Cranfield University

School of Mechanical Engineering

Ph.D.

Academic Year 2006-2007

Gary Dyson
Union Pumps

Investigation of the Closed Valve Head of Centrifugal Pumps

Supervisor: Dr J. Teixeira

Jan 2007

ACKNOWLEDGEMENTS

The author wishes to extend his thanks to his supervisor Mr J.Teixeira for his support and encouragement throughout this project.

The author also wishes to thank:

- Union Pump Textron for their support and funding
- Ron Palgrave for his tuition, guidance, encouragement and inspiration.
- Karen, Josh and Jess for not complaining (too much) about my love of pumps
- My parents –Thanks for the support over the years
- Albert Spencer for proof reading this thesis
- My colleagues at Union Pump who gave me support and contributed both directly and indirectly to this work.

Abstract

The ability to accurately predict the entire performance range of a centrifugal pump is commercially valuable. Pump manufacturers are reluctant to diversify their product portfolios unless they have confidence in their prediction methodologies. The prediction methodologies developed within this work are used to give Union Pump greater confidence in the prediction methods.

A methodology for using Computational Fluid Dynamics is presented which, when compared with time averaged pressure readings from the Union Pump test stand, accurately predicts the closed valve head of a centrifugal pump.

The work outlines the computational procedure used to achieve a successful CFD solution for a pump operating at closed valve. The procedure outlines the importance of including piping system elements within the simulation to allow the boundary conditions to be assigned correctly.

The methodology is applied to diffuser and volute pumps to give an insight into the flow regime. This work details the effects of rotor-stator interaction on the closed valve head.

Both diffuser and volute pumps exhibit a similar flow regime. At pump inlet the impeller experiences a strong steady outflow from the blade tip. The flow spirals out of the impeller eye into the pump suction channel. This spiralling flow is accommodated within the computational solution.

A new mental model, for use by designers, is proposed based on rotor-stator interaction analysis. The annular gap between the impeller and diffuser vane is filled with a pulsating the frequency of which is determined by the number of vanes within the impeller. The nature of this pulsation passed through to the stator passage influences the pressure at closed valve. This disagrees with the current mental model used by designers.

The minimum pressure fluctuation falls dramatically when the impeller vane number equals the diffuser vane number. This fall in minimum pressure is linked to the A2BB impeller dimension. This relationship is used to develop criteria for stability based on the pressure pulsation propagation through the diffuser.

This closed valve prediction method facilitates the redesign of existing unstable products to incorporate stable performance characteristics. Stable machines are more commercially acceptable as their performance is more reliable when they are operated in parallel with a similar machine. Unstable performance can be eradicated from pump performance characteristics through impeller redesign. The methodology also provides a roadmap for performance prediction of machines at off-design conditions for different pump configurations.

Contents

List of Figures

Nomenclature

General

a	Casing coefficient
A	Area
AR	Area ratio
API	American petroleum industry
b	Impeller passage width
B.E.P	Best efficiency point
Beta	Impeller vane angle
CFD	Computational fluid dynamics
C	Absolute velocity component
D	Diameter
g	Gravitational acceleration
HRTSO	Head rise to shut off
Ho	Impeller slip factor
H	Head
K	Von Karmen's constant
k	Turbulent kinetic energy
Kho	Casing constant
L	Length
LDA	Laser doppler anemometry
M	Mass
N	Rotational speed
Ns	Specific speed
P	Pressure
PLA	Phase locked averaging
q	Leakage flow rate
Q	Volumetric flow rate
r	Radius
Re	Reynolds number
RNG	Renormalized group
T	Time
U	Tangential velocity
u+	Dimensionless velocity
Vd	Velocity in discharge pipe
Vs	Velocity in suction pipe
W	Relative velocity
y+	Dimensionless distance from wall
Z	Number of blades

Greek

β	Impeller Blade Angle
θ	Angle
μ	Absolute Viscosity
ρ	Density
σ	Slip Factor
τ_{ω}	Wall shear stress
ν	Kinematic viscosity
Ψ	Closed valve correction coefficient
ω	Angular velocity

Subscript and Superscript

1	Impeller inlet
2	Impeller outlet
Imp	Impeller
so	Shut off
vol	Volute
z	Axial
t	time

1.0 The Importance of Performance Prediction

The performance prediction of a centrifugal pump across its complete operating envelope relies to some extent on empirically derived design coefficients. In particular the prediction of the closed valve head relies on a number of empirical methodologies. No analytical methodology exists. Design coefficients derived from a limited number of geometries are used to predict the closed valve head. These coefficients cannot account for many of the geometry changes and configurations that can be required in a final design.

The use of the empirically derived coefficients only predicts the closed valve head within 7%. For some extreme geometry the prediction error can be as much as 20%. These coefficients also cannot take account of the potential for unstable, drooping performance at closed valve.

The ability to predict closed valve performance of a centrifugal pump has widespread commercial significance. Pump manufacturers are reluctant to develop new machine configurations without the certainty of design prediction. Conventionally a combination of experimentation and the laws of similarity have been used to develop centrifugal pumps. This has lead to manufacturers specialising in certain machine types i.e. volute or diffuser. Developing machines outside these areas is viewed as expensive, requiring extensive testing and reworking prior to design launch.

The relative low capital cost of centrifugal pumps, compared to other turbo-machinery, limits the development budgets of pump manufacturers. Within the last 10 years no new pump manufacturer has emerged and many of the existing manufacturers have consolidated to form a single large company. This situation leaves the smaller manufacturers needing to develop design expertise away from their traditional product portfolio.

Union Pump has an extensive design database of volute machines that can be analysed to build design rules for similar new volute machines. The prediction of stability and closed valve head is a barrier to developing new complementary designs on a design for contract basis.

Furthermore the drooping, unstable closed valve characteristic is responsible for field failures of many pumps each year. Designing new stable machines with rising characteristics is essential in revitalising existing products and designing new products.

Union Pump's focus on volute machines is born from the conservative use of traditional design methodologies. The use of these methodologies and their appropriateness for diffuser design has reinforced a reluctance to develop a range of diffuser machines.

Diffuser machines have traditionally been viewed as difficult pumps to predict performance for across their entire spectrum. Many early diffuser machines exhibited drooping, unstable closed valve characteristics. Manufacturers of these machines developed empirical criteria over many decades. Shortcutting

this development cycle, and leapfrogging empirical design, is essential to developing a competitive range of diffuser machines to complement the companies existing volute range.

1.1Introduction to Pump Design

Many aspects of our lives are touched by pumps. Without even knowing it, people come across centrifugal pump in many aspects of their homes. Pumps are so numerous that their numbers are only exceeded by those of the motors which drive them. Centrifugal Pumps differ from all other rotating fluid machines in so much as they are expected to perform over an operating range which extends far beyond and far back from their design conditions.

To achieve this wide range of performance, an understanding of the entire flow spectrum is required. This level of understanding has previously been achieved by experimental techniques. With the advent of powerful computational resources it is now possible to computationally predict the flow structures of these machines as they operate at their most challenging performance points. Although it is prudent to be cautious when evaluating a computational solution, the extent and number of the validating cases both for on and off design conditions is growing.

The state of the art has advanced to such an extent that the computational solution can be compared with existing experimental research and time averaged performance data to give credibility to the analysis results. This chapter introduces some of the fundamental concepts of centrifugal pumps, as a background to the research into the closed valve head topic.

Section 1.2 deals with the definition of the pump performance envelope, the shape of the head capacity curve and why this is important.

Section 1.3 covers the pump construction and the common elements with the machines

Section 1.4 covers the theory of design using the Euler equations. This traditional development technique for blade design is explained.

Section 1.5 covers the theory of Similarity and its use in pump design.

1.2 Pump Performance Envelope

An analysis of the piping system into which a pump is placed is used to fix the performance parameters of the centrifugal pump. The system in which the pump operates has an effect on pump performance and as such defines the following parameters for pump selection/design

- Operating duty and performance curve
- Differential Pressure
- Head Rise To Shut off or particular curve shape
- Construction of pump
- Operating philosophy of the pumps

The system curve analysis is used to determine both the static and dynamic losses of any system into which a pump is to be fitted Fig.1.2.1 The static losses are fixed and are not related to the flow of the product. The dynamic losses due to friction are flow related and increase proportionally with flow.

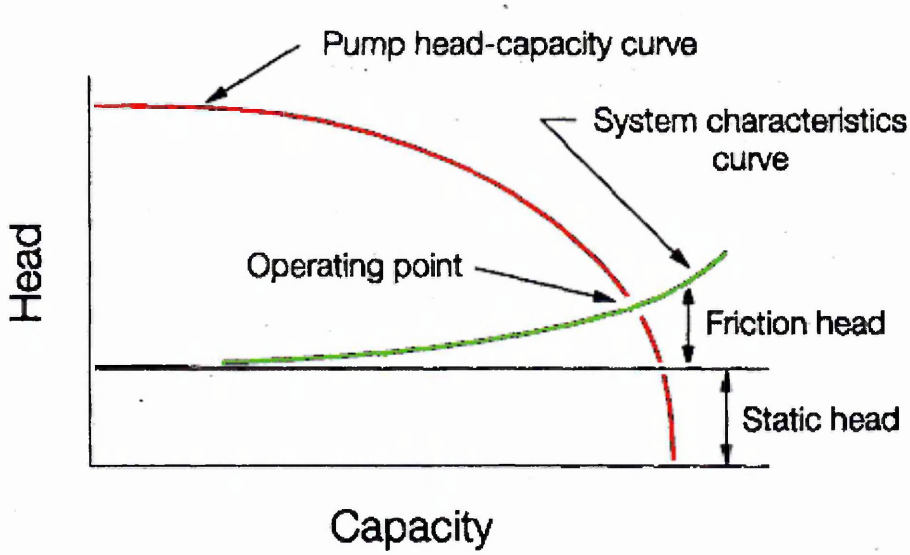

Fig 1.2.1 Pump Performance Curve and System Curve Intersection

The intersection of the system curve and the pump characteristic performance curve is used to fix the operating point of the pump. It should be noted that the dynamic proportion of the system curve can vary as mechanisms such as control valves are opened/closed to vary the pump flow.

The capacity of the pump is defined as the volume of liquid pumped and is generally measured in units of m3/hr in Europe and USGPM in the USA. These are plotted on the horizontal axis of the performance curve. The height to which a liquid level can be raised by a centrifugal pump is referred to as head and is measured in meters in Europe and feet in the USA. The use of head as a measure of pressure allows the pump performance to be judged

without reference to a particular liquid. The units of head being independent of specific gravity.

The pump is used to generate differential head. That is the discharge head minus the suction head.

For a horizontal pump the total differential head is defined as:-

$$H_{diff} = H_d - H_s + Vd^2/2g - Vs^2/2g$$

H_d is the discharge head
H_s is the suction head

Both these levels are adjusted and referred to the centreline of the pump.
The final two terms relate to the velocity head difference between the discharge and suction nozzles. Differential head values are plotted on the vertical axis of the pump performance curve. Fig.1.2.2 illustrates the performance map mandated by the API610 (2004) standard.

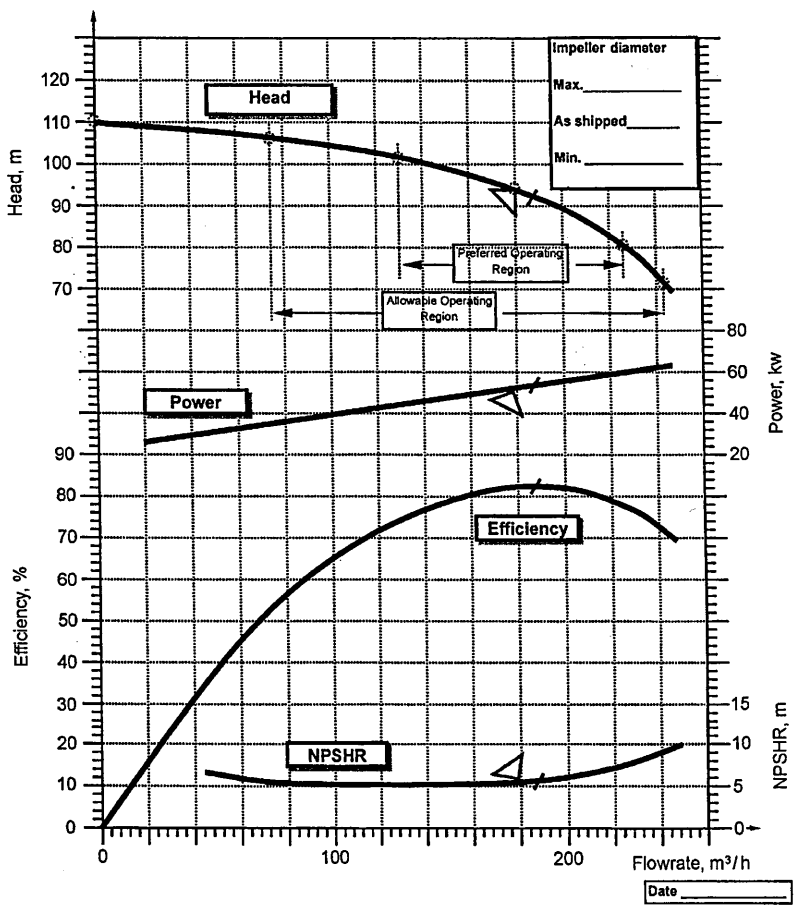

Fig 1.2.2 Typical Pump Performance Curve (AP610 2004)

The term Closed Valve Head applies to the differential head generated when the discharge valve is fully closed. This relates to the zero flow position on the horizontal axis of the performance curve. When a pump runs at closed valve

the flow across the discharge valve is zero. The flow passing through a pump however is not zero. A finite amount of liquid is passed through the wear ring landings and back to the pump low-pressure inlet.

This leakage is between 1-10% of the total best efficiency point (B.E.P) flow, depending on the geometry of the pump Fig.1.2.3. Designers quantify the amount of leakage flow and consider it within their design methods. When considering closed valve problems the difference between closed valve pressure incorporating this leakage and without this leakage is considered to be negligible as the performance curve has a shallow slope at such a low flow.

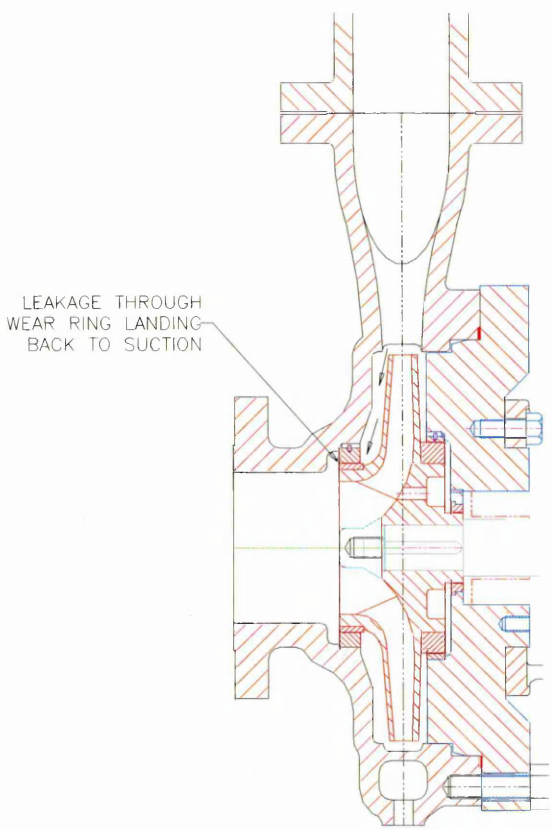

Fig 1.2.3 Discharge Flow Circulation Back to Pump Suction

The head of a centrifugal pump is expected to increase steadily with the reduction in flow rate from the pumps best efficiency point until the discharge valve is closed. This is commonly known as a constantly rising or stable curve. Many industry specifications limit, such as API 610 (2004), limit the minimum amount of head rise from B.E.P to closed valve. Some more stringent specifications, put forward by the petroleum industry, define a required head rise to closed valve or desired closed valve measurement.

In practice, some pumps will not exhibit a constantly rising head curve. These are referred to as unstable curves. The head of the pump at low flows may

start to decrease with the reduction in flow rate Fig.1.2.4. This unstable curve phenomenon is unacceptable for many applications.

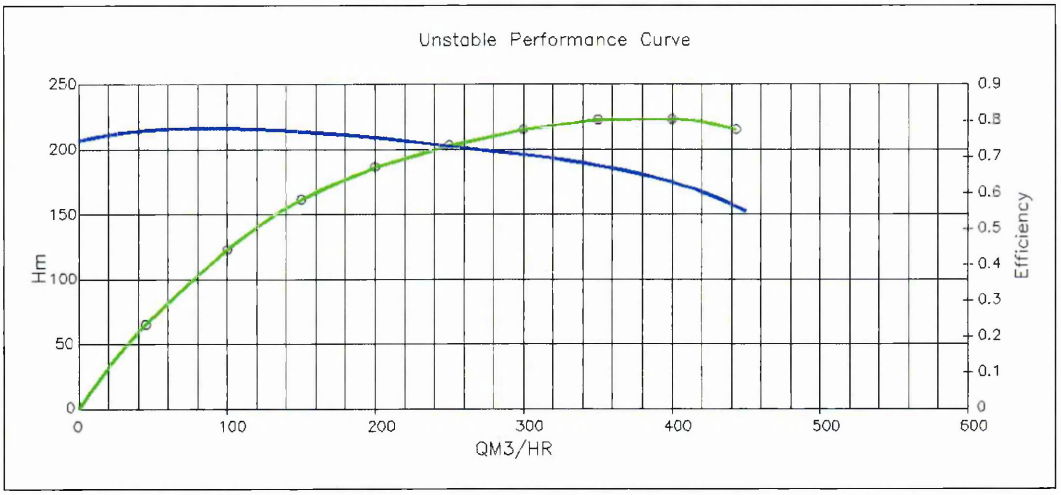

Fig 1.2.4 Unstable Pump Performance Curve

The consensus, from all the standards across the pump industry, is that a pump that is required to operate in parallel with another machine must have a head rise, between operating point and closed valve, of at least 10%.The specifications also mandate that all pumps have a constantly rising head curve (stable). The rise in differential head from operating point to closed valve is commonly referred to as head rise to shut off (HRTSO).

When two pumps are installed in a piping system as per Fig.1.2.5 the pump flows can be added together and their interaction with the system resistance curve is convergent at below twice the flow[1]. In this way higher flow pumping is achieved. This type of pumping system is particularly sensitive to HRTSO considerations.

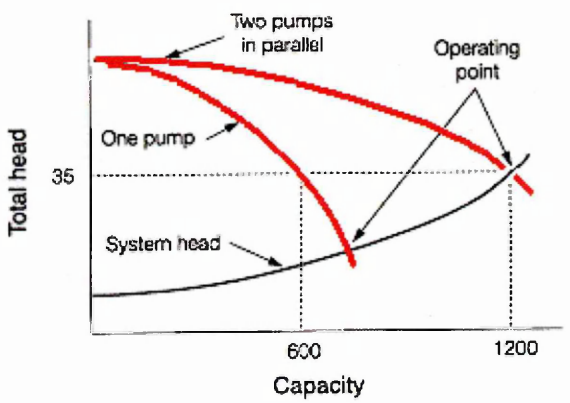

Fig.1.2.5 Performance Curves of Pumps Operating in Parallel

[1] Depending on the slope of the system resistance curve

The reason the specifications demand 10% HRTSO and a positive slope is due to the action of pumps which run in parallel. Two pumps operating in this scheme would synchronise at a common differential head. For an unstable pump, two flow conditions are satisfied by one common head reading. In this instance one of the machines may operate at a very low flow. Operation for any prolonged period at this low flow condition would lead to pump failure as the liquid within the machine heats up and flashes off.

The desired shape of the head capacity curve and the design for HRTSO is the main focus of this research. Whilst the prediction of the operating head is straightforward the prediction of the closed valve head is conventionally empirical and difficult in nature.

1.3 Pump Construction

The machines analysed within the research are common types of centrifugal pumps.

A volute machine is analysed as illustrated in Fig.1.3.1. In this example the impeller expels liquid into two passageways which diffuse the liquid. The passageways then join together at the pump discharge. This type of machine is common for medium to high end applications and in this case is a single stage machine. Fig.1.3.2 illustrates some of the mechanical features of this machine. The dominant rotor-stator interaction takes place as the impeller blades pass the two volute lips.

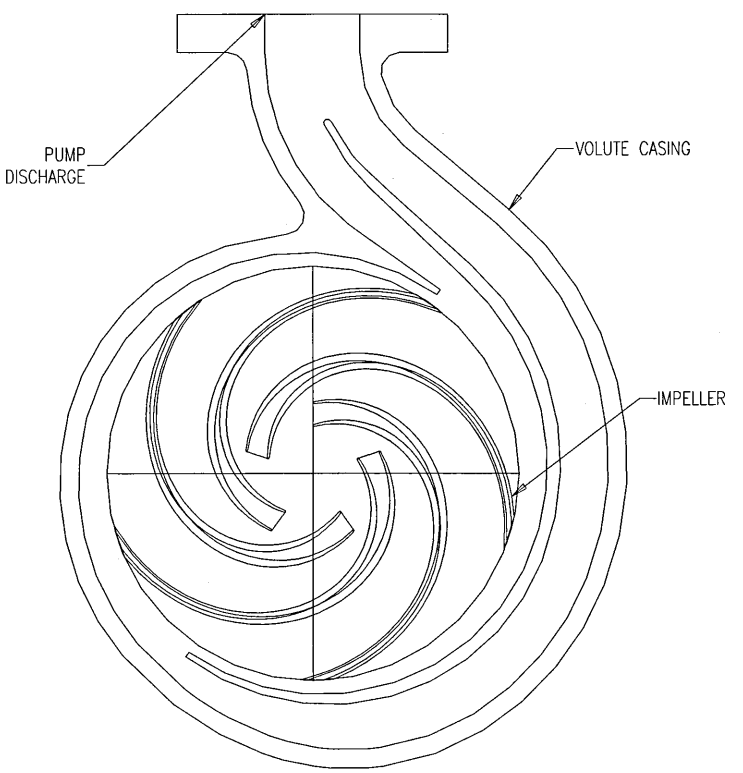

Fig.1.3.1 Hydraulic Passages in a Volute Machine

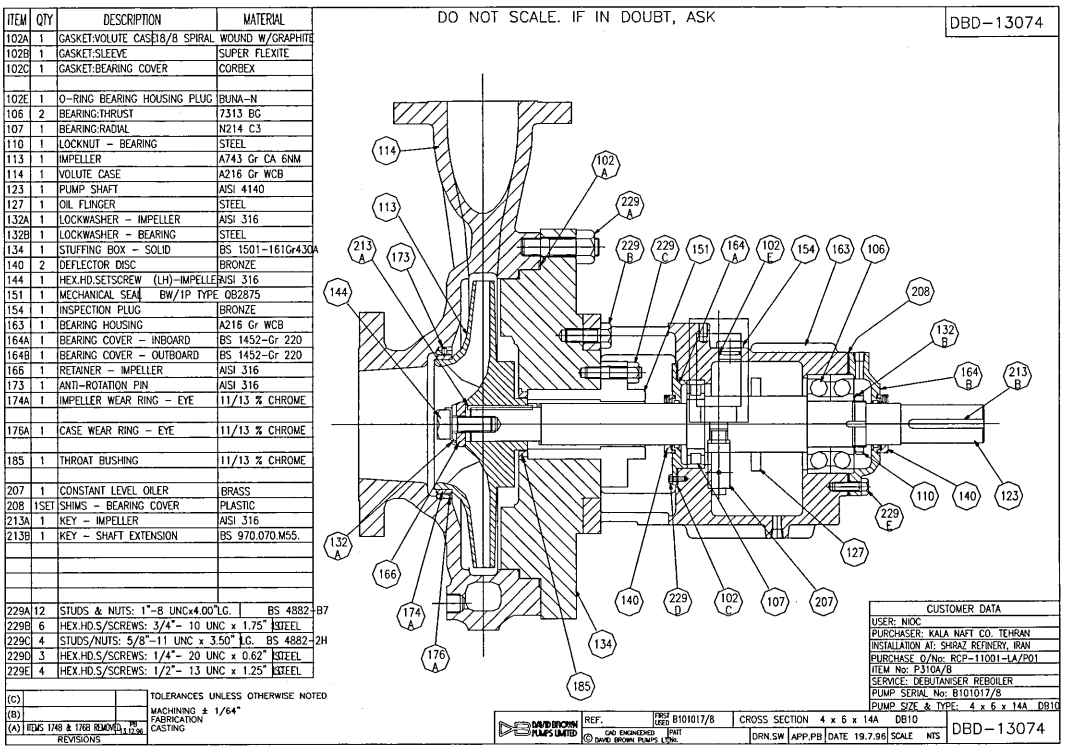

Fig 1.3.2 Cross Section of a Volute Pump

One stage of a diffuser machine is also analysed and is illustrated in Fig.1.3.3. This type of machine contains multiple blade rows in both the rotor and stator. This type of machine is common when high heads are required. Rather than use a very large impeller of a very high rotational speed, multiple impellers and diffusers are used on a common shaft. Fig 1.3.4 illustrates the mechanical construction of the machine. The dominant rotor stator interaction takes place as the impeller blades pass the multiple diffuser vane tips.

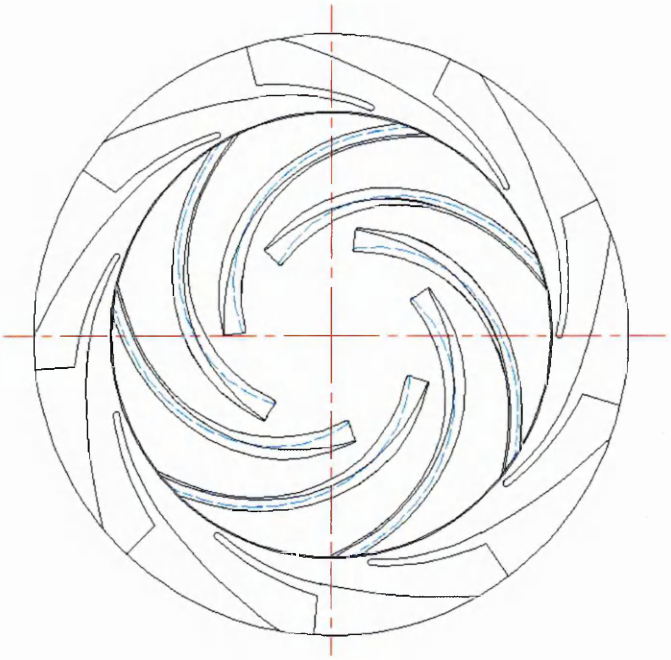

Fig.1.3.3 Hydraulic Passages in a Diffuser Machine

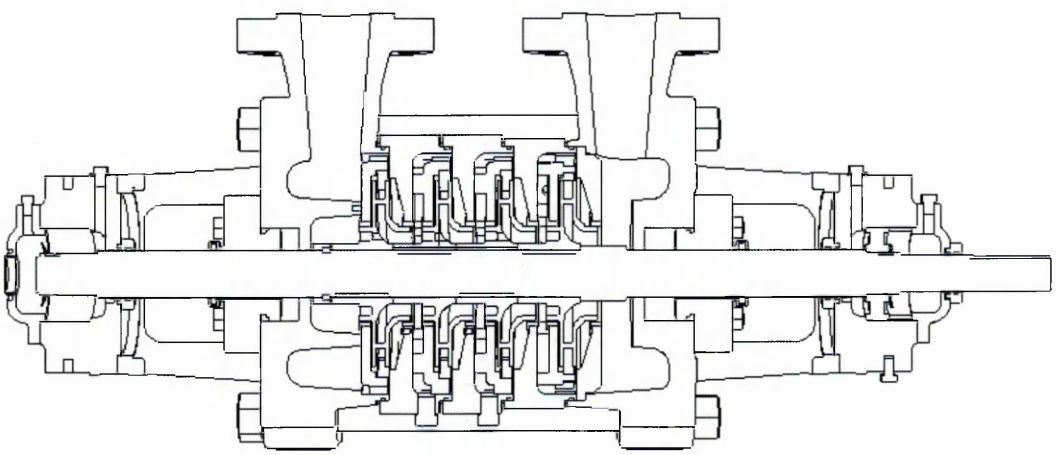

Fig. 1.3.4 Section through a Diffuser Machine

1.4 The Euler Pump Equation

Prediction methods for pump design are primarily based on the Euler Pump equation. This considers the transfer of energy from the rotating impeller into the fluid particles passing through it. Fundamentally, Newton's second law of motion is applied to the mean streamline fluid within the impeller.

This principle states that: -

The time rate of change of angular momentum of a body with respect to the axis of rotation is equal to the torque of the resultant force of the body with respect to the same axis.

For a mass of liquid travelling through one impeller passage,

When *time t = 0* the impeller passage way between the vane is filled with liquid as illustrated in Fig.1.4.1

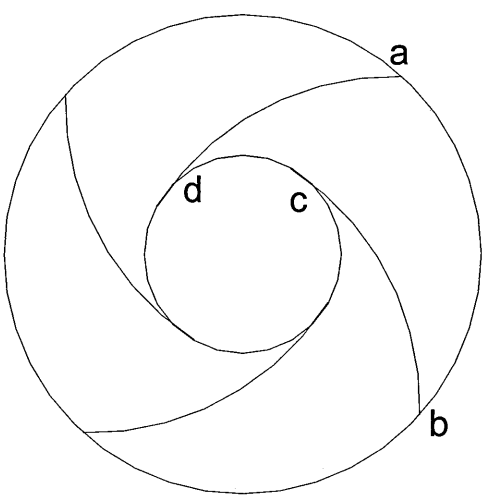

Fig.1.4.1 Impeller Passage Way Illustration When Time = 0

After a time period *time t = dt* the fluid between the vanes has progressed to positioning Fig.1.4.2. This figure also illustrates the proportion of a thin layer of fluid passing outside the impeller. The mass of this fluid exiting the impeller outlet is equal to the mass of the fluid entering the impeller at the inlet within the time period *dt*.

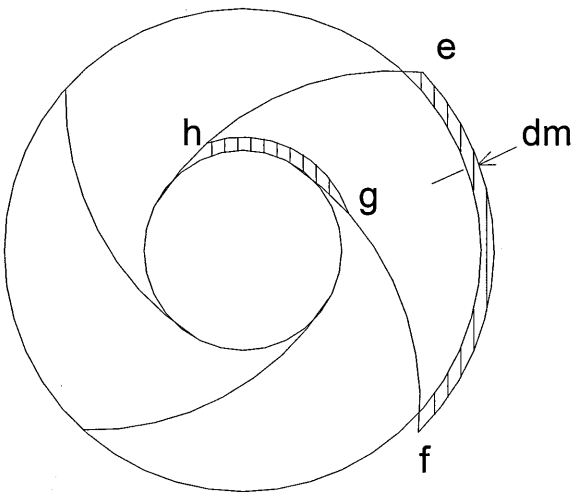

Fig.1.4.2 Liquid Progression with Time

The change in moment of momentum of the whole channel is represented by the change of moment of momentum of the mass *dm* entering and leaving the impeller.

The moment of external forces *T* is stated as

$$T = \frac{dm}{dt}(r_2 c_2 \cos\alpha_2 - r_1 c_1 \cos\alpha_1)$$

The external forces applied to the liquid are:

- Pressure difference between the suction and discharge side of the vane
- Pressure difference across the passage between vanes at inner and outer vane radius
- Hydraulic friction forces which oppose the relative flow.

If we consider the $\frac{dm}{dt}$ for all impeller channels this is the constant time rate of mass flow $\dot{M}$.

Substituting $\dot{M}$ and multiplying through by ω

$$T\omega = \dot{M}\omega(r_2 c_2 \cos\alpha_2 - r_1 c_1 \cos\alpha_1)$$

This is the equation for input power:

Substituting $U_2 = \omega(r_2)$

$U_1 = \omega(r_1)$

$c_2 \cos\alpha = cu_2$

$c_1 \cos\alpha = cu_1$

$$P = \dot{M}\left(u_2 cu_2 - u_1 cu_1\right)$$

If we assume that the no head is lost between the impeller and the measurement point the power is available as the pump output of an idealised pump

$$\dot{Q}H = \frac{\dot{Q}\left(u_2 cu_2 - u_1 cu_1\right)}{g}$$

Giving the Euler Equation

$$H = \frac{\left(u_2 cu_2 - u_1 cu_1\right)}{g}$$

Pump efficiency and cost constrains require engineers to eliminate the inlet pre-swirl into the impeller eye. This mandates that cu_1 = 0 and eliminates half of the equation.

$$H = \frac{\left(u_2 cu_2\right)}{g}$$

All the head of a centrifugal pump is generated by the impeller. The casing and other components contribute nothing to the generation of head but impact the final value by contributing losses. These include leakage losses back to suction, skin friction, diffusion losses due to sudden area changes and eddy losses which are inevitable due to the way a pump generates head.

To the fundamental Euler equation pump designers apply empirical constants to achieve realistic predictions of machine head. The difference between the theoretical head and the Euler head is accounted for by the term hydraulic efficiency.

Furthermore the Euler equation assumes that the angle of fluid leaving the impeller blade is equal to the impeller blade angle. This would only be true for an impeller with an infinite number of vanes. As the majority of centrifugal pumps do not have blade numbers more than eight the phenomenon of fluid slip occurs, and is considered, at the design stage as a refinement to the Euler equation.

The relative flow within the impeller outlet is regarded as a through flow upon which a relative eddy is imposed by the blade. The consequence of these

simultaneous actions forces the flow to leave the impeller at an angle β'_2 rather than the blade angle β_2.

This has the consequence of reducing the vane contribution from cu_2 to cu'_2 and its effect on the Euler equation reduces the proportion of the head the machine can produce Fig 1.4.3

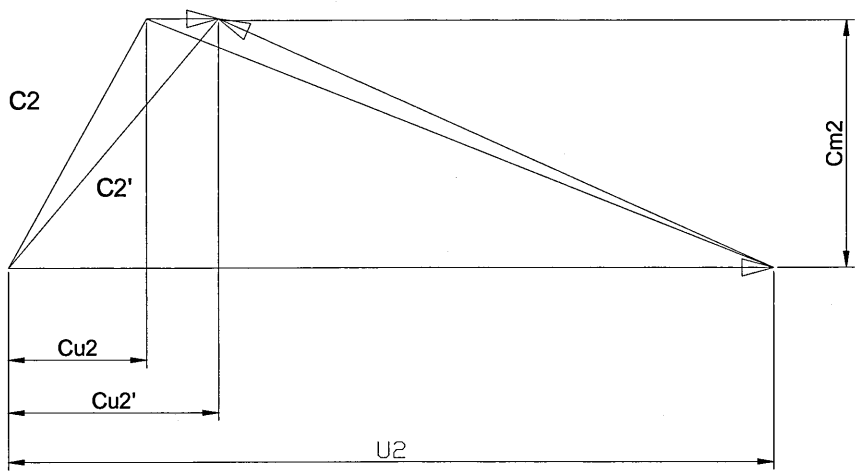

Fig.1.4.3 Discharge Velocity Triangle

A mathematically exact solution for the determination of slip factors was proposed by Busemann (1928) applying the theory to a two dimensional machine with logarithmic spiral vanes. Busemann (1928) ranked the influence on slip factor of outlet angle β_2 and vane number z.

The Busemann (1928) slip factor can be written as

$$\sigma_{bus} = \left(A - B\phi_2 \tan\beta'_2\right) \Big/ \left(1 - \phi_2 \tan\beta_2\right)$$

Where the constants A,B and β'_2 are functions of the blade angle, number and radius ratio. Other designers proposed alternative slip factors and these are reviewed for accuracy in the work by Patel (1981).

That being said, the pump industry designers have generally adopted the Busmann slip factors as the industry standard. One potential problem with Busmann slip factor adoption is that it is based on log spiral vane geometry. Impeller design rarely achieve a true log spiral over their whole length.

According to Stepanoff(1957) the flow through an impeller can be considered as consisting of two components: a circular motion around the axis as a result of the action of the vanes and the meridional flow caused by the energy of the gradient drop.

The circular component of flow forms a vortex motion. The type of vortex depends on the velocity and the pressure distribution and can be established by the Euler equation.

The importance of the Euler equation to the prediction of closed valve head can be characterised in part by the assumption that at zero flow the equation reduces to the form:-

$$H = \frac{\left(u_2^2\right)}{g}$$

The flow passing through the impeller is zero so only the geometric features that pertain to the peripheral velocity are considered by the equation.

Changing the impeller diameter or the rotational speed of the impeller changes the closed valve head. This is a commonly observed phenomenon and the Euler equation can be used to accurately predict changes in the closed valve head associated with both diameter and speed.

Designers of centrifugal pumps have noticed, after designing many machines, that there is a distinct difference between volute and diffuser pumps in terms of design for stability. Diffuser pumps appear, anecdotally, to have a higher closed valve head coefficient than volute pumps. Diffuser pumps are also more difficult to design with a stable performance curve.

One method employed by designers of diffuser machines is based on encouraging the $u_1 cu_1$ proportion of the Euler equation. Diffuser machines are commonly multi-stage as illustrated in Section 1.3. As the liquid is passed from the diffuser into the eye of the next impeller an inevitable amount of swirl is introduced into the fluid.

Associated with this swirl is a lessening of the head of the pump at best efficiency point. The head at closed valve is unaffected by this $u_1 cu_1$ proportion. This increases the HRTSO of the pump.

Designers have gone further than merely accepting the remnant swirl in this type of machine. On some occasions guide vanes are added to encourage the inlet swirl. This reduces the head of the machine at design flow whilst keeping the closed valve head unaltered.

This technique is unsatisfactory, reducing the machine efficiency. The pump must, therefore, contain more impeller stages to generate its final head to account for the head lost to ensure stability.

1.5 Pump Specific Speed Considerations

The pump industry associated with the design of pumps for oil and gas application has adopted, as standard, a method for ranking the design type of each centrifugal machine. Pump configurations are ranked in line with the following formula proposed by Camerer (1915):

$$Ns = \frac{n\sqrt{Q}}{H^{0.75}}$$

Unlike most ranking systems for centrifugal machines, this system requires the units to be assigned as follows:

Q = USGPM
H = Feet

The physical meaning of the equation is

Revolutions to produce 1gpm at 1 ft head with an impeller of with the same geometric characteristics as the one under consideration but scaled down in size.

Fig.1.5.1 Illustrates the geometry differences based on Ns.

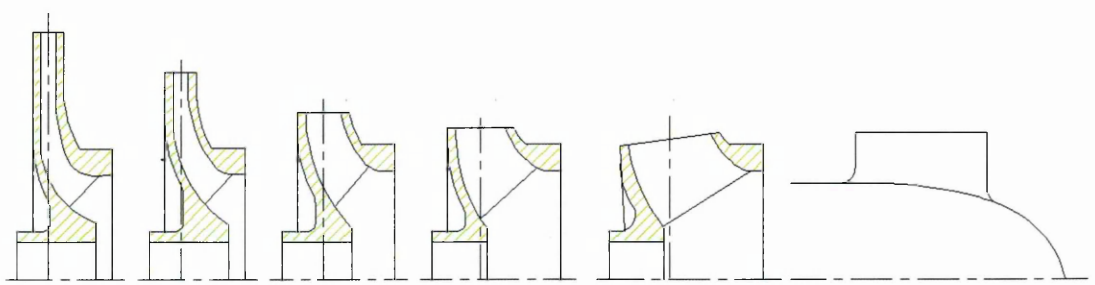

Fig.1.5.1 Illustration of How Geometry Changes with Specific Speed From Ns 500 (Radial Machine) to Ns 10000 (Axial Flow Machine)

For comparison purposes the industry has adopted this US dimensioned Ns value as standard. The full dimensional analysis can be found in Stepanoff (1957).

From a design standpoint the use of the Ns number is useful in so much as impellers with identical specific speeds can, theoretically, be scaled up and down in a predictable way.

This scaling effect also extends to the performance curve of the machine and is based on the following ratios:

$$\text{Linear Scale Factor Flow} = Q^3/Q$$
$$\text{Linear Scale Factor Head} = H^2/H$$

Designers have used this technique to create new designs with a predictable closed valve head value. This technique has some difficulties in as much as the design of a machine relies upon detailed geometric knowledge of a similar machine. Modifications to impeller blade numbers cause the scaled curve shape to change unpredictably at closed valve.

Some performance parameters, such as vibration, are not apparent from performance curves. Using the Ns value and scaling a poor performing machine inevitable leads to another poor performing machine. Although this technique can provide satisfactory results it is empirical in nature and is considered far from satisfactory for large scale changes.

1.6 Summary

The scope of this project investigates the prediction gap between the Euler theoretical maximum and the head which is actually achieved by the machine.

The commonly held belief in the pump industry is that unstable pumps cause operational problems. Whilst this fact is anecdotal, it is supported by the numerous specifications issued by pump purchasers, which mandate a constantly rising head curve (stable).

Yedidah (1993) presented evidence that, in practice, the use of a pump with an unstable curve was seldom an operation problem, but pumps of this type are still not accepted. Yedidah (1993) proposed that if a machine had a closed valve head which was greater than the duty head there would never be an operational problem.

One cause of the unstable curve can be the forced nature of the outlet impeller flow. Designers soon realised that high vane numbers in an impeller caused a drooping, unstable, closed valve head characteristic.

One proposed method for ranking the stability criteria based on vane number and outlet angle was proposed by Peck (1968). His paper proposed that the ratio of the relative velocity from inlet to outlet should be kept under unity to ensure a stable machine. This empirical methodology ignores the effect of the stator vanes and rotor-stator interaction.

This project contributes to the designer's ability to predict the close valve head of a machine by:-

- Providing a refined analytical method for ensuring a constantly rising head curve based on the empirical prediction methods.
- Aiding the understanding of the nature of the flow at closed valve and the consequences of common geometric changes.
- Providing a computational method to accurately predict closed valve head.
- Linking the vane number to the closed valve head development

Chapter 2 contains the literature search which describes the difficulties of experimental and computational analysis at closed valve. Worster (1963) described the analysis and prediction of closed valve head as the greatest challenge to pump designers. Forty years on from that statement the state of the art has hardly advanced.

Prediction methods studied in Section 2.3 reveal the difficulty of predicting closed valve head. An analysis of machines against the prediction methods available points to the empirical nature and inaccuracies contained in all the prediction methods.

Refinement coefficients are suggested in the literature review which improve the accuracy of the prediction methods. Although this offers some improvement the existing prediction methods are still not accurate enough to meet common specification requirements.

It should be noted that machines of identical design, with different impeller trim diameters behave in an identical way. This research is not aimed at the performance differences of these machines but at the unpredictable nature of a new design where the full range of vane numbers, outlet angles and diffuser types are available.

It can be observed from the literature that many of the geometries are compromised to aid either the access for experimental investigation. Many impellers run at low flow without a volute. Some machines have large throat areas which do not represent contemporary pump design.

Computational analysis is a valuable tool when investigating the flow physics within a machine. Whilst this technique has vast potential, its use must be checked against the experimental data that is available to ground the analysis. Many computational schemes and conditions are available. The science of Computational Fluid Dynamics (CFD) and its application to the closed valve problem is explored in Chapter 3. The parameters associated with grid density, turbulence modelling and time step independence are evaluated.

Chapter 4 uses the geometry from a commercially available machine as the basis for a computational analysis. This section is used to build an understanding of the nature of the flow physics within a volute pump. This has been previously attempted by Newton (1988) without accurately predicting the closed valve head

Chapter 5 extends the understanding of flow at closed valve by applying computational solutions to a centrifugal machine with a bladed diffuser stator. The analysis of a diffuser machine at closed valve has not been attempted.

With such a comprehensive study of the closed valve head flow phenomenon it is possible to use the analysis to propose a new criterion for the stability of a centrifugal pump. Chapter 6 concludes the project by outlining the proposed effect of changing impeller blade numbers within a diffuser pump and suggests criteria for stability based on linking unsteady analysis back to impeller geometry.

2.0 Literature Review and Prediction Methodologies - Overview

The literature review explores experimental work carried out to investigate flow physics within centrifugal pumps. It encompasses both on-design and off-design work.

On-design is conventionally considered to be the flow at which the pump efficiency is the greatest. The flow is considered to be independent of phase position between the impeller blade and the collector system. Although studies, Miner(1988), indicate that an unsteady temporal flow field exists, this is small and is ignored by pump designers to simplify the design problem. Off-design is considered to be at a flow significantly below the best efficiency point. This flow regime is considered to be highly time dependent, changing rapidly as the impeller blade position, with respect to the collector position, changes.

Much research in the area of on-design analysis has been carried out reflecting the designer's natural focus on pump efficiency. Less work is available on the unsteady flow behavior. The complex natures of the flow physics, the strong rotor stator interaction effects and the difficulty of the time dependent experimental investigation have proved obstacles.

The second section of the review is concerned with the computational solution of the flow physics within centrifugal pumps. On-design analysis has been successfully computed. Less work is available at off design conditions. The off-design work that is available is based on limited geometries which are often unrepresentative of commercial pump design.

Methods used to predict the closed valve head of a centrifugal pump are explored in the final section of the chapter. These methods are gauged against performance from a database of 200 pumps of varying configurations. Empirical modifications to the prediction methods are suggested to increase their accuracy.

2.1 Experimental Measurements and Investigation

The successful design of centrifugal pumps relies on the designer's mental picture of the flow behavior matching the actual behavior of the pump. To aid in the design process, experimental work has been carried out to determine the behavior of centrifugal pumps. The simplest case, impeller at design flow running without a collector (i.e. volute, diffuser or concentric enclosure), has received by far the most attention.

Recently attempts have been made to analyse the unsteady rotor stator interactions and complex re-circulating flows at the pump inlets for off-design conditions. Data is seldom taken at shut-off conditions. This may be due to the difficulties experienced in running a pump in this condition. Rapid heating of the product is experienced, the casing and seals are at maximum pressure and the flow is pulsing. The following sections of the literature review have been split between design point, low flow and closed valve flow analysis.

2.1.1 Best Efficiency Point Studies

A selection of papers were reviewed which typify the experimental work which has been carried out. Although not extensive the methodologies and geometries investigated are typical of this field.

Kumar and Rao (1977) developed a two-dimensional method of analysis for through flow in a centrifugal pump impeller with good agreement with experimental results for commercial pumps at B.E.P. Their predictions closely mirrored the Buseman (1928) predicted impeller head-line. One of the first papers to using the PLA (phase locked averaging) method was presented by Gostelow (1977). Using this technique it is possible to ascertain the unsteady pressure for different radii within the impeller flow channels. Although the impeller flow is not indicated in the paper, the steady nature of the flow patterns suggests that it is on or around B.E.P.

Alder and Levy (1979) successfully measured the B.E.P flow within a shrouded impeller in a large volute designed for ease of access. This volute design may have contributed to the poor inlet performance and distorted inlet flow. This is a characteristic of machines with large inlet areas. Recognising this fact, it is standard practice within the pump industry to incorporate flow straightening vanes and anti swirl vanes in the casing suction branches. These prevent pre-rotation of the flow into the impeller eye. This effectively eliminates the negative inlet proportion of the Euler head calculation, maximising head for a given impeller diameter and simplifying inlet design criteria.

Rose (1987) was one of the initial users of a new back scatter Laser Doppler Anemometry system. This requires optical access from one side only. Using a

high power laser he obtained a clean signal from the scattered light. He presented a study of a centrifugal multistage pump impeller operating in water at B.E.P.

From this experimental data the pump industry has refined the mental model used to build its prediction methodologies. Although the flow field is time dependent and unsteady the flow field fluctuations are so low that the industry successfully uses steady design methodologies rather than consider the low level pressure fluctuations.

2.1.2 Low Flow Studies

Whilst the investigation of the design point flow field was initially of most interest to pump researchers this quickly changed as the design methodologies evolved. The attention turned to the investigation of machine operating at extreme part load.

Peck (1950) carried out investigations on a single entry end suction pump, collecting experimental data through a visualisation window using a stroboscope. At very low flows he observed that a large re-circulation region "powerful forced vortex" was present. This extended far into the suction pipe. Pressure tappings in the casing indicated a circumferential pressure rise from cutwater to casing throat. Visualisation also confirmed a surging flow phenomenon at the cut-water.

Young (1956) used photographic tracking techniques involving tracers of unit specific gravity introduced into the pump. Observations at 50% of design flow indicated a complex flow pattern. Higher velocities on the leading blade face than on the trailing blade face were noted. Other observations indicated that the flow differs from passage to passage. This phenomenon, reported by Young, is identical to that previously observed by Fischer and Thoma (1952). It is explained as the stalling of alternate vane passages. No attempt in either paper is made to relate phase angle to the passage stall. This prevents any conclusions being drawn regarding the rotor/stator interaction effects.

At low flow rates a non-uniform pressure distribution within the volute was presented by Binder and Knapp (1958). As the area within the volute increased, from cut water to casing throat, the pressure was observed to increase. The minimum pressure encountered was local to the cutwater.

Simpson and Cinnamond (1964) carried out flow studies through centrifugal pump impellers with varying outlet angle. At lower flows vortices on the trailing face of the blade were observed. Conversely these occurred on the blade leading surface at high flows.

McDonald, Lennemann and Howard (1971) took experimental measurements using hot fill probes preceded by flow visualisation. They compared various changes of flow with potential invisid flow theory. They concluded that at low flow

their inviscid model could not account the region of low velocity near mid blade height on the suction side of the blade.

Brownall et al (1985), using streak photographic techniques, verified the existence of significant inflow to the impeller at the low-pressure region near to the tongue. Previous research by Alder and Levy (1979) had also noted this flow feature. Differing flow patterns were observed dependent on the phase position of the impeller blade with respect to the cut-water lip.

At the lowest flow (30% B.E.P) the tongue stagnation point moved into the volute indicating a large flow into the volute past the tongue. The separation zone, caused by the tongue, oscillated at vane pass rate demonstrating the impeller case interaction. This is consistent with Yedidah's (1985) earlier observations but not with Worster (1953).

Further to the work of Binder and Knapp(1958), Iversen(1960), Kikuyama et at (1987) determined the existence of the non-uniform circumferential pressure gradient around the volute. Using PLA they obtained periodic data on the hub side volute wall. At best efficiency point (B.E.P) a steady flow pattern was observed with respect to blade position. At "off design" flows the pattern became unsteady with large pressure oscillation at vane pass rate dependent on the blade relative position to the cut water. This gave an indication of the circumferential pressure distribution caused by the rotor stator interaction.

Goulas and Trouscott (1988) carried out experimental analysis of an end suction pump using LDA to explore the flow pattern at the impeller exit. At 27% of design flow the velocity vectors local to the cut-water were directed through the cut-water clearance, between the impeller and case. This indicated a low static pressure region. This agrees with earlier observations made by Binder and Knapp (1958), Brownall et al (1985), Kikuyama et al (1987). Goulas and Trouscott (1988) also found a reverse flow region past the tongue on the impeller side similar to the one suggested by Yedidiah (1993) for unstable pumps.

Roco (1990) correlated LDA data with shaft position to calculate the velocity field within a slurry pump at two flow rates. Data was plotted with respect to angular position. This is particularly important when studying the effects of rotor stator interactions.

Dong et al (1992a & 1992b) applied Particle Displacement Velocimetry (PDV) to obtain the pressure fluctuation within a pump. This study indicated that at low flows large flow structures exist determined by the blade orientation to the cut-water.

Hureau et al (1993) and also Stoffel and Weis (1994) used Phase Locked Average LDA to obtain tangential and radial velocity within an impeller. Their studies at low flows indicate that for flow to reverse and escape from the impeller

eye the re-circulating flow has to exceed the inlet tip speed of the impeller. Palgrave (1985) presented data to indicate that inlet vane angle was also significant in ascertaining the percentage of B.E.P flow at which this suction re-circulation occurred.

2.1.3 Closed Valve Studies

Following on from the low flow studies, investigators made the natural leap to the study of the closed valve head flow regime.

Ficher and Thoma (1952) carried out flow investigations in a centrifugal pump at closed valve. They used a rotating prism technique to freeze the flow. Their observations found a pulsating flow that was cyclical and sub-synchronous. Each impeller passage experienced a different flow regime dependent on its position in the cycle. Significant cross channel flow was witnessed at both pump inlet and outlet. Their observations concluded that a large proportion of the impeller was filled with "dead water".

Acosta (1954) and Acosta and Bowerman (1957) conducted experiments on a series of impellers. This experiment used a submerged impeller discharging into a test tank. At shut-off conditions they observed that for 80% of the impeller passages were filled with dead water. The 20% of the passages towards the outlet contained a relative eddy which rotated counter to the machine rotation. This experiment neglects rotor stator interaction.

Iversen (1960) encountered this same pressure distribution and found a similar pattern at shut–off. Pressure increased from cut-water to discharge around the collector circumference. Iversen was the first researcher to note a rapid pressure drop at the cut-water.

Worster (1953) in his work on shut-off head flow patterns concluded that the volute was responsible for 20% of the shut-off head. The pressure from the cut water was found to rise around the volute and be constant at the throat and in the discharge pipe. Worster (1953) also observed a considerable flow interchange between impeller and volute. He proposed that this exchange of energy was responsible for the closed valve head not reaching its maximum Euler value. It is not possible to ascertain if the pump displayed a stable head characteristic at closed valve.

At shut-off condition they observed the exit relative eddy previously observed by Acosta and Bowerman (1957). They also noted an inlet relative eddy rotating in the machine direction in the pump inlet Fig.2.1.3.1. This flow feature is not mentioned in any of the previous research.

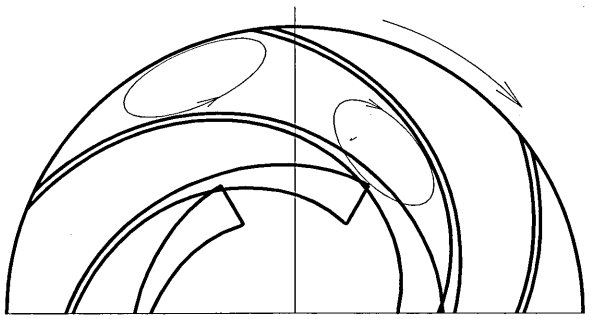

Fig.2.1.3.1 Visualised Eddy Distribution by Acosta and Bowerman (1957)

Levin and Poliokovsky (1965) carried out work to ascertain the nature of this suction re-circulation at shut-off conditions. Investigations took place on a radial un-shrouded machine. They found a large re-circulated region axially within the impeller and suction pipe Fig.2.1.3.2. Further unpublished work by Palgrave has shown that the recirculated region leaves the impeller at the inlet vane angle in the relative frame. This then spirals down the inlet pipe Fig.2.1.3.3.

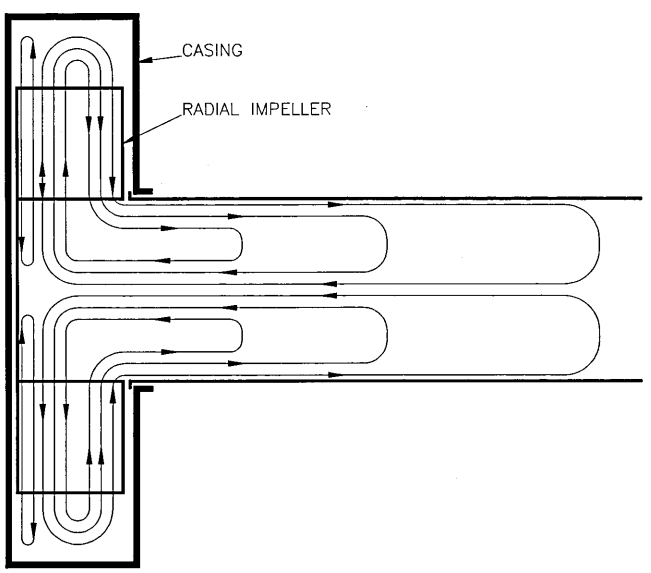

Fig.2.1.3.2 Flow Lines Of Radial Impeller at Zero Flow As Proposed By Levin And Poliokovsky (1965)

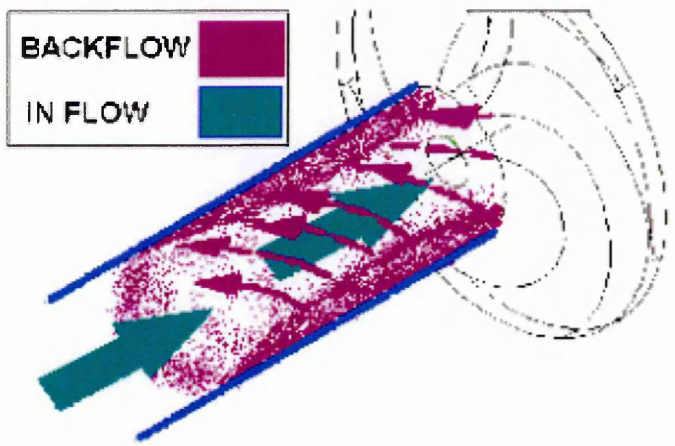

Fig.2.1.3.3 Flow Direction of Re-Circulating Liquid Proposed By Palgrave (2000)

Lennemann and Howard (1971) performed visualization studies using hydrogen bubbles. They examined the unsteady flow in radial impellers operating at shut-off conditions. Their findings were consistent with Acosta and Bowerman (1957). They observed a relative eddy at the impeller exit and 80% of the impeller exhibited solid body rotation. This contradicts the findings of Simpson and Cinnamond (1964). From the geometry given it is not possible to ascertain a reason for the exit relative eddy.

These cases are indicative of the difficulties encountered when attempting to separate out the effects of geometry on the flow features. The Simpson and Cinnamond (1964) pump may have had an overly large design of inlet, or significant inlet pre-swirl may have been present. Conversely Lennemann and Howard (1971) may just have overlooked the presence of the inlet relative eddy.

Yedidah (1985) used stroboscopic lighting to freeze the flow field on a single volute pump at zero flow. Two possible flow patterns were presented. For a pump with an unstable characteristic there is significant cyclic fluid interchange between casing and impeller Fig.2.1.3.4. For a stable pump characteristic there is no fluid interchange back into the impeller Fig.2.1.3.5. The energy lost during this interchange is proposed as the reason for the low closed valve head characteristic of an unstable pump.

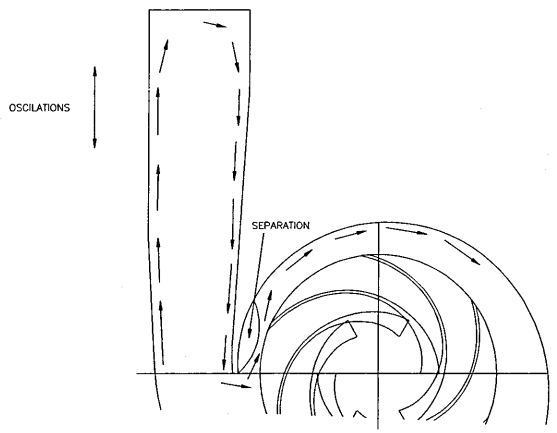

Fig.2.1.3.4 Yeddiah Proposed Flow Field for an Unstable Pump Characteristic

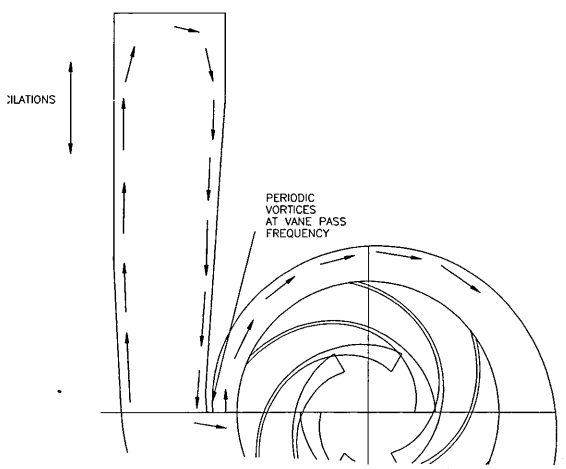

Fig.2.1.3.5 Yeddiah Proposed Flow Field For Stable Characteristic

Instability within pump impellers is caused by a number of factors, which pump designers consider, using empirical methods, when proposing a new design. It is not possible from the paper to ascertain which geometric features cause the instability or if the instability flow pattern is identical for all geometric cases. This flow phenomenon observed by Yeddiah (1985) is consistent with Worster's (1953) observations of an unstable head characteristic as is the oscillating flow feature observed by Peck (1950).

Abramian and Howard (1998) used LDA to gain an insight into pump flow by analysing an impeller with and without a volute. Their investigation differs from conventional investigations in that the subject was a low specific speed machine. This configuration introduces the difficulty of surface finish and leakage flow although these are not mentioned in the paper. Periodic unsteadiness,

fluctuations in the pressure fields and flow reversal into the impeller were all present at flows near to shutoff.

The measured flow patterns were in agreement with previous visualisation studies of Howard et al (1987). Vector measurements were taken at increments from the suction to the pressure side of the blade for differing phase angles with respect to the volute throat. The flow at the suction side continually exits the blade passage with no change of direction. There was a quickening of the flow as the blade passes the cut-water. Moving from suction to pressure side of the blade there is an increasingly strong flow rotation. At the pressure side of the blade the flow is turned inwards into the impeller. This flow reversal is repeated again 180 degrees around the volute. Although the pressure rise through the volute still exists this flow reversal is at odds with the flow pattern proposed by Frost (1991) and Newton (1998) where only one reversal near the cut-water interaction occurred.

The possibility of flow reversal even prior to the blade reaching the cut-water is suggested. These discrepancies may be explained by the double volute nature of the Abramian and Howard (1998) pump. The flow into the impeller was artificially swirled using an inducer so the effects of the re-circulated flow on the entrance flow are difficult to judge. Although the dimensions of the impeller and volute can be recreated from the paper the dimension of pre-swirl are not given.

Kaupert and Thomas (1999) presented two studies on the unsteady pressure field in a centrifugal pump impeller. The volute circumferential pressure variation was measured and mapped in agreement with Kikuyama (1987). This pressure variation, in the rotating frame of reference, is unsteady and dominated by vane pass frequency as established by Brownall et al (1985). The cutwater acted as a separator of two distinct flow regimes. This provides the pressure difference, which is responsible for the flow field fluctuation within the impeller. The unsteadiness of the flow increased as the flow was reduced with pressure fluctuations of 35% of total pump head. These pressure pulsations propagate at acoustic velocity.

Further work carried out within the same pump presented the difficulties of obtaining data and understanding the flow patterns as pump re-circulation commences. Binder and Knapp (1958), Brownall et al (1985), Iversen et al (1960), Kikuyama et al (1987) and Kaupert and Thomas (1999) all present data that illustrates the vane rate pressure fluctuation and the circumferential pressure distribution around the volute due to the rotor stator interaction.

2.1.4 Experimental Analysis using Air as the working Fluid

An alternative to using water as a product is to use air. Air is an easier product to use due to the lower working pressures involved. Leakage back to the pump inlets through wear ring landings though, can have a significant effect on the performance.

High flow machines, where leakage is small as a percentage of total flow, should be considered. The other consideration, in obtaining flow similarity, is to run the simulation with air at a greater speed. This replicates the Reynolds number defined as:

$$\mathrm{Re} = \frac{\rho \omega r_2^2}{\mu}$$

Yausa and Hinita(1979) used air as the pumped product and compared their results, on a dimensionless basis, to water. Identical agreement was obtained. Condenser microphones were also used to determine the unsteady pressure field.

Following on from this work Barrand et al (1984) and Caignaert et al (1985) both completed studies to determine the mechanisms of flow recirculation within an impeller. Their results, carried out on air and water were compared. The effect of increased leakage back to suction in the air model was responsible for measurement inaccuracies. A higher re-circulation flow rate was recorded for the air test pump.

Tourret et al (1985 and 1991) measured the unsteady pressure field with condenser microphones in an industrial pump using air. Considering three flow rates of 50%, B.E.P and 150% B.E.P, pressure increased within the impeller passage as it approached the cutwater and decreased immediately after. These measurements confirm the previous work by Binder and Knapp (1958).

Newton (1998) used air as the working fluid using LDA and condenser microphones to ascertain the unsteady flow pattern in a centrifugal fan of at closed valve. To minimised 3D effects the b2/D2 ratio was kept as small as possible. The inlet geometry was sealed to prevent inlet recirculation and a special sealing arrangement was adopted to minimise leakage losses.

2.1.5 Pump and System Interaction

The inability to accurately predict the closed valve head of a machine using computation methods has lead to a number of investigations which evaluate the impact of the pump system on the machines operation.

Work was published on the prediction for off design performance by Sun and Tsukamoto (2001). A method for predicting the off-design performance of a diffuser pump was presented, taking into account the rotor stator interaction effects. The paper covered the closed valve head condition. The methodology applied the pump system characteristic equation to the boundary conditions of the computational model. The effect of the system has previously been seen to have a significant effect on the pump flow regime. The system is responsible for the transient hysterisis observed by Kaupert and Staubli (2001).

The methodology realistically predicted the backflow onset at low flows, something that CFD has, anecdotally, struggled previously to achieve. The paper does not attempt to explain any of the flow features observed at closed valve. The linking of the characteristic equation to the closed valve condition is not necessary. If the mass flow through the system is zero, the effect of the characteristic equation on the flow regime is also zero. Longatte and Kueny (2001) also presented work which took into account the circuit interaction with the pump. This work quantified the pressure and flow fluctuations experienced by the stator. The intensity of the fluctuations was shown to be dependent on the pump system and the position of the pump within it. The distance of the boundary conditions from the pump was seen to effect the numerical simulations.

Although closed valve head calculations were not included in their work it may be significant to the closed valve problem. From the statistical work reviewed in Section 2.3 it is apparent that a mechanism may exist which is independent of the pump. The position of the discharge valve in relationship to the pump is difficult to quantify and differs from the test and site installation.

The level of closed valve head may be partly determined by the bound fluid, which is driven by the stalled impeller. The length of this re-circulating column has not been shown previously to influence the closed valve head value Fig.2.1.5.1.

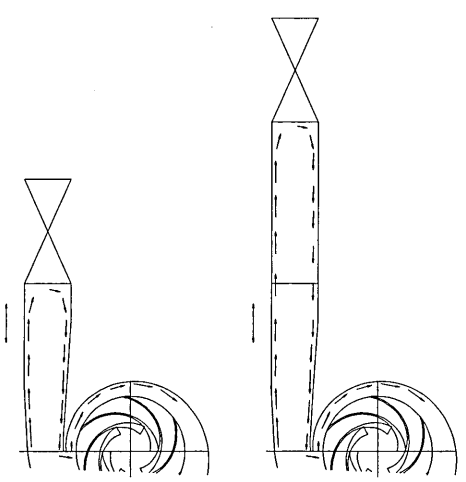

Fig.2.1.5.1 Illustration of the Proposed Effect of the Discharge Valve Position

If the position of the discharge valve has an effect on the closed valve head position, it is reasonable to assume that multistage pumps with high number of stages, will have a more consistent closed valve head coefficient. This is due to the liquid being bound and driven in the consistent environment of the inter-volute crossovers. The discharge valve position will only have an effect on the final impeller stage. The interaction of the bound liquid in a multistage pump crossover and the expelled liquid from that pump's subsequent stage impeller inlet is an area of pumping that has received little research attention. Only Worster's (1953) research has commented that the pressure with the volute passageways is steady and uniform.

2.2 Computational Methods

The investigation of centrifugal pumps using CFD (Computational Fluid Dynamics) is not as common as with other turbo-machines. The following papers are representative of the state of the art, regarding pump CFD study.

Graf (1993) compared results from three computational methods applied to a blade channel. Tascflow, Q-3D and a NASA simplified Q-3D codes were considered. The results were compared with flow visualisation data. At design flow the three codes were comparable. At "off design" conditions the only successful prediction was obtained from Tascflow.

Cooper and Graf (1994) used the commercially available CFD software CFX Tascflow, which is dedicated turbo machinery code, to assess the computational performance against experimental data. The researchers computed both suction and discharge re-circulation with good qualitative comparison of the flow field from 5% B.E.P to 21% B.E.P. The researchers showed that CFD had been integrated into the design process.

Work carried out by Yates et al (1995), Tourlidakis et al (1995) and Hamil et al (1995) has applied CFD to the solution of pump flow. Comments on accuracy are difficult as these were all published without corresponding experimental data, but all point towards the vast potential of CFD.

Chen and Liaw (1997) presented a CFD study incorporating an on-design analysis with particular attention paid to the interaction between rotor and stator. A full transient computation simulation was carried out with the flow field calculated for every 18 degrees of revolution. Mesh incompatibility from impeller to volute is handled by employing a small gap, which is ignored in the computation. The evaluation of an "on design" impeller solution only concluded that in a small time frame with a course grid accurate results of the flow field can be gained from the analysis.

The impeller-casing interaction is complicated at off design conditions, with solution times increasing considerably. The flow field observed agrees with the mental picture designer work with. At design flow there was no separation at the cut-water, the flow is squeezed between the impeller and casing. The flow rate in differing impeller passages is dependent upon its position within the casing. The paper again showed the non-linear diffuser effect of the volute as the pressure rose from cutwater to throat. This illustrates the importance of modelling the volute in unsteady analysis.

Miner et al (1988, 1989, 1992) analysed a 2D centrifugal pump using a finite element method based on potential flow. The goal was to refine the prediction method by considering both the impeller and volute. 9 grids were generated, each

with a fixed impeller orientation. Validation was carried out by comparing the results with LDA data.

Miner et al (1989) results show that at design flow the measured velocity and predicted velocity were within 17%. Miner concluded that below design flow the potential flow method was not suitable. The qualitative agreement was good but quantitative errors were attributed to poor grid refinement.

Dyson (1999) presented an overview of how CFD has become an everyday design tool, fully integrated into the design process. Palgrave & Dyson (2000) later demonstrated using CFD how flow physics effects the vibration potential of a pump. In both these cases only on-design analysis was considered.

The only notable study of closed valve head Newton (1998) used Fluent's sliding mesh to simulate the shut off conditions a 2D centrifugal fan. The results were compared with LDA and condenser microphone methods taken with air as the working fluid. The intention was to provide an insight into the flow mechanisms at closed valve and gaining an indication of the potential for using CFD to predict closed valve head. The experimental pump impeller had a closed inlet and the volute had a closed outlet. 3D effects were limited by making the pump d2/b2 ratio as large as possible.

The major conclusions drawn from this work by Newton (1998) are divided into flow and computational.

Flow physics

- The fluid within the rotor does not exhibit solid body rotation. This disagrees with the conventional mental model designers have traditionally used. It also disagrees with Frost's (1991) work.
- Rather than solid body rotation, large vortices occur within the blade passages driven by the turbulent shear stress around the rotor periphery. This agrees with the observations of Simpson and Cinnamond (1964).

- The proposed flow field by Frost (1991) was qualitatively correct.

- The mechanism of volute pressure rise proposed by Frost (1991) is incorrect. Radial variations in pressure around the volute are small. The volute acts as a diffuser with pressure rising from cutwater to discharge circumfrentialy.

The pump geometry for Newton's (1998) experimental analysis, particularly the volute layout bears no relation to conventional pump design. It is difficult to believe that such a distorted geometric layout could hold for Frost's (1991) prediction method, which is derived from actual pump geometry.

In this layout the casing throat is tall and narrow. The diffusion around the volute is too great to represent contemporary pump design Fig.2.2.1. It is possible that differing radial velocity streams across the throat, which are the basis of Frost's (1991) model, will have been mixed out by time/distance to such an extent that they are undetectable.

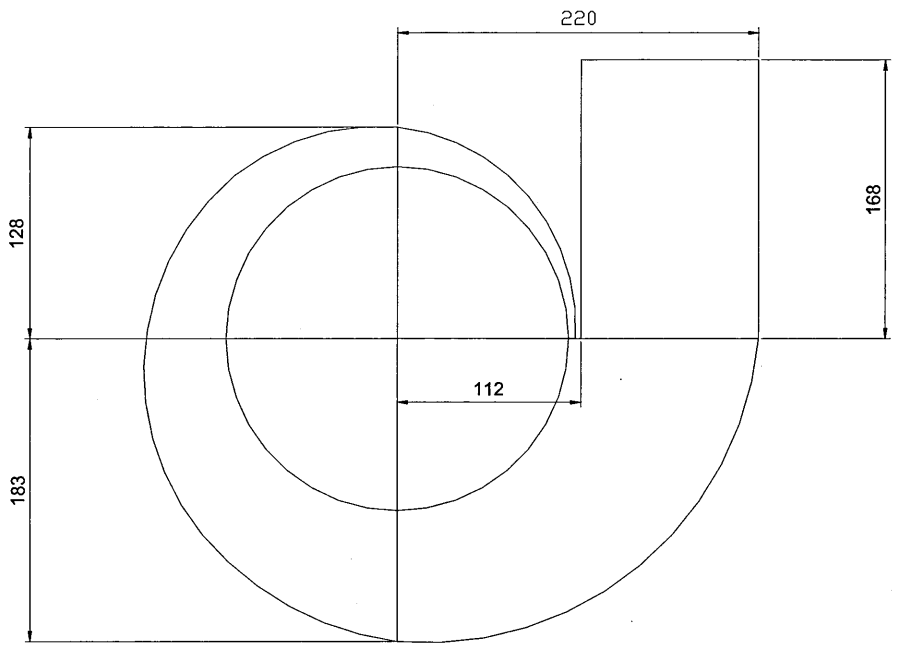

Fig.2.2.1 Newton's (1998) Volute Layout

One major difference between the Newton (1998) research and the "real-world" situation is the treatment of the pump suction. Newton's (1998) research relies on a closed impeller inlet. This does not allow the inlet-backflow proportion of the closed valve flow regime to develop as observed by Fraser (1991) and others. Whilst instructive, from a realistic standpoint Newton's (1998) work is incomplete

Computational

Newton (1998) found the commercial software package Fluent 4.4 acceptable for this analysis. The qualitative agreement of the flow pattern was good.

- The major error in the computational analysis was the over prediction of the shut-off head associated with the volute pressure rise. This was directly linked to the validity of the rotor/stator interaction prediction within the research.
- The sliding mesh did not appear to introduce significant errors into the solution.
- A Higher order spacial discretisation scheme did not affect the solution.

- Momentum balance and convergence were major obstacles. Torque errors between rotor and stator were as much as 20% out and could not be reduced.
- The standard k-epsilon turbulence model did not have a significant impact on the solution. k-epsilon standard giving better results than the more advanced RNG k-epsilon model. Viscosity prediction appears to be the problem. This was not true under steady state analysis where the RNG k-epsilon model performed better.
- It is important to include the rotor/stator interaction effects in any attempted off-design solution where unsteady interactions are expected.

Newton (1998) disagreed with the supposition that the impeller exhibits solid body rotation. This is the basis of the work by Frost (1991).

2.3 Analysis of Closed Valve Head Prediction Methods

There are several methods available which can be used to predict the levels of closed valve head. All incorporate the rotational speed and the impeller diameter as major contributing factors. The influence of other geometry is seldom accounted for. These methods are evaluated for accuracy by using a database of 200 pumps of different configurations.

Many of the prediction methods were devised using a statistical approach based on a limited number and configuration of pump. By using such a larger sample of pumps, the suitability and accuracy of each method can be evaluated. A modifying design coefficient is suggested for each method with a corresponding evaluation of the improvement in accuracy.

2.3.1 Stepanoff (1957)

Simplifying the Euler equation for a condition where flow through the pump is zero gives a maximum theoretical value for closed valve head of:

$$Headcv = \left(\frac{U_2^2}{g} \right)$$

From this basis many statistical investigations have attempted to correct this theoretical maximum by application of a universal correction. Stepanoff (1957) proposed the use of a design coefficient to modify the Euler head equation.

$$Headcv = \Psi \left(\frac{U_2^2}{g} \right)$$

The coefficient for ψ is defined by Stepanoff (1957) as 0.585. This factor was derived from a review of a number of centrifugal pumps. An analysis of ψ, based around the closed valve head design coefficients derived from the database, shows this correction factor to be statistically true, as the arithmetic mean of the analysed geometry. As a method of predicting closed valve head its use is limited. The spread of error is over 20%.

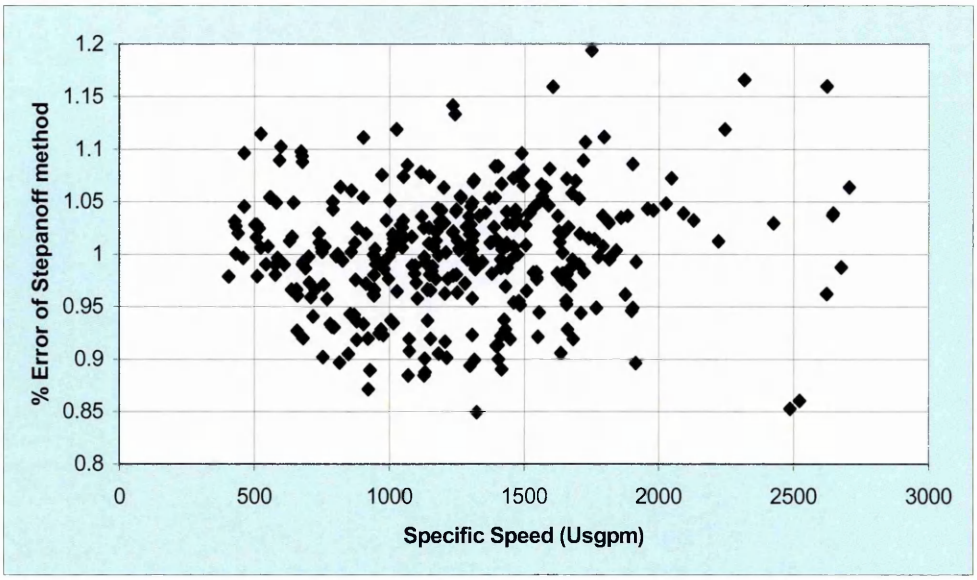

Fig.2.3.1.1 Error of Stepanoff (1957) Prediction Method Based on the Pumps in the Database vs. Specific Speed

The method only links the peripheral velocity to the closed valve head value and as such the impeller outside diameter is the only geometric feature considered by the prediction method. Fig.2.3.1.1 illustrates the Stepanoff (1957) Euler Closed Valve head modifier assessed for varying geometry of David Brown Pumps.

2.3.2 Peck (1968)

A similar modifier to the Euler equation is proposed by Peck (1968), who also presented work based on the statistical analysis of pump geometry giving the formula.

$$Headcv = \frac{\Psi}{2}\left(\frac{U_2^2}{g}\right)$$

He proposed that the pump configuration affected the empirical constant. This lead to a constant $\frac{\Psi}{2}$ for volute pumps of 0.5 to 0.55. Although this value is different to Stepenoff's proposed constant, which was verified by the database geometry, it is within the error band.

The consideration of pump configuration, combined with impeller diameter, as geometric considerations, does not add to the accuracy of the predicted closed valve head in Peck's method. If we apply the reasoning that pump configuration

has an effect on closed valve head coefficient to the pump database, it is clear that different types of pumps have differing closed valve head coefficients.

Fig.2.3.2.1 contains a frequency analysis of closed valve head coefficients for different pump configurations. The frequency analysis can be used to refine the head coefficients for pump configuration, but the spread of the results is still too wide to be of use in design.

Hocv Single Entry - 0.575
Hocv Multistage - 0.6
Hocv Double Entry - 0.625

From the frequency data, the multistage pump has the lowest spread of results.

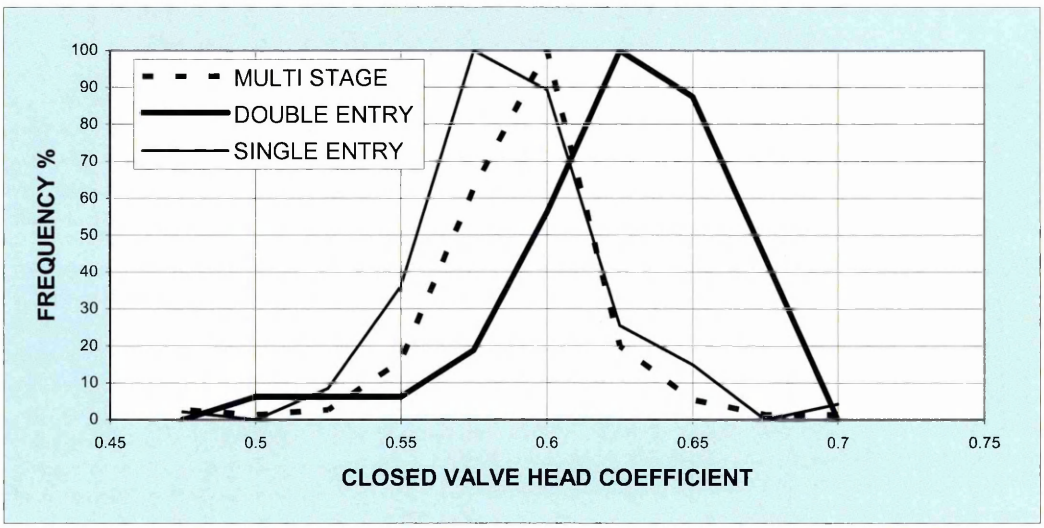

Fig.2.3.2.1 Frequency Analysis of Closed Valve Head Coefficients For Differing Pump Configurations

2.3.3 Patel (1981)

Patel (1981) proposed the theory that the specific speed of the pump has an effect on the value of closed valve head. Typically a low specific speed pump may exhibit a flat or drooping performance curve, whilst a high specific speed pump will have a high head rise to shut off. From statistical data Patel proposed a modifier to the Euler head based on this observation.

$$\Psi cv = 0.65 - 0.004Ns(metric)$$

From the database geometry a dependency on specific speed can be identified. This is as expected due to the characteristic nature of the performance curves for the types of machine. The geometric differences between low specific and high specific speeds are striking so the link between geometric configuration and closed valve head value should show a strong trend. A further factor is the difficulty in maintaining the prescribed design geometry for low specific speed machines. The impeller outlet widths, which have an effect on pump stability, are sensitive to the inherent errors found in sand casting technology.

Using the database to separate out pump configurations a difference is apparent for pump type. The data suggests the prediction method can be further modified to take into account the specific speed slope and also the pump configuration, based on the pumps within the database. Fig.2.3.3.1 illustrates the percentage error of Patel (1981) prediction method based on specific speed. Patel's formula increases in accuracy if the following modifications are used.

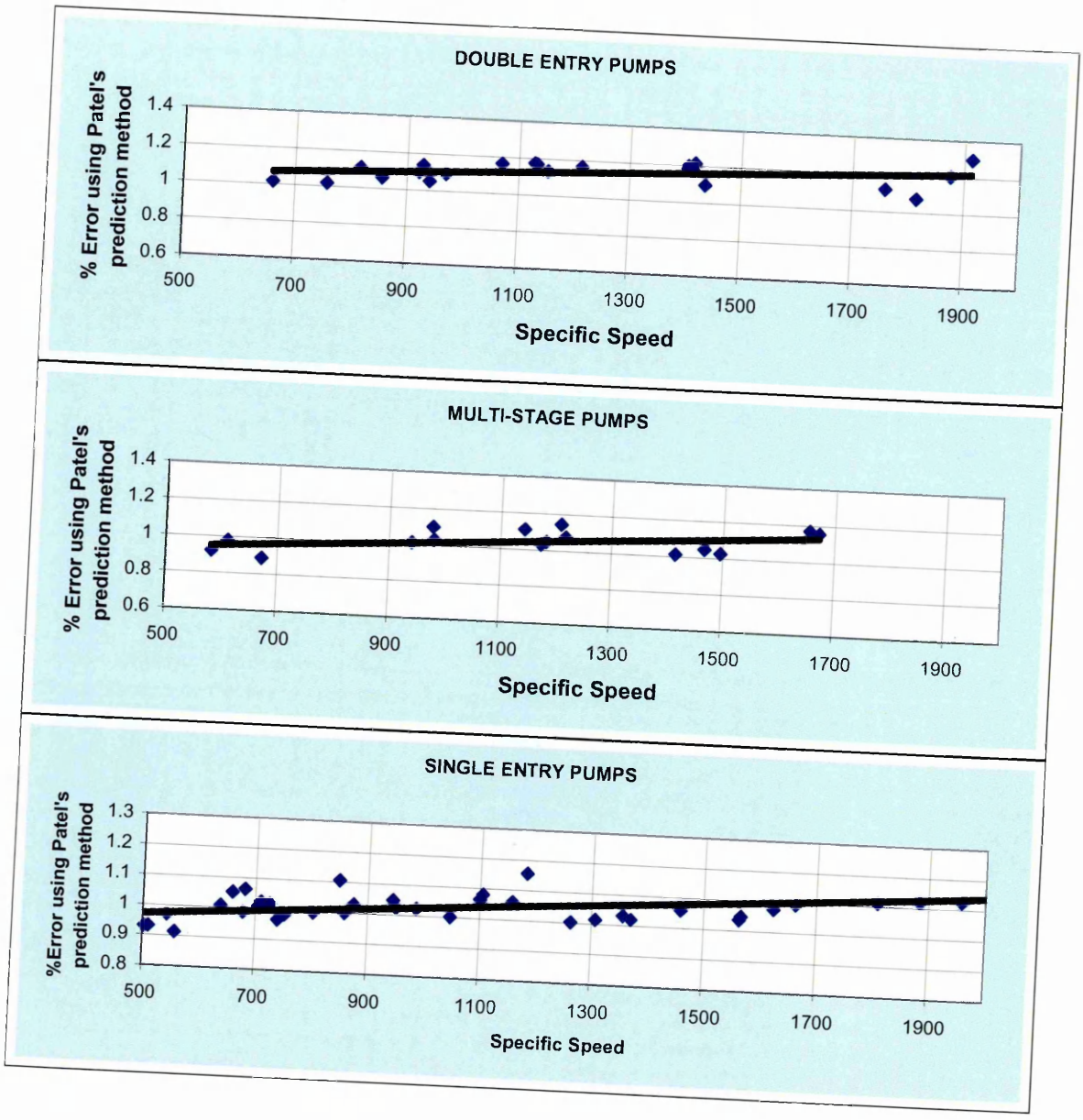

Fig.2.3.3.1 Percentage Error of Patel (1981) Prediction Method Based On Specific Speed

Single Suction

$$Headcv = \frac{Patelcvhead}{0.9165 + 0.0001NS(us)}$$

Double Suction

$$Headcv = \frac{Patelcvhead}{0.9923 + 0.0001NS(us)}$$

Multi-stage

$$Headcv = \frac{Patelcvhead}{0.8559 + 0.0002NS(us)}$$

From a frequency analysis of the error spread the accuracy of the prediction method has been increased Fig.2.3.3.2.

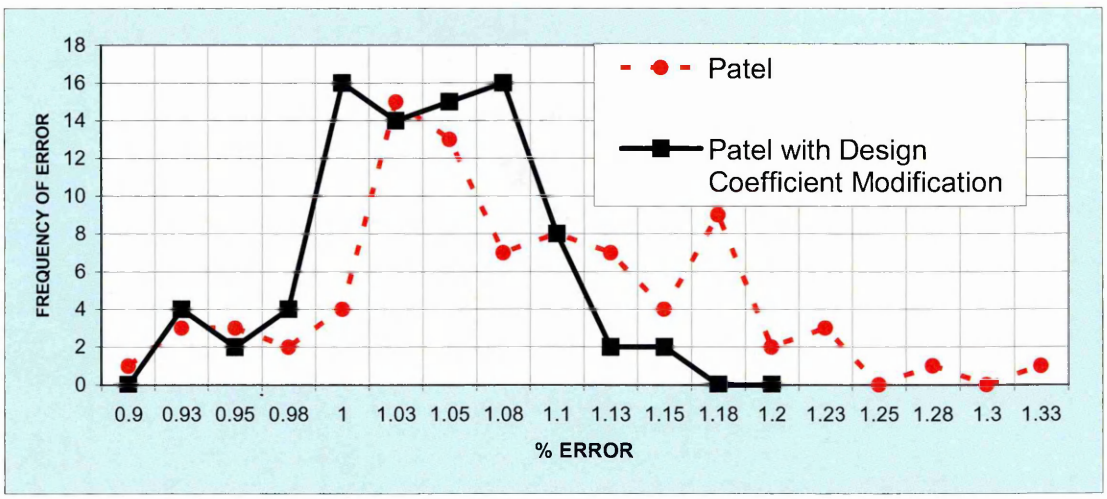

Fig.2.3.3.2 Frequency Analysis of Accuracy Increase Due To Design Coefficients

2.3.4 Thorne (1988)

Thorne (1988) used a more complex modifier for the Euler equation based on empirical constants for the impeller and casing.

$$Headcv = \left(\frac{U_2^2}{g}\right)\left[\left(\frac{1}{slip}\right) - \left(\frac{C_{1m}}{2U1}\right)\left(A^2 + \frac{B^2}{slip^2}\right)\right]$$

$$Slip = 1 + \left(\frac{a}{z}\right)\left(\frac{1 + Beta2}{60}\right)\left(\frac{2}{1 - \left(\frac{D_1}{D_2}\right)^2}\right)$$

The casing coefficient in the slip formula a=0.77

The prediction method attempts to incorporate the impeller outlet diameter to satisfy the known link to the Euler equation with impeller inlet parameters of eye size, which influence inlet re-circulation and as such may have a negative effect on the closed valve head. The vane geometry is also considered by taking some account of the slip value of the relative velocity, Weisner (1967). Casing considerations are accounted for by including an empirically derived coefficient. The configuration of the pumps is not considered. It is difficult to imagine a mechanism, following on from the experimental review, where slip factor is the actual mechanism which influences the closed valve head. More likely is the geometric change that occurs when changing vane number or discharge angle.

As shown in Fig.2.3.4.1, this prediction method consistently over predicts the value of closed valve head, with the errors over 20%. When pump type is taken into consideration the amount of error is influenced by the pump configuration. The following denominators for the Thorne (1988) prediction method increase the accuracy of the methods over a range of specific speeds

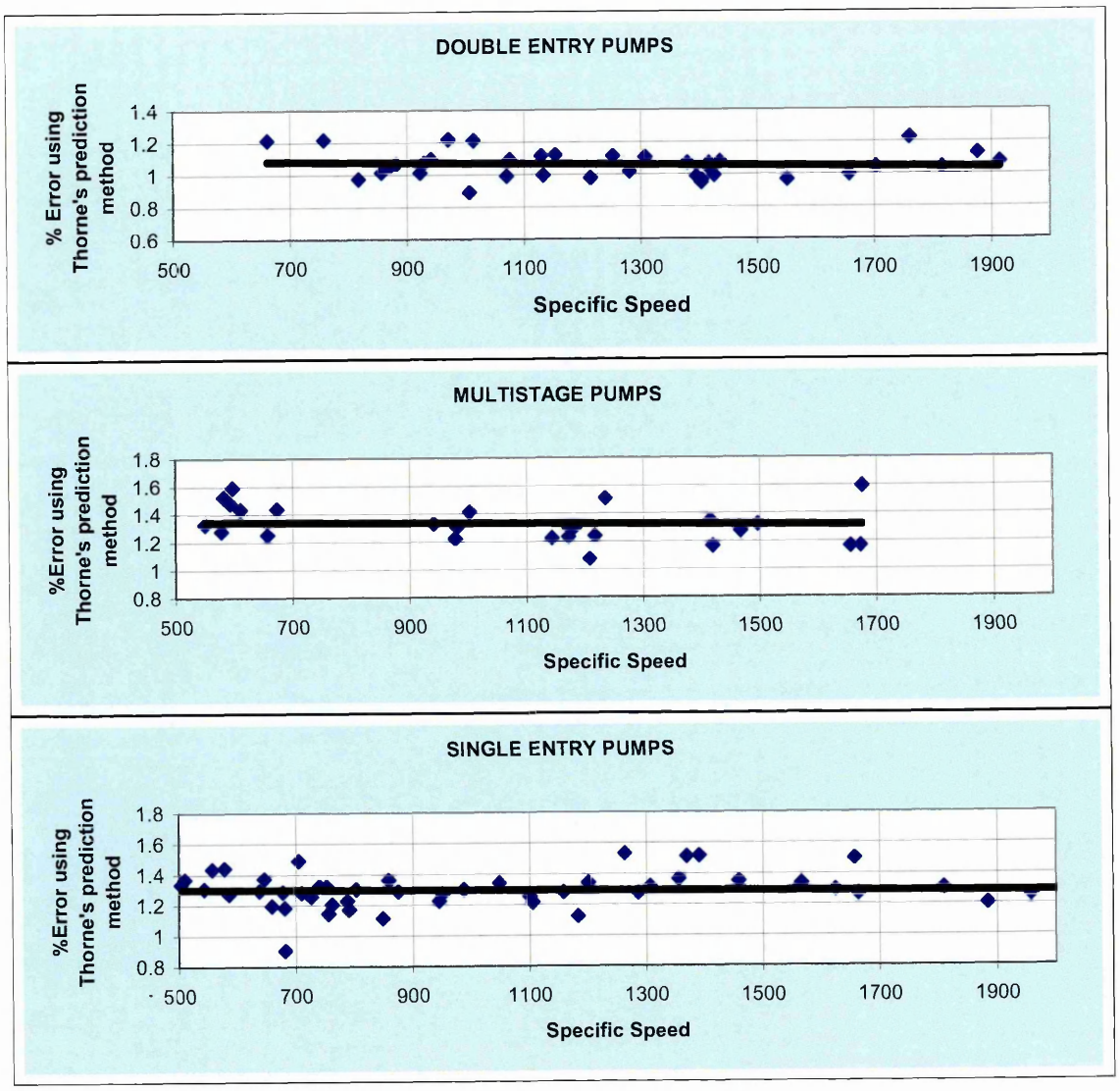

Fig.2.3.4.1 Configuration Of Pumps Analysed Using Thorne(1988) Prediction Method

Single Entry Pumps 1.31
Multistage Pumps :- 1.36
Double Entry Pumps:- 1.1

There is an accuracy increase due to the modifiers proposed. This is illustrated by the frequency analysis in Fig.2.3.4.2.

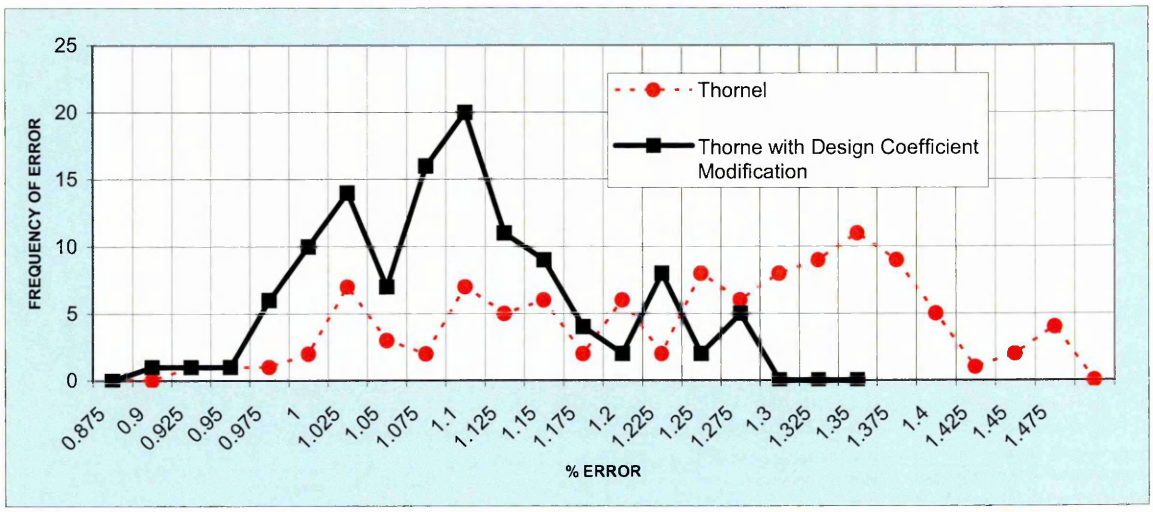

Fig.2.3.4.2 Frequency Analysis of Accuracy Increase Due To Design Coefficients

2.3.5 Stirling (1982)

Stirling (1982) used a method based on the contribution of the impeller added to a volute contribution. The impeller contribution was taken from Levin and Poliokovsky (1965) who investigated re-circulating flow in a free impeller at shut-off. Stirling (1982) proposed that the closed valve head of a centrifugal pump was composed of three components.

2.3.5.1 Impeller Contribution

The impeller acts as if it were a solid body with no fluid interchange between rotor and collector. Whist this ignores the rotor/stator interaction effects if serves as an analogy for the strong viscous forces driving the collector flow.

$$Hsoimp = \frac{1}{2g}\left(U_2^2 - \frac{U_1^2}{2}\right)$$

2.3.5.2 Volute Contribution

The collector throat area is considered significant by the inclusion of Anderson's (1947) area ratio.

$$Hsovolute = \frac{U_2^2}{2g}\left(ho - \left(\frac{\phi R}{(\tan(beta2 - \delta A))} \right) \phi R.AR \right)$$

AR = Anderson area ratio
Ho = Weisner's slip factor

$$\delta A = 1.17x10^{-3}\left(\frac{P_2 Beta_2}{Cm} \right)$$

2.3.5.3 Inlet Back-flow

As the flow through a pump is reduced the liquid exits from the impeller eye and flows into the inlet channel. To escape the impeller liquid has to exceed the impeller inlet tip speed. This high energy liquid has a negative contribution on the closed valve head of the pump.
The re-circulating flow factor is derived empirically by analysis of a number of pumps

$$\phi R = -0.2331\left(\frac{r_1}{r_2} \right) + 0.1952$$

The negative contribution of the inlet back-flow cannot be valid for more than one configuration of pump. The inlet channel for an end suction pump will inevitable have a differing contribution to closed valve head from a multi-stage or top entry pump. This is further supported by Kovats (1979) whose work exposed the higher head coefficients of pumps with splitters which extend into the impeller eye.

This is the first prediction method to characterise the contribution of the three distinct geometric features of suction diameter, impeller diameter and volute into a prediction method. Fig.2.3.5.3.1 demonstrates the Percentage Error vs. Specific Speed for the Stirling (1982) prediction method.

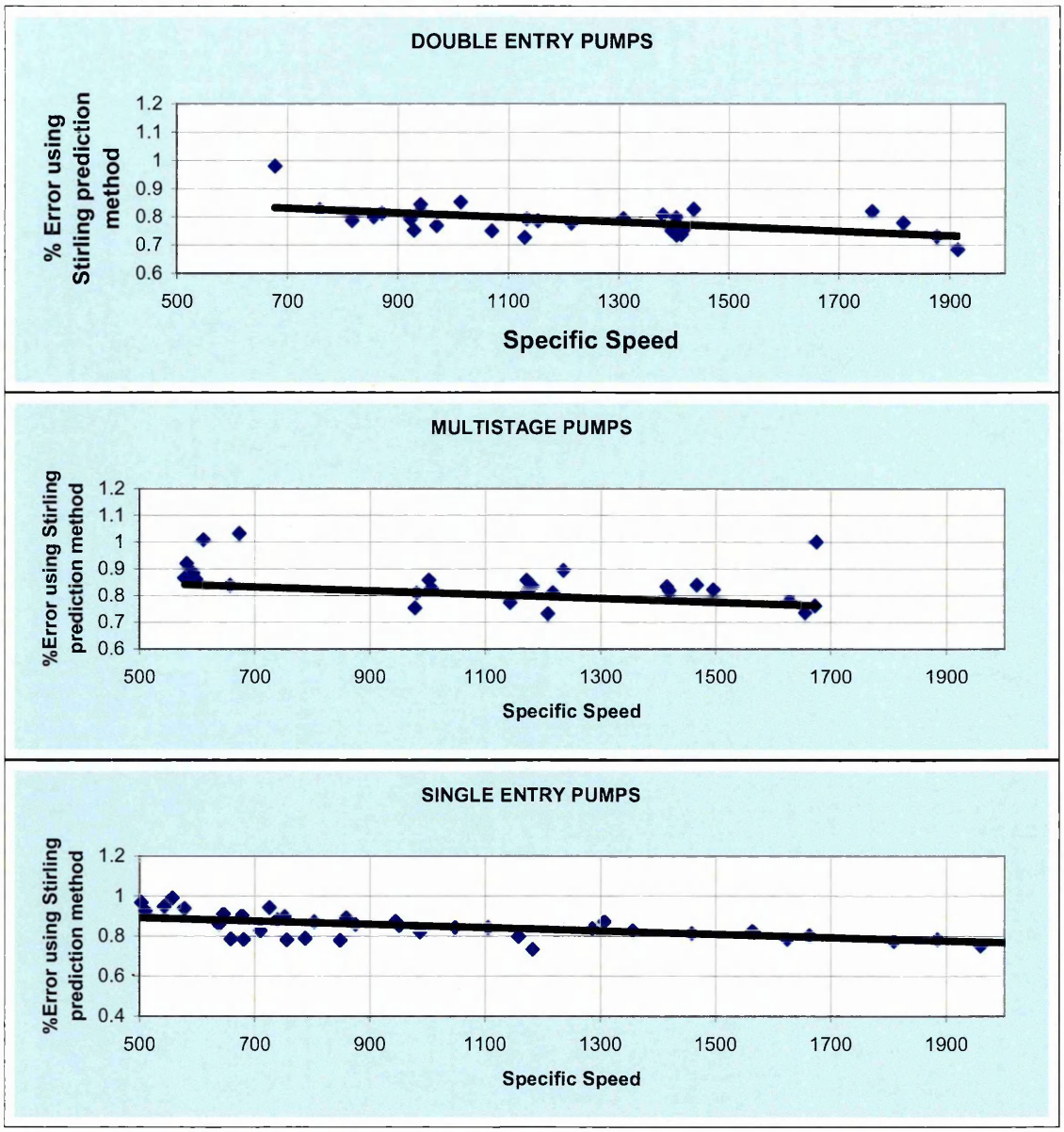

Fig.2.3.5.3.1 Percentage Error Vs. Specific Speed For Stirling (1982) Prediction Method

This method, whilst linking some of the geometry to the closed valve head value, still relies on empirically derived constants. The pump configuration does not have a marked statistical effect on the predicted head, but the method consistently under predicts the closed valve head level.

A modifying factor can be applied to the Stirling (1982) equation to increase its accuracy

$$Headcv = \frac{Stirlingcvhead}{0.938 - 0.0001NS(us)}$$

Fig 2.3.5.3.2 contains a frequency analysis of accuracy increase due to Dyson design coefficients. The error spread is improved by the design coefficient and the accuracy is increased.

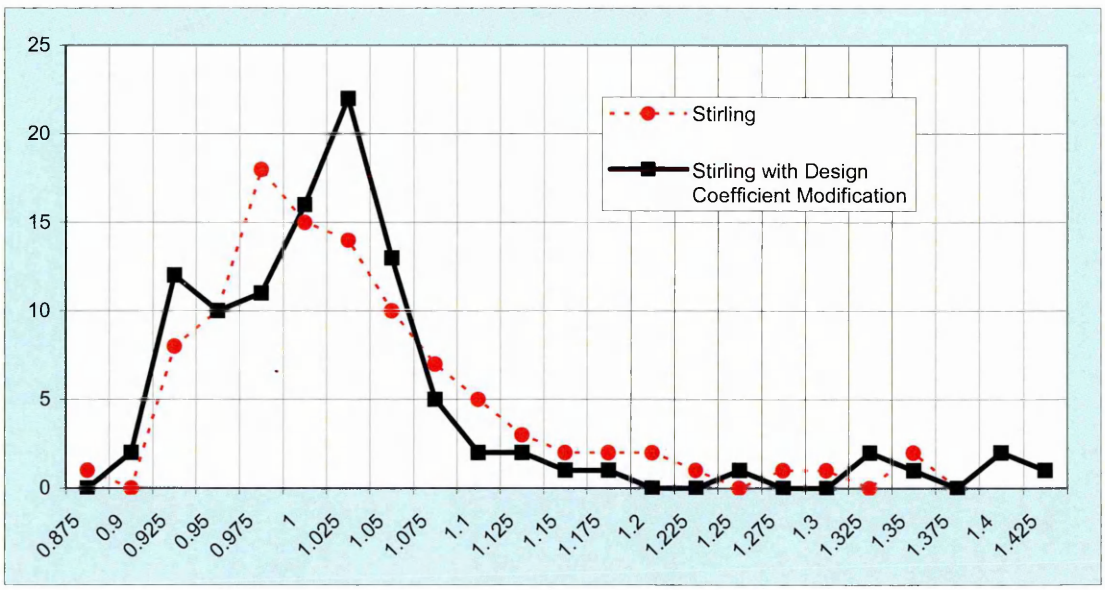

Fig 2.3.5.3.2 Frequency Analysis Of Accuracy Increase Due To Design Coefficients

2.3.6 Frost and Neilsen (1988)

Frost and Neilsen (1988) produced significant work in the area of shut-off head predication when they proposed a model for the volute pressure rise added to the head developed by the impeller. Although Stirling (1982), using empirical coefficients, had previously proposed this, the Frost and Neilsen (1988) method

was the first purely analytical method. To calculate the contribution of the impeller Frost (1988) assumed the flow in the rotor exhibited solid body rotation although this still ignores the rotor stator interaction effects. This implied a shut off head contribution from the impeller OD.

$$Himpso = \frac{U_2^2}{2g}\left(1-\left(\frac{r_1}{r_2}\right)^2\right)$$

Considering the velocity distribution across the casing throat area and obtaining the associated pressure from this velocity profile we can derive the volute contribution.

$$Hsovolute = \left(\frac{\varphi r_2}{(r_m - r_2)^2}\right)\left[r_m \ln\left(\frac{r_4}{r_2}\right) - 2r_m(r_4 - r_2) + \left(\frac{r_4^2 - r_2^2}{2}\right)\right]\frac{1}{g}$$

Where r_4 is the height from impeller centerline to the throat and r_2 is the radius at the middle of the throat (centroid).

Fig 2.3.6.1 contains a chart of Error vs. Specific Speed for Frost (1998) prediction method. Although this method does not assess the negative contribution from the inlet back-flow, it is more accurate than previous methods.

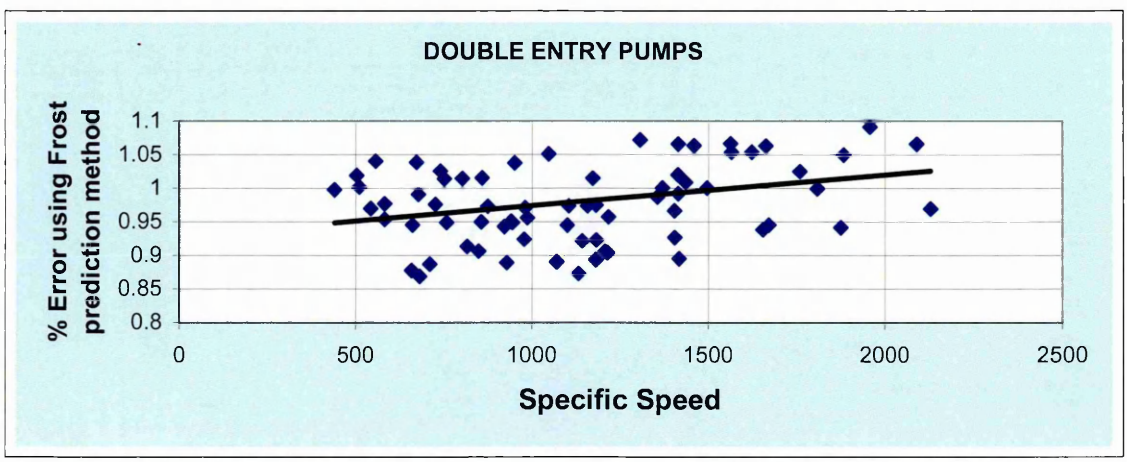

Fig 2.3.6.1 Error Vs. Specific Speed For Frost (1998) Prediction Method

No error trend is shown to be dependent on the pump configuration, but a modifying factor can be applied to the Frost (1998) equation to increase its accuracy.

$$Headcv = \frac{Frostcvhead}{0.9282 - 0.00005NS(us)}$$

A frequency analysis of accuracy increase due to the new design coefficient is demonstrated in Fig.2.3.6.2. The accuracy of the method is increased and the error spread is reduced.

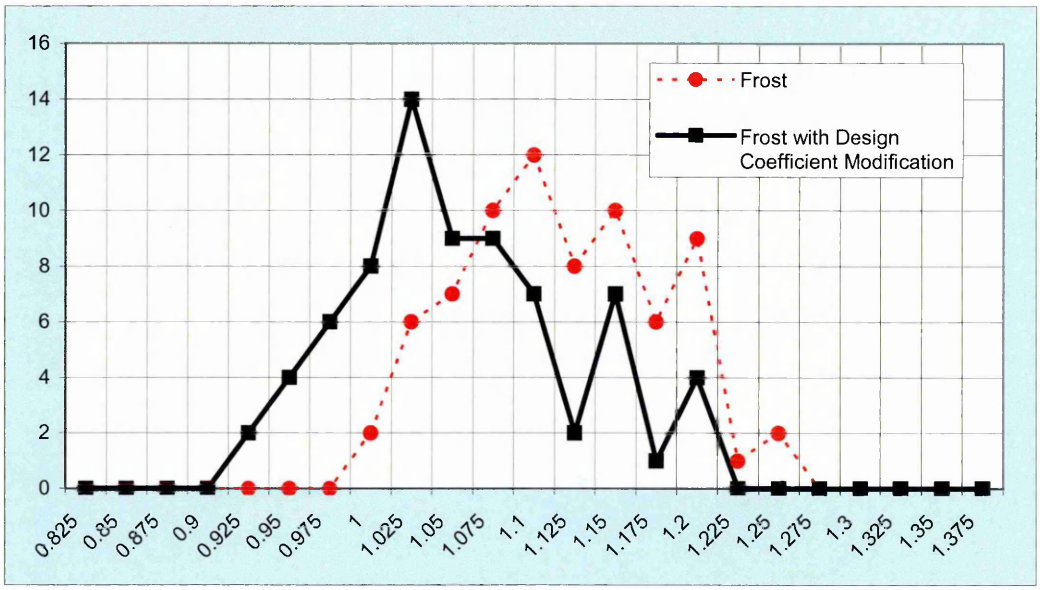

Fig.2.3.6.2 Frequency Analysis of Accuracy Increase Due To Design Coefficients

2.4 Summary of Literature Review

The problems associated with the prediction of closed valve head are complex. The existing prediction methods only offer an empirically derived solution to the prediction on the pump closed valve head. Refinement techniques based on statistical analysis improve the accuracy but not to a satisfactory extent.

From the experimental and computational research that has been reviewed it is possible to draw the following conclusion.
These conclusions can be divided between the three distinct geometric regions within the pump:

- The contribution of the impeller.

It is a common view held among pump designers that the pressure contribution to closed valve head from the impeller is analogous to a rotating solid body. There is some debate over whether the internal radii of the solid body is based on the impeller eye diameter, hub diameter or is zero. This view, based on the work by Frost, is based on conversations with pump designers from Guninard Pumps (Gilbert Gauze), Weir Pumps (Ron Palgrave), Union Pump USA (George Cheng) Flowserve Pumps (Paul Cooper). The designers from this community are representative of all the major API pump manufacturers. It is important to state that solid body should only be considered an analogy at this stage of the research. Pump designers have adopted this theory as a representation of the actual flow mechanism based on the work by Frost. The current research is unclear as to whether the is the case or the mechanism accurately represents the flow.

Recent work by Newton (1998) has suggested that the assumption is not true. This has added little to help the designer in assessing the contribution of the impeller as not alternative was suggested. It is difficult to ascertain from Newton's work if the experimental fan had a stable characteristic. If not the flow phenomenon witness by Yeddiah (1993) may be responsible for inaccurate volute contribution prediction.

As previously discussed, the contrived geometry may be responsible for Frost's (1988) pressure rise volute prediction not holding true but it is more likely problems with the codes inability to predict weak interaction effects or the solution methodology that cased the errors. The existence of an inlet relative eddy and the geometric features responsible for this phenomenon are unknown. This aspect of the research was compromised by the experiment inlet conditions.

- The contribution of the volute

The pressure rise due to the diffusive nature of the volute has been assessed, by Frost (1991), assuming zero net-mass flow at a particular point within the volute

and establishing its associated pressure. There is some debate over the position of zero net mass flow within the volute.

Newton found the CFD code over predicted the pressure rise within the volute. Experimental work has determined a non-linear pressure distribution around the volute at closed valve and the presence of separation regions on unstable pumps.

- The contribution of inlet back-flow

The liquid re-circulating out through the pump inlets has a rotational effect on the incoming fluid, notionally causing a loss of closed valve head. No experimental data is available to quantify the effects of this re-circulating fluid.

Designers have also noticed how differing geometric features can have an effect on closed valve head.
A volute with a high width to height ratio or have differing shapes will have a lower closed valve head than expected as liquid is trapped either side of the impeller. This partly supports the theory proposed by Frost (1991) in which volute throat shape is a factor in closed valve head value.

Diffuser pumps which are somewhat different from volute pumps in the respect that the diffusion is carried out through a stationary multiple blade row which contains upwards of 5 diffusing passageways. A volute pump never contains more that two passages. The diffuser type of machine anecdotally has a higher closed valve head characteristic than a volute machine. This discrepancy is not explained in the literature.

The number of vanes and the vane outlet angle causes changes in flow slip and thus changes in closed valve head, supporting Newton (1998) supposition that the impeller's contribution is not analogous to solid body rotation.

Attempts at CFD analysis at closed valve have been partly successful. Convergence is a major issue and the validity of the results whilst qualitatively representative are quantitatively poor. Experimental data gained from commercially representative machines is insufficient. The only comprehensive study carried out was on a closed inlet fan pump, which was unrepresentative of commercial geometry.

Modelling of the system elements has increased the CFD accuracy for closed valve head prediction.

From the experimental data reviewed it is possible to gain some agreement on the flow physics:

- The nature of the flow field is unsteady.

- The rotor/stator interaction has a direct effect on the flow field. Passage velocity profiles are dependent on their position with respect to the collector cut waters.
- There is a flow pulsation within the discharge pipe.
- Non-linear circumferential pressure gradient exists around the volute with a low-pressure region existing at the casing lip.
- The impeller drives a relative eddy, in the majority of the literature, at the outlet counter to the machine rotation.
- Inlet re-circulation occurs extending into the collector inlet pipe.
- The system has an influence on the off-design performance of the pump.

2.0 Literature Review and Prediction Methodologies - Overview

The literature review explores experimental work carried out to investigate flow physics within centrifugal pumps. It encompasses both on-design and off-design work.

On-design is conventionally considered to be the flow at which the pump efficiency is the greatest. The flow is considered to be independent of phase position between the impeller blade and the collector system. Although studies, Miner(1988), indicate that an unsteady temporal flow field exists, this is small and is ignored by pump designers to simplify the design problem. Off-design is considered to be at a flow significantly below the best efficiency point. This flow regime is considered to be highly time dependent, changing rapidly as the impeller blade position, with respect to the collector position, changes.

Much research in the area of on-design analysis has been carried out reflecting the designer's natural focus on pump efficiency. Less work is available on the unsteady flow behavior. The complex natures of the flow physics, the strong rotor stator interaction effects and the difficulty of the time dependent experimental investigation have proved obstacles.

The second section of the review is concerned with the computational solution of the flow physics within centrifugal pumps. On-design analysis has been successfully computed. Less work is available at off design conditions. The off-design work that is available is based on limited geometries which are often unrepresentative of commercial pump design.

Methods used to predict the closed valve head of a centrifugal pump are explored in the final section of the chapter. These methods are gauged against performance from a database of 200 pumps of varying configurations. Empirical modifications to the prediction methods are suggested to increase their accuracy.

2.1 Experimental Measurements and Investigation

The successful design of centrifugal pumps relies on the designer's mental picture of the flow behavior matching the actual behavior of the pump. To aid in the design process, experimental work has been carried out to determine the behavior of centrifugal pumps. The simplest case, impeller at design flow running without a collector (i.e. volute, diffuser or concentric enclosure), has received by far the most attention.

Recently attempts have been made to analyse the unsteady rotor stator interactions and complex re-circulating flows at the pump inlets for off-design conditions. Data is seldom taken at shut-off conditions. This may be due to the difficulties experienced in running a pump in this condition. Rapid heating of the product is experienced, the casing and seals are at maximum pressure and the flow is pulsing. The following sections of the literature review have been split between design point, low flow and closed valve flow analysis.

2.1.1 Best Efficiency Point Studies

A selection of papers were reviewed which typify the experimental work which has been carried out. Although not extensive the methodologies and geometries investigated are typical of this field.

Kumar and Rao (1977) developed a two-dimensional method of analysis for through flow in a centrifugal pump impeller with good agreement with experimental results for commercial pumps at B.E.P. Their predictions closely mirrored the Buseman (1928) predicted impeller head-line. One of the first papers to using the PLA (phase locked averaging) method was presented by Gostelow (1977). Using this technique it is possible to ascertain the unsteady pressure for different radii within the impeller flow channels. Although the impeller flow is not indicated in the paper, the steady nature of the flow patterns suggests that it is on or around B.E.P.

Alder and Levy (1979) successfully measured the B.E.P flow within a shrouded impeller in a large volute designed for ease of access. This volute design may have contributed to the poor inlet performance and distorted inlet flow. This is a characteristic of machines with large inlet areas. Recognising this fact, it is standard practice within the pump industry to incorporate flow straightening vanes and anti swirl vanes in the casing suction branches. These prevent pre-rotation of the flow into the impeller eye. This effectively eliminates the negative inlet proportion of the Euler head calculation, maximising head for a given impeller diameter and simplifying inlet design criteria.

Rose (1987) was one of the initial users of a new back scatter Laser Doppler Anemometry system. This requires optical access from one side only. Using a

high power laser he obtained a clean signal from the scattered light. He presented a study of a centrifugal multistage pump impeller operating in water at B.E.P.

From this experimental data the pump industry has refined the mental model used to build its prediction methodologies. Although the flow field is time dependent and unsteady the flow field fluctuations are so low that the industry successfully uses steady design methodologies rather than consider the low level pressure fluctuations.

2.1.2 Low Flow Studies

Whilst the investigation of the design point flow field was initially of most interest to pump researchers this quickly changed as the design methodologies evolved. The attention turned to the investigation of machine operating at extreme part load.

Peck (1950) carried out investigations on a single entry end suction pump, collecting experimental data through a visualisation window using a stroboscope. At very low flows he observed that a large re-circulation region "powerful forced vortex" was present. This extended far into the suction pipe. Pressure tappings in the casing indicated a circumferential pressure rise from cutwater to casing throat. Visualisation also confirmed a surging flow phenomenon at the cut-water.

Young (1956) used photographic tracking techniques involving tracers of unit specific gravity introduced into the pump. Observations at 50% of design flow indicated a complex flow pattern. Higher velocities on the leading blade face than on the trailing blade face were noted. Other observations indicated that the flow differs from passage to passage. This phenomenon, reported by Young, is identical to that previously observed by Fischer and Thoma (1952). It is explained as the stalling of alternate vane passages. No attempt in either paper is made to relate phase angle to the passage stall. This prevents any conclusions being drawn regarding the rotor/stator interaction effects.

At low flow rates a non-uniform pressure distribution within the volute was presented by Binder and Knapp (1958). As the area within the volute increased, from cut water to casing throat, the pressure was observed to increase. The minimum pressure encountered was local to the cutwater.

Simpson and Cinnamond (1964) carried out flow studies through centrifugal pump impellers with varying outlet angle. At lower flows vortices on the trailing face of the blade were observed. Conversely these occurred on the blade leading surface at high flows.

McDonald, Lennemann and Howard (1971) took experimental measurements using hot fill probes preceded by flow visualisation. They compared various changes of flow with potential invisid flow theory. They concluded that at low flow

their inviscid model could not account the region of low velocity near mid blade height on the suction side of the blade.

Brownall et al (1985), using streak photographic techniques, verified the existence of significant inflow to the impeller at the low-pressure region near to the tongue. Previous research by Alder and Levy (1979) had also noted this flow feature. Differing flow patterns were observed dependent on the phase position of the impeller blade with respect to the cut-water lip.

At the lowest flow (30% B.E.P) the tongue stagnation point moved into the volute indicating a large flow into the volute past the tongue. The separation zone, caused by the tongue, oscillated at vane pass rate demonstrating the impeller case interaction. This is consistent with Yedidah's (1985) earlier observations but not with Worster (1953).

Further to the work of Binder and Knapp(1958), Iversen(1960), Kikuyama et at (1987) determined the existence of the non-uniform circumferential pressure gradient around the volute. Using PLA they obtained periodic data on the hub side volute wall. At best efficiency point (B.E.P) a steady flow pattern was observed with respect to blade position. At "off design" flows the pattern became unsteady with large pressure oscillation at vane pass rate dependent on the blade relative position to the cut water. This gave an indication of the circumferential pressure distribution caused by the rotor stator interaction.

Goulas and Trouscott (1988) carried out experimental analysis of an end suction pump using LDA to explore the flow pattern at the impeller exit. At 27% of design flow the velocity vectors local to the cut-water were directed through the cut-water clearance, between the impeller and case. This indicated a low static pressure region. This agrees with earlier observations made by Binder and Knapp (1958), Brownall et al (1985), Kikuyama et al (1987). Goulas and Trouscott (1988) also found a reverse flow region past the tongue on the impeller side similar to the one suggested by Yedidiah (1993) for unstable pumps.

Roco (1990) correlated LDA data with shaft position to calculate the velocity field within a slurry pump at two flow rates. Data was plotted with respect to angular position. This is particularly important when studying the effects of rotor stator interactions.

Dong et al (1992a & 1992b) applied Particle Displacement Velocimetry (PDV) to obtain the pressure fluctuation within a pump. This study indicated that at low flows large flow structures exist determined by the blade orientation to the cut-water.

Hureau et al (1993) and also Stoffel and Weis (1994) used Phase Locked Average LDA to obtain tangential and radial velocity within an impeller. Their studies at low flows indicate that for flow to reverse and escape from the impeller

eye the re-circulating flow has to exceed the inlet tip speed of the impeller. Palgrave (1985) presented data to indicate that inlet vane angle was also significant in ascertaining the percentage of B.E.P flow at which this suction re-circulation occurred.

2.1.3 Closed Valve Studies

Following on from the low flow studies, investigators made the natural leap to the study of the closed valve head flow regime.

Ficher and Thoma (1952) carried out flow investigations in a centrifugal pump at closed valve. They used a rotating prism technique to freeze the flow. Their observations found a pulsating flow that was cyclical and sub-synchronous. Each impeller passage experienced a different flow regime dependent on its position in the cycle. Significant cross channel flow was witnessed at both pump inlet and outlet. Their observations concluded that a large proportion of the impeller was filled with "dead water".

Acosta (1954) and Acosta and Bowerman (1957) conducted experiments on a series of impellers. This experiment used a submerged impeller discharging into a test tank. At shut-off conditions they observed that for 80% of the impeller passages were filled with dead water. The 20% of the passages towards the outlet contained a relative eddy which rotated counter to the machine rotation. This experiment neglects rotor stator interaction.

Iversen (1960) encountered this same pressure distribution and found a similar pattern at shut–off. Pressure increased from cut-water to discharge around the collector circumference. Iversen was the first researcher to note a rapid pressure drop at the cut-water.

Worster (1953) in his work on shut-off head flow patterns concluded that the volute was responsible for 20% of the shut-off head. The pressure from the cut water was found to rise around the volute and be constant at the throat and in the discharge pipe. Worster (1953) also observed a considerable flow interchange between impeller and volute. He proposed that this exchange of energy was responsible for the closed valve head not reaching its maximum Euler value. It is not possible to ascertain if the pump displayed a stable head characteristic at closed valve.

At shut-off condition they observed the exit relative eddy previously observed by Acosta and Bowerman (1957). They also noted an inlet relative eddy rotating in the machine direction in the pump inlet Fig.2.1.3.1. This flow feature is not mentioned in any of the previous research.

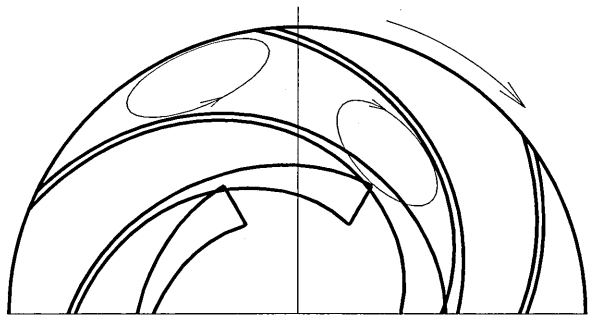

Fig.2.1.3.1 Visualised Eddy Distribution by Acosta and Bowerman (1957)

Levin and Poliokovsky (1965) carried out work to ascertain the nature of this suction re-circulation at shut-off conditions. Investigations took place on a radial un-shrouded machine. They found a large re-circulated region axially within the impeller and suction pipe Fig.2.1.3.2. Further unpublished work by Palgrave has shown that the recirculated region leaves the impeller at the inlet vane angle in the relative frame. This then spirals down the inlet pipe Fig.2.1.3.3.

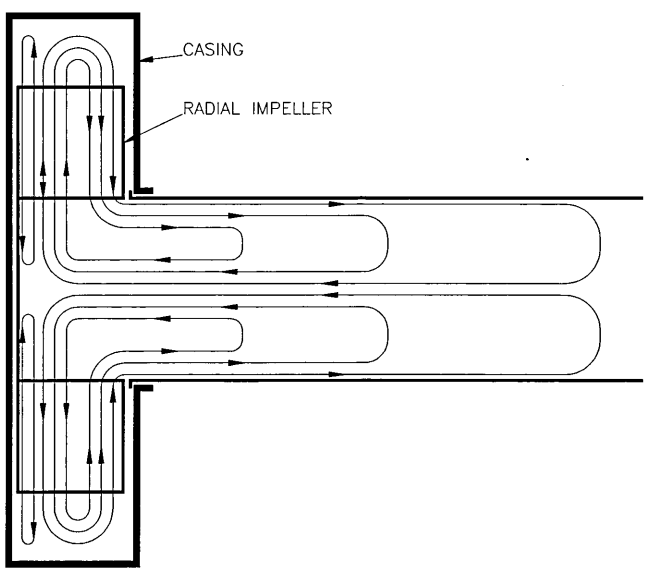

Fig.2.1.3.2 Flow Lines Of Radial Impeller at Zero Flow As Proposed By Levin And Poliokovsky (1965)

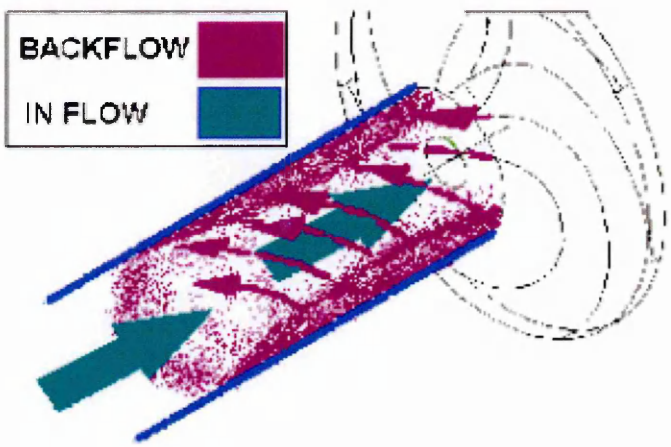

Fig.2.1.3.3 Flow Direction of Re-Circulating Liquid Proposed By Palgrave (2000)

Lennemann and Howard (1971) performed visualization studies using hydrogen bubbles. They examined the unsteady flow in radial impellers operating at shut-off conditions. Their findings were consistent with Acosta and Bowerman (1957). They observed a relative eddy at the impeller exit and 80% of the impeller exhibited solid body rotation. This contradicts the findings of Simpson and Cinnamond (1964). From the geometry given it is not possible to ascertain a reason for the exit relative eddy.

These cases are indicative of the difficulties encountered when attempting to separate out the effects of geometry on the flow features. The Simpson and Cinnamond (1964) pump may have had an overly large design of inlet, or significant inlet pre-swirl may have been present. Conversely Lennemann and Howard (1971) may just have overlooked the presence of the inlet relative eddy.

Yedidah (1985) used stroboscopic lighting to freeze the flow field on a single volute pump at zero flow. Two possible flow patterns were presented. For a pump with an unstable characteristic there is significant cyclic fluid interchange between casing and impeller Fig.2.1.3.4. For a stable pump characteristic there is no fluid interchange back into the impeller Fig.2.1.3.5. The energy lost during this interchange is proposed as the reason for the low closed valve head characteristic of an unstable pump.

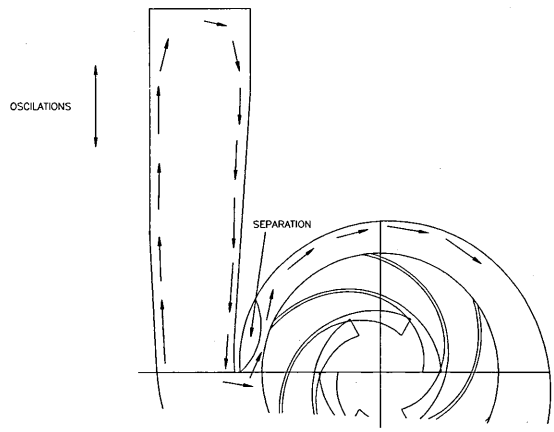

Fig.2.1.3.4 Yeddiah Proposed Flow Field for an Unstable Pump Characteristic

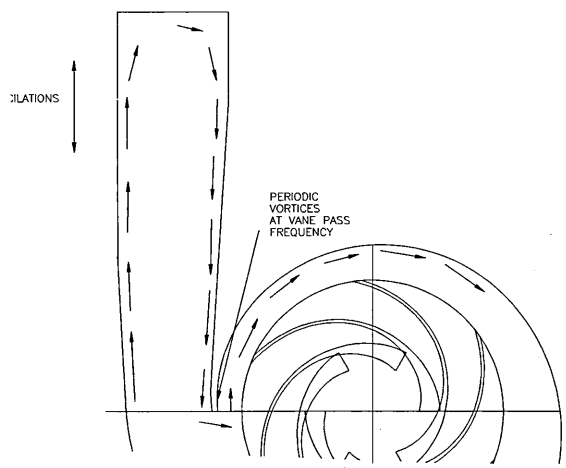

Fig.2.1.3.5 Yeddiah Proposed Flow Field For Stable Characteristic

Instability within pump impellers is caused by a number of factors, which pump designers consider, using empirical methods, when proposing a new design. It is not possible from the paper to ascertain which geometric features cause the instability or if the instability flow pattern is identical for all geometric cases. This flow phenomenon observed by Yeddiah (1985) is consistent with Worster's (1953) observations of an unstable head characteristic as is the oscillating flow feature observed by Peck (1950).

Abramian and Howard (1998) used LDA to gain an insight into pump flow by analysing an impeller with and without a volute. Their investigation differs from conventional investigations in that the subject was a low specific speed machine. This configuration introduces the difficulty of surface finish and leakage flow although these are not mentioned in the paper. Periodic unsteadiness,

fluctuations in the pressure fields and flow reversal into the impeller were all present at flows near to shutoff.

The measured flow patterns were in agreement with previous visualisation studies of Howard et al (1987). Vector measurements were taken at increments from the suction to the pressure side of the blade for differing phase angles with respect to the volute throat. The flow at the suction side continually exits the blade passage with no change of direction. There was a quickening of the flow as the blade passes the cut-water. Moving from suction to pressure side of the blade there is an increasingly strong flow rotation. At the pressure side of the blade the flow is turned inwards into the impeller. This flow reversal is repeated again 180 degrees around the volute. Although the pressure rise through the volute still exists this flow reversal is at odds with the flow pattern proposed by Frost (1991) and Newton (1998) where only one reversal near the cut-water interaction occurred.

The possibility of flow reversal even prior to the blade reaching the cut-water is suggested. These discrepancies may be explained by the double volute nature of the Abramian and Howard (1998) pump. The flow into the impeller was artificially swirled using an inducer so the effects of the re-circulated flow on the entrance flow are difficult to judge. Although the dimensions of the impeller and volute can be recreated from the paper the dimension of pre-swirl are not given.

Kaupert and Thomas (1999) presented two studies on the unsteady pressure field in a centrifugal pump impeller. The volute circumferential pressure variation was measured and mapped in agreement with Kikuyama (1987). This pressure variation, in the rotating frame of reference, is unsteady and dominated by vane pass frequency as established by Brownall et al (1985). The cutwater acted as a separator of two distinct flow regimes. This provides the pressure difference, which is responsible for the flow field fluctuation within the impeller. The unsteadiness of the flow increased as the flow was reduced with pressure fluctuations of 35% of total pump head. These pressure pulsations propagate at acoustic velocity.

Further work carried out within the same pump presented the difficulties of obtaining data and understanding the flow patterns as pump re-circulation commences. Binder and Knapp (1958), Brownall et al (1985), Iversen et al (1960), Kikuyama et al (1987) and Kaupert and Thomas (1999) all present data that illustrates the vane rate pressure fluctuation and the circumferential pressure distribution around the volute due to the rotor stator interaction.

2.1.4 Experimental Analysis using Air as the working Fluid

An alternative to using water as a product is to use air. Air is an easier product to use due to the lower working pressures involved. Leakage back to the pump inlets through wear ring landings though, can have a significant effect on the performance.

High flow machines, where leakage is small as a percentage of total flow, should be considered. The other consideration, in obtaining flow similarity, is to run the simulation with air at a greater speed. This replicates the Reynolds number defined as:

$$\mathrm{Re} = \frac{\rho \omega r_2^2}{\nu}$$

Yausa and Hinita(1979) used air as the pumped product and compared their results, on a dimensionless basis, to water. Identical agreement was obtained. Condenser microphones were also used to determine the unsteady pressure field.

Following on from this work Barrand et al (1984) and Caignaert et al (1985) both completed studies to determine the mechanisms of flow recirculation within an impeller. Their results, carried out on air and water were compared. The effect of increased leakage back to suction in the air model was responsible for measurement inaccuracies. A higher re-circulation flow rate was recorded for the air test pump.

Tourret et al (1985 and 1991) measured the unsteady pressure field with condenser microphones in an industrial pump using air. Considering three flow rates of 50%, B.E.P and 150% B.E.P, pressure increased within the impeller passage as it approached the cutwater and decreased immediately after. These measurements confirm the previous work by Binder and Knapp (1958).

Newton (1998) used air as the working fluid using LDA and condenser microphones to ascertain the unsteady flow pattern in a centrifugal fan of at closed valve. To minimised 3D effects the b2/D2 ratio was kept as small as possible. The inlet geometry was sealed to prevent inlet recirculation and a special sealing arrangement was adopted to minimise leakage losses.

2.1.5 Pump and System Interaction

The inability to accurately predict the closed valve head of a machine using computation methods has lead to a number of investigations which evaluate the impact of the pump system on the machines operation.

Work was published on the prediction for off design performance by Sun and Tsukamoto (2001). A method for predicting the off-design performance of a diffuser pump was presented, taking into account the rotor stator interaction effects. The paper covered the closed valve head condition. The methodology applied the pump system characteristic equation to the boundary conditions of the computational model. The effect of the system has previously been seen to have a significant effect on the pump flow regime. The system is responsible for the transient hysterisis observed by Kaupert and Staubli (2001).

The methodology realistically predicted the backflow onset at low flows, something that CFD has, anecdotally, struggled previously to achieve. The paper does not attempt to explain any of the flow features observed at closed valve. The linking of the characteristic equation to the closed valve condition is not necessary. If the mass flow through the system is zero, the effect of the characteristic equation on the flow regime is also zero. Longatte and Kueny (2001) also presented work which took into account the circuit interaction with the pump. This work quantified the pressure and flow fluctuations experienced by the stator. The intensity of the fluctuations was shown to be dependent on the pump system and the position of the pump within it. The distance of the boundary conditions from the pump was seen to effect the numerical simulations.

Although closed valve head calculations were not included in their work it may be significant to the closed valve problem. From the statistical work reviewed in Section 2.3 it is apparent that a mechanism may exist which is independent of the pump. The position of the discharge valve in relationship to the pump is difficult to quantify and differs from the test and site installation.

The level of closed valve head may be partly determined by the bound fluid, which is driven by the stalled impeller. The length of this re-circulating column has not been shown previously to influence the closed valve head value Fig.2.1.5.1.

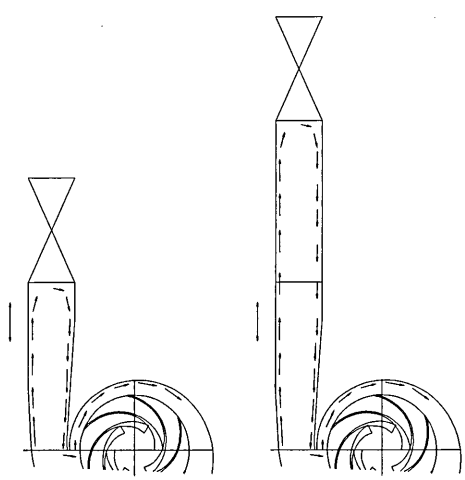

Fig.2.1.5.1 Illustration of the Proposed Effect of the Discharge Valve Position

If the position of the discharge valve has an effect on the closed valve head position, it is reasonable to assume that multistage pumps with high number of stages, will have a more consistent closed valve head coefficient. This is due to the liquid being bound and driven in the consistent environment of the inter-volute crossovers. The discharge valve position will only have an effect on the final impeller stage. The interaction of the bound liquid in a multistage pump crossover and the expelled liquid from that pump's subsequent stage impeller inlet is an area of pumping that has received little research attention. Only Worster's (1953) research has commented that the pressure with the volute passageways is steady and uniform.

2.2 Computational Methods

The investigation of centrifugal pumps using CFD (Computational Fluid Dynamics) is not as common as with other turbo-machines. The following papers are representative of the state of the art, regarding pump CFD study.

Graf (1993) compared results from three computational methods applied to a blade channel. Tascflow, Q-3D and a NASA simplified Q-3D codes were considered. The results were compared with flow visualisation data. At design flow the three codes were comparable. At "off design" conditions the only successful prediction was obtained from Tascflow.

Cooper and Graf (1994) used the commercially available CFD software CFX Tascflow, which is dedicated turbo machinery code, to assess the computational performance against experimental data. The researchers computed both suction and discharge re-circulation with good qualitative comparison of the flow field from 5% B.E.P to 21% B.E.P. The researchers showed that CFD had been integrated into the design process.

Work carried out by Yates et al (1995), Tourlidakis et al (1995) and Hamil et al (1995) has applied CFD to the solution of pump flow. Comments on accuracy are difficult as these were all published without corresponding experimental data, but all point towards the vast potential of CFD.

Chen and Liaw (1997) presented a CFD study incorporating an on-design analysis with particular attention paid to the interaction between rotor and stator. A full transient computation simulation was carried out with the flow field calculated for every 18 degrees of revolution. Mesh incompatibility from impeller to volute is handled by employing a small gap, which is ignored in the computation. The evaluation of an "on design" impeller solution only concluded that in a small time frame with a course grid accurate results of the flow field can be gained from the analysis.

The impeller-casing interaction is complicated at off design conditions, with solution times increasing considerably. The flow field observed agrees with the mental picture designer work with. At design flow there was no separation at the cut-water, the flow is squeezed between the impeller and casing. The flow rate in differing impeller passages is dependent upon its position within the casing. The paper again showed the non-linear diffuser effect of the volute as the pressure rose from cutwater to throat. This illustrates the importance of modelling the volute in unsteady analysis.

Miner et al (1988, 1989, 1992) analysed a 2D centrifugal pump using a finite element method based on potential flow. The goal was to refine the prediction method by considering both the impeller and volute. 9 grids were generated, each

with a fixed impeller orientation. Validation was carried out by comparing the results with LDA data.

Miner et al (1989) results show that at design flow the measured velocity and predicted velocity were within 17%. Miner concluded that below design flow the potential flow method was not suitable. The qualitative agreement was good but quantitative errors were attributed to poor grid refinement.

Dyson (1999) presented an overview of how CFD has become an everyday design tool, fully integrated into the design process. Palgrave & Dyson (2000) later demonstrated using CFD how flow physics effects the vibration potential of a pump. In both these cases only on-design analysis was considered.

The only notable study of closed valve head Newton (1998) used Fluent's sliding mesh to simulate the shut off conditions a 2D centrifugal fan. The results were compared with LDA and condenser microphone methods taken with air as the working fluid. The intention was to provide an insight into the flow mechanisms at closed valve and gaining an indication of the potential for using CFD to predict closed valve head. The experimental pump impeller had a closed inlet and the volute had a closed outlet. 3D effects were limited by making the pump d2/b2 ratio as large as possible.

The major conclusions drawn from this work by Newton (1998) are divided into flow and computational.

Flow physics

- The fluid within the rotor does not exhibit solid body rotation. This disagrees with the conventional mental model designers have traditionally used. It also disagrees with Frost's (1991) work.
- Rather than solid body rotation, large vortices occur within the blade passages driven by the turbulent shear stress around the rotor periphery. This agrees with the observations of Simpson and Cinnamond (1964).

- The proposed flow field by Frost (1991) was qualitatively correct.

- The mechanism of volute pressure rise proposed by Frost (1991) is incorrect. Radial variations in pressure around the volute are small. The volute acts as a diffuser with pressure rising from cutwater to discharge circumfrentialy.

The pump geometry for Newton's (1998) experimental analysis, particularly the volute layout bears no relation to conventional pump design. It is difficult to believe that such a distorted geometric layout could hold for Frost's (1991) prediction method, which is derived from actual pump geometry.

In this layout the casing throat is tall and narrow. The diffusion around the volute is too great to represent contemporary pump design Fig.2.2.1. It is possible that differing radial velocity streams across the throat, which are the basis of Frost's (1991) model, will have been mixed out by time/distance to such an extent that they are undetectable.

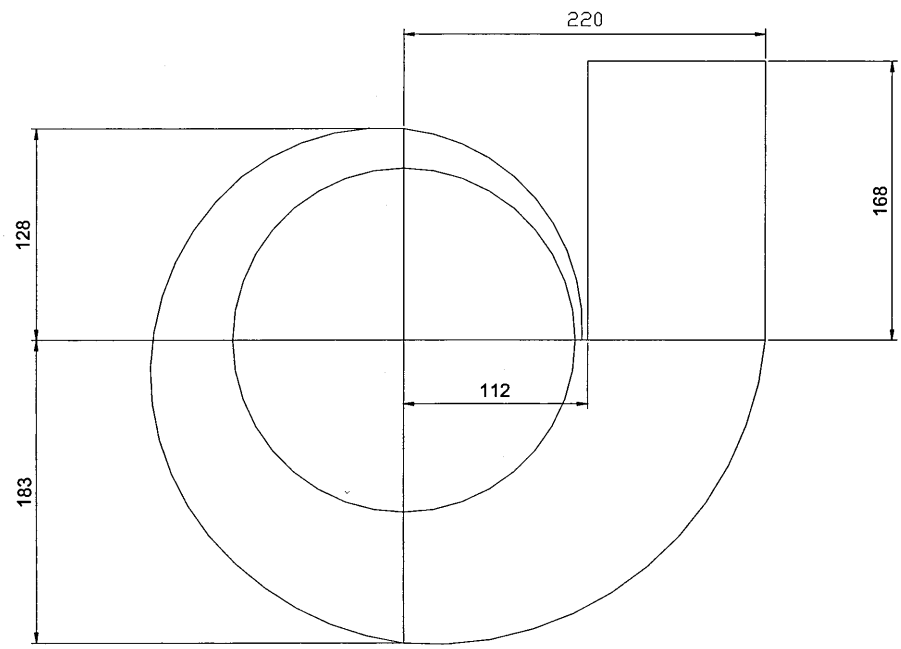

Fig.2.2.1 Newton's (1998) Volute Layout

One major difference between the Newton (1998) research and the "real-world" situation is the treatment of the pump suction. Newton's (1998) research relies on a closed impeller inlet. This does not allow the inlet-backflow proportion of the closed valve flow regime to develop as observed by Fraser (1991) and others. Whilst instructive, from a realistic standpoint Newton's (1998) work is incomplete

Computational

Newton (1998) found the commercial software package Fluent 4.4 acceptable for this analysis. The qualitative agreement of the flow pattern was good.

- The major error in the computational analysis was the over prediction of the shut-off head associated with the volute pressure rise. This was directly linked to the validity of the rotor/stator interaction prediction within the research.
- The sliding mesh did not appear to introduce significant errors into the solution.
- A Higher order spacial discretisation scheme did not affect the solution.

- Momentum balance and convergence were major obstacles. Torque errors between rotor and stator were as much as 20% out and could not be reduced.
- The standard k-epsilon turbulence model did not have a significant impact on the solution. k-epsilon standard giving better results than the more advanced RNG k-epsilon model. Viscosity prediction appears to be the problem. This was not true under steady state analysis where the RNG k-epsilon model performed better.
- It is important to include the rotor/stator interaction effects in any attempted off-design solution where unsteady interactions are expected.

Newton (1998) disagreed with the supposition that the impeller exhibits solid body rotation. This is the basis of the work by Frost (1991).

2.3 Analysis of Closed Valve Head Prediction Methods

There are several methods available which can be used to predict the levels of closed valve head. All incorporate the rotational speed and the impeller diameter as major contributing factors. The influence of other geometry is seldom accounted for. These methods are evaluated for accuracy by using a database of 200 pumps of different configurations.

Many of the prediction methods were devised using a statistical approach based on a limited number and configuration of pump. By using such a larger sample of pumps, the suitability and accuracy of each method can be evaluated. A modifying design coefficient is suggested for each method with a corresponding evaluation of the improvement in accuracy.

2.3.1 Stepanoff (1957)

Simplifying the Euler equation for a condition where flow through the pump is zero gives a maximum theoretical value for closed valve head of:

$$Headcv = \left(\frac{U_2^2}{g} \right)$$

From this basis many statistical investigations have attempted to correct this theoretical maximum by application of a universal correction. Stepanoff (1957) proposed the use of a design coefficient to modify the Euler head equation.

$$Headcv = \Psi \left(\frac{U_2^2}{g} \right)$$

The coefficient for ψ is defined by Stepanoff (1957) as 0.585. This factor was derived from a review of a number of centrifugal pumps. An analysis of ψ, based around the closed valve head design coefficients derived from the database, shows this correction factor to be statistically true, as the arithmetic mean of the analysed geometry. As a method of predicting closed valve head its use is limited. The spread of error is over 20%.

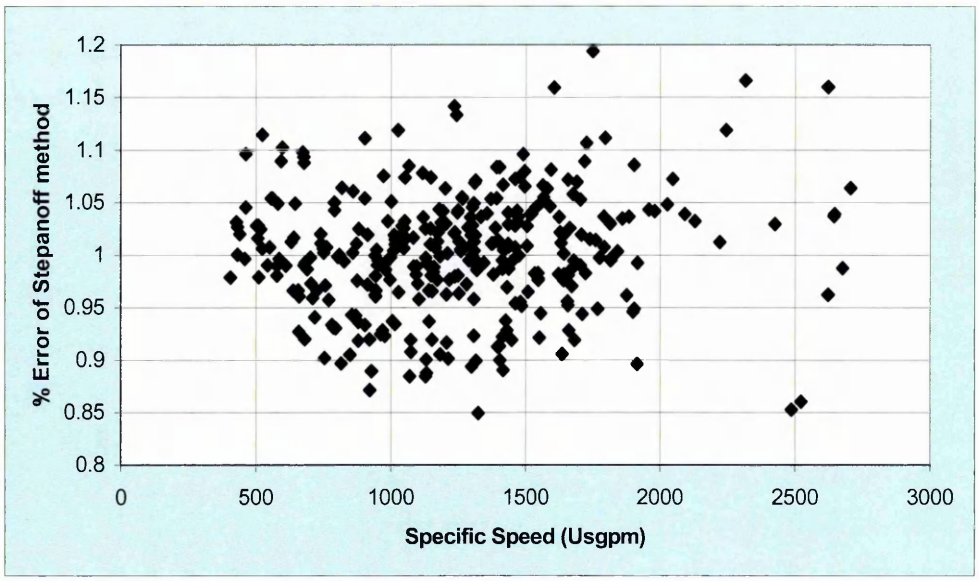

Fig.2.3.1.1 Error of Stepanoff (1957) Prediction Method Based on the Pumps in the Database vs. Specific Speed

The method only links the peripheral velocity to the closed valve head value and as such the impeller outside diameter is the only geometric feature considered by the prediction method. Fig.2.3.1.1 illustrates the Stepanoff (1957) Euler Closed Valve head modifier assessed for varying geometry of David Brown Pumps.

2.3.2 Peck (1968)

A similar modifier to the Euler equation is proposed by Peck (1968), who also presented work based on the statistical analysis of pump geometry giving the formula.

$$Headcv = \frac{\Psi}{2}\left(\frac{U_2^2}{g}\right)$$

He proposed that the pump configuration affected the empirical constant. This lead to a constant $\frac{\Psi}{2}$ for volute pumps of 0.5 to 0.55. Although this value is different to Stepenoff's proposed constant, which was verified by the database geometry, it is within the error band.

The consideration of pump configuration, combined with impeller diameter, as geometric considerations, does not add to the accuracy of the predicted closed valve head in Peck's method. If we apply the reasoning that pump configuration

has an effect on closed valve head coefficient to the pump database, it is clear that different types of pumps have differing closed valve head coefficients.

Fig.2.3.2.1 contains a frequency analysis of closed valve head coefficients for different pump configurations. The frequency analysis can be used to refine the head coefficients for pump configuration, but the spread of the results is still too wide to be of use in design.

Hocv Single Entry - 0.575
Hocv Multistage - 0.6
Hocv Double Entry - 0.625

From the frequency data, the multistage pump has the lowest spread of results.

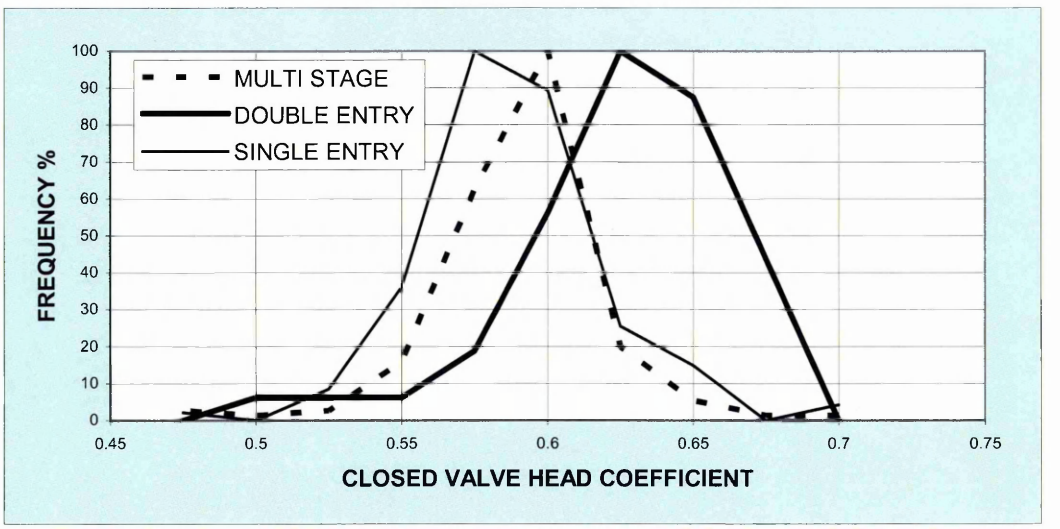

Fig.2.3.2.1 Frequency Analysis of Closed Valve Head Coefficients For Differing Pump Configurations

2.3.3 Patel (1981)

Patel (1981) proposed the theory that the specific speed of the pump has an effect on the value of closed valve head. Typically a low specific speed pump may exhibit a flat or drooping performance curve, whilst a high specific speed pump will have a high head rise to shut off. From statistical data Patel proposed a modifier to the Euler head based on this observation.

$$\Psi cv = 0.65 - 0.004Ns(metric)$$

From the database geometry a dependency on specific speed can be identified. This is as expected due to the characteristic nature of the performance curves for the types of machine. The geometric differences between low specific and high specific speeds are striking so the link between geometric configuration and closed valve head value should show a strong trend. A further factor is the difficulty in maintaining the prescribed design geometry for low specific speed machines. The impeller outlet widths, which have an effect on pump stability, are sensitive to the inherent errors found in sand casting technology.

Using the database to separate out pump configurations a difference is apparent for pump type. The data suggests the prediction method can be further modified to take into account the specific speed slope and also the pump configuration, based on the pumps within the database. Fig.2.3.3.1 illustrates the percentage error of Patel (1981) prediction method based on specific speed. Patel's formula increases in accuracy if the following modifications are used.

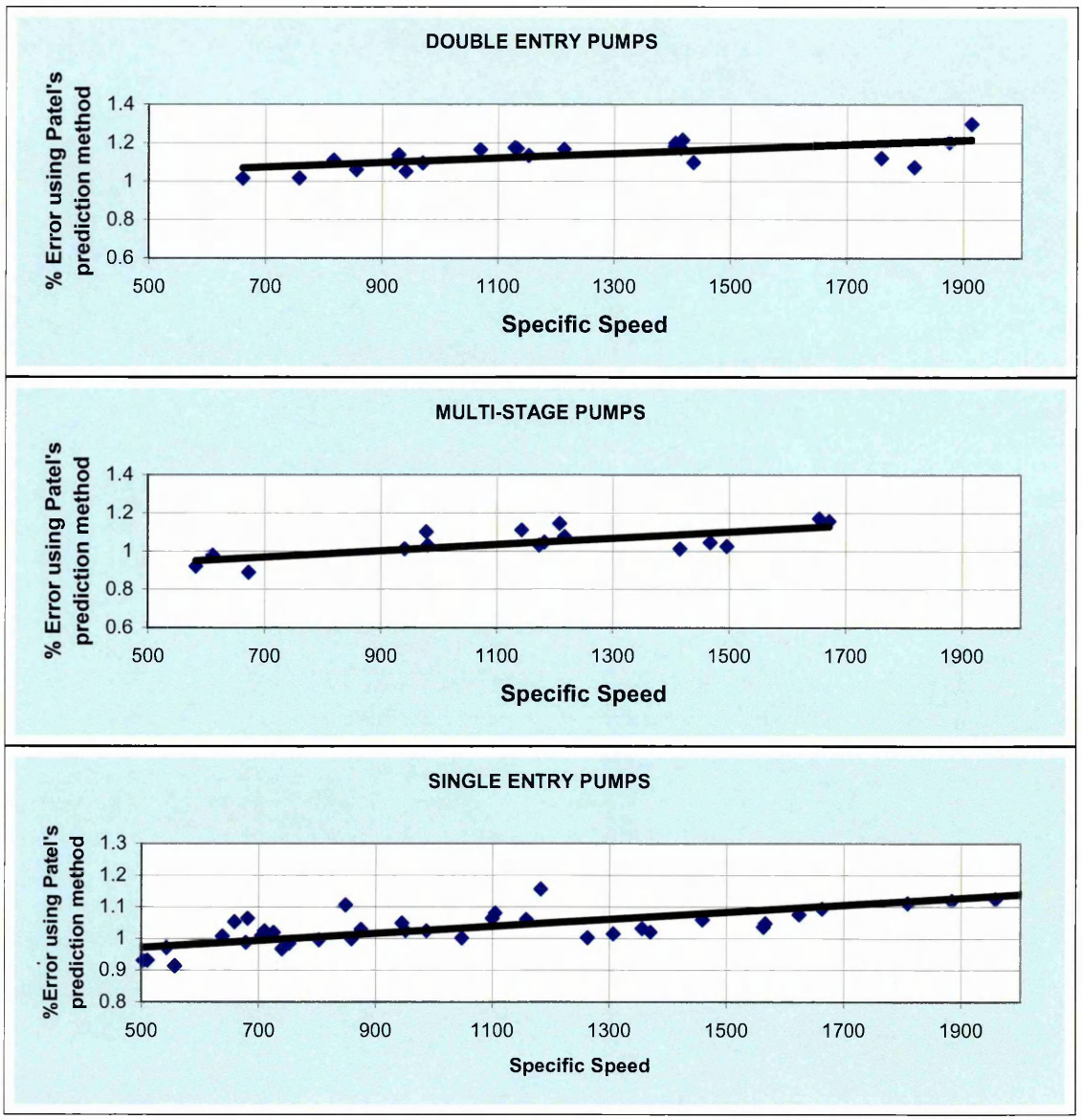

Fig.2.3.3.1 Percentage Error of Patel (1981) Prediction Method Based On Specific Speed

Single Suction

$$Headcv = \frac{Patelcvhead}{0.9165 + 0.0001NS(us)}$$

Double Suction

$$Headcv = \frac{Patelcvhead}{0.9923 + 0.0001NS(us)}$$

Multi-stage

$$Headcv = \frac{Patelcvhead}{0.8559 + 0.0002NS(us)}$$

From a frequency analysis of the error spread the accuracy of the prediction method has been increased Fig.2.3.3.2.

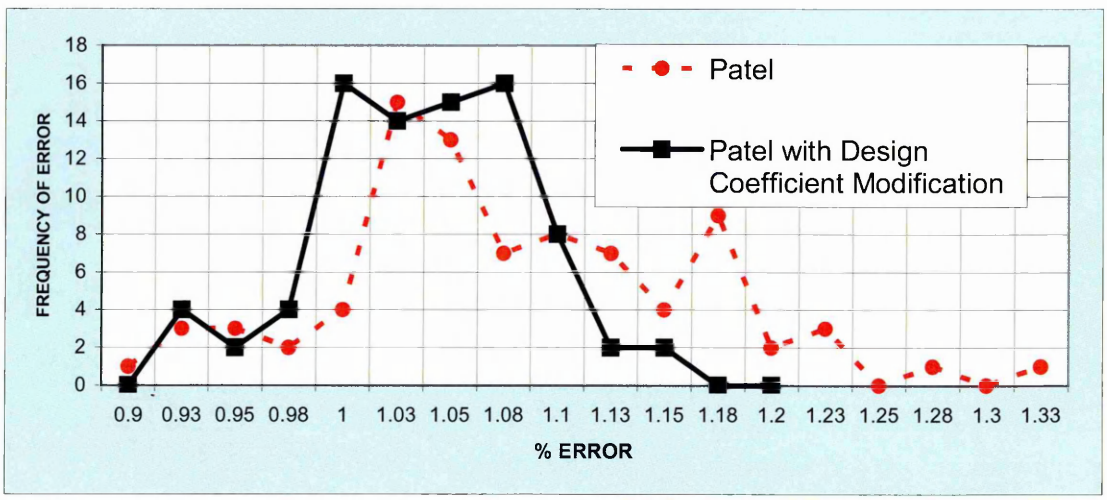

Fig.2.3.3.2 Frequency Analysis of Accuracy Increase Due To Design Coefficients

2.3.4 Thorne (1988)

Thorne (1988) used a more complex modifier for the Euler equation based on empirical constants for the impeller and casing.

$$Headcv = \left(\frac{U_2^2}{g} \right) \left[\left(\frac{1}{slip} \right) - \left(\frac{C_{1m}}{2U1} \right) \left(A^2 + \frac{B^2}{slip^2} \right) \right]$$

$$Slip = 1 + \left(\frac{a}{z} \right) \left(\frac{1 + Beta2}{60} \right) \left(\frac{2}{1 - \left(\frac{D_1}{D_2} \right)^2} \right)$$

The casing coefficient in the slip formula a=0.77

The prediction method attempts to incorporate the impeller outlet diameter to satisfy the known link to the Euler equation with impeller inlet parameters of eye size, which influence inlet re-circulation and as such may have a negative effect on the closed valve head. The vane geometry is also considered by taking some account of the slip value of the relative velocity, Weisner (1967). Casing considerations are accounted for by including an empirically derived coefficient. The configuration of the pumps is not considered. It is difficult to imagine a mechanism, following on from the experimental review, where slip factor is the actual mechanism which influences the closed valve head. More likely is the geometric change that occurs when changing vane number or discharge angle.

As shown in Fig.2.3.4.1, this prediction method consistently over predicts the value of closed valve head, with the errors over 20%. When pump type is taken into consideration the amount of error is influenced by the pump configuration. The following denominators for the Thorne (1988) prediction method increase the accuracy of the methods over a range of specific speeds

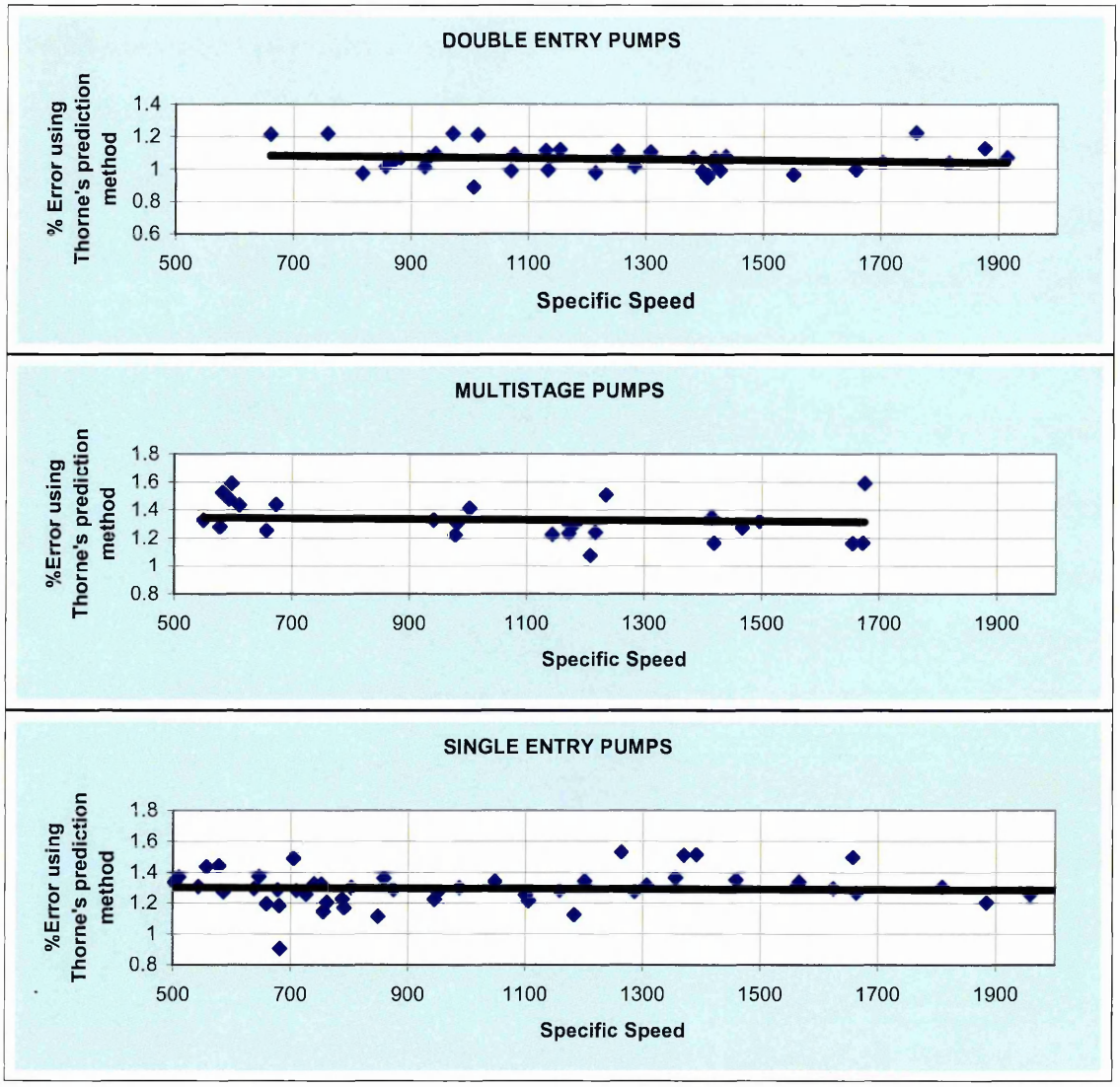

Fig.2.3.4.1 Configuration Of Pumps Analysed Using Thorne(1988) Prediction Method

Single Entry Pumps 1.31
Multistage Pumps :- 1.36
Double Entry Pumps:- 1.1

There is an accuracy increase due to the modifiers proposed. This is illustrated by the frequency analysis in Fig.2.3.4.2.

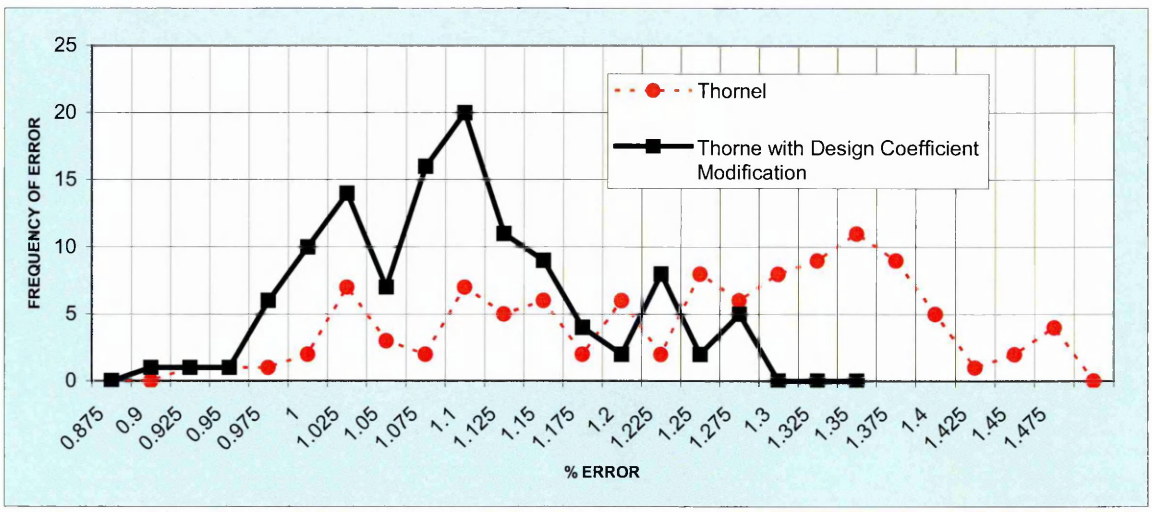

Fig.2.3.4.2 Frequency Analysis of Accuracy Increase Due To Design Coefficients

2.3.5 Stirling (1982)

Stirling (1982) used a method based on the contribution of the impeller added to a volute contribution. The impeller contribution was taken from Levin and Poliokovsky (1965) who investigated re-circulating flow in a free impeller at shut-off. Stirling (1982) proposed that the closed valve head of a centrifugal pump was composed of three components.

2.3.5.1 Impeller Contribution

The impeller acts as if it were a solid body with no fluid interchange between rotor and collector. Whist this ignores the rotor/stator interaction effects if serves as an analogy for the strong viscous forces driving the collector flow.

$$Hsoimp = \frac{1}{2g}\left(U_2^2 - \frac{U_1^2}{2}\right)$$

2.3.5.2 Volute Contribution

The collector throat area is considered significant by the inclusion of Anderson's (1947) area ratio.

$$Hsovolute = \frac{U_2^2}{2g}\left(ho - \left(\frac{\phi R}{(\tan(beta2 - \delta A))} \right) \phi R.AR \right)$$

AR = Anderson area ratio
Ho = Weisner's slip factor

$$\delta A = 1.17x10^{-3}\left(\frac{P_2 Beta_2}{Cm} \right)$$

2.3.5.3 Inlet Back-flow

As the flow through a pump is reduced the liquid exits from the impeller eye and flows into the inlet channel. To escape the impeller liquid has to exceed the impeller inlet tip speed. This high energy liquid has a negative contribution on the closed valve head of the pump.
The re-circulating flow factor is derived empirically by analysis of a number of pumps

$$\phi R = -0.2331\left(\frac{r_1}{r_2} \right) + 0.1952$$

The negative contribution of the inlet back-flow cannot be valid for more than one configuration of pump. The inlet channel for an end suction pump will inevitable have a differing contribution to closed valve head from a multi-stage or top entry pump. This is further supported by Kovats (1979) whose work exposed the higher head coefficients of pumps with splitters which extend into the impeller eye.

This is the first prediction method to characterise the contribution of the three distinct geometric features of suction diameter, impeller diameter and volute into a prediction method. Fig.2.3.5.3.1 demonstrates the Percentage Error vs. Specific Speed for the Stirling (1982) prediction method.

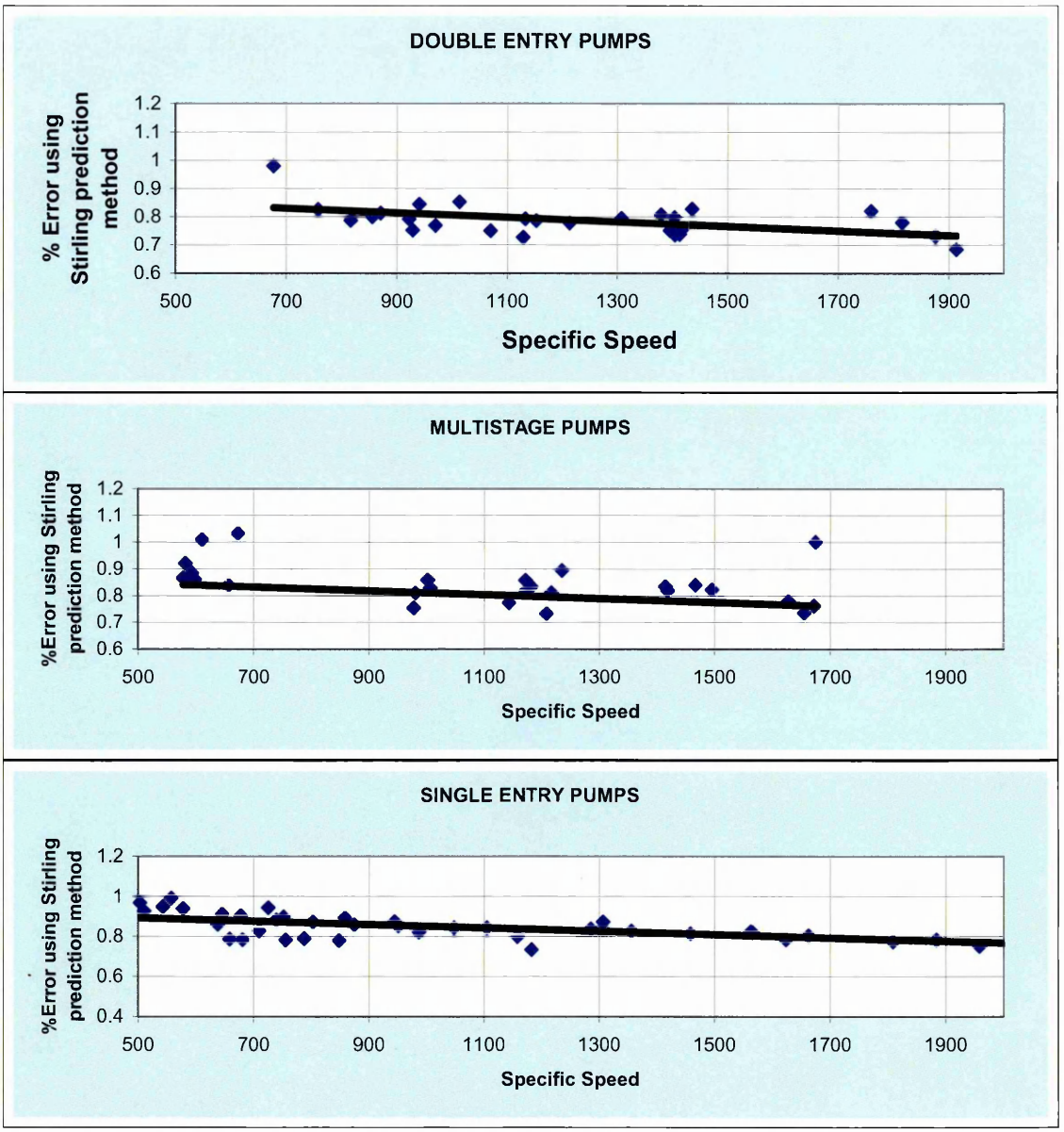

Fig.2.3.5.3.1 Percentage Error Vs. Specific Speed For Stirling (1982) Prediction Method

This method, whilst linking some of the geometry to the closed valve head value, still relies on empirically derived constants. The pump configuration does not have a marked statistical effect on the predicted head, but the method consistently under predicts the closed valve head level.

A modifying factor can be applied to the Stirling (1982) equation to increase its accuracy

$$Headcv = \frac{Stirlingcvhead}{0.938 - 0.0001NS(us)}$$

Fig 2.3.5.3.2 contains a frequency analysis of accuracy increase due to Dyson design coefficients. The error spread is improved by the design coefficient and the accuracy is increased.

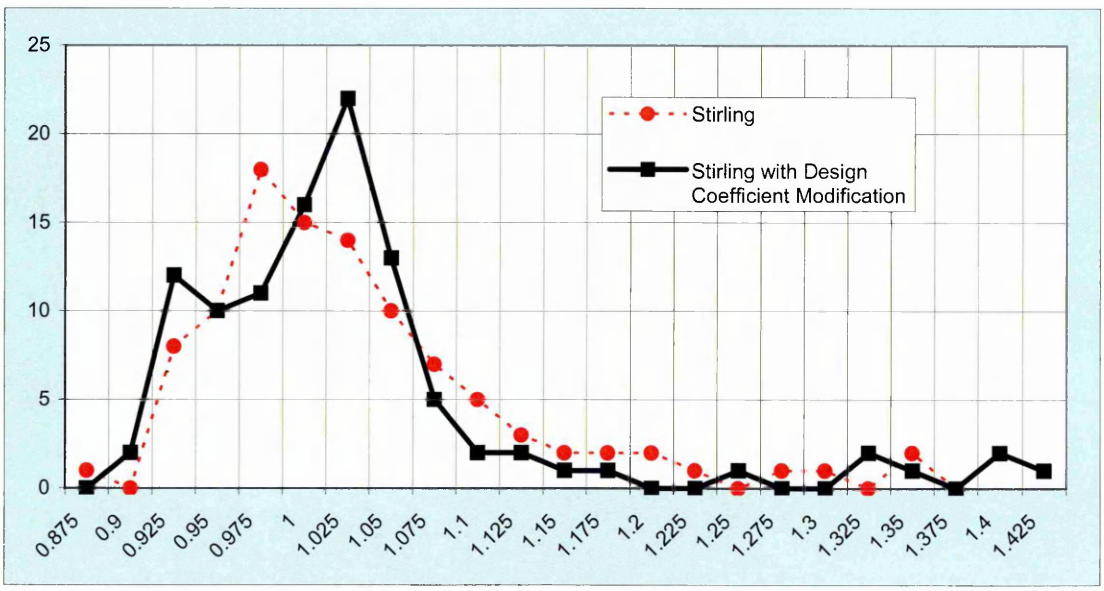

Fig 2.3.5.3.2 Frequency Analysis Of Accuracy Increase Due To Design Coefficients

2.3.6 Frost and Neilsen (1988)

Frost and Neilsen (1988) produced significant work in the area of shut-off head predication when they proposed a model for the volute pressure rise added to the head developed by the impeller. Although Stirling (1982), using empirical coefficients, had previously proposed this, the Frost and Neilsen (1988) method

was the first purely analytical method. To calculate the contribution of the impeller Frost (1988) assumed the flow in the rotor exhibited solid body rotation although this still ignores the rotor stator interaction effects. This implied a shut off head contribution from the impeller OD.

$$Himpso = \frac{U_2^2}{2g}\left(1-\left(\frac{r_1}{r_2}\right)^2\right)$$

Considering the velocity distribution across the casing throat area and obtaining the associated pressure from this velocity profile we can derive the volute contribution.

$$Hsovolute = \left(\frac{\mathcal{G}r_2}{(r_m - r_2)^2}\right)\left[r_m \ln\left(\frac{r_4}{r_2}\right) - 2r_m(r_4 - r_2) + \left(\frac{r_4^2 - r_2^2}{2}\right)\right]\frac{1}{g}$$

Where r_4 is the height from impeller centerline to the throat and r_2 is the radius at the middle of the throat (centroid).

Fig 2.3.6.1 contains a chart of Error vs. Specific Speed for Frost (1998) prediction method. Although this method does not assess the negative contribution from the inlet back-flow, it is more accurate than previous methods.

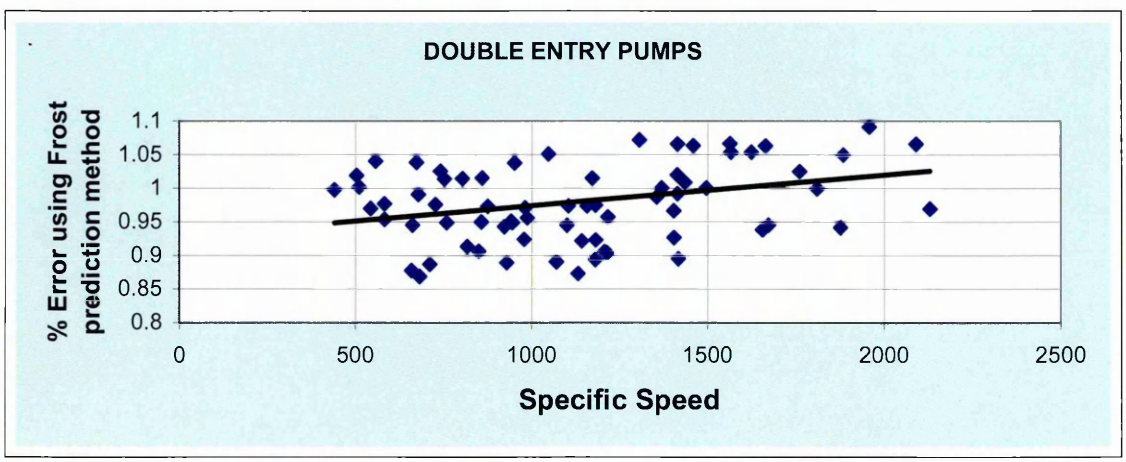

Fig 2.3.6.1 Error Vs. Specific Speed For Frost (1998) Prediction Method

No error trend is shown to be dependent on the pump configuration, but a modifying factor can be applied to the Frost (1998) equation to increase its accuracy.

$$Headcv = \frac{Frostcvhead}{0.9282 - 0.00005NS(us)}$$

A frequency analysis of accuracy increase due to the new design coefficient is demonstrated in Fig.2.3.6.2. The accuracy of the method is increased and the error spread is reduced.

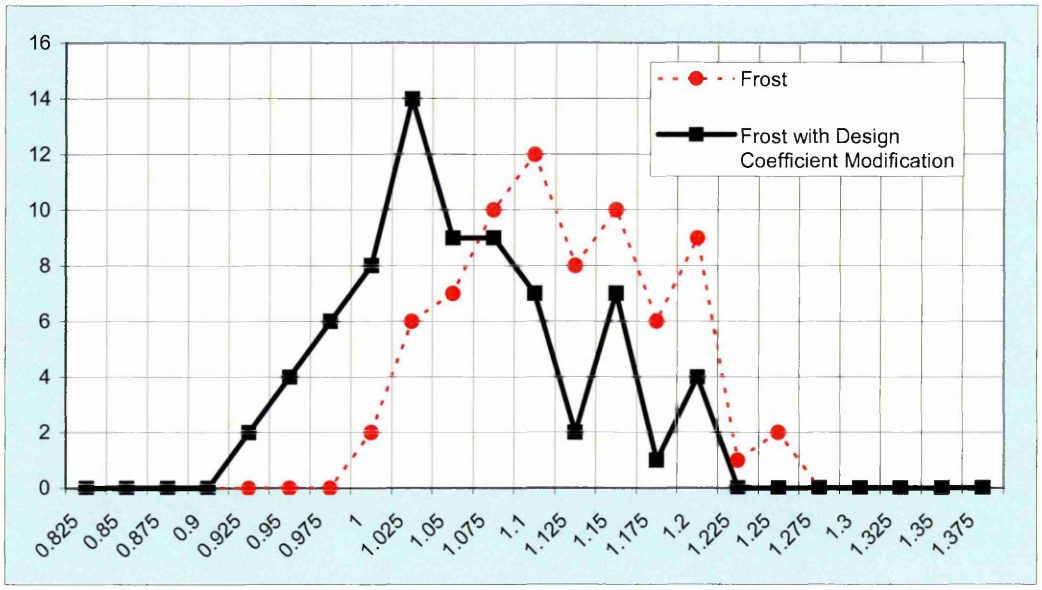

Fig.2.3.6.2 Frequency Analysis of Accuracy Increase Due To Design Coefficients

2.4 Summary of Literature Review

The problems associated with the prediction of closed valve head are complex. The existing prediction methods only offer an empirically derived solution to the prediction on the pump closed valve head. Refinement techniques based on statistical analysis improve the accuracy but not to a satisfactory extent.

From the experimental and computational research that has been reviewed it is possible to draw the following conclusion.
These conclusions can be divided between the three distinct geometric regions within the pump:

- The contribution of the impeller.

It is a common view held among pump designers that the pressure contribution to closed valve head from the impeller is analogous to a rotating solid body. There is some debate over whether the internal radii of the solid body is based on the impeller eye diameter, hub diameter or is zero. This view, based on the work by Frost, is based on conversations with pump designers from Guninard Pumps (Gilbert Gauze), Weir Pumps (Ron Palgrave), Union Pump USA (George Cheng) Flowserve Pumps (Paul Cooper). The designers from this community are representative of all the major API pump manufacturers. It is important to state that solid body should only be considered an analogy at this stage of the research. Pump designers have adopted this theory as a representation of the actual flow mechanism based on the work by Frost. The current research is unclear as to whether the is the case or the mechanism accurately represents the flow.

Recent work by Newton (1998) has suggested that the assumption is not true. This has added little to help the designer in assessing the contribution of the impeller as not alternative was suggested. It is difficult to ascertain from Newton's work if the experimental fan had a stable characteristic. If not the flow phenomenon witness by Yeddiah (1993) may be responsible for inaccurate volute contribution prediction.

As previously discussed, the contrived geometry may be responsible for Frost's (1988) pressure rise volute prediction not holding true but it is more likely problems with the codes inability to predict weak interaction effects or the solution methodology that cased the errors. The existence of an inlet relative eddy and the geometric features responsible for this phenomenon are unknown. This aspect of the research was compromised by the experiment inlet conditions.

- The contribution of the volute

The pressure rise due to the diffusive nature of the volute has been assessed, by Frost (1991), assuming zero net-mass flow at a particular point within the volute

and establishing its associated pressure. There is some debate over the position of zero net mass flow within the volute.

Newton found the CFD code over predicted the pressure rise within the volute. Experimental work has determined a non-linear pressure distribution around the volute at closed valve and the presence of separation regions on unstable pumps.

- The contribution of inlet back-flow

The liquid re-circulating out through the pump inlets has a rotational effect on the incoming fluid, notionally causing a loss of closed valve head. No experimental data is available to quantify the effects of this re-circulating fluid.

Designers have also noticed how differing geometric features can have an effect on closed valve head.
A volute with a high width to height ratio or have differing shapes will have a lower closed valve head than expected as liquid is trapped either side of the impeller. This partly supports the theory proposed by Frost (1991) in which volute throat shape is a factor in closed valve head value.

Diffuser pumps which are somewhat different from volute pumps in the respect that the diffusion is carried out through a stationary multiple blade row which contains upwards of 5 diffusing passageways. A volute pump never contains more that two passages. The diffuser type of machine anecdotally has a higher closed valve head characteristic than a volute machine. This discrepancy is not explained in the literature.

The number of vanes and the vane outlet angle causes changes in flow slip and thus changes in closed valve head, supporting Newton (1998) supposition that the impeller's contribution is not analogous to solid body rotation.

Attempts at CFD analysis at closed valve have been partly successful. Convergence is a major issue and the validity of the results whilst qualitatively representative are quantitatively poor. Experimental data gained from commercially representative machines is insufficient. The only comprehensive study carried out was on a closed inlet fan pump, which was unrepresentative of commercial geometry.

Modelling of the system elements has increased the CFD accuracy for closed valve head prediction.

From the experimental data reviewed it is possible to gain some agreement on the flow physics:

- The nature of the flow field is unsteady.

- The rotor/stator interaction has a direct effect on the flow field. Passage velocity profiles are dependent on their position with respect to the collector cut waters.
- There is a flow pulsation within the discharge pipe.
- Non-linear circumferential pressure gradient exists around the volute with a low-pressure region existing at the casing lip.
- The impeller drives a relative eddy, in the majority of the literature, at the outlet counter to the machine rotation.
- Inlet re-circulation occurs extending into the collector inlet pipe.
- The system has an influence on the off-design performance of the pump.

3.0 The Need for Computational Fluid Dynamics

Computational Fluid Dynamics is a simulation technique, which plays an important role in engineering disciplines. CFD has been used for many years within the pump industry, primarily as a problem solution tool after a test or field failure. Now with the increased computer capacity available it has become more common place within the upfront design environment.

Over the last 5 years CFD has increased in importance to such an extent that it is often an integral part of the design process. Pump manufacturers have turned to CFD to refine the hydraulic performance of their machines and to investigate the important flow features that exists at off-design conditions.

The inability to predict the performance of a new product can have serious consequences for pump manufacturers. High development and pattern costs mean that pump companies design on a bespoke basis. A non-performing machine may result in financial penalties and the loss of reputation. The subsequent re-work cost for the design can also be substantial. The alternative to simulations is experimental analysis. In pump terms, this approach is time consuming and costly on a design for contact basis. The analysis of streamline data without intrusive methods is almost impossible.

The speed and memory capability of computers has increased greatly over the last few years. With this extent of computational development the complexity and depth of the solutions can be expected to increase to the same extent. The use of a 250000-node grid is analogous to using 250000 non-intrusive probes. The insight gained from this type of CFD analysis can be more valuable than that available from experiments.

The case for using CFD as an experimental test upfront of manufacture is compelling. The number of validation studies for pump design problem is growing (Chapter 2). This section of the research deals with the theory behind the CFD analysis and the schemes available within the commercial software package CFX5.1 and CFX Tascflow.

In this Chapter comparisons are made with a simplified pump research case study to provide evidence for the reliability of CFD when predicting b.e.p. performance. Experimental data is difficult to obtain at closed valve but unsteady pressure pulsations were taken on a commercial pump as it underwent its factory testing. These results are also presented as a background to the following CFD studies at closed valve presented in later chapters of the work.

3.1 Basic Equations

Laws governing the movement of fluids are constructed from the three important physical laws:-

- Conservation of Mass
- Conservation of Momentum
- Conservation of Energy

Whilst important for compressible fluids, the energy equation cannot be directly linked to the first two stated laws without change in density. As such, problems can be solved with the mass and momentum equations.

3.1.1 Conservation of Mass

The law governing conservation of mass relates to the transfer of mass flow into and out of a control volume. A full explanation of the derivation of this law is found in Versteeg and Malalasekera (1995). The final state is shown here for brevity

$$\frac{\partial u}{\partial x}+\frac{\partial v}{\partial y}+\frac{\partial w}{\partial z}=0$$

3.1.2 Conservation of Momentum

Newton's second law states that the rate of change of momentum of a particle is equal to the sum of the forces acting on the particle.
These can be covered by two distinct areas within fluids.

- Surface forces such as pressure and viscous forces
- Body forces such as centrifugal and Coriolis forces.

The derivation of the momentum equation can be found again in Versteeg and Malalasekera (1995) but the final equation is shown here.

$$\rho\frac{Du}{Dt}=\frac{\partial\left(-p+\tau_{xx}\right)}{\partial x}+\frac{\partial\tau_{yx}}{\partial y}+\frac{\partial\tau_{zx}}{\partial z}+S_{mx}$$

-p :- Compressive pressure
τ :- viscous stresses in j direction
Smx :- Source term including the body forces

$\frac{D}{Dt}$:- derivative following the fluid, including local unsteady and convectional accelerations
This equation can also be written for y and z directions.

The introduction of the viscous stress, require a methodology for the solution of these unknowns.

This methodology, for a Newtonian fluid, supposes that the individual viscous stresses are proportional to the rate of change of deformation of a fluid element. For the x direction the viscous stresses can be written as:

$$\tau_{xx} = 2\mu\frac{\partial u}{\partial x}$$

This represents the result of linear elongation, deformation

$$\tau_{xx} = \mu\left(\frac{\partial u}{\partial y} + \frac{\partial v}{\partial x}\right)$$

$$\tau_{xx} = \mu\left(\frac{\partial u}{\partial z} + \frac{\partial w}{\partial x}\right)$$

These represent the effects of linear shearing deformation

μ :- dynamic viscosity

The above equations can be substituted into the momentum equation to give:

$$\rho\frac{Du}{Dt} = \frac{\partial p}{\partial x} + \frac{\partial}{\partial x}\left(2\mu\frac{\partial u}{\partial x}\right) + \frac{\partial}{\partial y}\left[\mu\left(\frac{\partial u}{\partial y} + \frac{\partial v}{\partial x}\right)\right] + \frac{\partial}{\partial z}\left[\mu\left(\frac{\partial u}{\partial z} + \frac{\partial w}{\partial x}\right)\right] + S_{mx}$$

This is commonly re-written as

$$\frac{\partial u}{\partial t} + div(uu) = -\frac{1}{p}\frac{\partial p}{\partial x} + \upsilon div grad u + Smx$$

υ :- kinematic viscosity

The substantive derivatives $\frac{Du}{Dt}$ and $\frac{\mu}{\rho}$ have been split into a local unsteady acceleration $\frac{\partial u}{\partial t}$ and a convective acceleration div(uu).

The y and z components of the Navier-Stokes equations can also be found in this way.

Four equations have been generated, the mass conservation and the three Navier-Stokes equations. These can be solved for four unknowns.

3.1.3 Rotating and Stationary Reference Frames

With a model of a rotating machine two frames of reference exist. Each of the frames shares the same coordinate system.

The impeller sits in the rotating frame of reference and rotates with an angular velocity ω. The impeller is arranged so the axis of rotation coincides with the z-axis.

The impeller volute and its associated suction inlet geometry sit in the stationary frame of reference. These components are stationary in the absolute frame.

For the rotating reference frame it is essential that the equations of motion contain extra terms. These additional body force terms ensure that the overall accelerations are correct when viewed in the stationary frame.

These acceleration terms are:-

$-2\omega_z w_\theta - \omega_z^2 r$
Radial direction

$-2\omega_z w_r - \omega_z^2 r\theta$
Circumferential direction

w_r and w_θ are relative velocities in the radial and circumferential directions.

3.2 Turbulence Modelling

In principle the unsteady Navier-Stokes equations give a complete description of the physics of fluid flow. Direct solution of the Navier-Stokes equations for turbulent flow is computationally complex for industrial applications. The solution times are large and the computing capacity needed is beyond the level of most industries.

To counteract this limitation, a practical, engineering solution is incorporated. The time averaged properties of the flow are important to the solution. The details of each individual eddy are not required. CFX solves the problems by modelling the time-averaged effects of turbulence.

This section explains why turbulence models are used and details the strengths of some of the turbulence models available within the code.
Near wall treatments available under the code are also covered.

The final section includes a comparison of results from a centrifugal impeller operating at design flow. This analysis compares important pump design criteria, assessing the relative effects of changing the turbulence model.

3.2.1 Basic Mathematics of Turbulent Flows

For flow within a rotating impeller, the instantaneous velocity is generated by the blade rotation. Superimposed on this periodic fluctuation is the more random fluctuating turbulence Fig.3.2.1.1.

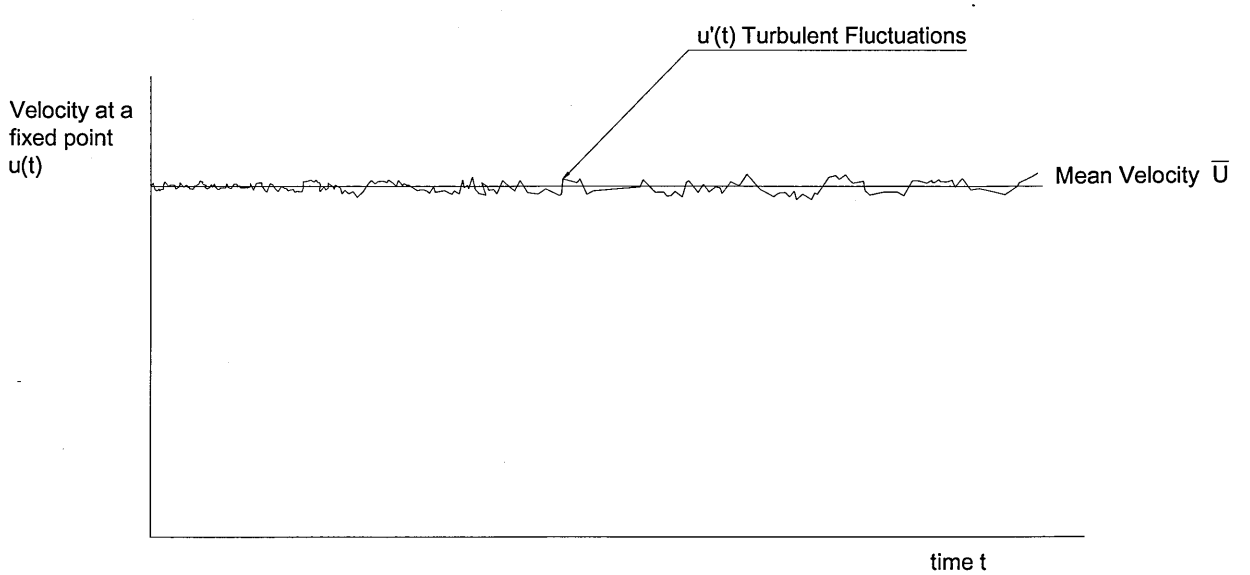

Fig.3.2.1.1 Turbulence Illustration (CFX Tascflow)

The analysis of this problem is simplified by breaking down the velocity at a fixed point into steady, mean and fluctuating components.

This can be written as:

$$u(t) = \bar{u} + u'(t)$$

The mean flow is time averaged and is given as

$$\bar{u} = \frac{1}{t_o}\int_0^{t_0} u\,dt$$

The nature of the turbulence means that both negative and positive fluctuations are likely to occur. The time averaged turbulent component can be written as

$$\bar{u} = \frac{1}{t_o}\int_0^{t_0} u'(t)dt = 0$$

To obtain the mean turbulent flow equations for the combined mean and fluctuating components Reynolds averaging has to be applied as found in CFD textbooks such as Versteeg and Malalasekera (1995).

Considering the 'x' component only for simplification the 2D Navier Stokes Equation is :-

$$u\frac{\partial u}{\partial x} + v\frac{\partial u}{\partial y} = -\frac{1}{\rho}\frac{\partial p}{\partial x} + \nu\left[\frac{\partial^2 u}{\partial x^2} + \frac{\partial^2 u}{\partial y^2}\right]$$

applying the rules of Reynolds averaging the following time averaged instantaneous Navier-Stokes equation can be found after re-arrangement:-

$$\bar{u}\frac{\partial \bar{u}}{\partial x} + \bar{v}\frac{\partial \bar{u}}{\partial y} = -\frac{1}{\rho}\frac{\partial \bar{p}}{\partial x} + \frac{\partial}{\partial x}\left[\nu\frac{\partial \bar{u}}{\partial x} - \overline{u'^2}\right] + \frac{\partial}{\partial y}\left[\nu\frac{\partial \bar{u}}{\partial y} - \overline{u'v'}\right]$$

This is the time-averaged Reynolds Stress Equation for an incompressible fluid. The quantities $\overline{u'^2}$ and $\overline{u'v'}$ are the Reynolds stresses.
The fluctuating instantaneous velocity components have been discarded and the concentration is on the time averaged flow components.
Unfortunately the components now contain the two unknowns due to these Reynold stresses. The appropriate turbulence model is used to predict these stresses.

This project is in no way intended to give a full explanation or derivation of each of the turbulence models available. The intention is only to assess the suitability of the model. Each of the turbulence models within CFX has been compared for a steady state rotating impeller operating at design flow.

3.2.2 Near Wall Treatment of Turbulent Flows

The numerical treatment of the region close to the wall within the computational solution is deemed important in industrial flow problems. This treatment can determine the development of the boundary layer and can influence the onset of separation.

Close to the wall the turbulence is damped and a thin boundary layer exists. This is commonly known as the laminar sub-layer and lies immediately adjacent to the wall. There are strong velocity gradients at the outer part of the near wall region that must be accounted for. The viscous effects must also be accounted for along with the rapid variations in flow across the boundary layer.

To capture this data a fine grid close to the walls must be employed. This increases the solution times and as such is not a favoured industrial approach.

A more popular technique is to employ a semi-empirical function to represent the layer between the wall and the full turbulent flow. This lower cost approach allows coarser grid problems to be evaluated as the wall region does not have to be modelled and the near wall viscous effects do not have to be accounted for in the turbulence model.

3.2.3 Mathematical Wall Treatment

Fig 3.2.3.1 illustrates how the near wall region is treated by CFX software. The standard wall functions within CFX have been replaced with a scalable wall function. This approach is an extension of the wall function approach proposed by Launder and Spalding (1972).

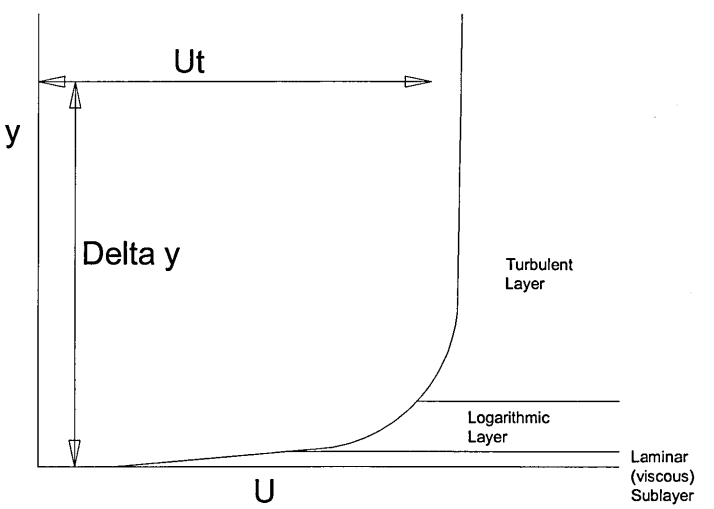

Fig.3.2.3.1 Near Wall Flow (CFX Tascflow)

The near wall tangential velocity is related to the wall shear stress by means of a logarithmic relationship.

$$u^{=} = \frac{1}{k}\ln(y^{+}) + C$$

where

$$u^{+} = \frac{Ut}{u_r}$$

$$y^{+} = \frac{\rho \Delta y u_r}{\mu}$$

$$u_r = \left(\frac{\tau_w}{\rho}\right)^{1/2}$$

y^{+} is the non-dimensional wall distance
τ_{ω} is the wall shear stress
U_r is the tangential velocity to the wall
Δy is the distance from the wall
k is the Von Karmen constant
C is a wall roughness constant

When the tangential velocity approaches zero at separation points the equation becomes singular. This is the main problem with the standard wall function.
This can be overcome by using an alternative

$$u^{*} = c\mu^{1/4}\sqrt{k}$$

This gives the benefit that when the tangential velocity becomes zero it does not go to zero. In turbulent flow k is never truly zero. Based on this definition the following equation for wall shear stress is obtained.

$$\tau_w = \tau_{visc}\frac{y^{*}}{u^{+}}$$

$$\tau_{visc} = \frac{\mu Ut}{\Delta y}$$

$$y^{*} = \frac{\rho u^{*} \Delta y}{\mu}$$

$$u^+ = \frac{1}{k}\ln(y^*) + C$$

One of the problems with the wall function approach is that predictions are dependent on the density of the mesh near the wall. Refining the mesh does not always increase the accuracy of the solutions Grotjans and Menter(1998). The problem of the inconsistencies in the wall function in the case of fine grids can be overcome by using the scalable wall function formulation developed by CFX. It allows the user to carry out consistent grid refinements independent of the Reynolds number of the application.

The premise of the scaleable wall function is to assume that the surface coincides with the edge of the viscous sub-layer which is determined to be y+=11. This is in the region between the logarithmic and linear region wall profile. The computed y+ is not allowed to fall below this limit. All grid points are outside the viscous sub-layer thus avoiding the fine grid inconsistencies.

3.2.3.1 Near Wall Treatment for the $k-\omega$ Based Models

The scalable wall function approach previously demonstrated allows for consistency in grid refinement. This approach is based on physical assumptions that are problematic especially at low Reynolds numbers because the sub-layer is neglected in the underlying mass and momentum equations.

3.2.4 Comparison of Turbulence Models through a Single Impeller Passage

The simplest technique employed for pump CFD analysis is the study of the flow regime through one impeller passage, at the pump design flow, without its collector system. This is computationally inexpensive and solution times are low. The stator, undoubtedly, has an effect on the impeller flow regime when the pump is in operation, but benefits encountered by refining the impeller design through single passage analysis are manifest in the final design.

Managing the flow field from inlet to outlet and presenting the collector with a more uniform flow field can only benefit the machine. The choice of grid density and turbulence model is perceived to have an effect on the quality of the solution and the time taken to solve the problem.

The following models were compared using a single impeller passage at design flow.

1. $k-\varepsilon$
2. $k-\varepsilon ASM$
3. $k-\varepsilon RNG$
4. $k-\varepsilon$ With a scaleable wall function
5. $k-\varepsilon ASM$ With a scaleable wall function
6. $k-\varepsilon RNG$ With a scaleable wall function
7. $k-\omega$
8. $k-\omega SST$

The following Design Parameters were compared:

1. Outlet tangential velocity distribution, hub to shroud
2. Outlet radial velocity distribution, hub to shroud
3. Average Pressure inlet to outlet
4. Velocity U inlet to outlet
5. Velocity V inlet to outlet
6. Velocity W inlet to outlet
7. Tangential velocity inlet to outlet along streamline
8. Radial velocity inlet to outlet along streamline

Fig.3.2.4.2-Fig.3.2.4.9 contains comparisons of these design parameters. Although these comparisons are taken at design flow through a single centrifugal pump passage the geometry is purposefully 2 dimensional. The blades have no rake effect from hub to shroud.

Figure 3.2.4.1 illustrates the 2D nature of the impeller analysed for this problem.

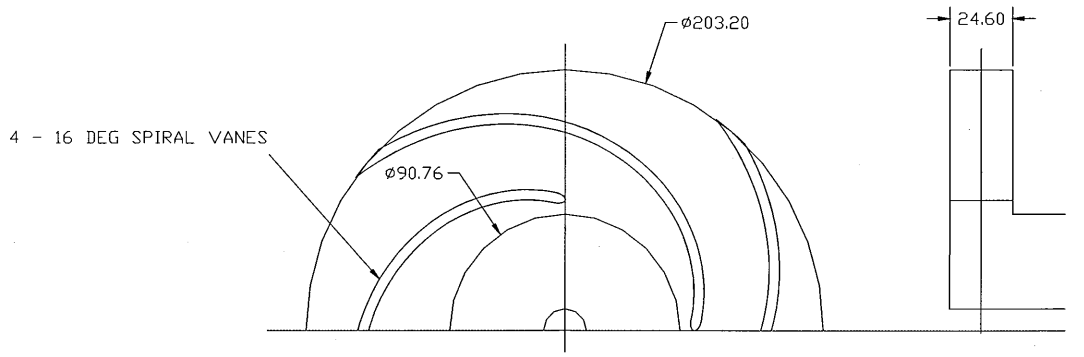

Fig3.2.4.1 Test Case Geometry for Turbulence Model Evaluation

The graphs compare data important in the design of a pump impeller.
In each case the effect of the turbulence model on the important design values of each solution is considered to be small.

Fig 3.2.4.2 contains 3 plots. The first plot compares the tangential velocity component across the impeller outlet from hub to shroud. Qualitatively the shape of the velocity profile differs little with turbulence model. The effect of the impeller side wall boundary is notably consistent in all models. The second graph for this figure is more illustrative of the difference apparent due to turbulence model. Taking the K-Epsilon model as the baseline there is no difference between this baseline and the K-Epsilon RNG model.

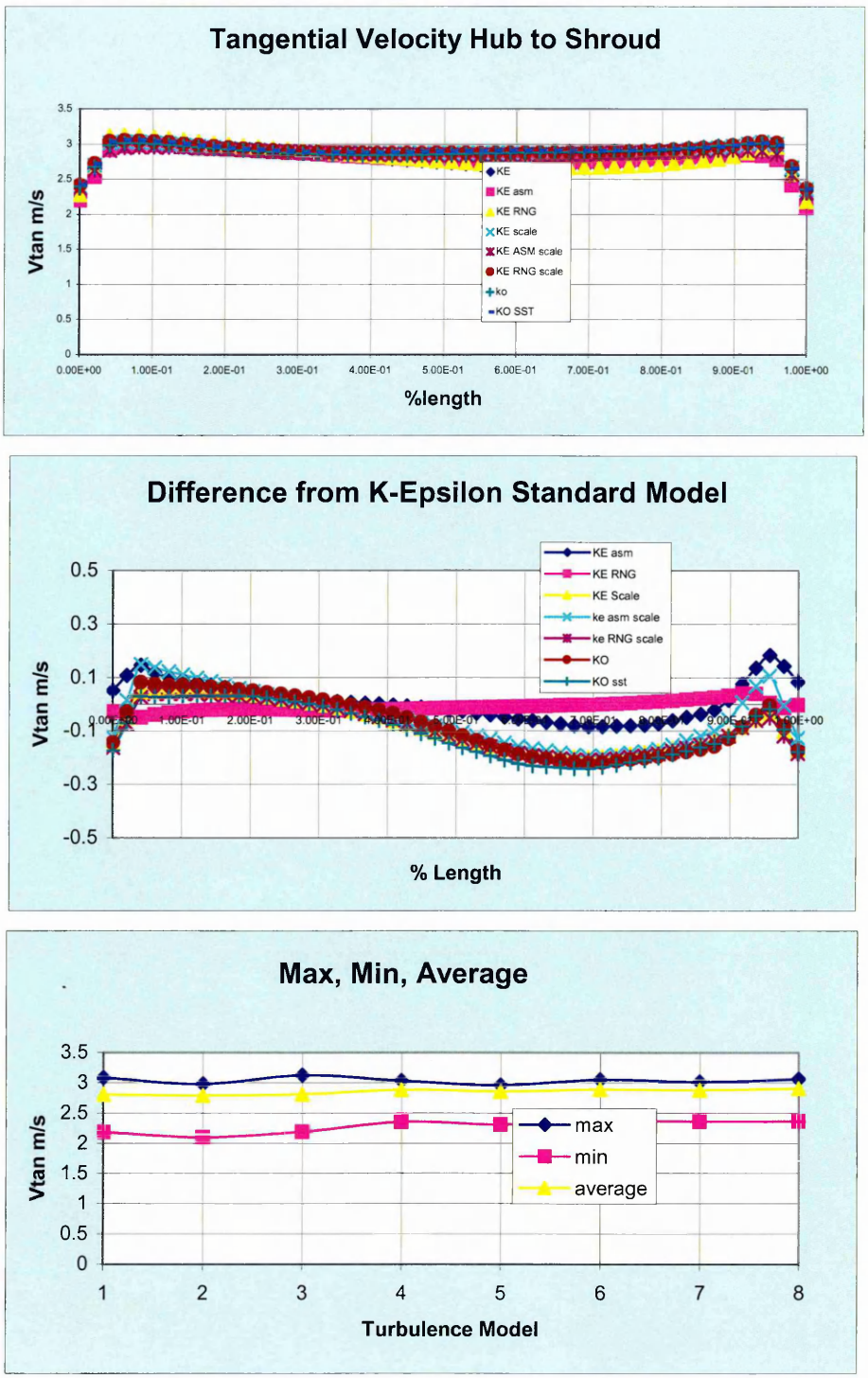

Fig.3.2.4.2 Tangential Velocity Hub-Shroud

The application of the scalable wall function to the model causes a decrease in the tangential velocity away from the boundary wall in the free stream. This deviation approaches 5% of the total velocity.
To quantify the absolute values graph the third graph is used to compare the maximum, minimum and average velocities. Average velocities remain

consistent with small changes in maximum velocity being mirrored by equal changes in minimum velocity.

Figure 3.2.4.3 contains an analysis of the radial velocity from hub to shroud and presents results similar to those of the previous figure. Deviations remain within 5% and the average radial velocity for all turbulence models.

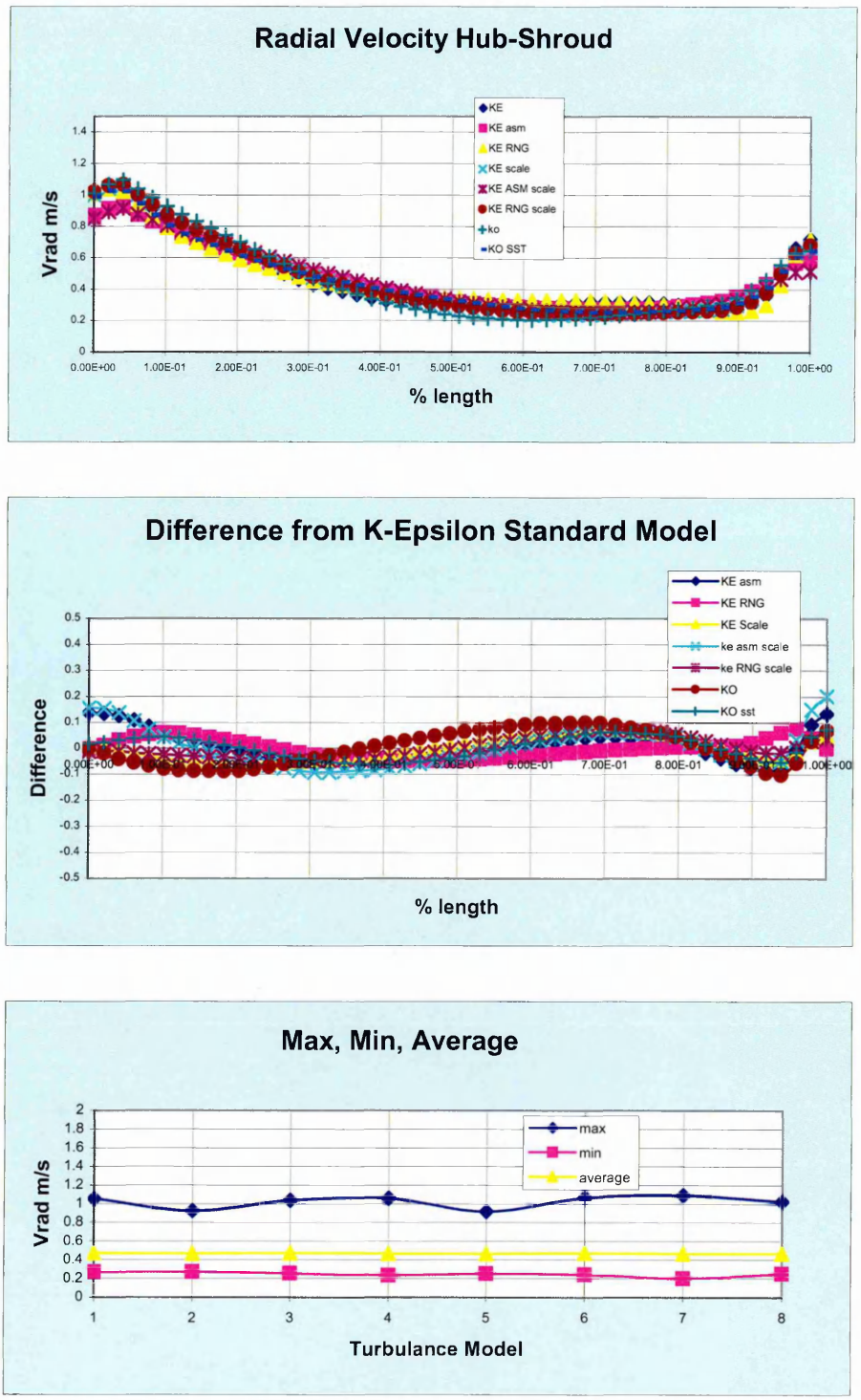

Fig.3.2.4.3 Radial Velocity Hub-Shroud

As the main focus of the research will be pressure development through the pump it is interesting to ascertain the differences in pressure development for each turbulence model as illustrated in Figure 3.2.4.4.

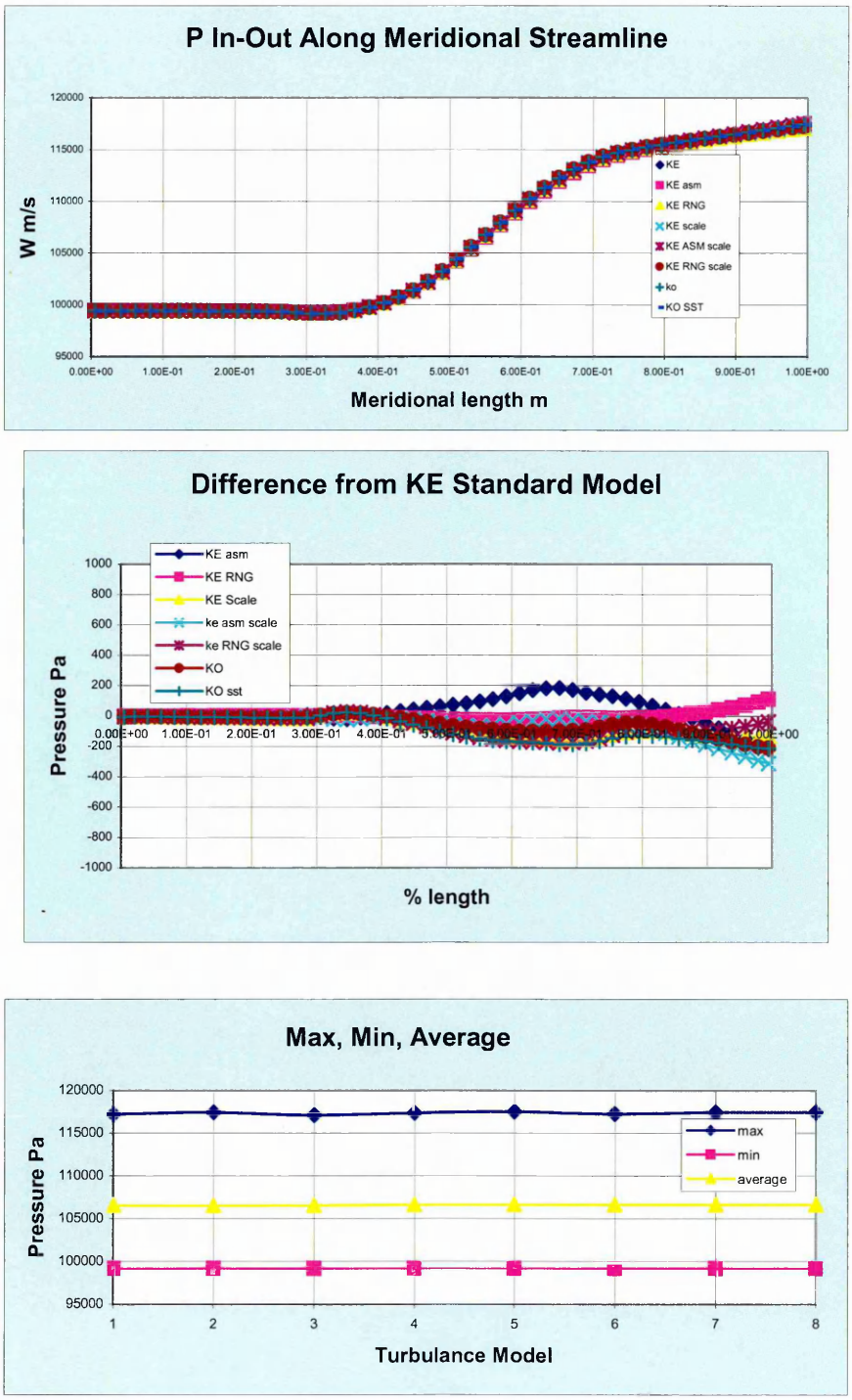

Fig.3.2.4.4 Average Pressure Inlet – Outlet

Along the meridional streamline the shape of the pressure development plot is consistent. Comparisons of the deviations from the K-Epsilon model indicated that prior to the blade inlet the turbulence model has no effect. The turbulence model effect on the blade is 200Pa through the blade passage. There is a stronger influence once the fluid has left the zone of blade influence with the ko model accounting for a deviation of 325Pa. The third graph illustrates maximum, minimum and average pressure development independent of turbulence model.

Figures 3.2.4.5 – Figure 3.2.4.9 takes a view of the velocity development through the domain along the massage streamline from inlet to outlet for the turbulence models. All these figures demonstrate small deviations from the K-epsilon model away from the influence of the impeller blade. In each case there is a consistency independent of turbulence model for maximum, minimum and average values.

Qualitatively all the velocity and pressure profiles through the impeller follow the same pattern with only small differences appearing at the impeller exit far away from the wake.

Although this is a limited study and gives a crude assessment of the influence of the turbulence models available there is little reason to doubt the perceived wisdom that the turbulence models have little significant effect on the important design parameters used within impeller design. As such the k-epsilon turbulence model with scaleable wall function was chosen to continue this study. It is considered to be the most robust of the turbulence models available and was also used by Newton (1998), in his study of a centrifugal fan operating at closed valve, after evaluation against the k-epsilon RNG model.

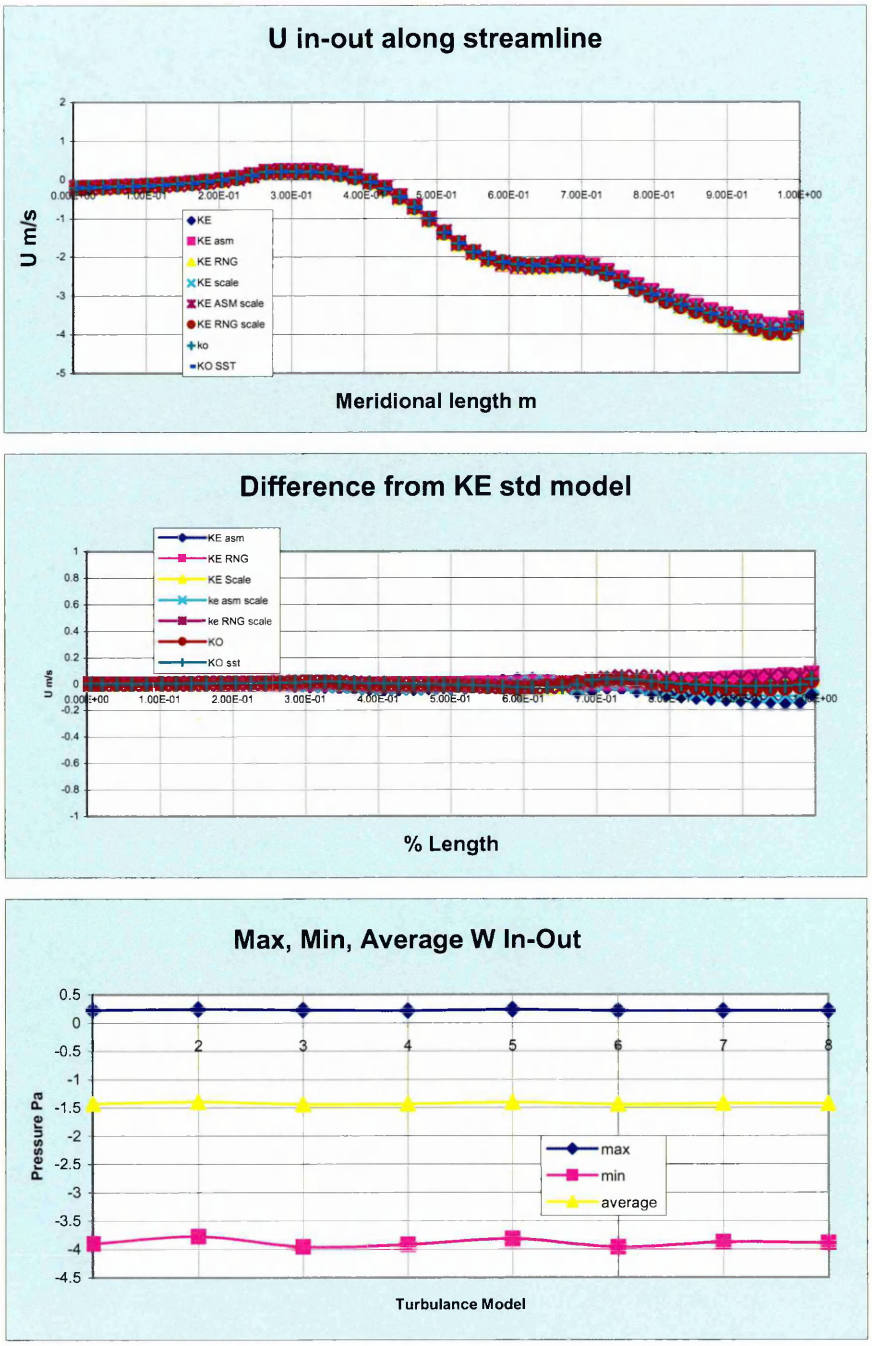

Fig.3.2.4.5 Velocity U inlet -Outlet

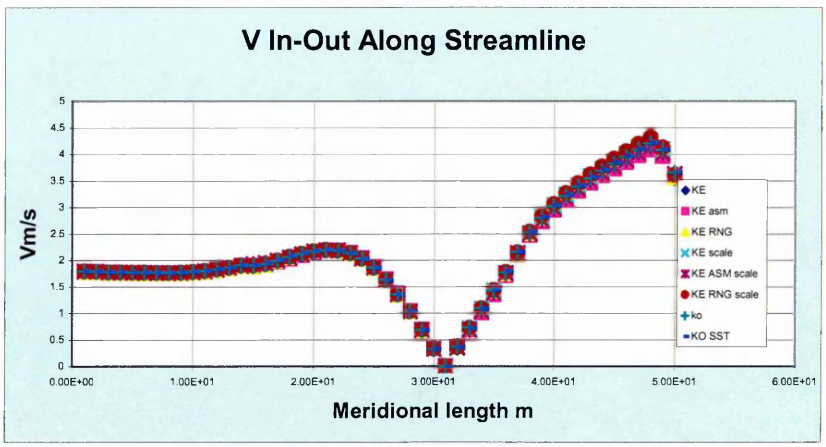

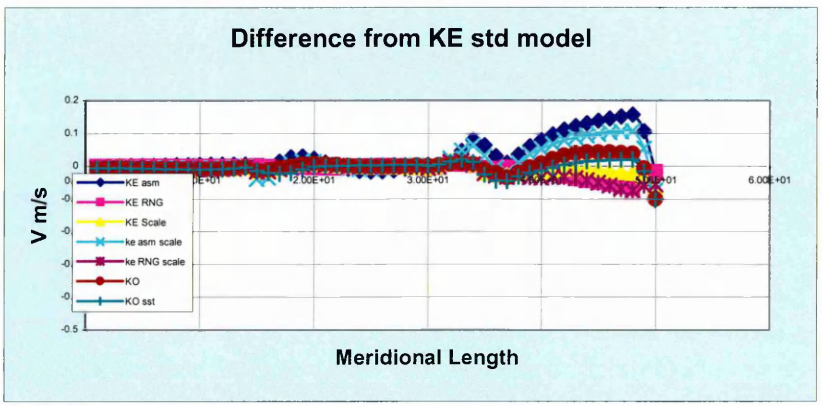

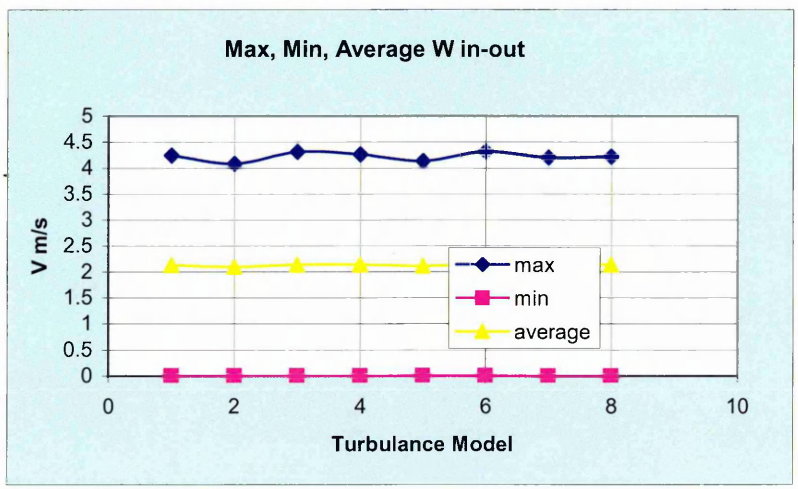

Fig.3.2.4.6 Velocity V inlet -Outlet

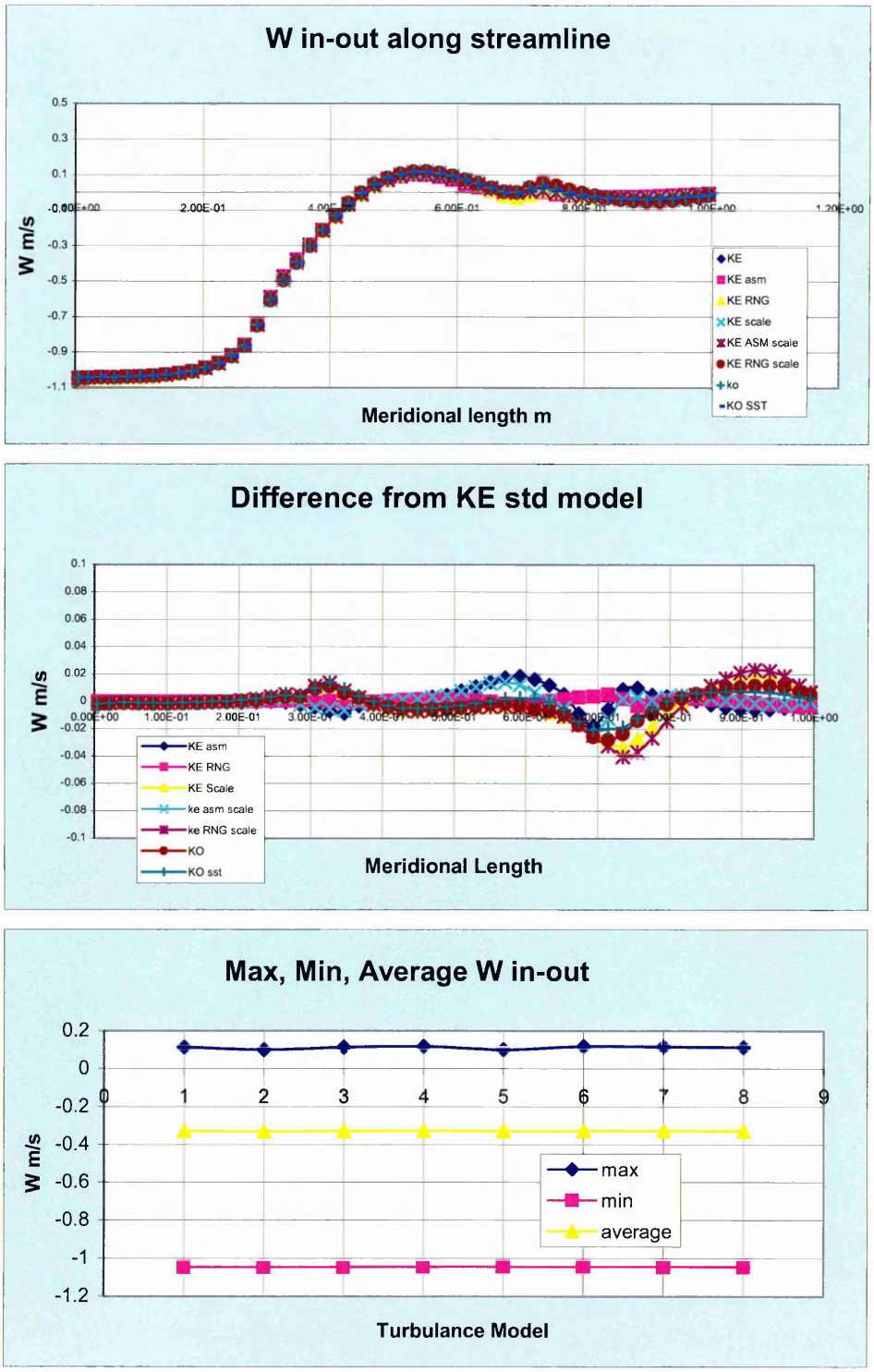

Fig.3.2.4.7 Velocity W Inlet -Outlet

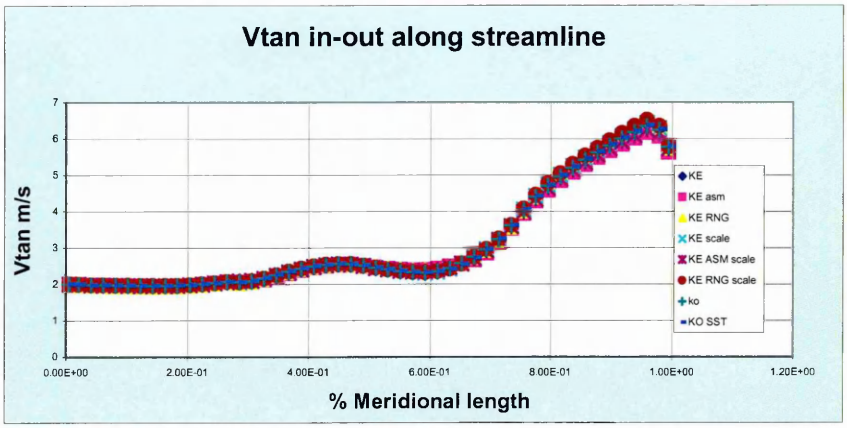

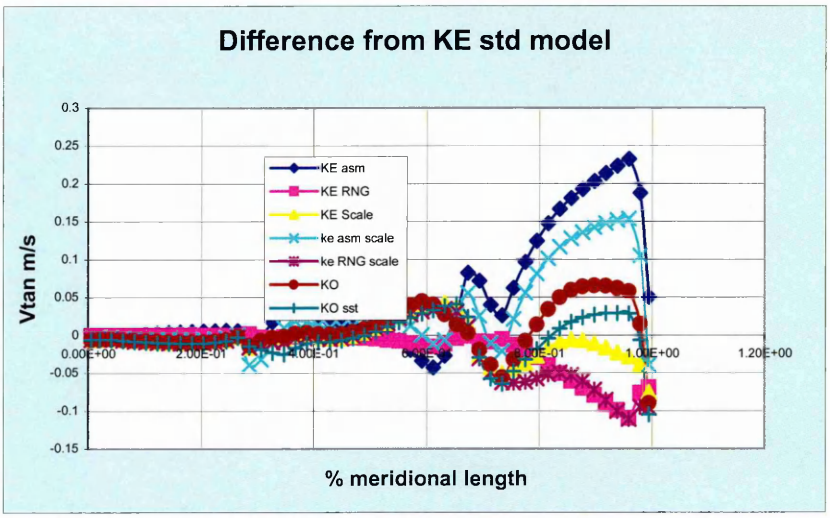

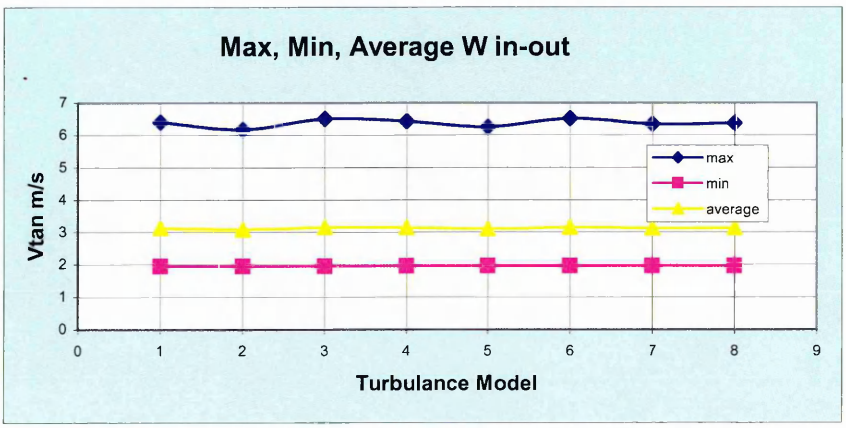

Fig.3.2.4.8 Tangential Velocity Inlet- Outlet

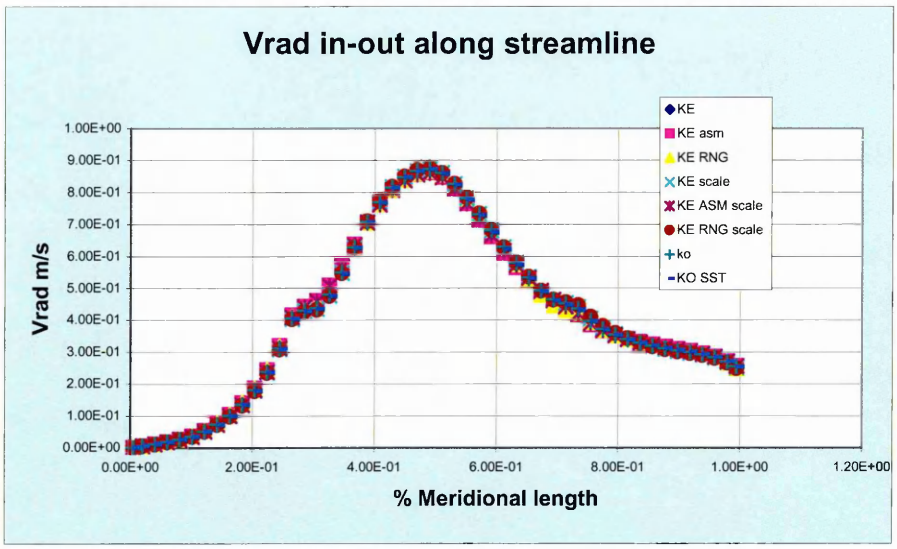

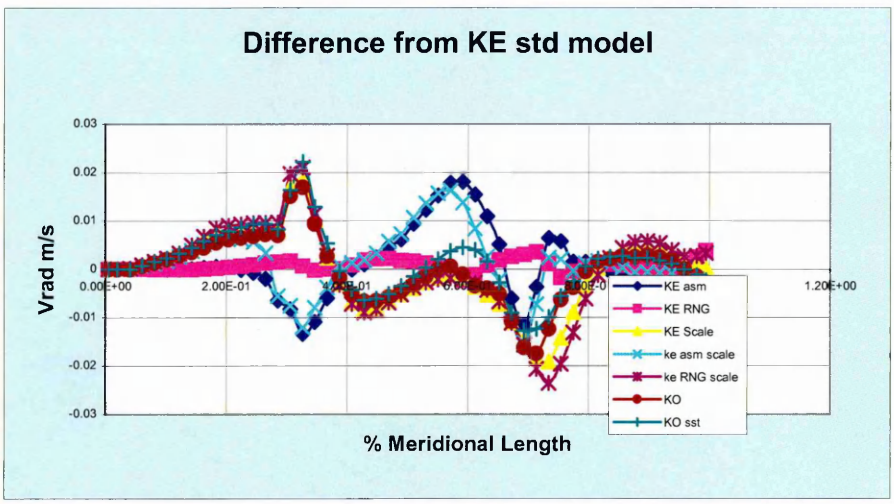

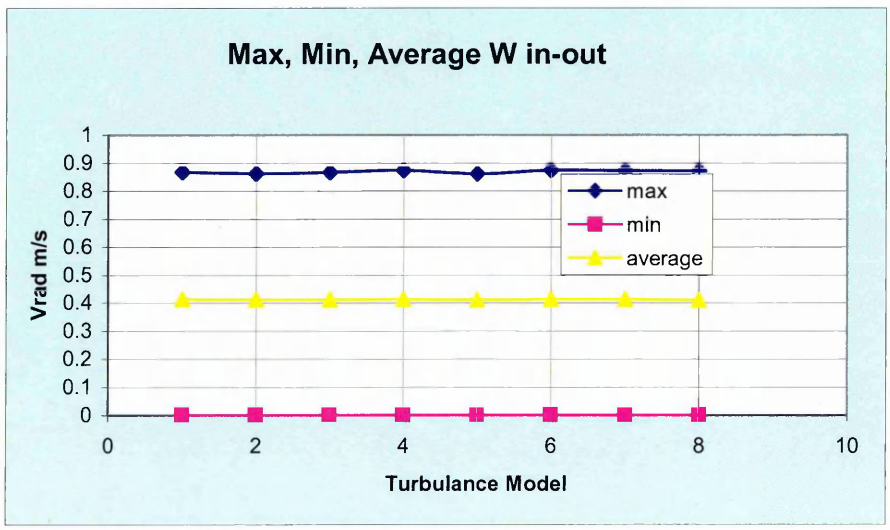

Fig.3.2.4.9 Radial Velocity Inlet- Outlet

3.3 Grid Sensitivity

Within the Tascflow/CFX codes a number of options are available which can have an effect on the validity of the solution.
Of primary consideration in this section is the evaluation of the effect of grid density on the solution accuracy. There is no doubt from the theory or the research that CFD predicts accurately the flow parameters. An evaluation is needed to ascertain if the density of the grid within the impeller can cause errors in the solution.

A further consideration must be given to the schemes within the code which take account of the fluid being passed between rotor and stator. An incorrect choice of scheme in this case could have a dramatic effect on the solution viability.

3.3.1. Impeller Geometry

The impeller used for this sensitivity study is pictured in Fig 3.4.1.1. The impeller is typical of a radial machine. It is a shrouded 6 blade design with an outlet angle of 28 degrees and a varying inlet angle across the blade to match the design incidence condition. The inlet diameter on the front shroud is 90mm whilst the outlet diameter is 222mm.

The impeller is designed to run in a volute at 2980rpm at a design flow of 112m3/hr.

3.3.2 Grid Particulars

One issue, previously mentioned in Section 3.2, relates to the controlled refinement of grid mesh. It is important to consider the method of refinement when changing the grid density

For all the cases the scaleable wall function described in the previous section was used to provide a controllable method for consistent refinement of the grid density. This takes away from the problem the issues related to controlling the y+ values.

The wall-function approach in CFX-TASCflow is an extension of the method of Launder and Spalding (1974). The near wall tangential velocity is related to the wall-shear-stress by means of a logarithmic relation.

One of the major drawbacks of the wall-function approach is that the predictions depend on the location of the point nearest to the wall and are sensitive to the near-wall meshing; refining the mesh does not necessarily give a unique solution of increasing accuracy Grotjans and Menter (1998).

The problem of inconsistencies in the wall-function in cases of fine grids can be overcome with the use of the *scaleable* wall-function formulation developed by CFX. It can be applied on arbitrarily fine grids and allows the

user to perform a consistent grid refinement independent of the Reynolds number of the application.

The scaleable wall-function approach assumes that the surface coincides with the edge of the viscous sub-layer. This sub-layer is defined to be at y+=11. This is the intersection between the logarithmic and the linear near wall profile. The computed y+ is not allowed to fall below this limit. Therefore, all grid points are outside the viscous sub-layer and all grid inconsistencies are avoided. A more detailed explanation of the development of the scalable wall function approach is available in the CFX Tascflow Theory documentation.

The simplest case of a single impeller blade running without a volute is considered. This allows the analysis to be simplified as each blade passage undergoes a steady flow regime with each blade passage experiencing the same flow phenomenon.

The generated grids are pictured in Fig.3.3.2.1 for densities 10000, 50000 and 100000.

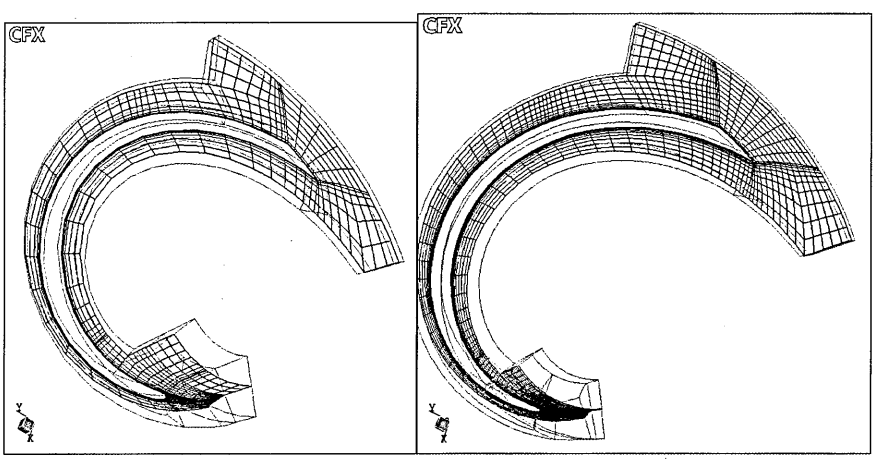

10000 Node Grid 50000 Node Grid

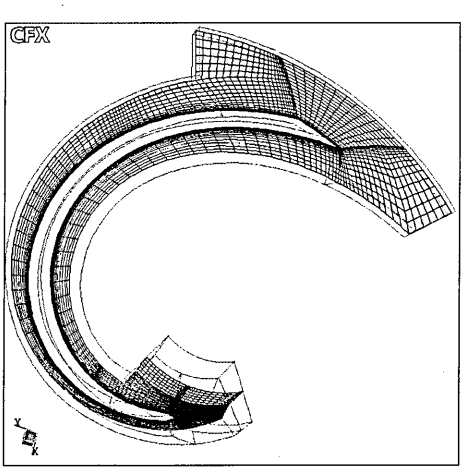

100000 Node Grid

Fig 3.3.2.1 Grid for Sensitivity Study

The flow into the impeller inlet is assumed to be axial. For the test case the following boundary conditions were applied to the periodic surface ABCD:

Pressure = 20000Pa

Although this is a reasonable condition for the suction of the pump, in this case it makes little difference to the final analysis we are ultimately interested in differential pressure.

The discharge boundary conditions are set at EFGH:

Flow = 18.66m3/hr

This is the total machine flow divided by the number of flow channels within the impeller.

Periodic boundaries are assigned along the centre of the impeller flow passages. Fig 3.3.2.2 illustrates both the boundary condition regions for inlet and outlet and the periodic boundaries between impeller passages.

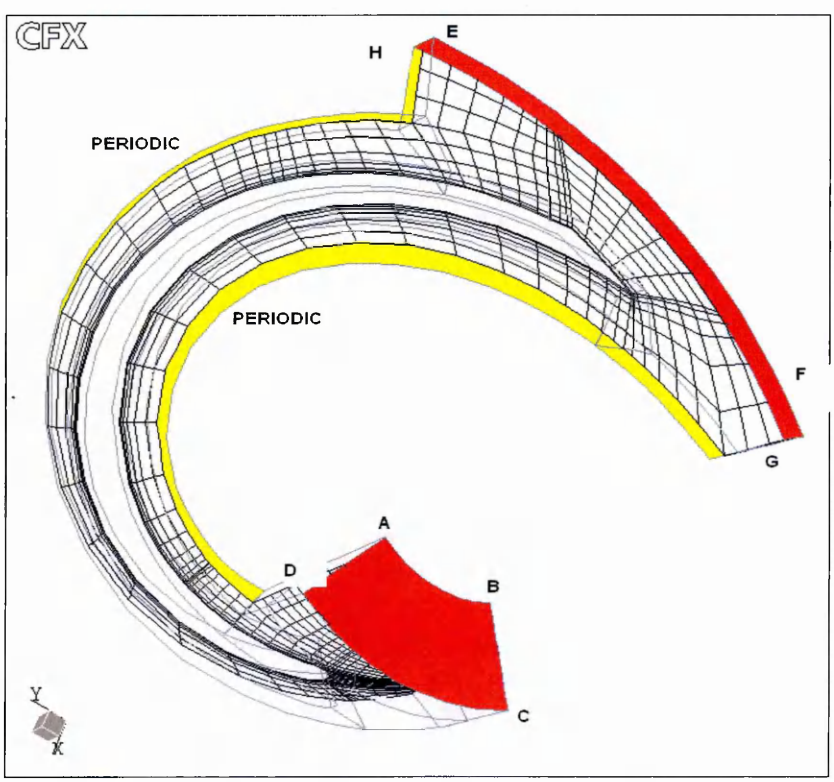

Fig 3.3.2.2 Grid Boundaries and Periodic

For the sensitivity study this mesh is considered suitable as it has a uniform distribution of elements, periodic boundaries are assigned to simplify the solution, the element distortion limits are set to a maximum of 20degrees. It is desirable that the mesh elements retain a rectangular shape throughout the refinement process.

3.3.3 Comparison of Results

The flow distribution in the impeller meridional plane is non uniform and dominated by turning the flow from axial to radial. This span-wise non-uniform velocity distribution has an effect on the blade design.

The derivation of the impeller blade angles and the meridional profiles is traditionally based on empirical analysis of successful designs and estimation of averaged through-flow velocities. This inlet span-wise meridional velocity distribution is important to the pump designer in refining his blade inlet angles. 2D methods cannot capture 3D and the boundary layer effects.

Fig.3.3.3.1 demonstrates the effect of grid density on the meridional velocity distribution. Grid density at inlet has little effect on the span-wise meridional velocity. Estimates of incidence and effect of thickness profiles can be gauged by low-density grids with rapid solution times.

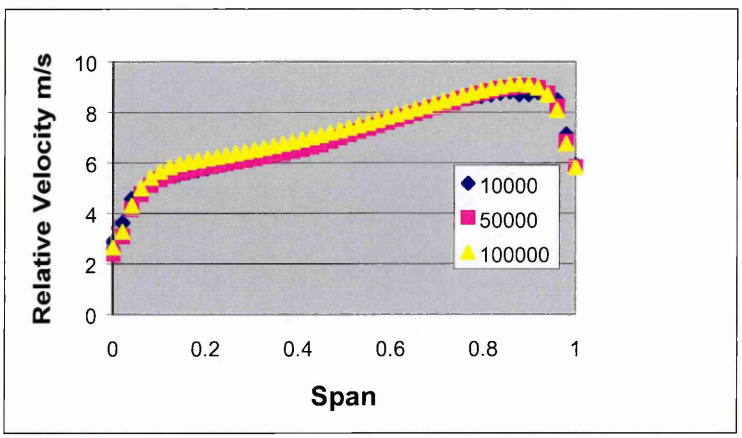

Fig.3.3.3.1 Comparison of Inlet Meridional Velocity Distribution for Varying Grid Densities

It is also important to the designer to have control over the velocity distribution at the impeller outlet. This presents the pump collector with a more uniform velocity field. This can increase machine efficiency and lower vibration levels. Fig 3.3.3.2 compares the meridional outlet velocity distribution for different grid densities.

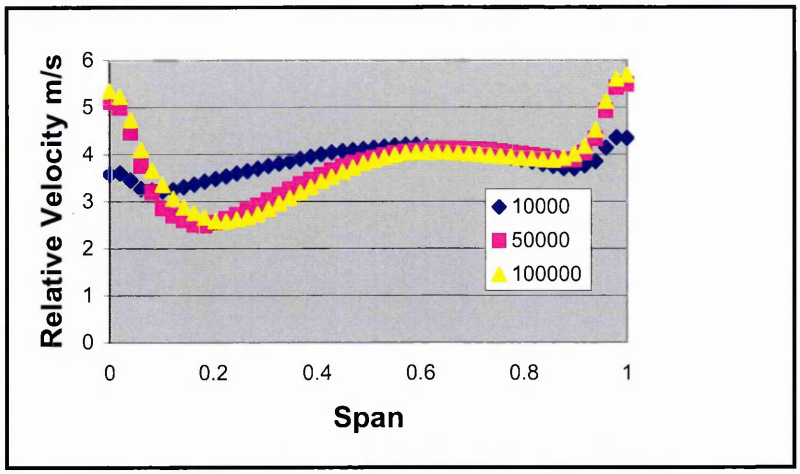

Fig.3.3.3.2 Comparison of Outlet Meridional Velocity Distribution for Varying Grid Densities

As the grid is spread out in the radial direction the solution becomes less accurate. At its least dense, at the impeller outlet, the coarse grid does not capture the true meridional velocity profile. There is little difference between the 50000 and 100000 node grids.

Stream-wise, the designer is looking to smooth away any non-uniformity in the velocity distribution. High incidence or disturbance at the pump inlet is manifest in a disturbed mid-passage mixing loss on the pressure side of the blade. This type of velocity distribution, once started, is difficult to recover later in the passage.
Other fields of interest to the pump designer are listed in the table in fig 3.3.3.3 for different grid densities.

	10000	50000	100000
CIRCUMFRENTIAL AREA AVERAGED MERIDIONAL VELOCITY (INLET)	7.068	7.011	7.064
CIRCUMFRENTIAL AREA AVERAGED MERIDIONAL VELOCITY (OUTLET)	4.13	4.22	4.26
HEADRISE THROUGH IMPELLER (INLET-OUTLET)	151m	151.6m	152.1m
RELATIVE FLOW ANGLE OUTLET	11deg	10deg	10.5deg

Fig.3.3.3.3 Comparison of Important Design Values for Varying Grid Densities

For all the above cases the scaleable wall function described was used to provide a controllable method for consistent refinement of the grid density.

3.4 Impeller-Stator Simulations

Whenever sets of blade rows run relative to one another there is an unsteady interaction between the blades. In fact for a pump to function it is unavoidable that this unsteady behaviour takes place Deans (1959). The difficulty for a CFD solution lies with handling this unsteady interaction. Within the CFD codes three distinct schemes are available to solve the problem.

3.4.1 Geometry

The impeller geometry used is as stated in Fig 3.4.1.1. This geometry is used with the diffuser geometry pictured in Fig 3.4.1.2.

The diffuser contains 10 stationary vanes designed to accept the b.e.p flow from the impeller. The diffuser's inlet angle is arranged to match the average absolute flow angle from the impeller blades.

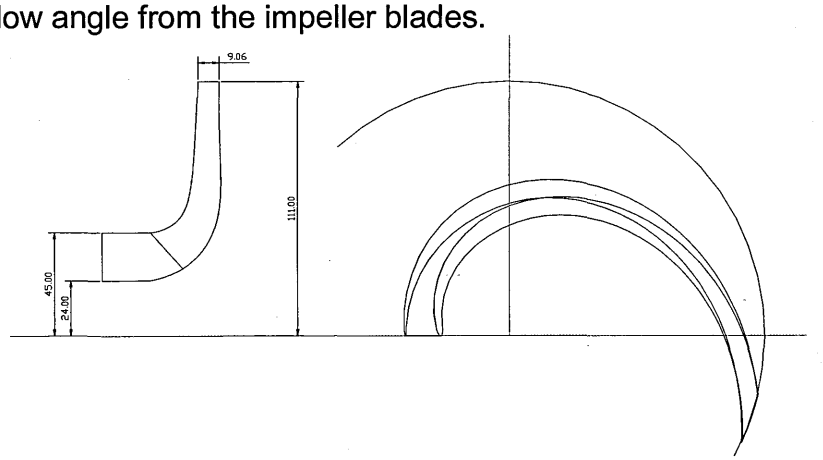

Fig 3.4.1.1 Impeller Geometry for Grid Sensitivity Study

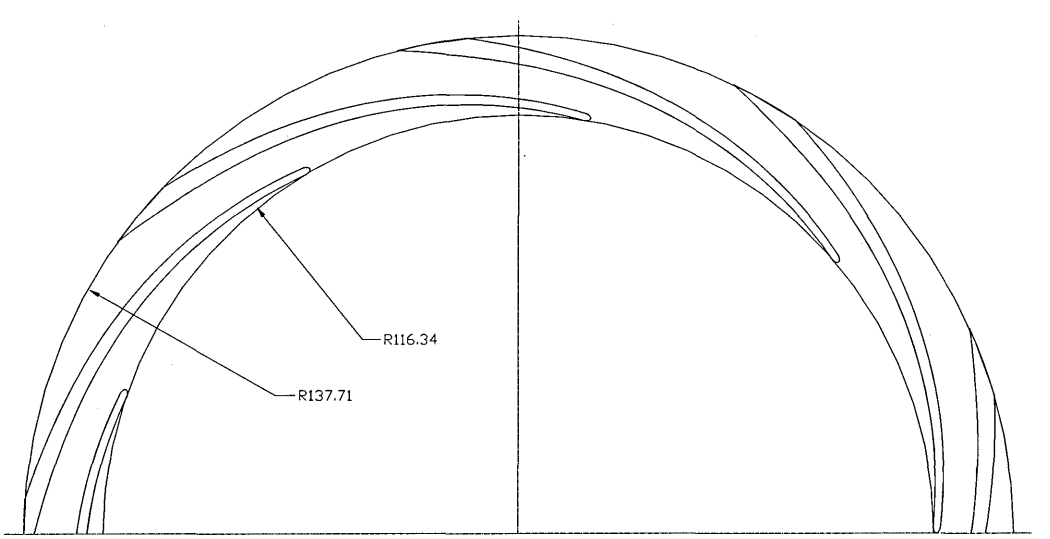

Fig 3.4.1.2. Diffuser Geometry

3.4.2 Stage Interface

The simplest computational solution is to employ circumferential averaging to the unsteady interactions. This presents the stator with a time averaged velocity pattern. The stage calculation was developed by Denton and implemented within CFX Tascflow by Galpin.

Stage calculations require a mixing plane midway between the stationary and rotating components. This simulates the steady state interaction between the impeller and stator components in the pump. Each component is calculated in its own frame of reference. Blade numbers can be reduced with periodic boundaries.

The scheme will accommodate pitch variance. Since designers tend to use unequal multiples of blades on the rotor and stator it is not necessary to model more than one rotating channel and one stator channel.

It is difficult to solve Stage problems for the Rotor-Stator without some compromise on geometry. Pump design methods require the design to be fixed at the impeller maximum diameter. This, when carried through to the computational problem means the impeller blades run close to the diffuser blades.

The stage interface works effectively when relative space between the components is large enough for the velocity profile of the rotating component to mix out before entering the stationary collector. This is not the case with impeller diffuser pump interaction. The strong unsteady rotor-stator effects and the large circumferential differences in velocity cause convergence stall or failure.

To allow the solution to converge to a satisfactory level the impeller geometry should be modified. The diameter should be reduced by a minimum of 7% and the stage interface positioned centrally between the components. The boundary conditions should be modified according to the affinity laws.

This reduction in diameter causes some problems with the validity of the analysis. Typically the impeller of a pump can be physically reduced by a maximum of 15%. With such a large gap between the impeller and diffuser the span-wise solution does not represent the true situation

Despite this the solution is still instructive as a design tool. The data is easy to associate with the diffuser geometry. The circumferential averaging allows the diffuser incidence and diffusion rate to be assessed irrespective of the pitch effect. Fig 3.4.2.1 contains an illustration of the velocity vectors for the Stage interface for an impeller-diffuser simulation.

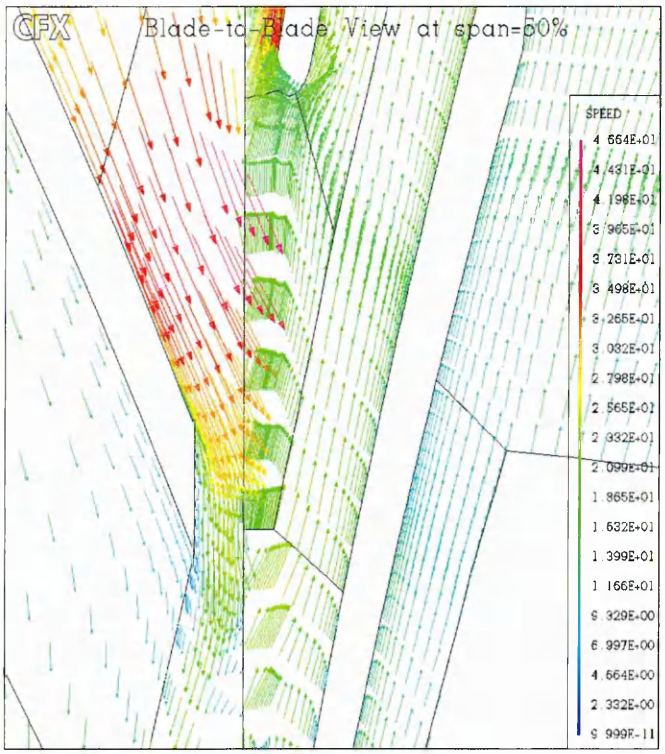

Fig.3.4.2.1 Illustration of Velocity Vectors for Stage Interface for Impeller Diffuser Simulation

3.4.3 Frozen Rotor

The frozen rotor scheme is used to predict the steady state flow between the rotor and stator. The relative position of the rotor to the stator is frozen in time. In this way the solution provides a snapshot of the flow regime.

For this type of solution to be instructive it its necessary to take care with the blade passage pitch arrangements. An equal circumferential interface length is required and it is prudent to model more than one stator passage to try to capture the pitch effects.

The solution for the frozen rotor when applied to the maximum impeller diameter running at a close clearance to the diffuser has few problems; although the convergence is slow, there is no stalling effect

With the frozen rotor interface the designer is free to make his own assessment of incidence and diffusion but the picture is complicated by the rotor-stator pitch differences. In Fig 3.4.3.1 the model is configured so the effect of the rotor blade relative to the stator blades can be judged for three positions from one solution.

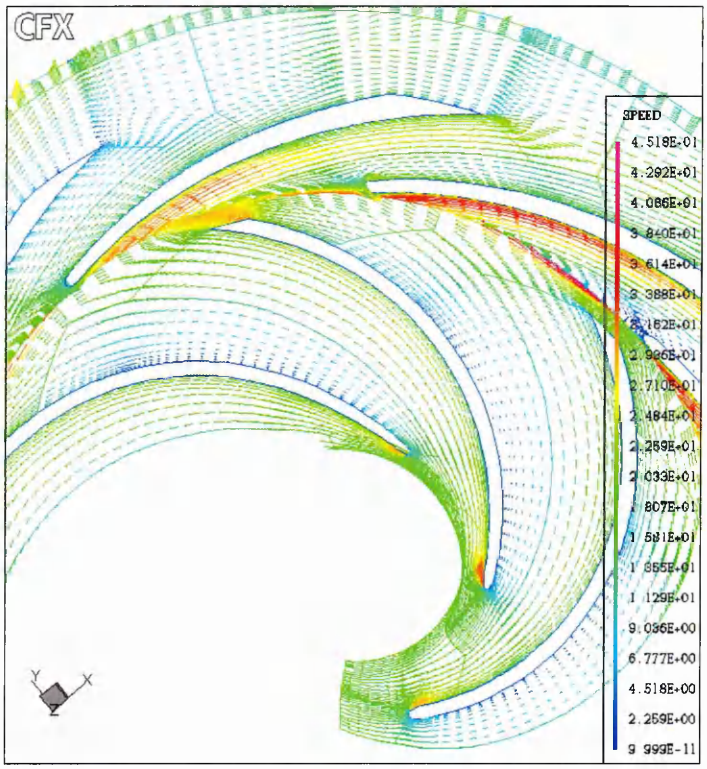

Fig.3.4.3.1 Illustration of Velocity Vectors for Frozen Rotor Interface for Impeller Diffuser Simulation

One impeller blade is set central to the diffuser passage. Two further blades are modelled, one just leaving the diffuser tip, the other approaching the diffuser tip. In this way only one solution captures the flow regime at different relative positions. The blade number ratio determines this configuration and this type of solution is not always possible without compromise.

3.4.4 Fully Transient Solution

This scheme involves the solution of multiple problems based on the varying pitch positions. It provides the ultimate solution accounting for all interaction effects between components of differing relative motion. This type of solution scheme requires large computational resources in terms of processing and disc space. The solution times are large for the routine design environment.

Modelling of all the impeller and diffuser passages is required. Pump impeller/diffuser problems have inherent pitch variance, designed in to lower vibration levels. Simplification of the scheme by geometry modifications to model one-one pitch ratios will affect the validity of the solution.

3.4.5 Unsteady Interactions

The solution of the closed valve head problem depends on choosing the correct scheme to handle the interaction between rotor and stator. The previous experimental data from Newton suggests that the relationship between the phase positions of the impeller blade with respect to the stator blade has an influence on the pressure field within both the impeller and collector. Fig 3.4.5.1. Illustrates the unsteady pressure at closed valve

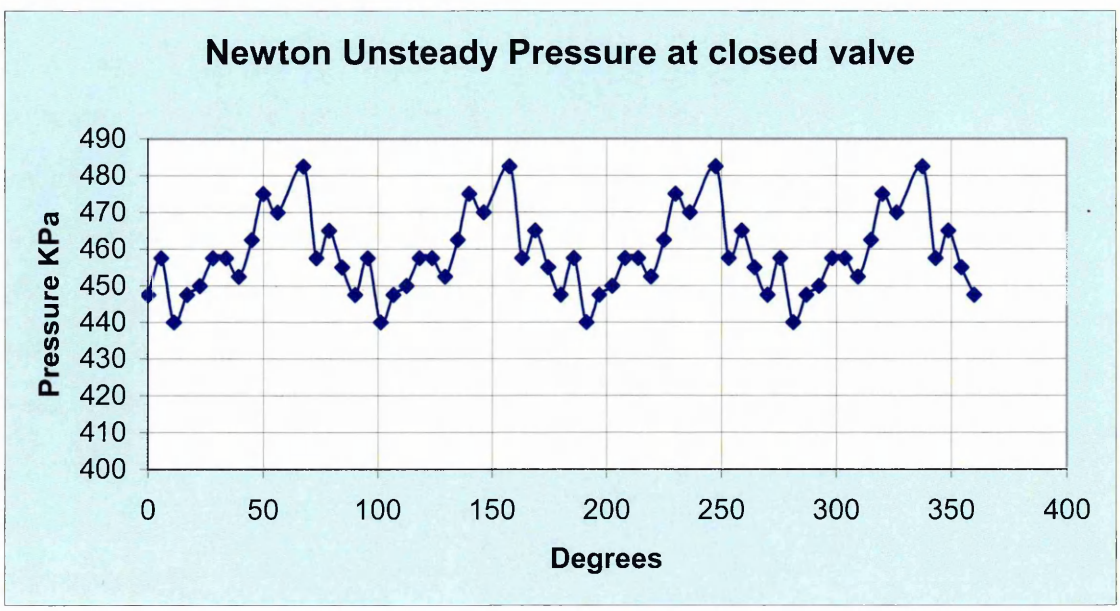

Fig.3.4.5.1 Unsteady Pressure at Closed Valve

Further to this, work by Fraser (1991), Palgrave (1985) points towards the existence of a flow field within the suction channel and associated pipe-work of the pump. This is also related to the phase position of the impeller blade particularly if a suction splitter is incorporated within the pump or piping design.

Examination of the deviations from the average velocity from the experimental pump investigations by Newton suggests that the only scheme suitable for the simulation is the Transient Solution.

A transient rotor stator interface is assigned at outlet from the impeller into the stator/diffuser and a further Transient interface is assigned at the impeller inlet where it joins to the suction pipe-work. Comparisons in Fig.3.4.5.2 show the deviations from the average velocity and Pressure shown in the Newton Experimental Pump.

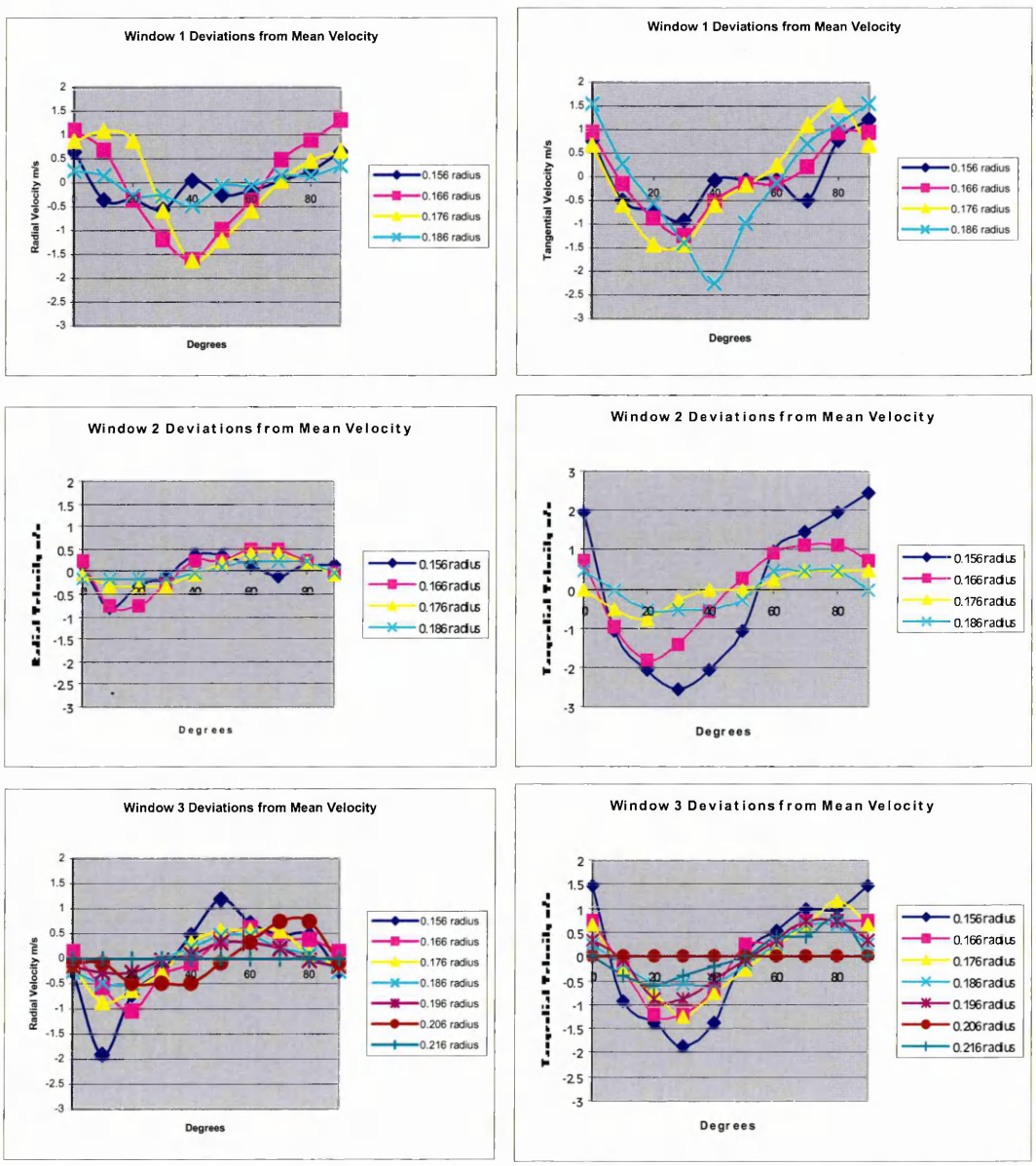

Fig.3.4.5.2 Deviations from Average Velocity and Pressure from Newton Pump

From this analysis we can conclude that the transient Rotor-Stator interface must be used to account for the unsteady interaction at the suction duct to impeller and the impeller to casing.

3.5 Comparison with Experimental Data

To evaluate the code's ability to predict the performance of a centrifugal pump an "on-design" solution was compared with the experimental data obtained by Miner (1989). Miner's work centred on the comparison of potential theory with LDA measurements within both volute and impeller. Fig 3.5.1 illustrates the pump used by Miner for his experiments and the positions of the experimental windows.

Four positions were analysed along the centre of the impeller at different radii.

- Position 1 –2.5" radii
- Position 2 - 3.0" radii
- Position 3 – 3.5" radii
- Position 4 – 3.88" radii

Axial positions at differing radii in the volute were also analysed

- Position 1 –4.05" radii
- Position 2 - 5.01" radii
- Position 3 – 5.4" radii

In this study the grid sensitivity was at its least refined in the span-wise direction conforming to a ratio less that that experienced in the following section that is attributed to the axial density at 10000 nodes. For the purpose of the final analysis a refinement in the span-wise direction associated with a grid density of at least 50000 nodes was used. In this way the effects of grid sensitivity are minimised.

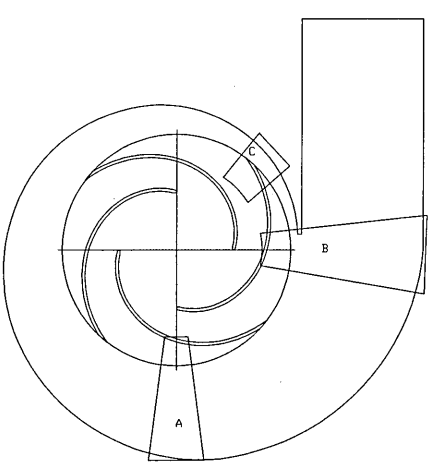

Fig.3.5.1 Miner Pump Illustration

3.5.1 Grid Generation

To begin an analysis of the pump, it is necessary to construct 3D models and grids for the casing and impeller.

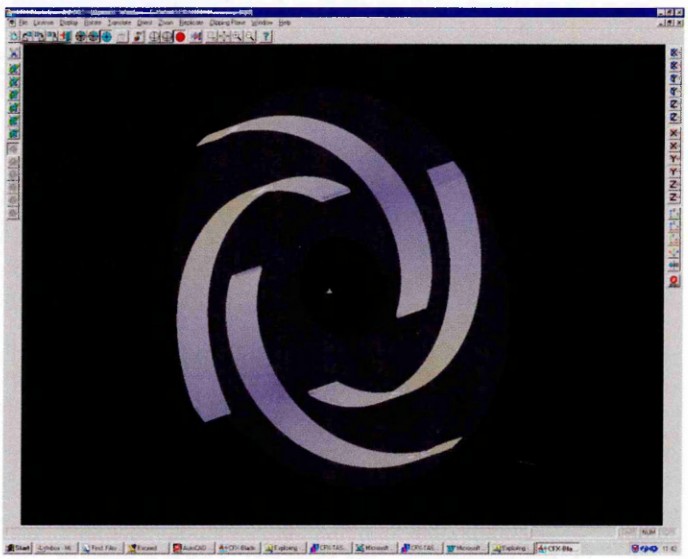

Fig 3.5.1.1 3D Model of Impeller

A 10000-node per channel course grid has been developed for the impeller using CFX Turbogrid.

The volute design has been modelled using Solidworks Modelling tools and imported into CFX Build to allow Meshing to take place. The sliding mesh interface was placed mid-way between impeller and casing clearance.

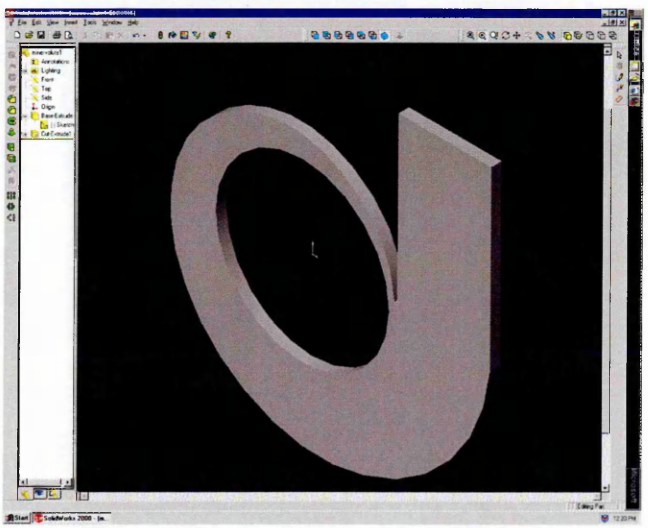

Fig 3.5.1.2 Solidworks Volute Model

This type of casing configuration is difficult to model and mesh and as such a technique was developed, breaking down the model in to simpler components, meshing and gluing the various elements back together using the Tasctool commands.

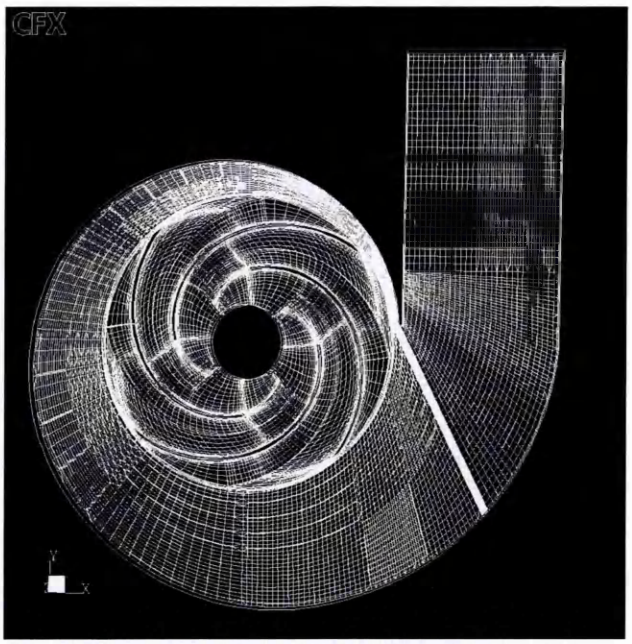

Fig 3.5.1.3 Grid Representation

This method allows easy checking for skewness due to the rectangular nature of individual meshed elements.

The impeller skewness was limited to 25degrees. This was achieved by iterating the configuration of the grid using the CFX Turbogrid tool. Negative volumes were also eliminated using this tool.

3.5.2 Evaluation of Results

Fig.3.5.2.1-fig.3.5.2.9 contains the graphical comparisons through the Miner pump with a CFD solution. The comparison to experimental data is reasonable through the impeller for the unsteady analysis. The sensitivity to the grid is demonstrated by the poor results span-wise.

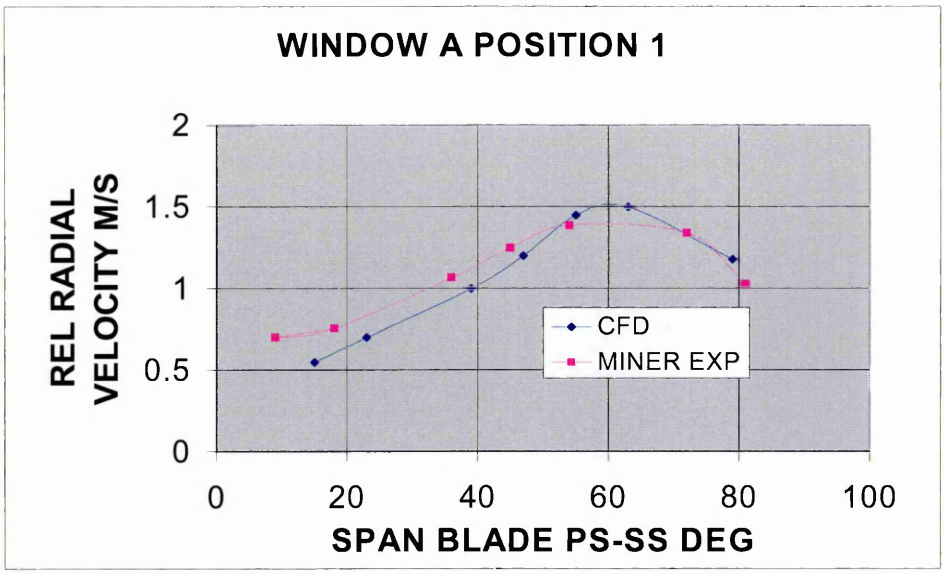

Fig.3.5.2.1 Passage Averaged Radial Velocity across Volute Window A Position 1

Figure 3.5.2.1 illustrates the radial velocity comparisons between the Miner Experimental Pump and the CFX Tascflow simulation. There is reasonable agreement between the velocity profile of the two curves. The differences between the two curves, although appearing small, are up to 27% of the radial velocity.

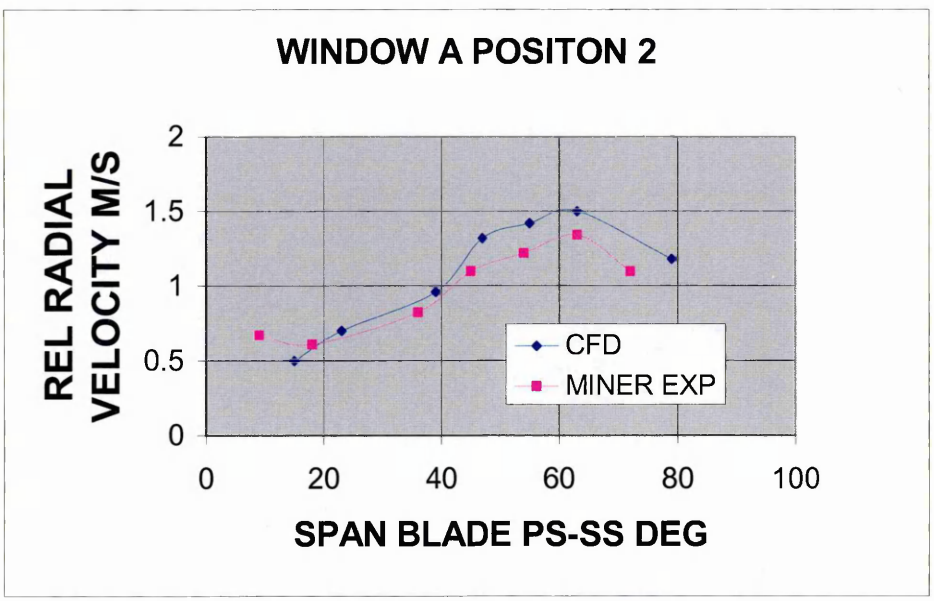

Fig.3.5.2.2 Passage Averaged Radial Velocity across Volute Window A Position 2

Figure 3.5.2.2 illustrates the radial velocity comparisons between the Miner Experimental Pump and the CFX Tascflow simulation. There is good agreement between the velocity profile of the two curves. The differences between the two curves are small, differing by 7% as a maximum.

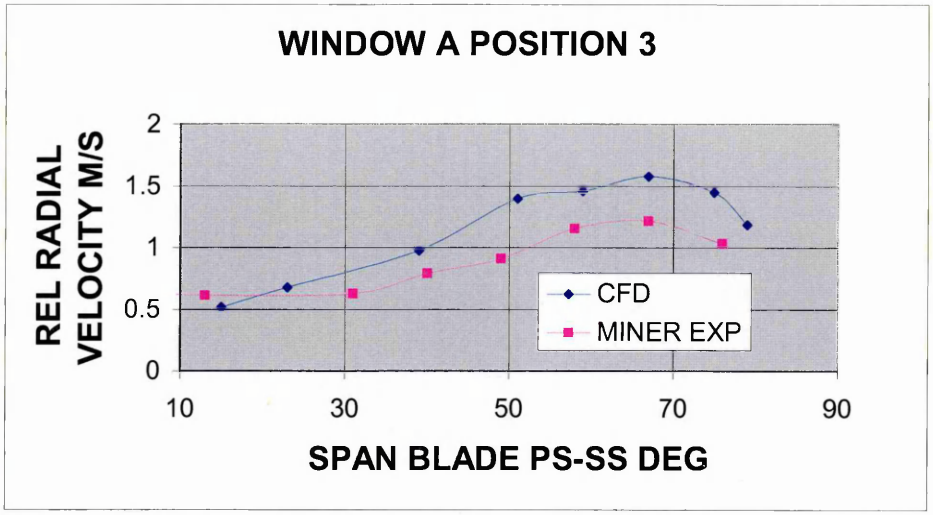

Fig.3.5.2.3 Passage Averaged Radial Velocity across Volute Window A Position 3

Figure 3.5.2.3 illustrates the radial velocity comparisons between the Miner Experimental Pump and the CFX Tascflow simulation. There is reasonable agreement between the shape of the velocity profiles of the two curves. The differences between the two curves appear small but differ by 30% as a maximum.

Fig.3.5.2.4 Passage Averaged Radial Velocity across Volute Window A Position 4

The velocity values we are dealing with are relatively small compared to the tip speed of the impeller. Small errors in terms of absolute values represent large percentage differences. This window is sited furthest away from the volute lip and experiences minimal rotor-stator interaction effects. Figure 3.5.2.4 contains the greatest deviation between the two chart lines. This point, which would experience the least unsteady influence from the rotor stator

interaction and experiences the greatest error. CFD for this point over predicts the radial velocity component by 50%.

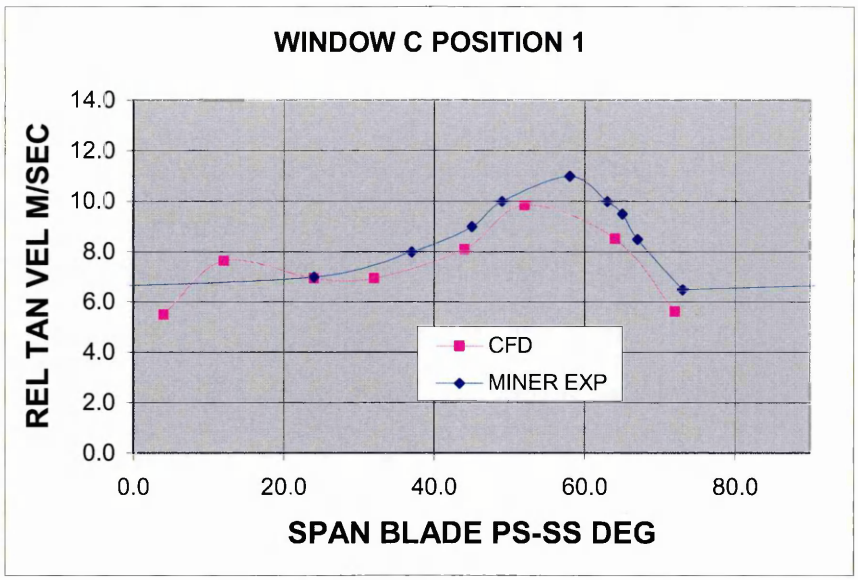

Fig.3.5.2.5 Passage Averaged Radial Velocity across Volute Window C Position 1

Figure 3.5.2.5 illustrates the radial velocity comparisons between the Miner Experimental Pump and the CFX Tascflow simulation through window B closest to the volute lip. There is good agreement between the velocity profiles of the two curves. The differences between the two curves are small, differing by 2% as a maximum. In absolute terms the value of the error is greater than that experienced at Window A.

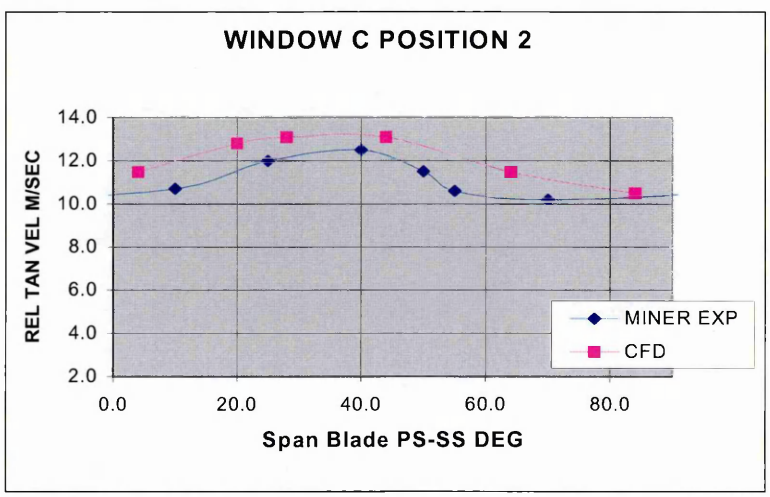

Fig.3.5.2.6 Passage averaged Radial Velocity across Volute Window C Position 2

Figure 3.5.2.6 illustrates the radial velocity comparisons and, as with the comparisons through Window A, the difference between the two curves begins to increase.

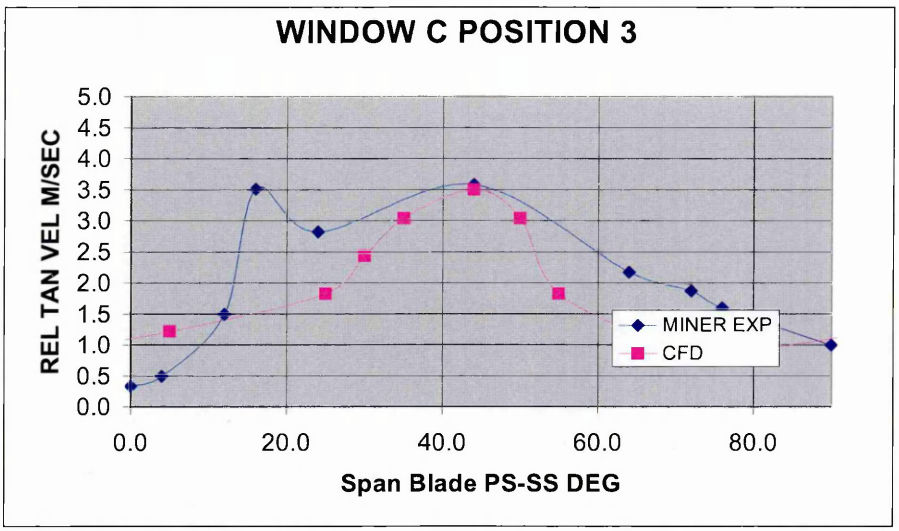

Fig.3.5.2.7 Passage Averaged Radial Velocity across Volute Window C P3

Figure 3.5.2.7 illustrates the radial velocity comparisons and, as with the comparisons through Window A, the difference between the two curves has increased with a maximum deviation over 50%. The Miner experimental results contain a spike at 16deg which is not evident in the CFD results

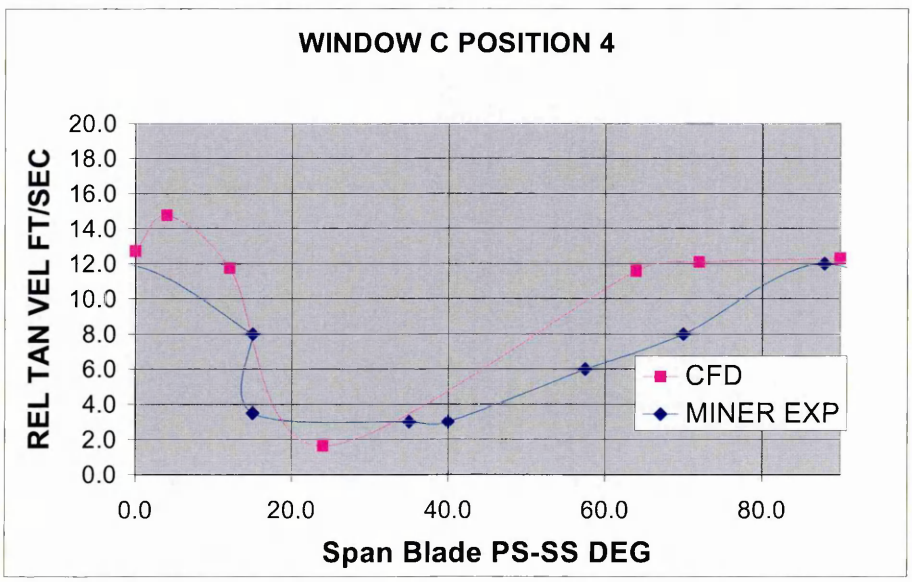

Fig.3.5.2.8 Passage Averaged Radial Velocity across Volute Window C P4

At the greatest radius through Window C the deviation from experimental data remains at a maximum of 50% but there is still evidence that the velocity

profile curve shape is at least representative of that found in the experimental analysis.

Fig 3.5.2.9 represents the velocity profile across the volute. Computational limitation forced the grid refinement in this direction to be at it's least refined. The points given in this figure are the only ones available from the solution such was the coarseness of the grid.

The pattern of increasing deviation form the experimental results as the radius increases is evident also in these plots. This grid, as represented in Fig 3.5.1.3, is less refined as the radius through the domains increases. The increasing radius requires the same number of nodes to occupy a large arc length and as a result the accuracy of the comparison suffers. This is particularly significant where the absolute velocity values are small and the interaction effects are weak.

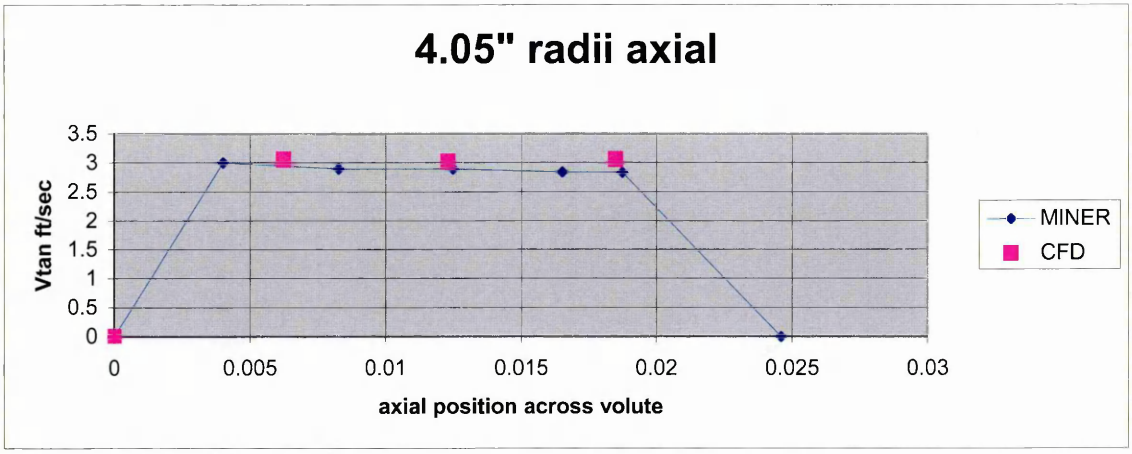

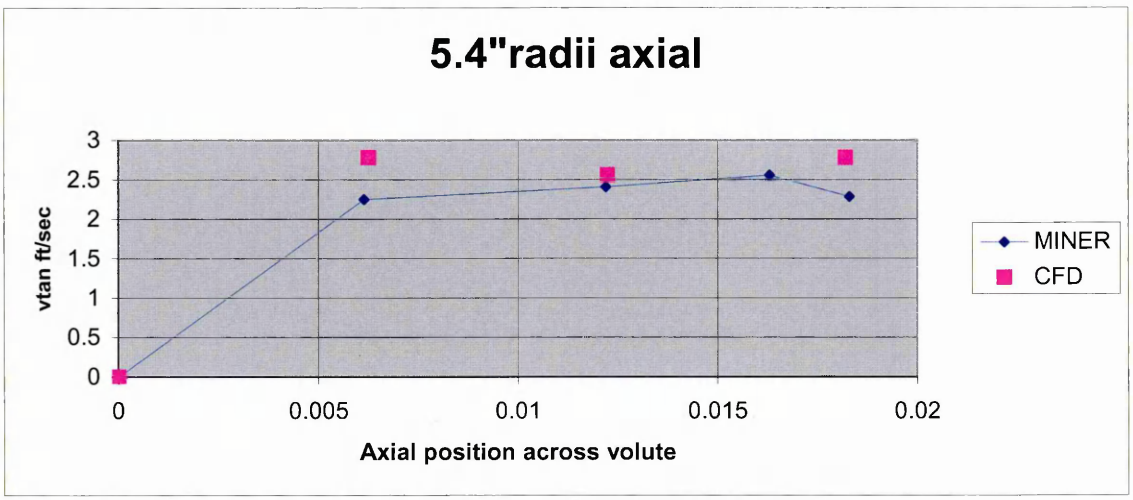

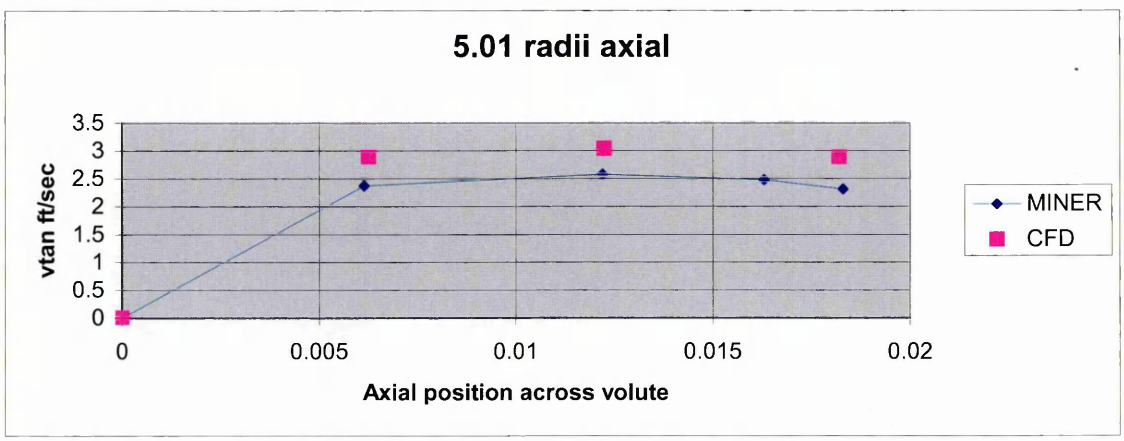

Fig.3.5.2.9 Passage Averaged Tangential Velocity across Volute Window B

3.6 Boundary Conditions

It is important to the accuracy of any computational solution that the boundary conditions assigned represent the real situation.

In the case of the solution of a closed valve head simulation, special consideration must be given to the assignment and selection of the boundary conditions and the model must be adjusted to allow the boundary conditions to be valid.

The work by Sun et al (2002) suggests that the pump cannot be treated in isolation for the computational solution. The system in which the pump runs has an effect.

3.6.1 Inlet Duct

Palgrave and Fraser both observed the nature of the re-circulatory flow within the inlet duct of centrifugal pumps running at extreme part load. This re-circulatory flow does not dissipate until approximately 20 pipe diameters downstream of the pump. This situation imposes an unsteady boundary condition close to the impeller inlets. To counter this, the inlet duct has to be modelled on all computational simulations to allow this reversed flow to be accounted for. By modelling the inlet pipe, an inlet pressure condition can be assigned to the suction duct inflow boundary.

3.6.2 Outlet Flow

To correctly represent the impeller flow field, a finite amount of flow, not greater than the volumetric flow through the wear ring landings, is assigned as the mass flow at the exit of the casing.
The model treatment includes a blockage at the pump outlet to represent the effect of a flow control valve. The size of the outflow duct is controlled to allow a minimum walling over the outflow area. The walling is constructed by the solver to prevent unwanted outflow re-entry.

3.6.3 Working Fluid

Water is used as the working fluid.

The temperature rise within the pump at closed valve is ignored as the change in specific gravity due to temperature rise is accounted for in the calculation procedure from test measurements.

3.6.4 Time Dependency

The unsteady nature of the solution means that the length of the time step used may have an affect on the accuracy of the solution.
The number of time steps taken affects the amount of time take for the solution to converge.

A small number of time steps would require fewer converged solutions but would require more iteration per time step. A small time step would result in many solutions but with less iterations in each time step. To optimise the computational resources full independent solution from the time step size was sought.

For the study four different time step sizes were considered. These corresponded to the impeller rotating 4 degrees, 2 degrees, 1 degree and 0.5 degrees. The average pressure at outlet within each solution component was plotted after each solution run.

From the plot in Fig.3.6.4.1 of the average velocity in the volute it is shown that the solution for the 2-degree solution is not independent of time step.

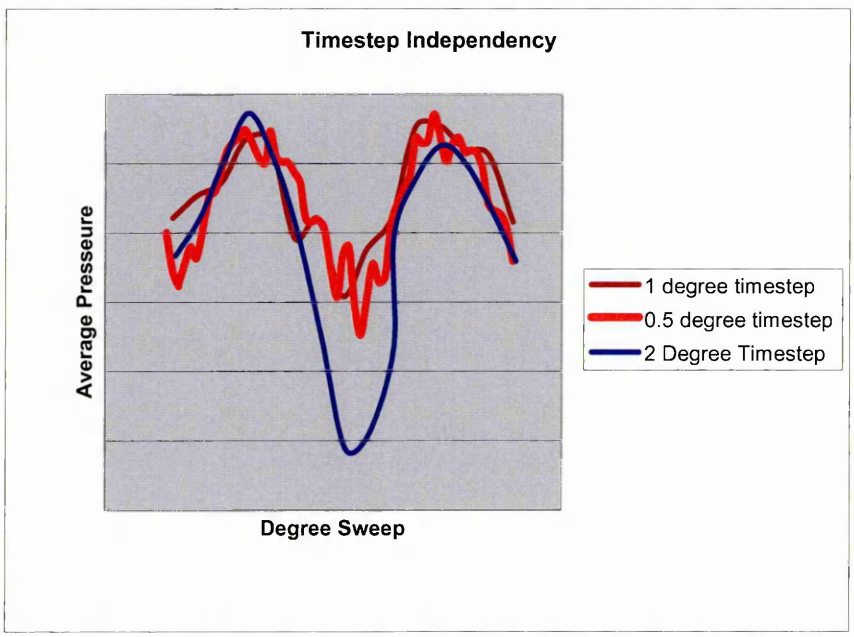

Fig.3.6.4.1 Comparison of Average Pressure in Volute for 1 Blade Pitch for Different Time Steps

The smaller time steps of 0.5 degrees and 1 degree produce solutions, which are within 2% of each other, and as such the 0.5-degree time step is considered independent.

3.6.5 Solution Procedure

A process of iterative selections used the following procedure to produce the optimum solution, independent of time step.

- 5 Degree time steps for 6 sweeps of the impeller within the stator to handle the larger unsteady elements of the solution
- 0.5 Degree time steps to ensure a repeatable pattern of pressure and velocity per vane periodic within the rotating and stationary components

This solution procedure is refined in subsequent problems. Fig 3.6.4.1 shows comparisons of average pressure in a volute for 1 blade pitch for different time steps

3.7 Experimental Analysis

This section contains the experimental data obtained from three production pump units. These values were taken during a standard performance test. Although the CFD code is the primary source of investigation, experimental observations were taken on pump units. These observations, whilst rudimentary, give grounding to the simulated flow regime.

Since the primary concern of the project is pressure prediction, the unsteady nature of the pressure pulsations observed at closed valve is important. The levels and frequencies of the pressure pulsations were taken in the both the suction and discharge nozzles. These pressure spectra are contained in Fig.3.7.1 with the associated performance curve for this machine included in Fig 3.7.2.

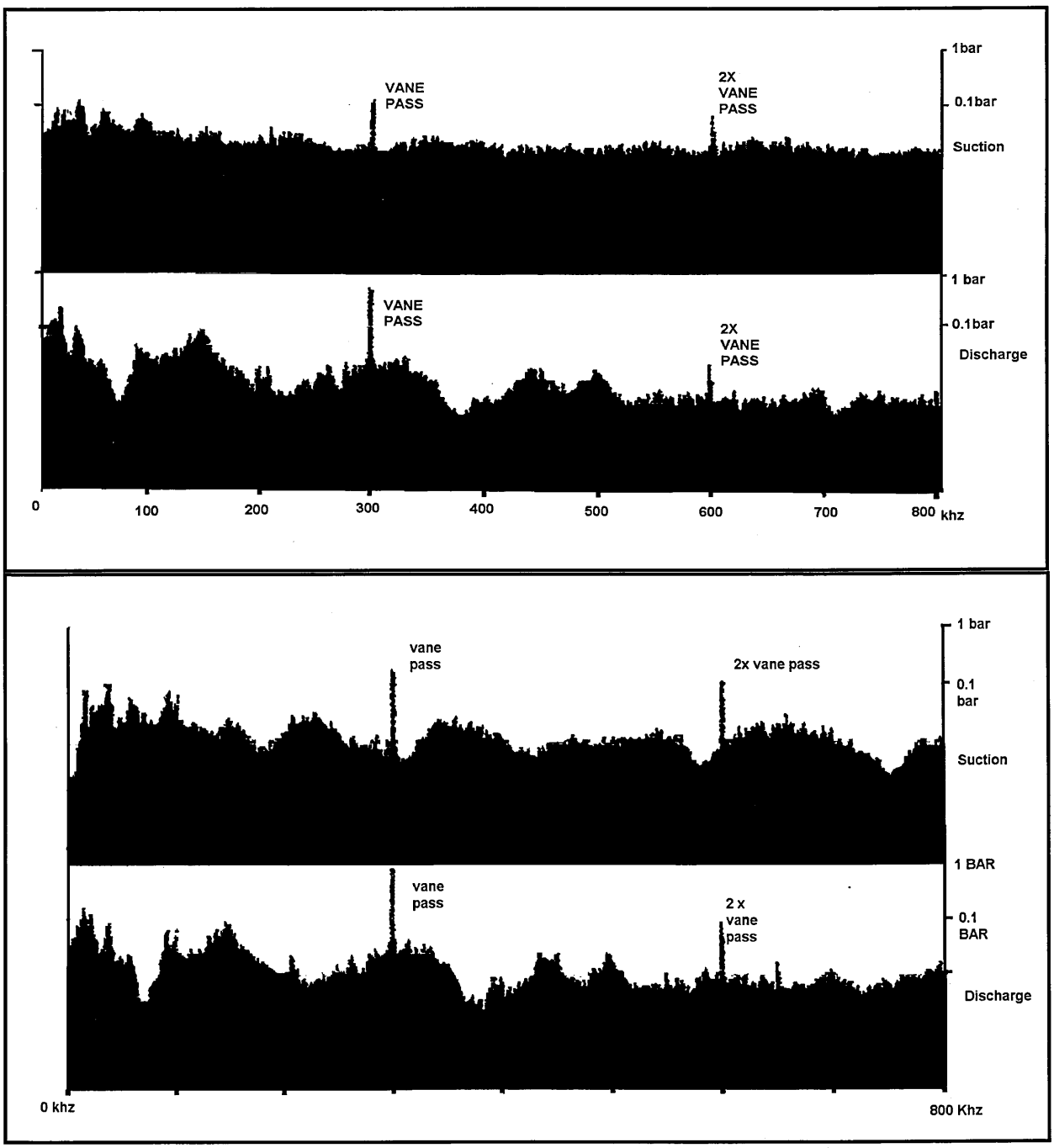

Fig.3.7.1 Pressure Pulsation Spectra in Suction and discharge Nozzles 372mm & 381mm Diameter

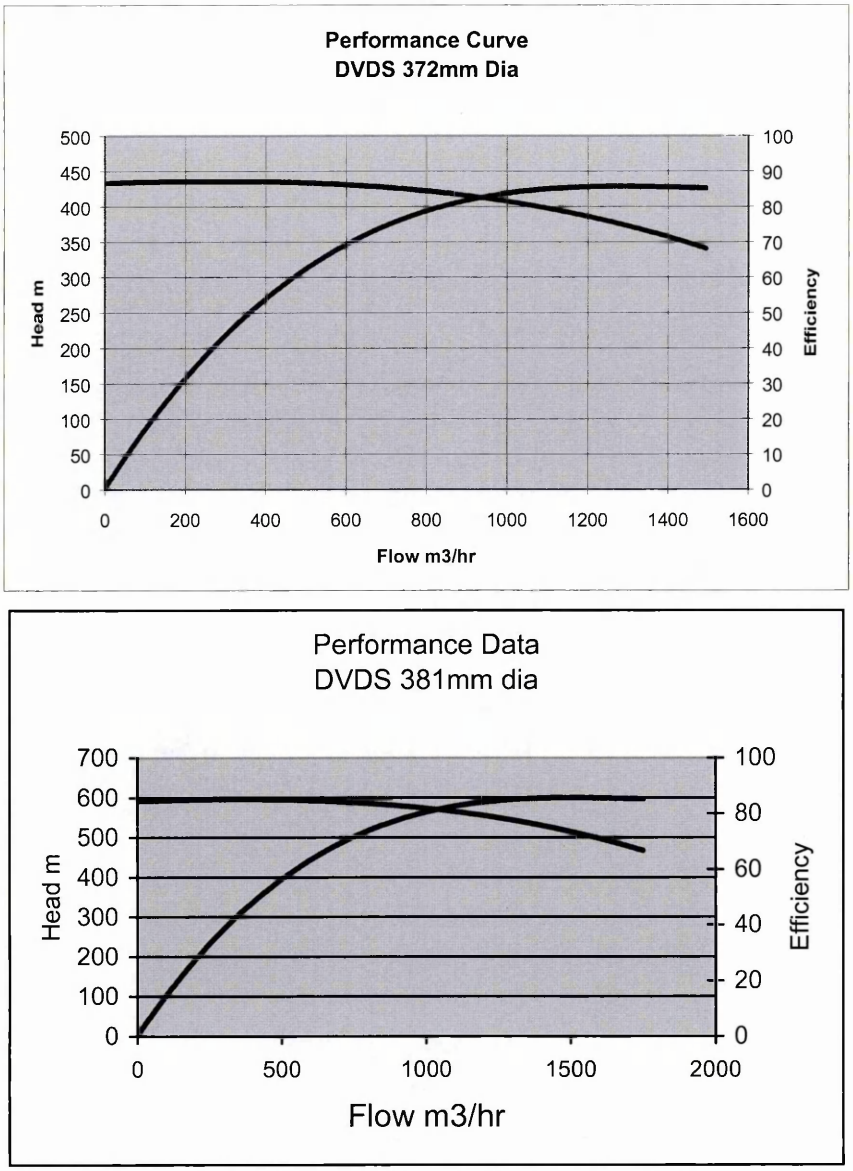

Fig.3.7.2 Performance Curve

The pressure spectrum for the discharge is dominated by the multiples of the vane frequency. Present also are sub-synchronous elements associated with the stalled discharge vane re-circulation eddy. This is faithful to the picture propose by Simister and Cinammond(1964) who first reported this counter rotation sub-synchronous eddy.

The dominance of the vane pass frequency is not unexpected. The literature suggests that the stalled nature of the collector and the squeezing of the flow through the gap between stator and rotor blade would lead to high pressure fluctuations at vane pass frequency.

This is also true of the suction channel. Whilst the flow, expelled from the inlets would be free to spiral down the inlet duct in an end suction pump Fig 3.7.3 this particular pump contains a suction splitter.

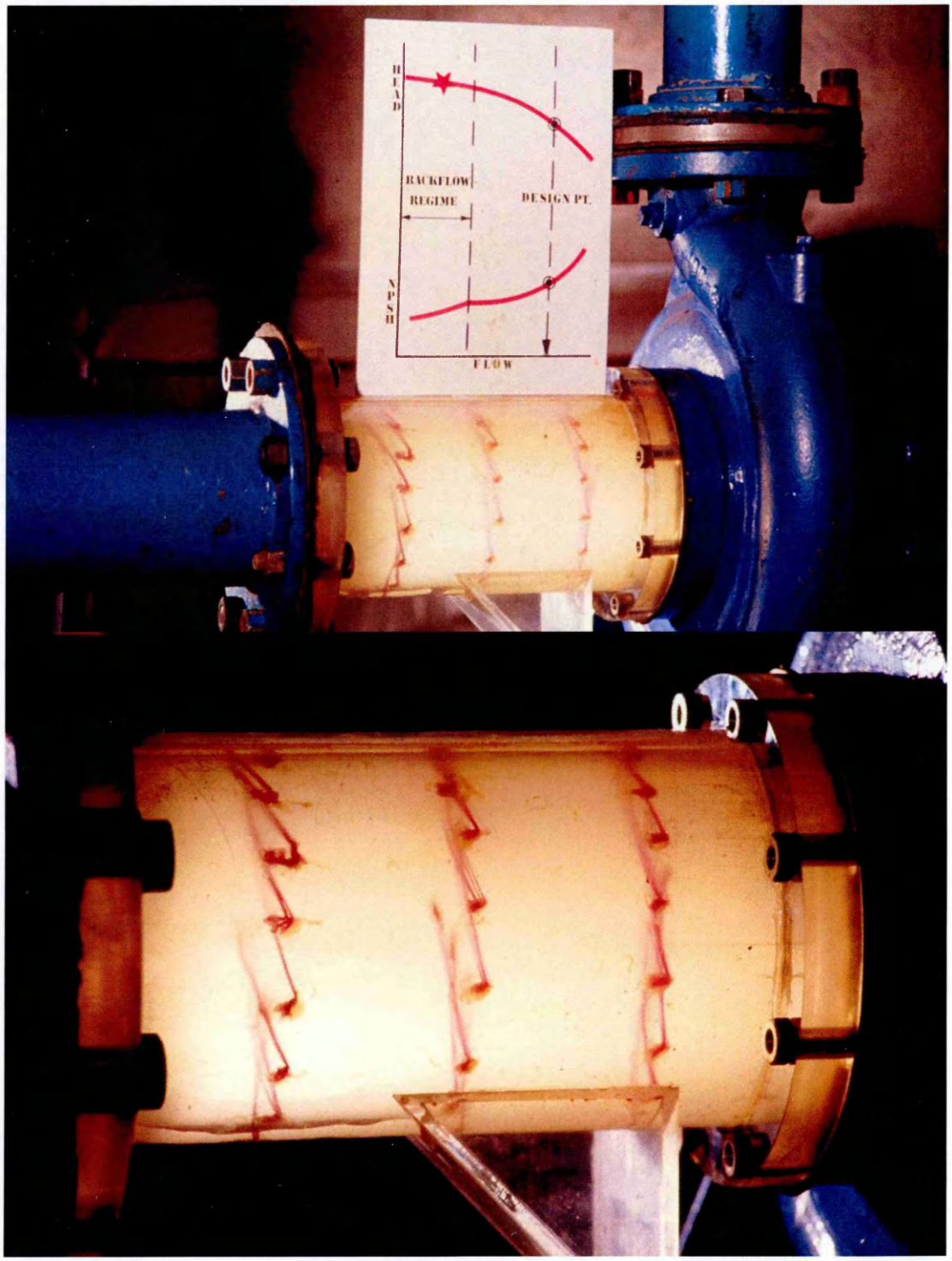

Fig.3.7.3 Pump Test to Qualitatively Illustrate the Suction Re-circulation Effect at Extreme Low Flow

To escape from the impeller inlets the fluid velocity at the impeller eye has to exceed the inlet tip speed of the impeller. This high energy liquid impacts on the pump suction splitter. Continuity considerations account for the pressure pulsations in the suction at multiples of vane pass frequency.

This pump required a reduction in impeller diameter to tune the performance. Further readings were taken at this reduced diameter and the associated spectra are shown in Fig 3.7.4 with the pump performance curve being included in Fig 3.7.5.
Again the pressure spectra are consistent with the flow feature observed in the literature.

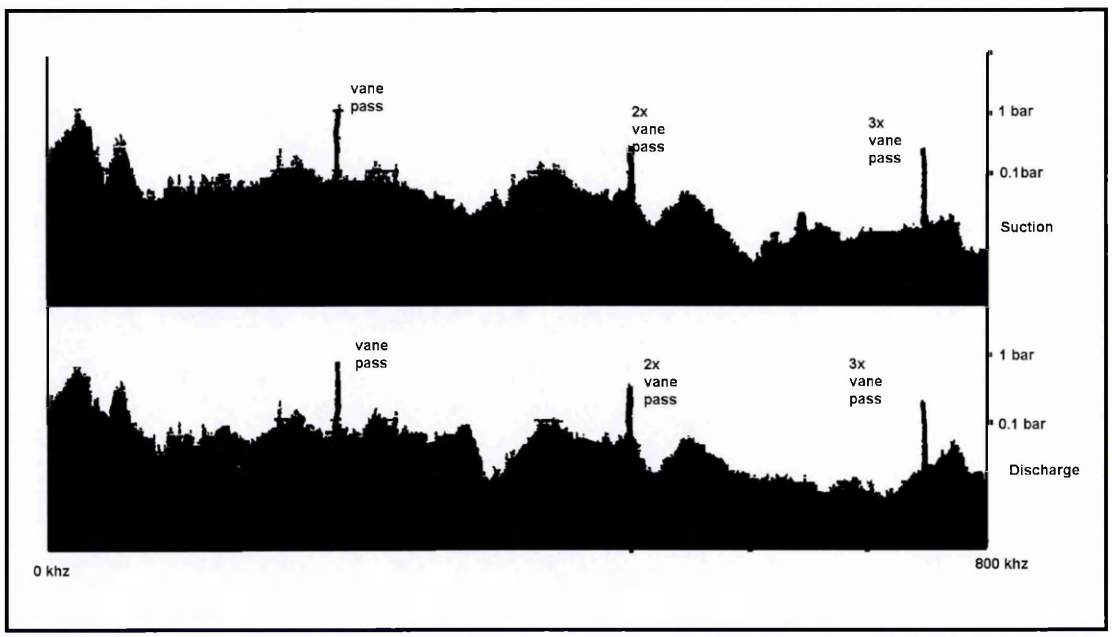

Fig.3.7.4 Pressure Pulsation Spectra in Suction and discharge Nozzles 365mm Diameter

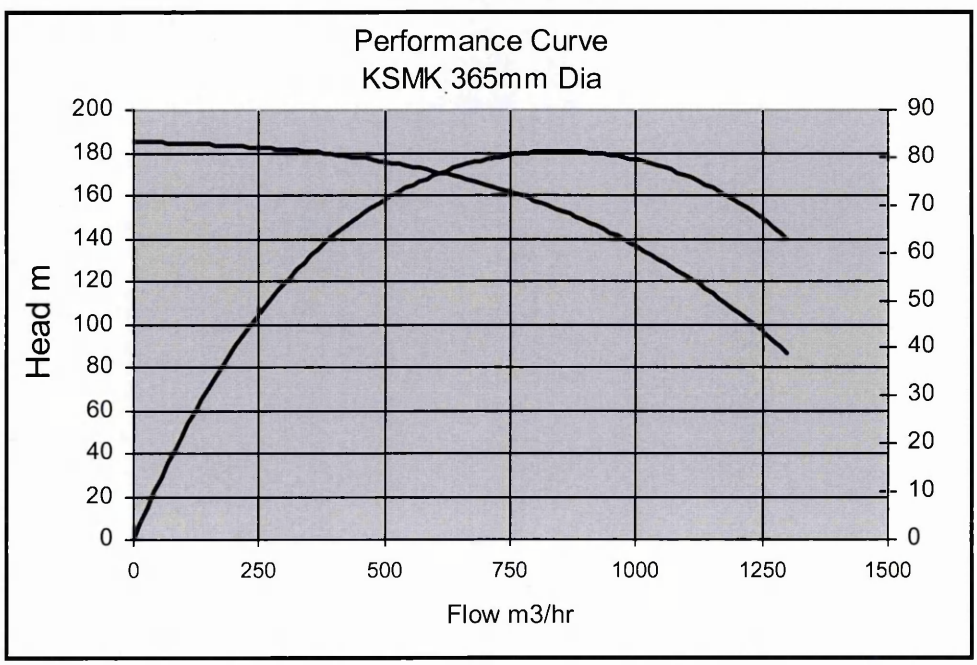

Fig.3.7.5 Performance Curve

3.8 Summary

The case for using CFD as an experimental test of pump performance is compelling but it is important to carefully select appropriate modelling parameters and schemes from the commercially available software.

The experimental analysis comparison carried out against the Miner (1988) indicates that whilst there is good agreement between the unsteady velocity pulsation shapes the absolute values can contain difference of up to 50%. These occurred in the span-wise direction where the grid was at its least refined. Solution accuracy is linked to the refinement of the grid.

Grid sensitivity studies and refinement studies favoured the scaleable wall function approach available within the code CFX Tascflow. Controlled refinement of the grid from 10000-100000 nodes indicates that differences in pressure development are smaller above 50000 nodes. Whilst this grid density would ideally be used for future simulations the 10000 node grid was still instructive.

Selection of turbulence models is a difficult area with little validating work for pumps operating at off design conditions. The perceived wisdom within the industry that the $k-\varepsilon$ model is the most suitable is borne out by the comparisons. Newton's(1998) thesis, being the only other study available, came to the same conclusion. Only small deviations were found between all the schemes.

Time step independence, from this chapter, is the one area which has a dramatic effect on the solution accuracy. Time steps above one degree contain pressure amplitudes which greater than experience with those below one degree.

The schemes available to handle the interface between relatively moving blade rows are also important. Although it is not definitively defined within the literature, the interaction between the rotor and stator blades is unsteady and must be handled using a transient rotor-stator interface. This is supported by the experimental pressure readings taken within the suction and discharge nozzles of a centrifugal machine on the Union Pump test-bed.

Assignment of boundary conditions must reflect the way in which a pump conventionally operates. For closed valve head this requires a pressure inlet boundary to be assigned away at the suction pipe away from the outflow suction region as described by Fraser(1991) and Palgrave(1985)

4.0 Description of Flow Features through a Volute Pump

The major study by Newton (1998) used, as its basis, a volute pump. Using air as the working fluid the CFD predicted the flow regime but over predicted the volute pressure rise by 160%. In terms of contemporary pump design the geometry analysed only crudely represented commercial design. Features such as a blocked inlet and the large height of the throat contributed to flow features that would not be apparent in a more traditional design.

This section contains an analysis of a volute pump which has the following feature that are similar to the Newton (1998) machine.

- The pump suction enters the impeller along the rotating axis of the machine. This limits inlet pre-swirl.
- The impeller discharges into a spiral volute
- The discharge is initially tangential to the impeller

The pump contains the following features that are typical of modern pump design that were not included in the Newton (1998) research.

- The impeller inlet angles are arranged for zero incidence at design flow.
- The spiral volute contains two throats to balance the radial loads.
- The impeller meridional profile is curved to accept the inflow.
- The impeller blade width is not equal to the throat width.

The machine has a specific speed of 700 (US units). This would be considered a low Specific speed machine.

From a comparison standpoint with the Newton (1998) machine the impeller is considered to be radial. This pump is comparable also with the machine analysed by Peck (1950) in which he observed the "powerful forced vortex" extending into the suction pipe of the pump.

This chapter contains a description of the flow features through this double volute centrifugal pump. The flow regimes are described for casing, impeller and inlet pipe flow. Some experimental data and comparisons with existing work are included as a background to the CFD analysis. This experimental data is intended to reinforce the findings of CFD analysis.

4.1 Geometry

The geometric features of a centrifugal pump volute casing can be divided into a number of discrete regions for the purpose of describing the flow features. The pump within this example is typical of medium to high power machines. The casing passageways are divided by a central splitter to limit radial loads applied on the bearings.

- The volute is the region of the casing around the periphery of the impeller. A double volute machine contains two of these regions which extend between the throat areas. Each region covers half of the impeller periphery.
- The casing contains two diffusing passageways. One is long and the other is short. These passages join together at the pump discharge. Each passageway is used to diffuse the liquid passed to it from the impeller.
- The two passageways are divided by the casing splitter
- The area where the liquid enters the passageways from the volute is named the casing throat. The area of this throat, along with the impeller outlet area (A2BB), is used to control the flow at which the pump's best efficiency point occurs.
- The two portions of the casing that form the inlet to the casing throat and act closest to the impeller blades at the throat entrance are named "lips" or "casing cutwaters". These two terms are used interchangeably throughout the following chapter.

These geometric features are illustrated in Fig.4.1.1

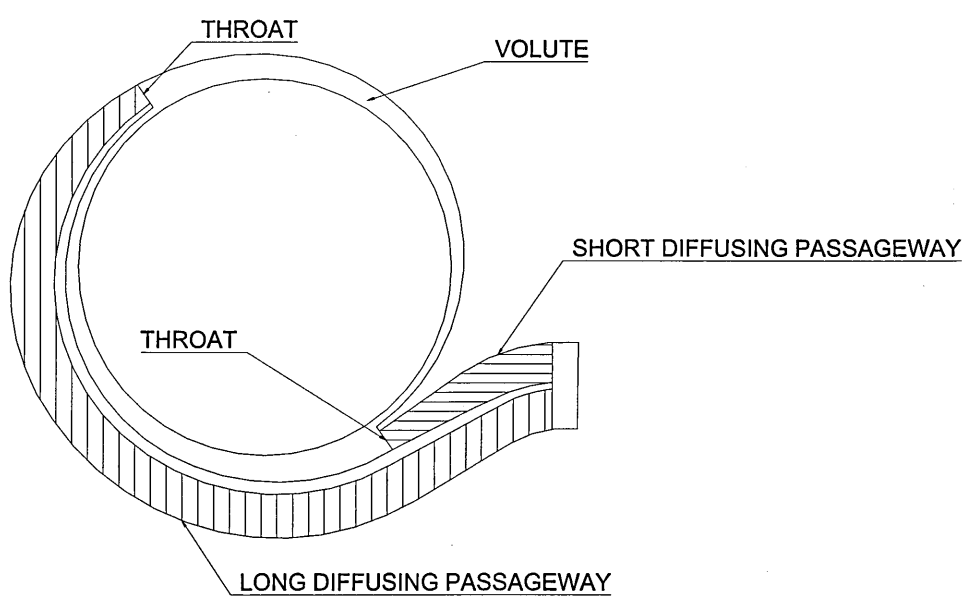

Fig 4.1.1 Construction of a Double Volute Casing

To ascertain the flow regime within each section of the volute a number of monitor points are assigned. Fig.4.1.2 illustrates the position of these monitor points around the volute.

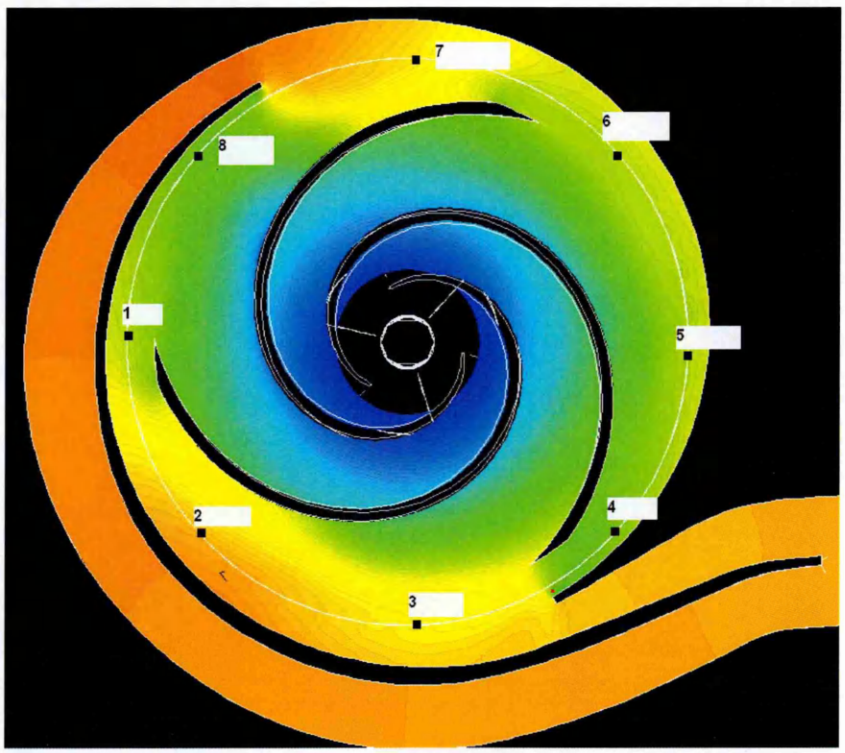

Fig 4.1.2 Monitor Points Location

Fig.4.1.3 contains the positions of monitor lines within the short and long passageways, and across the pump discharge. These lines are used to monitor the pressure properties of the CFD solution along the centre of the passages.

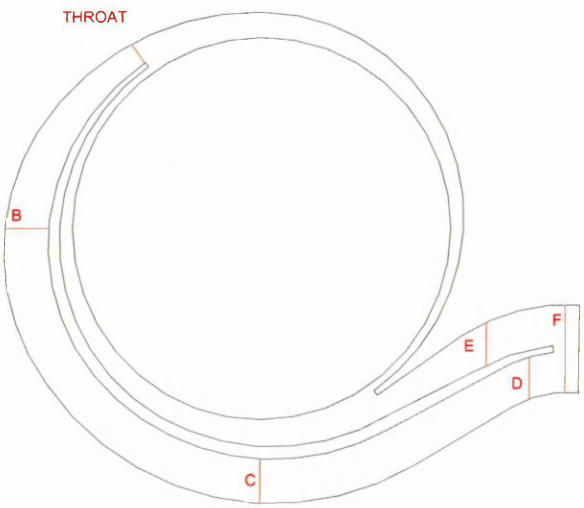

Fig 4.1.3 Diagram of Monitor Linear Sections Through The Pump Casing

Fig 4.1.4 contains the impeller geometry used in this machine; Fig 4.1.5 illustrates the volute geometry and Fig 4.1.6. contains the performance map for the machine.

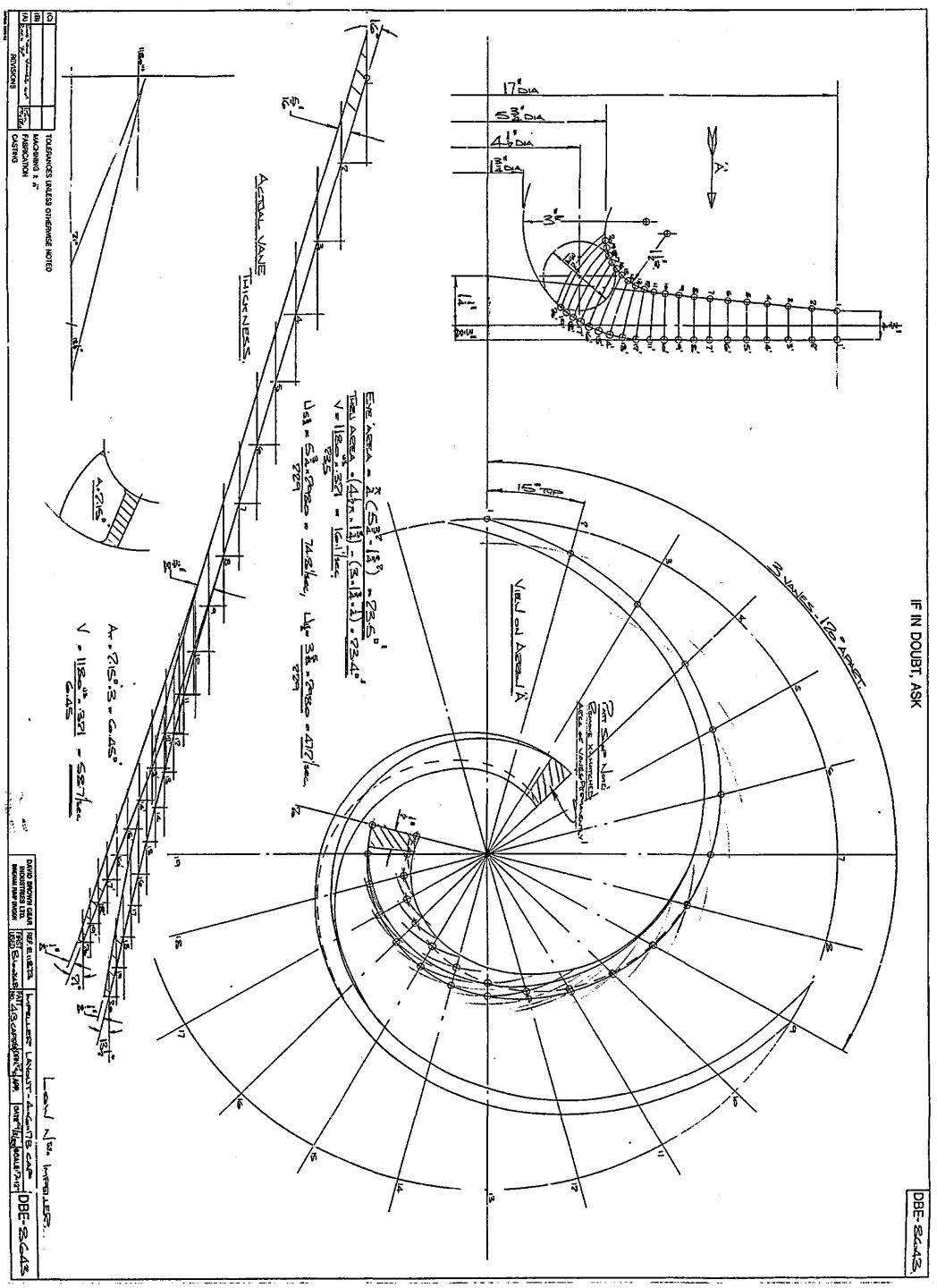

Fig 4.1.4 Impeller Geometry

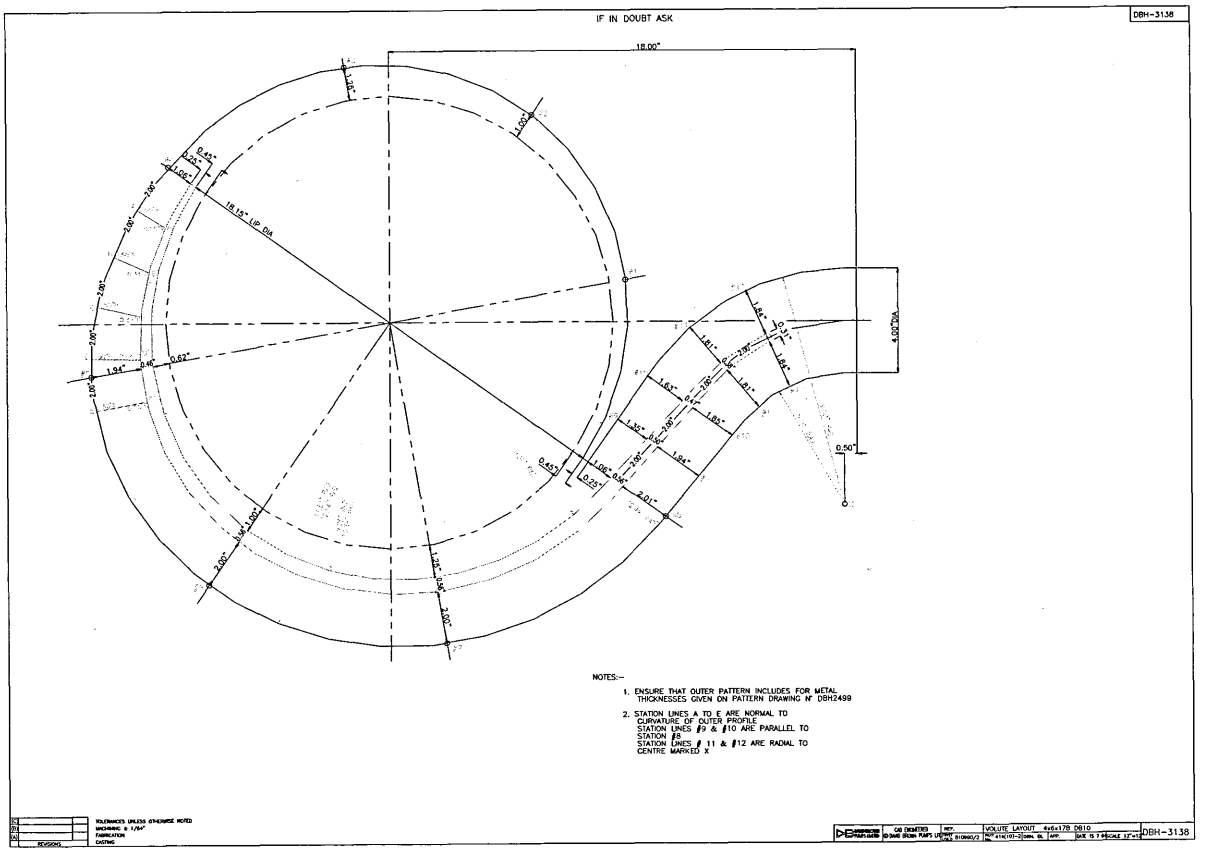

Fig 4.1.5 Volute Geometry

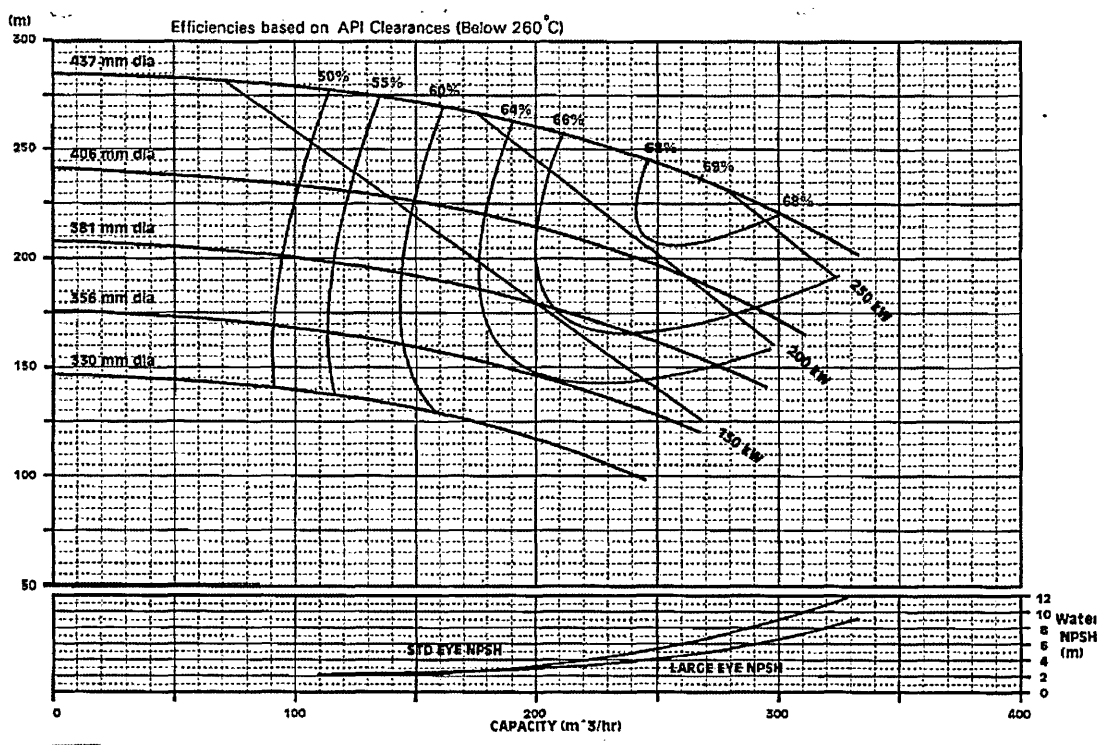

Fig 4.1.6 Performance Envelope for Pump

4.2 Solution Parameters

The development of the computational procedure, based on the research incorporated in Chapter 3, uses the following parameters and boundary conditions. The parameters and conditions and procedure outlined within this section are the culmination of a computational campaign with solution run times extending over a 6 month period. Using a process of successive iteration the schemes and conditions available within CFX 5.1 were refined and assimilated into this final technique.

It is important in any computational simulation that the boundary conditions accurately reflect those experienced by an actual pump.
Primarily a pump runs at a specific suction pressure, this suction pressure is used to suppress cavitation within the impeller inlet. Pump designers are familiar with this concept so a pressure boundary as a pump inlet boundary condition is a favourable choice. Although the choice of pressure, notionally, is unimportant for the computational solution it should represent the actual pump suction pressure to enable pump designers to better picture the link between the simulation and the actual situation.

Inlet boundary – Pressure Boundary :- 100000 Pa

Inlet boundary conditions based on mass flow input were found to be produce walling of the inlet boundary by the solver. This was perceived to be caused by the solvers attempt to simulate the inlet backflow proportion of the flow where outflow may be apparent at the inflow boundary. Switching to a pressure boundary and moving the inflow further from the impeller prevented this walling.

The outlet boundary requires a finite outflow through the boundary to enable a converged solution. Since pump designers talk in terms of discharge flow, from a perception standpoint an outlet mass flow is desirable.

Final Outlet boundary – Mass flow outlet: - 0.001 kg/s

The outlet boundary is placed close to the pump discharge but away from the central splitter between the long and short rotating passageways. The solution evolution is slow if the discharge passage is left to wall by the solver. To better aid this situation incorporating a blockage at the discharge to represent the tapered nature of a closed discharge valve reduces walling and speeds the solution.

Other boundary conditions are as follows

Rotational Speed: - 1480rpm

This is a synchronous speed of a 50hz motor and would be recognisable to pump designers

Working Fluid:- Water

Although pumps are used for many liquids they are commonly only tested by pump manufactures on water and then the results are adjusted for specific gravity and viscosity after the water test.

4.3 Solution Procedure

Using the above solution parameters we can apply the following solution procedure to the problem.

4.3.1 Initial Conditions

The initial conditions are established using the methodology available within the CFX code. These conditions require refinement by allowing the rotating impeller grid to rotate 1 complete revolution with a 5 degree time-step.
These rotations are carried out in the following manner:-

- B.e.p flow – 1 complete sweep
- 50% b.e.p flow 1 complete sweep
- 25% b.e.p flow 1 complete

At the 25% b.e.p. flow condition the inlet backflow proportion of the flow is fully established.

4.3.2 Solution Process Part 2

The final solution is evolved utilising the 25% b.e.p flow solution as the initial condition. The outlet boundary flow condition is modified to its final value. Through this stage a process of time step reduction is followed:-

- 1 sweep of the impeller at 1 degree time-step
- multiple sweeps of the impeller at 0.5 degree time-step until the periodic pulsations monitored within the solved are converged to with 3% of each other
- 1 final sweep of one blade pitch with outputs to individual results for every degree of time-step for final analysis.

It is important to implement the final output run to conserve disc capacity. The individual results files can contain 60Mb of data. Individual file outputs of this size per time-step quickly utilise disk space and solver failure occurs when no disc space remains.

The results from the final sweep are used for the subsequent analysis.

4.4 Time Averaged Evaluation

Many experimental measurements are available for the closed valve head of centrifugal pumps. These measurements are a standard requirement when plotting the performance envelope of the machine (Fig 4.4.6). All these measurements are time averaged and only take into account the unsteady pressure in so much as they are formed from the components of this pressure.

Complicating the picture of the time averaged pressure is the nature of the pressure rise around the volute. The literature review contains examples of a non-linear pressure rise around the volute of a centrifugal pump at low volume flux, Binder and Knapp (1958). Explanations are not given for this non-linearity but Newton points out that these variations in the radial direction are small and the likely mechanism is diffusion. Kikuyama et al (1987) also noted this non-uniform pressure distribution around the volute.

This non-linear pressure rise is illustrated in Fig.4.4.1 for the analysed machine. The time averaged pressure is calculated at 4 points around half the volute. Position 4 conforms to the point closest to the volute lip. Continuity considerations would expect this to exhibit the lowest level of time averaged pressure. This is supported by the observations made by Brownall et al (1985).

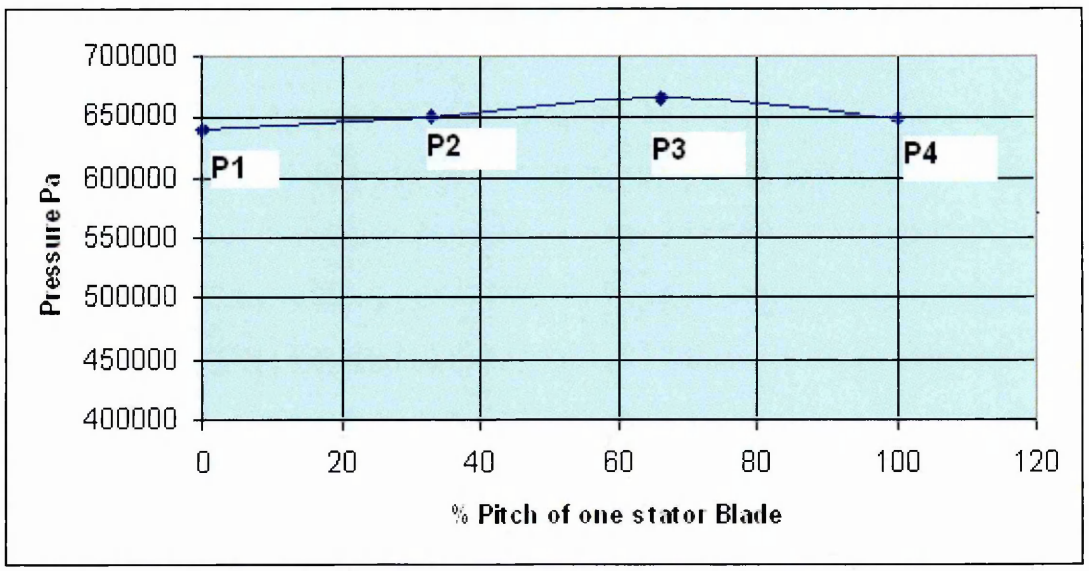

Fig 4.4.1 Time Averaged Pressure at Monitor Point 1-4

The stalled nature of the short and long passageways is inhibiting the impeller outlet flux. The liquid trapped within the upper proportion of the impeller and volute is subject to velocity variations from the rotating impeller blades approaching the volute lips. When the impeller vanes are congruent to the lip a finite volume of liquid is squeezed between this small gap causing an

increase in velocity and a decrease in the instantaneous pressure. This is supported by observations made by Goulas and Trouscott (1988).

Fig 4.4.1 indicates that the time averaged non-linear pressure distribution is not identical at each volute lip.

Although the impeller and lip geometry is identical, the lip closest to the short diffusing passage way (P4) experiences a higher value of time-averaged pressure. The geometry downstream of the throat i.e. the passageway configuration has an effect on the pressure development within the machine. This is a significant observation that is absent form all other experimental and computational studies. From this non uniform pressure between the long and short passageways we would expect some cross passage flow driven by the pressure differential. This is alluded to by Kikuyama et al (1987) as they describe their volute flow to be divided by the central splitter of a double volute pump.

Many of the other available studies use simplified geometries. Fischer and Thome (1952), Goulas and Trouscoutt (1988), Binder and Knapp(1958) and Iversen (1960), all use single volute machines for their experimental analysis. These do not represent typical geometries for medium and high power machines. Only Brownall (1985) uses a double volute machine for his experimental analysis.

Papers such as Acosta (1954) and Acosta and Bowermann (1957) use impeller geometry submerged in a tank. This, by nature, has no rotor-stator interaction component and no casing flow component.

Investigation of this phenomenon using a machine with multiple stator blades to explore the development and effect of this non-linear passageway dependent flow is undertaken is Chapter 5.

The nature of the pressure evolution, over and above the time averaged data is interesting. Time averaging represents the ultimate head of the machine as it will be viewed at its performance test but it is essential to demonstrate that this time averaged pressure is made up from the unsteady constituents of the pressure pulsations generated by the rotor stator interactions. This builds towards eliminating solid body rotation theory as a true representation of the flow regime.

4.4.1 Unsteady Pressure Readings Taken At Monitor Point 1

The position of Monitor Point 1 is central between the impeller outside diameter and the volute lip on the horizontal centre line. This is illustrated in Fig.4.1.2.

Fig.4.4.1.1 contains a fringe plot of the blade position which coincides with the maximum pressure developed at this point. The maximum pressure precedes the blade as it approaches the monitor point.

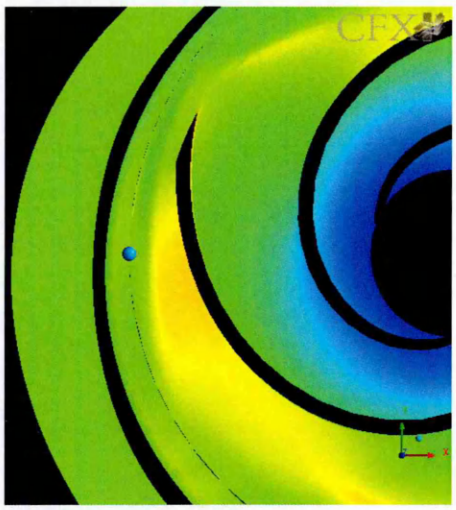

Fig 4.4.1.1 Monitor Point 1 Maximum Pressure

The unsteady pressure readings generated by the computational solution are depicted in Fig 4.4.1.2. The time signal history illustrates a repeating pattern of pressure peaks which are directly related to the interaction of the rotating and stationary components.

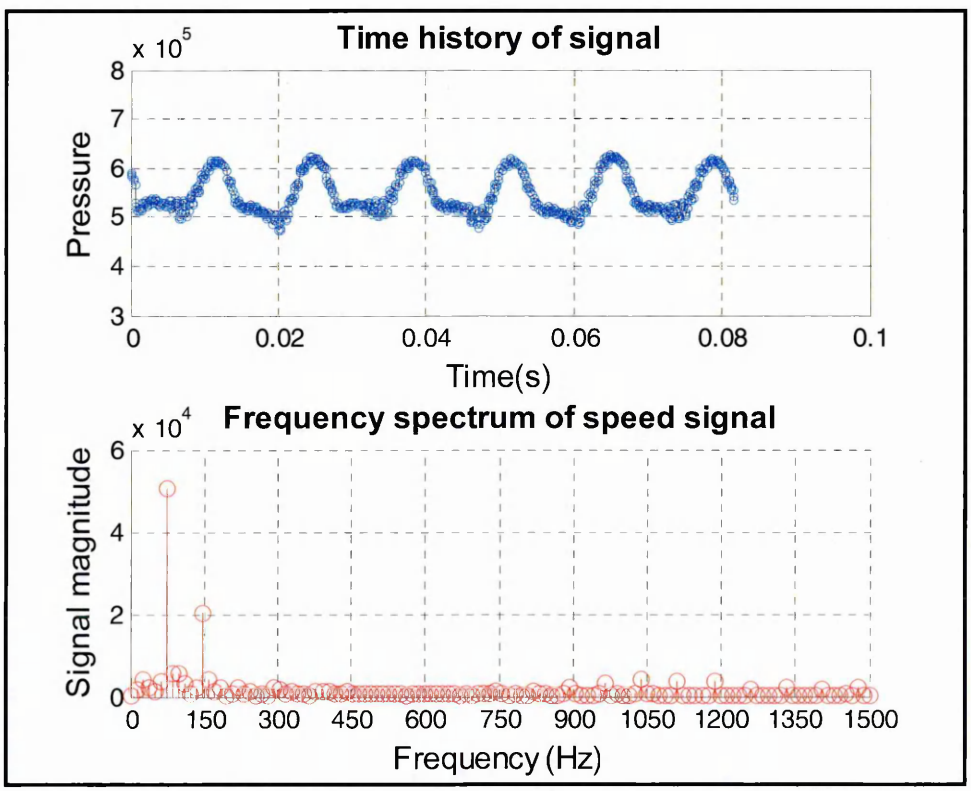

Fig 4.4.1.2 Pressure Pulsation at Monitor Point 1

The frequency spectrum of the signal contains two dominant frequencies. By far the most prominent frequency depicted is the one which can be attributed to the vane passing frequency. This is calculated by multiplying the rotational speed of the pump impeller in Hz by the number of vanes in the impeller.

Also of significance is a frequency that is double the vane pass frequency. This frequency is attributed by pump designers to the blade wake effects. A further description of this effect is contained in Section 4.7.

Fig.4.4.1.3 illustrates the effect of the turbulent wake as it passes the monitor point. The discrete frequency that conforms to twice the vane rate is attributed to this turbulent wake (Dyson and Palgrave 2000).

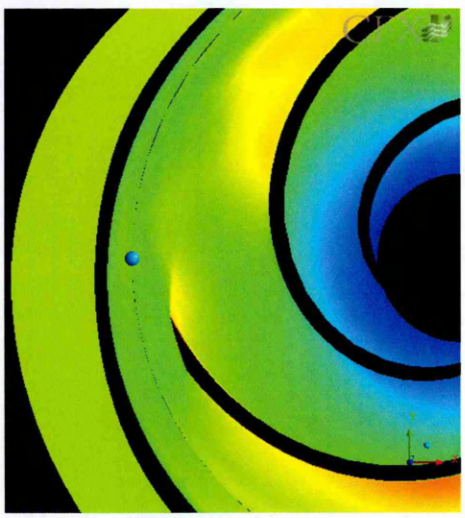

Fig 4.4.1.3 Monitor Point 1 Pressure Due To Turbulent Wake

Both these flow features account for the common vibration phenomenon encountered by centrifugal pumps running at low flow. Designers consider the vibrations these unsteady fluctuations (Dyson 2005) exert on the rotor system and counter them with mechanical modifications to increase machine reliability.

The minimum unsteady pressure at point 1 occurs close to 40% of the blade row span. This represents the position where the both blades are far from the monitor point Fig.4.4.1.4. The pressure rises by 27% from the minimum pressure in front of the approaching blade

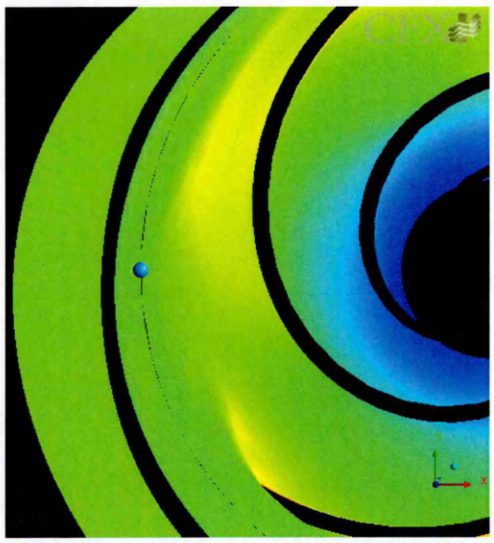

Fig 4.4.1.4 Monitor Point 1 Minimum Pressure

The average minimum pressure is 572840 Pa. The average pressure from blade to blade is 652271 Pa. The maximum pressure peak is 725880 Pa.

Whilst the unsteady pressure pulsations around the volute lip are well documented, Brownall (1985) and Kikuyama et al (1987), the unsteady pressure has previously been neglected in CFD and experimental studies. This section links the phase position of the impeller blades to the amplitude of the pressure pulsations.

4.4.2 Unsteady Pressure Readings Taken At Monitor Point 2

Point 2 is centrally positioned between the impeller outside diameter and the volute lip Fig.4.1.2. The impulsive nature of the pressure development is linked to the position of the blade angle with respect to the point and with respect to the proximity of the volute lip.

The maximum pressure occurs in at 50% of the blade row span. This represents the position where the both blade are furthest from the monitor point as illustrated in Fig.4.4.2.1. This is different from the maximum pressure position encountered at monitor point 1.

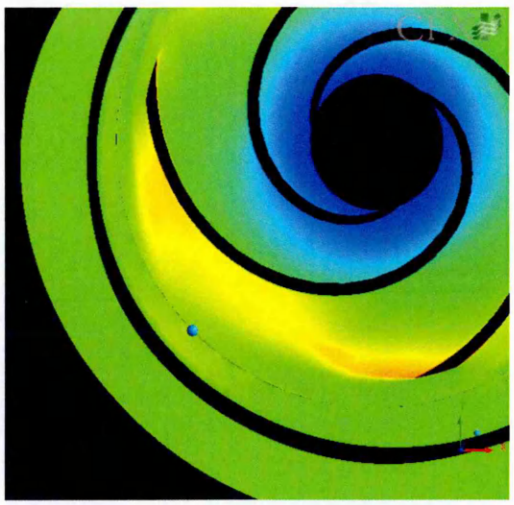

Fig 4.4.2.1 Monitor Point 2 Maximum Pressure

The wake pressure level which was evident at Monitor Point 1 is no longer apparent; suggesting the influence of the volute lip has dissipated. The pressure wave is sinusoidal and completely dominated by the vane pass frequency Fig.4.4.2.2.

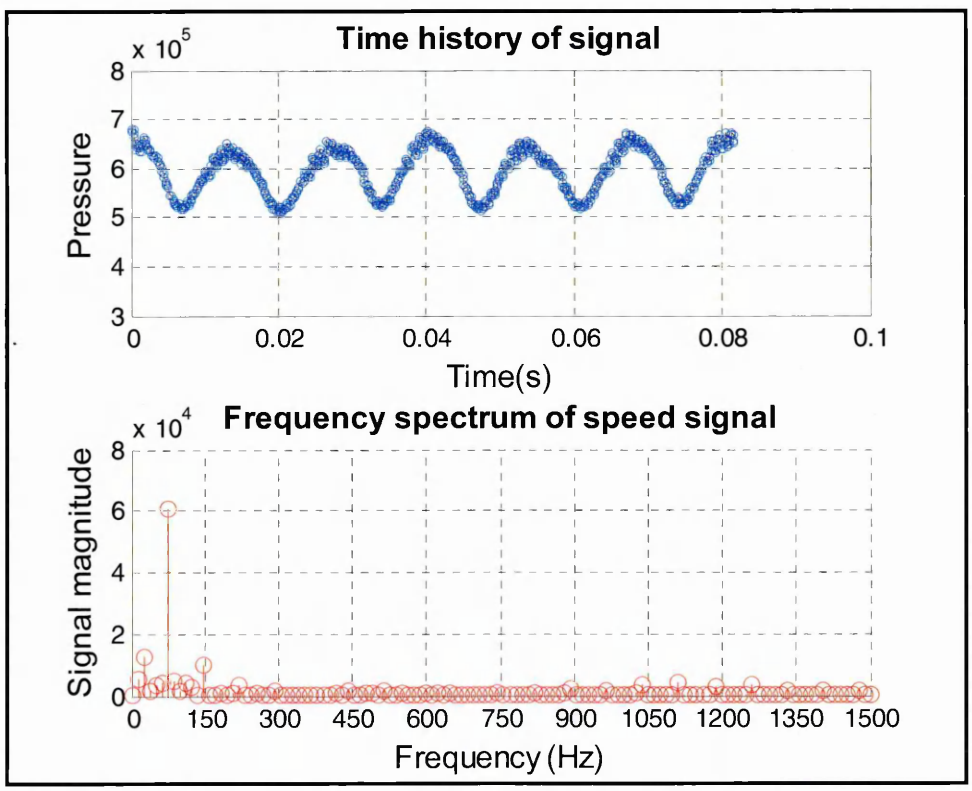

Fig 4.4.2.2 Pressure Pulsation at Monitor Point 2

The minimum pressure occurs as the blade passes the monitor point. This is illustrated in Fig 4.4.2.3.
This is again opposed to the position of minimum pressure encountered at Monitor point 1 where the minimum pressure occurred at mid-pitch.

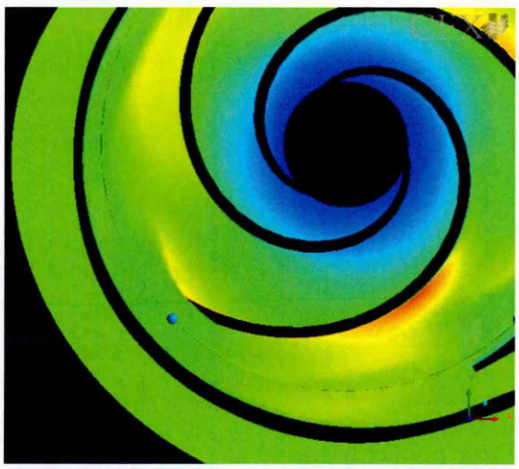

Fig 4.4.2.3 Monitor Point 2 Minimum Pressure

This reverse in positions of the maximum and minimum pressures encountered by points 1 & 2 can be explained, in part, by examination of the position of the previous blade to the measurement point.

Monitor point one experiences its highest pressure as the blade approaches. Analysis of the previous blade position in the row indicates its equidistance from the volute lip. Conversely monitor point 2 experiences the maximum pressure at its mid pitch. This conforms to a position close to the volute lip for the following blade.

The pressure fluctuations encountered by the monitor points are influenced by the blades passing the volute lips not from the blades passing the monitor points.

The wake effect apparent in monitor point 1 is also a consequence of the blade lip interaction effect.

The pressure rises at monitor point 2 by 32% from baseline minimum pressure. The baseline minimum pressure is 574710Pa. The average pressure from blade to blade is 675980 Pa. the maximum pressure peak is 759160Pa.

4.4.3 Unsteady Pressure Readings Taken At Monitor Point 3

Point 3 is centrally positioned between the impeller outside diameter and the volute lip Fig.4.1.2 on the approach to the volute throat. The impulsive nature of the pressure development is linked to the position of the blade angle with respect to the lip.

At this point the nature of the unsteadiness has significantly diminished, demonstrating that volute lip has a strong influence on the unsteadiness. Fig

4.4.3.1 illustrates that the vane rate again dominates the frequency spectra but at a reduced level.

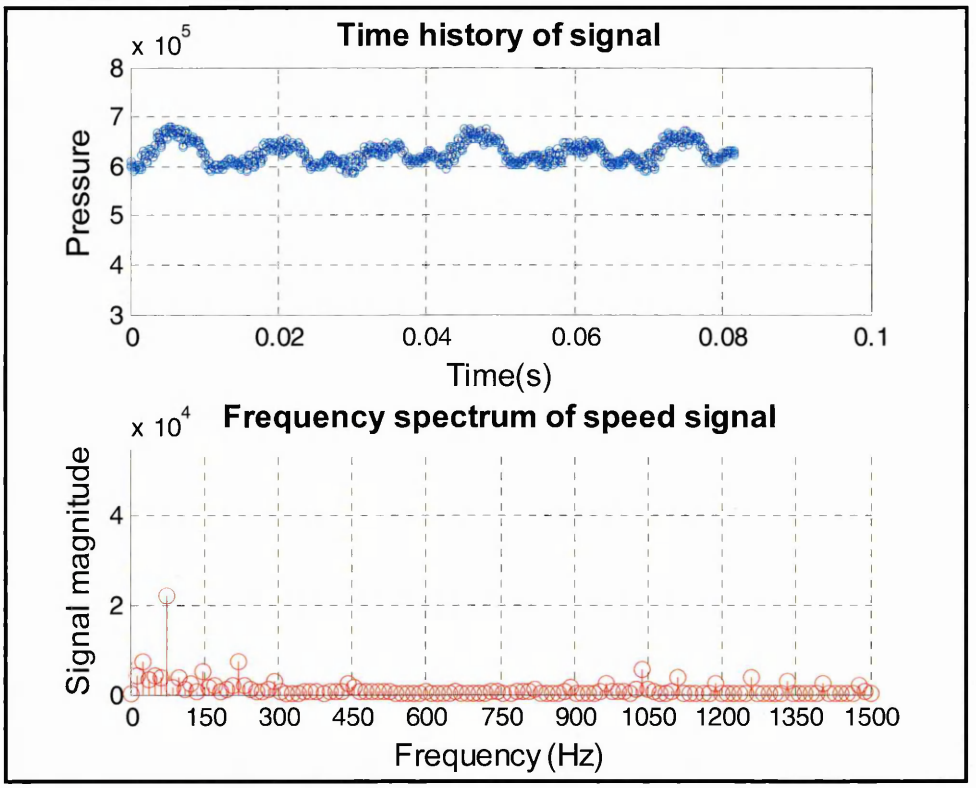

Fig 4.4.3.1 Pressure Pulsation at Monitor Point 3

The pressure reaches a maximum in front of the approaching blade Fig.4.4.3.2.

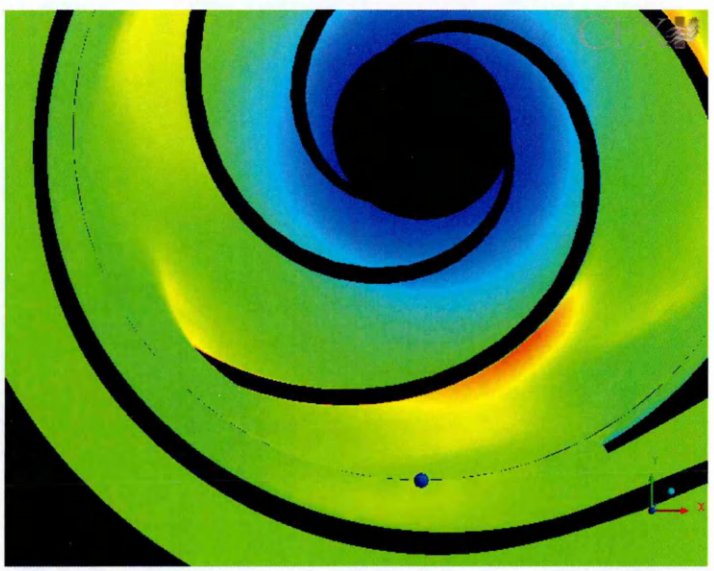

Fig 4.4.3.2 Monitor Point 3 Maximum Pressure

The minimum pressure occurs at 50% of the blade row span Fig.4.4.3.3. The pressure rises by 17.5% from baseline minimum pressure. The baseline

minimum pressure is 643060 Pa. The average pressure from blade to blade is 693865 Pa. The maximum pressure peak is 755650 Pa.

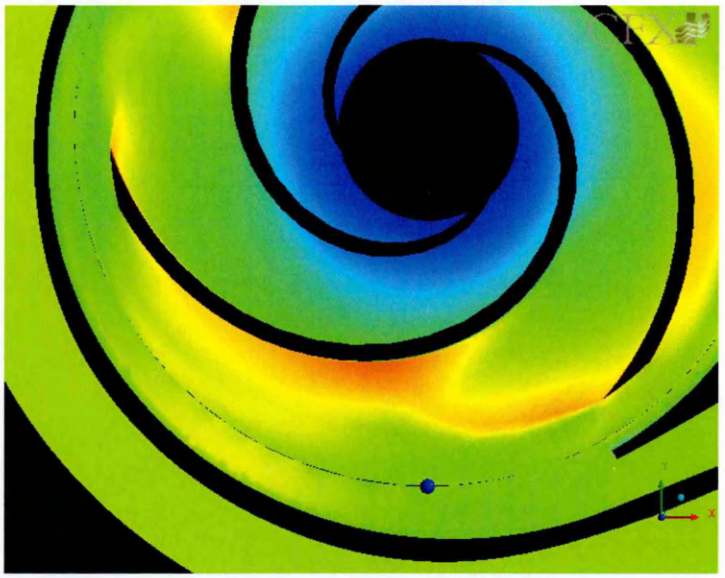

Fig 4.4.3.3 Monitor Point 3 Minimum Pressure

The maximum and minimum pressures are again linked to the pressure fluctuation generated by the lip-impeller interaction and are not directly linked to the blade position with respect to the monitor point.

4.4.4 Unsteady Pressure Readings Taken At Monitor Point 4

Point 4 is centrally positioned between the impeller outside diameter and the volute lip Fig 4.1.2. The impulsive nature of the pressure development is linked to the position of the blade angle with respect to the point and is illustrated in Fig.4.4.4.1.

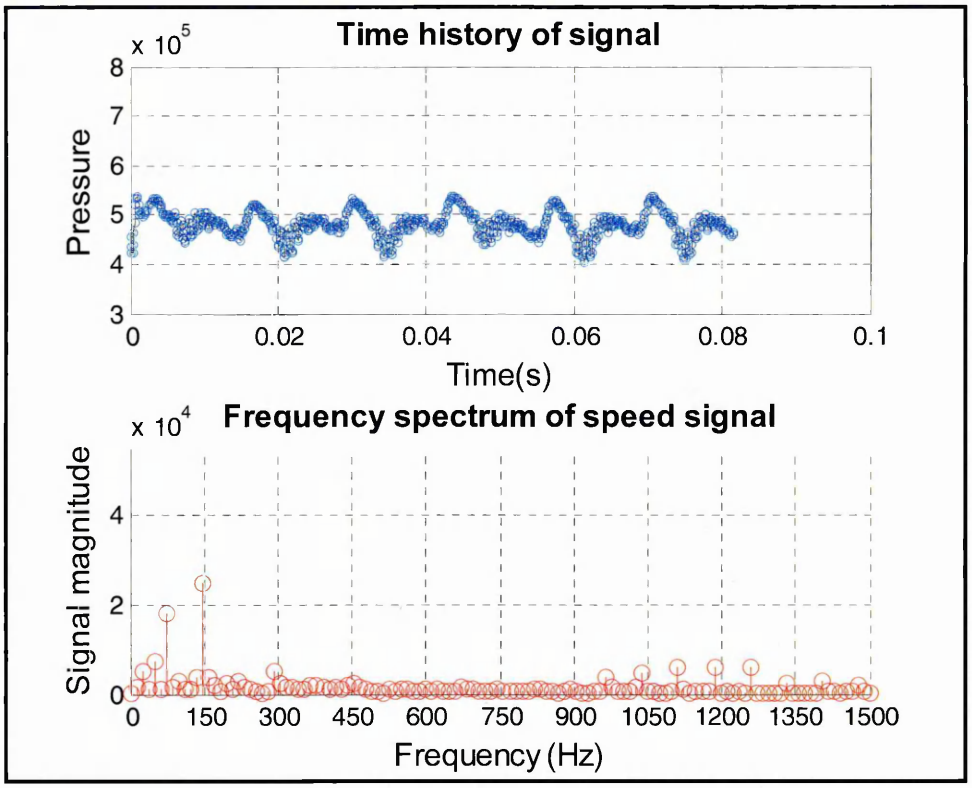

Fig 4.4.4.1 Pressure Pulsation At Monitor Point 4

At this point the nature of the unsteadiness has increased. The monitor point is the closest to the volute lip. Proximity to the volute lip increases the unsteady pressure pulsations. Fig.4.4.4.1 showing the frequency spectrum is now dominated by the twice vane rate level. This is a consequence of both vane and wake passing the lip.

The pressure reaches a maximum as the blade passes the monitor point Fig.4.4.4.2.

Fig 4.4.4.2 Monitor Point 4 Maximum Pressure

The minimum pressure occurs at 50% of the blade row span Fig.4.4.4.3.

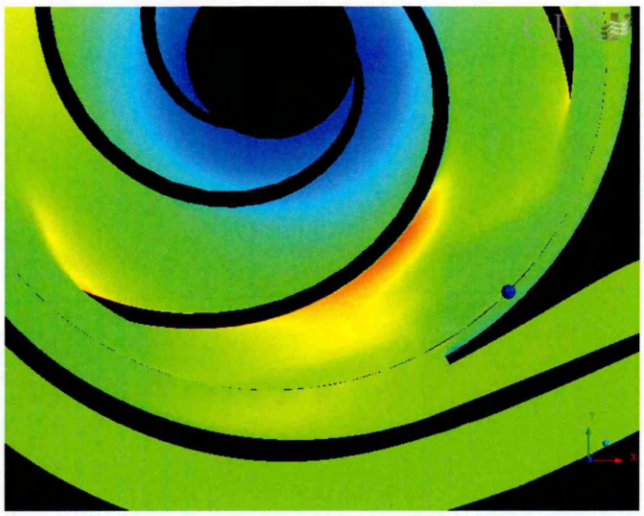

Fig 4.4.4.3 Monitor Point 4 Minimum Pressure

The pressure rises by 35% from baseline minimum pressure. The baseline minimum pressure is 547150 Pa. The average pressure from blade to blade is 651033 Pa. The maximum pressure peak is 736920 Pa.

This conforms to the experimental data generated by Kikuyama et al (1987) which demonstrated the reduction in pressure after the volute lip caused by the impeller vane-lip interaction. Iversen (1960) also observed this phenomenon.

From the comparison of phase position and pressure pulsation, we can agree with observation and experimental analysis of Kaupert and Thomas (1999). These observations, that unsteadiness is 35%, are borne out by the CFD analysis. Kaupert and Thomas also observed that within the diffusing volute the pressure pulsations generated by the lip-vane interaction propagated, not at vane rate, but at acoustic velocities. This accounts for the changing pressure pulsation phases observed within the CFD.

4.4.5 Comparison with Experimental Results

Fig.4.4.5.1 compares the experimental frequency spectra from unsteady pressure readings, taken within the volute of double suction centrifugal pump, with the unsteady pressure spectrum from the CFD solution. Although this machine has some geometric differences from the machine in the CFD analysis the frequency of pressure pulsations is identified at vane rate and twice vane rate. Centrifugal pump spectra are dominated by these two frequencies.

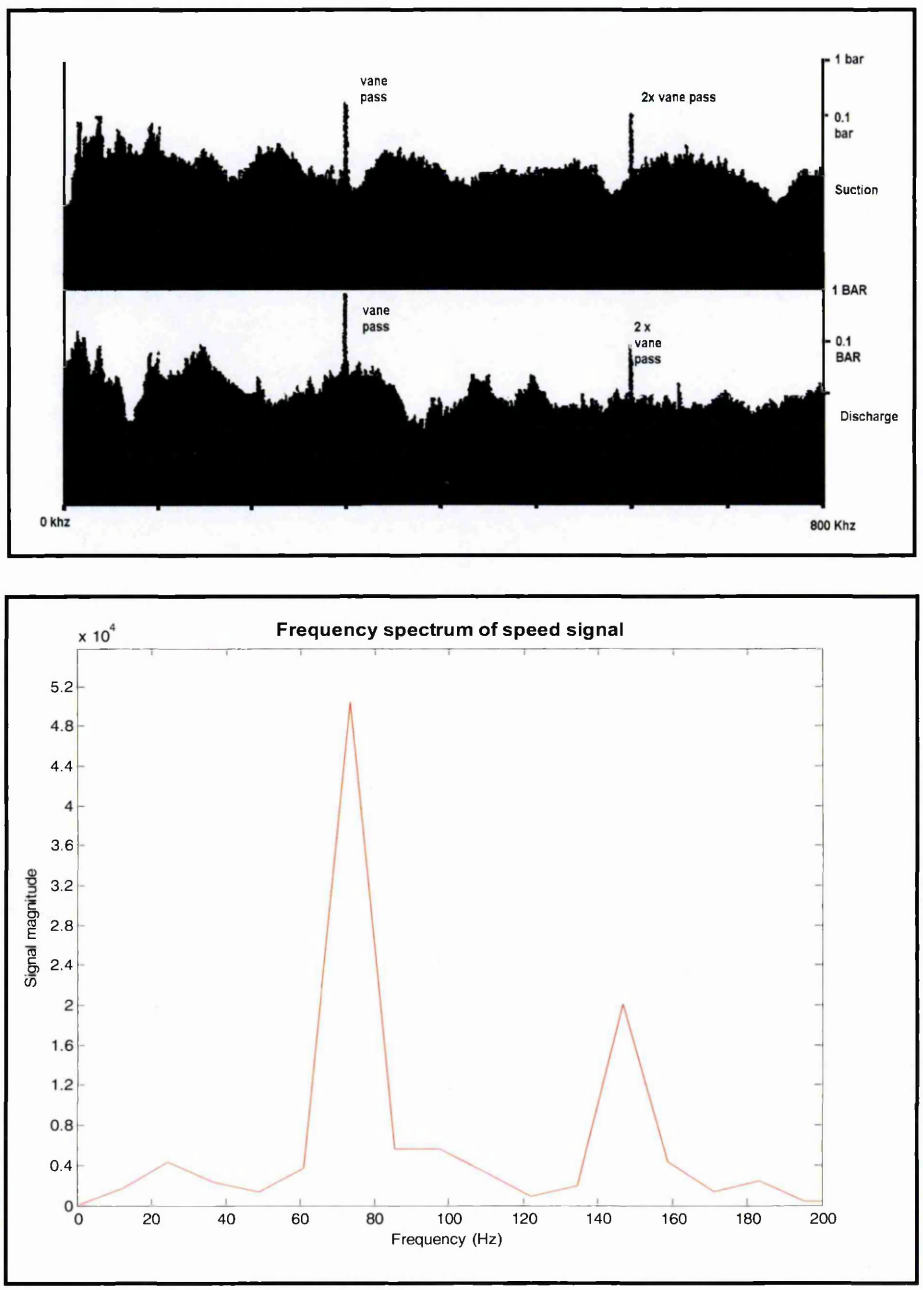

Fig.4.2.5.1 Comparison Of Experimental Spectrum With CFD Spectrum

This correlation added to the accurately predicted time averaged pressure level builds evidence of the credibility of the CFD solution as a means of accurately predicting closed valve head.

4.5 Overview of Volute and Impeller Flow Regime

The following section is used to reveal that the impulsive nature of the pressure development is linked to the position of the blade angle in relation to the volute lip. Fig.4.5.1 illustrates this instantaneous fluctuation in pressure with respect to the blade position. Within this figure the pressure is shown to develop as the blade approaches the volute lip and diminish as the blade passes the lip. This surging flow was observed in the work by Kaupert and Thomas (1999).

The pressure picture, viewed through a cruder breakdown of the fringe plot gives us further insight into the flow features evident in the machine. The strength of the wake is particularly noticeable as the blade approaches the volute lip. This strong feature diminishes then disappears when the impeller blade has passed the volute lip illustrated in Fig 4.5.2.

This can also be seen in Fig 4.5.3 which take account of the velocity profiles to illustrate the flow features. The diffusing passage ways are filled with a slow moving liquid. Pressure pulsations drive into the slow moving body of fluid at vane pass frequency. Also apparent is a distinct frequency at rotational speed.

This again is in conflict with the perceived wisdom that the impeller acts as a solid disc (Nielsen 1989) driving the fluid with the volute by cylindrical viscous forces alone. Newton's(1998) analysis of the solid body theory concluded that the impeller solid body rotation did not exist, but his experimental evaluation was flawed. He merely closed off the impeller outlets with a circumferential strip of metal and measured the generated pressure. This approach negates the rotor-stator blade interaction pressure fluctuations.

Fig 4.5.4 also provides some insight in into the rotor stator interactions and is able to demonstrate why the vane pass frequency exists in the diffusing passageways.

The velocity vectors are observed to be driven between the impeller blade and the casing cutwater as proposed by Kaupert and Thomas (1999). This provides a peristaltic effect at closed valve. The diffusing passages experience a forcing of the fluid into the fixed area chamber. They then are relieved as the impeller blade passes beyond the cutwater and the large A2BB area is congruent with the casing cutwater.

Research papers, including Abraman and Howard (1988) and Fischer and Thoma(1952), pointed out the strong links between phase position and flow features. Pressure plots from the CFD presented in Fig 4.5.2 denote the strong wake effects that propagate then diminish as the impeller blade passes the casing cutwater.

Fig 4.5.3 is illustrative of different flow regimes that can be observed in different areas of the pump. The long and short diffusing passage ways are filled with slow moving liquid. All the dynamic rotor-stator interaction effects take place within the volute, around the impeller periphery.

Fig 4.5.4 demonstrates this dynamic effect as the stalled nature of both impeller and volute drive the liquid trapped between these components into the annular gap.

The nature of the impeller geometry causes the wake effect, streaming from the suction side of the blade, to be trapped by the liquid in the annular gap between the impeller and volute and, looking in the relative frame, to be turned inwards as it is bound by the higher velocity stream within this gap.

The resulting vortex in the outer proportion of the impeller is as observed by Acosta and Bowermann (1957) who described this as "dead water". Looking in the absolute frame this observation would hold true. Worsters (1953) observations where these exit relative eddies were first observed, also supports the CFD qualitative predictions.

Acosta and Bowermann (1957) observed their eddy rotating counter to the machine rotation. The CFD predicts that the eddy is always apparent but its extent pulses with the impeller blade interaction. This pulsing phenomenon would appear to rotate counter to the machine rotation and would agree with the Acosta and Bowermann (1957) observations.

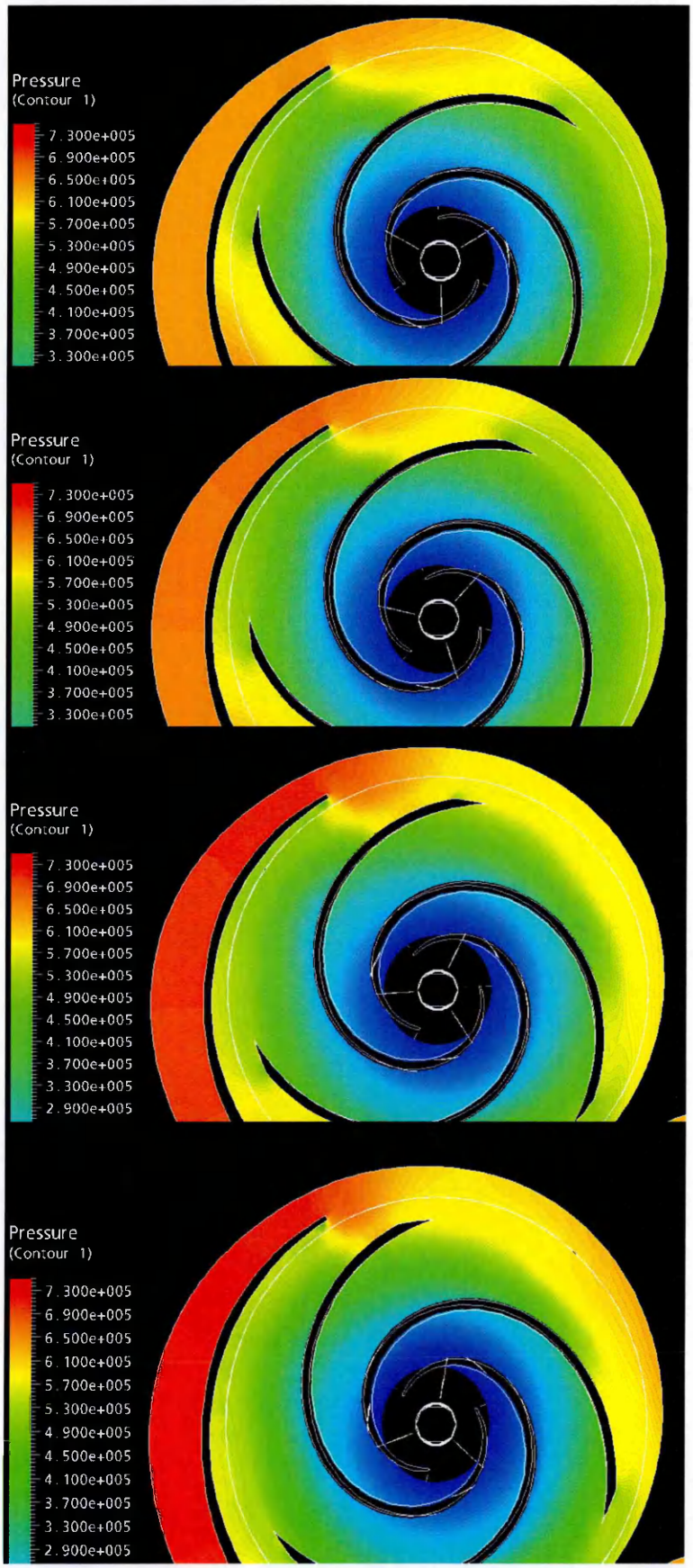

Fig 4.5.1 Unsteady Non Linear Pressure Increase Around The Volute

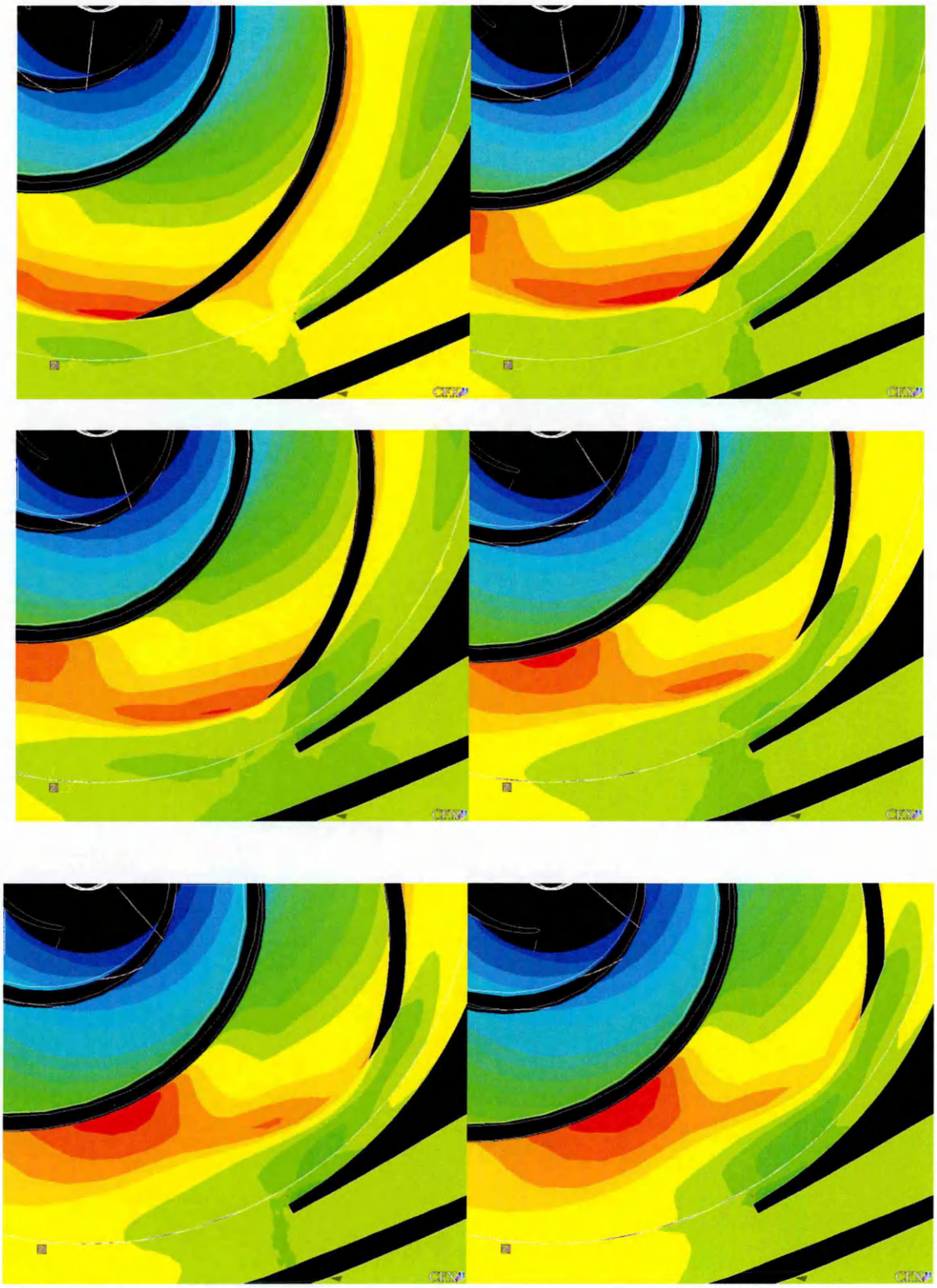

Fig 4.5.2 Pressure Plot of Impeller Vane and Stator Interaction

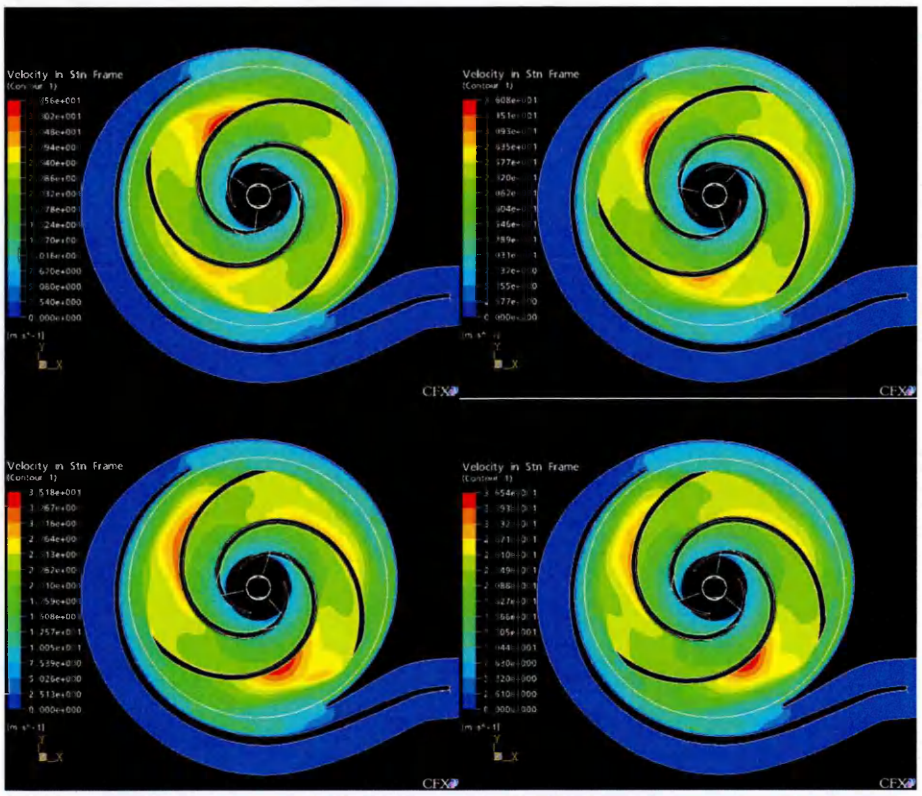

Fig 4.5.3 Comparison of Velocity Plots at Mid Streamline

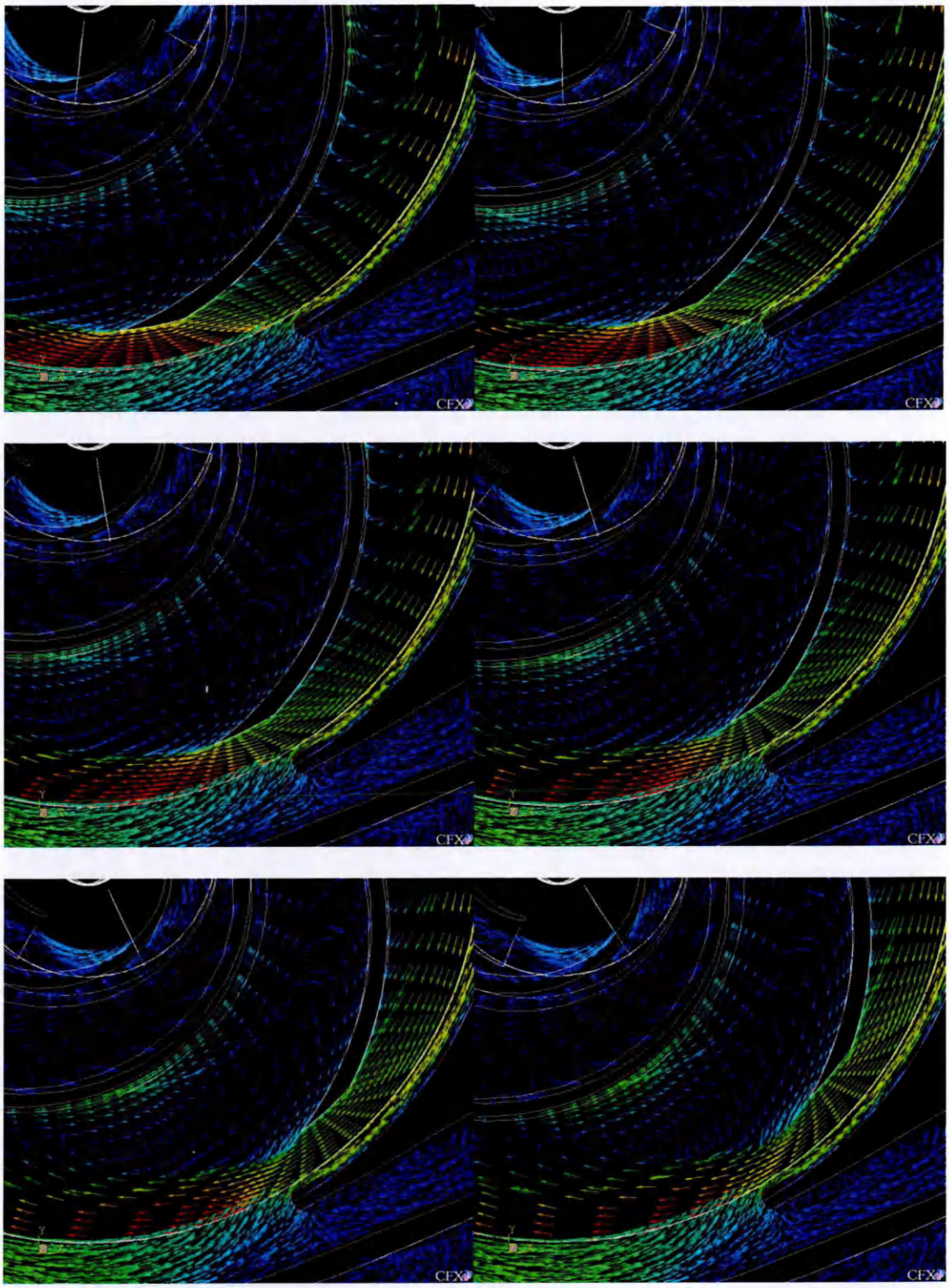

Fig 4.5.4 Vector Plot of Impeller Vane and Stator Interaction

4.6 Volute Passageways

The nature of the unsteady pressure pulsations within the stalled short and long passage ways is weak. Pressure pulsations passed from the approaching blade are manifest within the volute passageways. If we take a radial view across the volute throat and plot the maximum and minimum pressure levels we see that the pressure level close to the volute lip is the greatest. Away from the lip the pressure level is constant with consistent unsteadiness Fig.4.6.1. The point Positions are depicted in Fig 4.6.2.

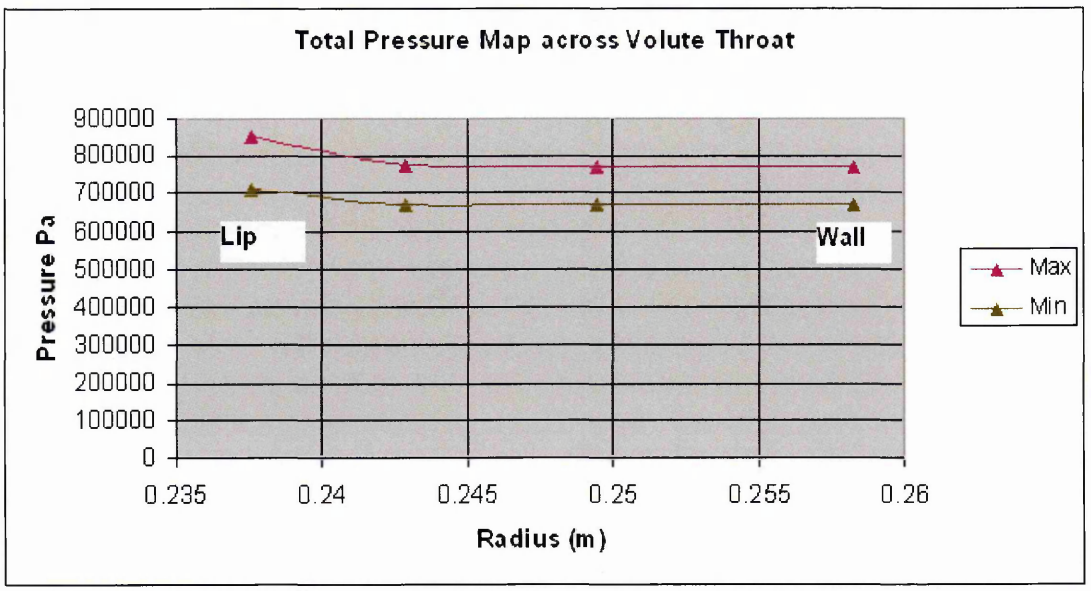

Fig 4.6.1 Pressure Map across Volute Throat

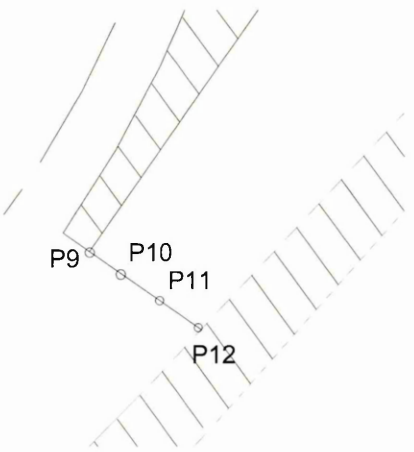

Fig 4.6.2 Position of Points across the Volute Throat

A phase shift in the fluctuations in Fig.4.6.3 and Fig.4.6.4 can be seen within the volute sections The unsteady pressure fluctuates by 14%

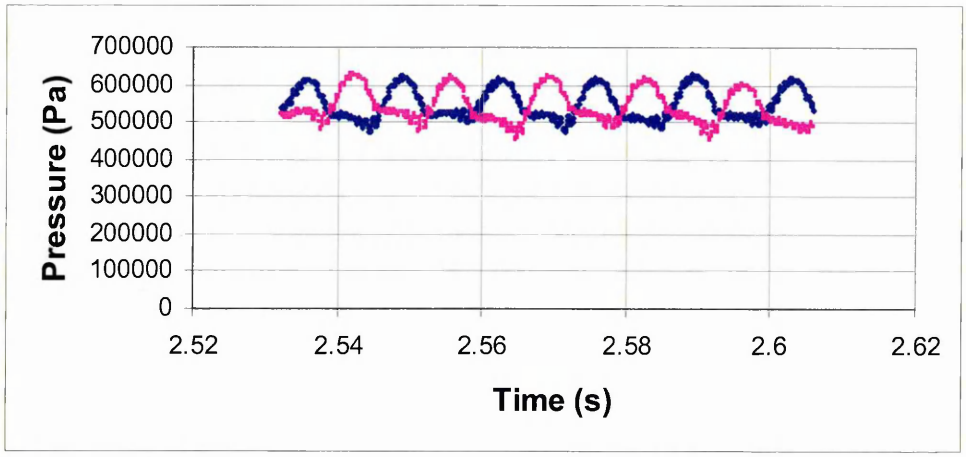

Fig 4.6.3 Comparison of P1 & P5 from Fig 4.1.2

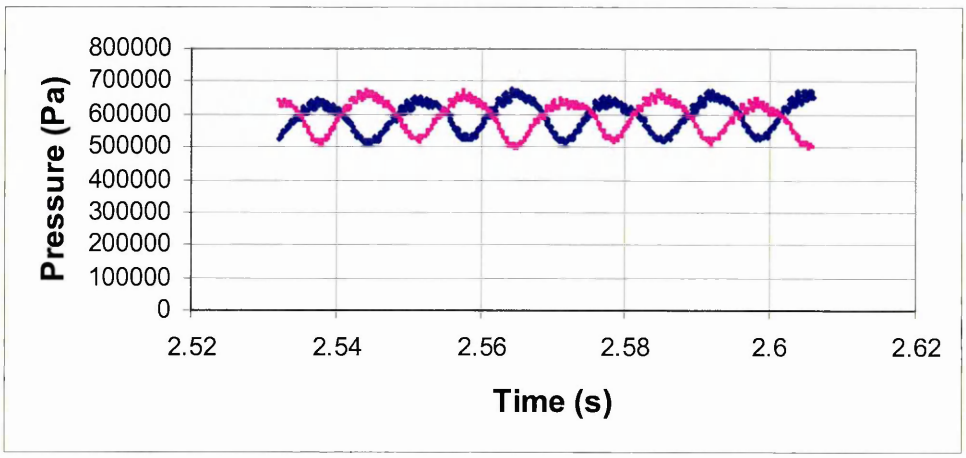

Fig 4.6.4 Comparison of P2 & P6 from Fig 4.1.2

As expected with a 3 vane impeller operating within a double volute machine there is a 180 degree phase shift between the pressure pulsations in the long and short passageways.

Inspection of the pressure profile across the casing throat and its associated frequency spectrum again illustrates the dominance of the vane rate frequency Fig.4.6.5.

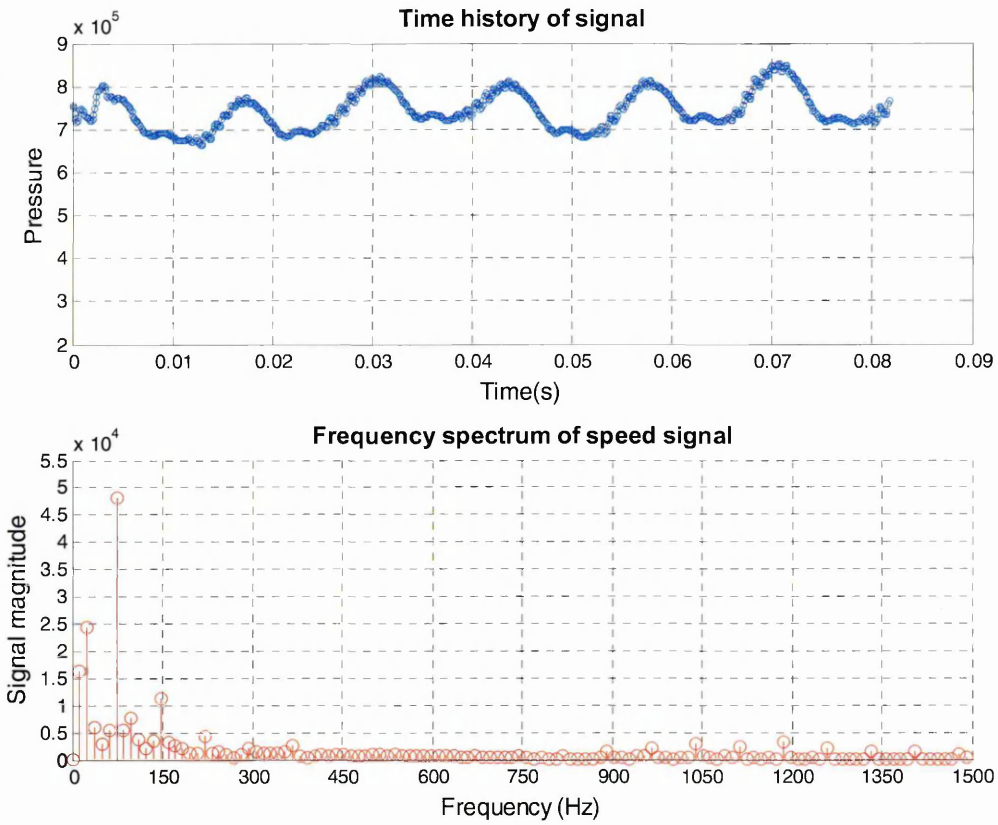

Fig 4.6.5 P9 Throat Close To Lip

The diffusing discharge passages of the pump are filled with a low velocity fluid. The pressure fluctuations within these passages are driven by the blade frequency. As the impeller blade tip approaches the volute lip, the pressure within the discharge duct reaches a maximum. As the blade tip passes the lip the pressure within the discharge duct decreases, but a pressure rise within the impeller is manifest.

The double design of the volute spiral casing is popular with centrifugal pump designers as it is used to balance the radial loads imposed on the bearings. The design consists of two discharge ducts, used to transport 50% of the flow. These two ducts then join together at the pump discharge nozzle. These two ducts experience pressure pulsations at independent periods based on the impeller blade position.

Fig.4.6.6 illustrates the pressure rise within the volute passages across the throat. The time-step horizontal scale represents the period over which one impeller blade passes the cutwater.

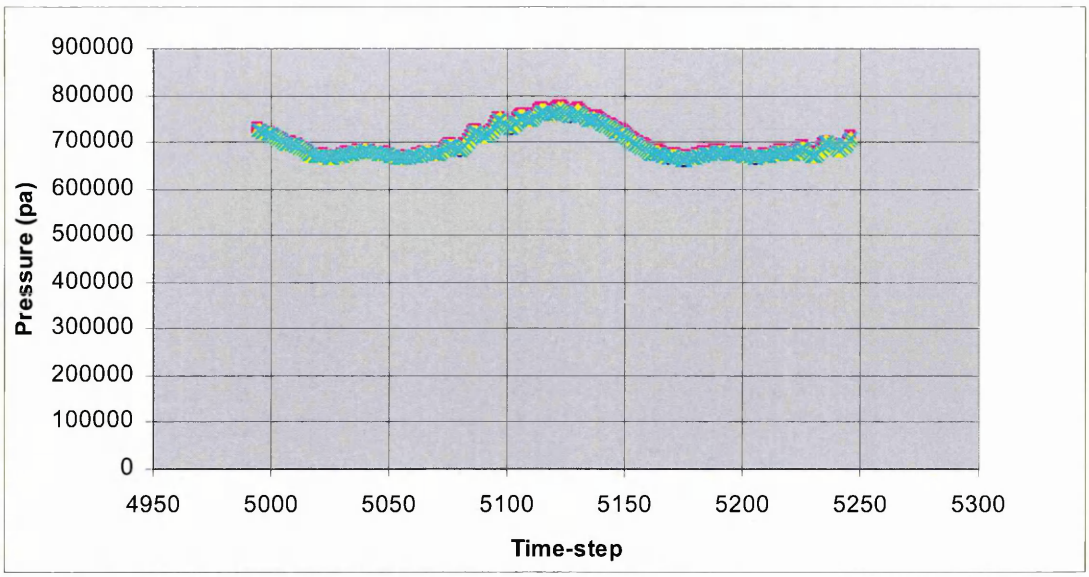

Fig 4.6.6 Pressure Map across Volute Throat

This illustrates that the unsteady pressure levels for P9-12 do not differ from each other in the radial direction. The spectrum is dominated by vane frequency at all points across the throat as illustrated in Fig 4.6.7.

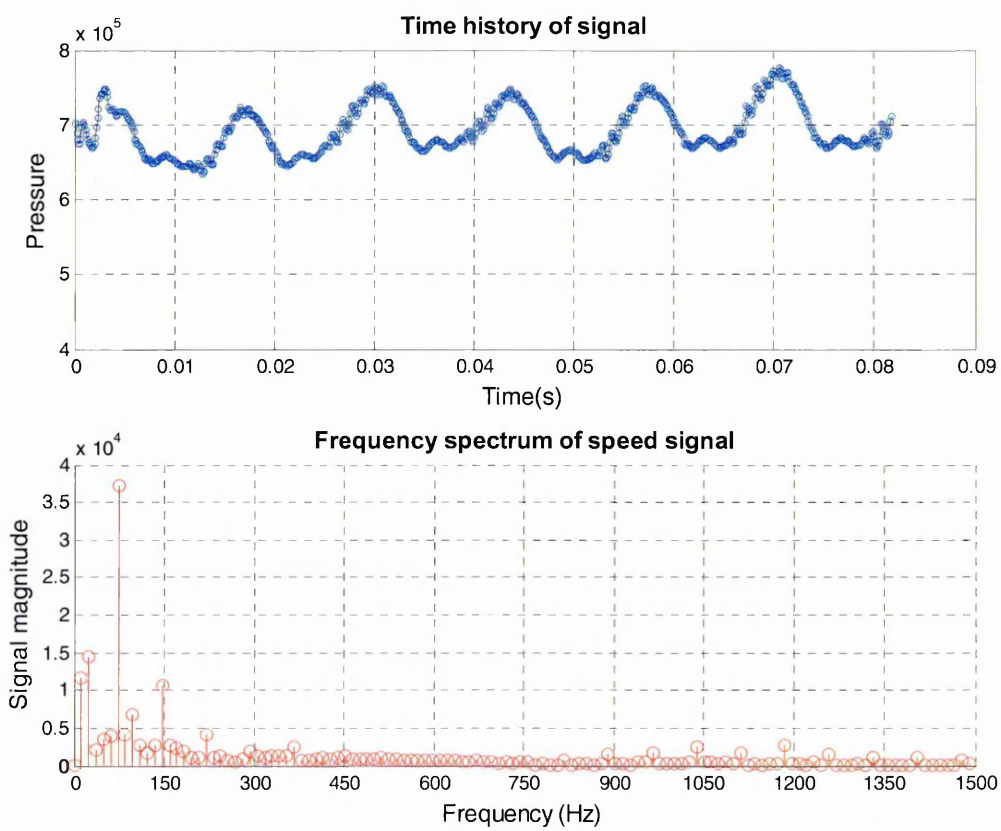

Fig 4.6.7 P9-12 Pressure across Throat Equal For All

The discharge duct described in the Newton (1998) single volute proposition, contains a rotating eddy in the discharge passage driven by the viscous forces imposed by the impeller discharge flow. This situation is not representative of the flow regime within a double volute pump.

Although the fluid within the duct is moving at low speed, the situation of a driven vortex as suggested by Newton (1998) does not occur. The vortex is broken by the addition of a volute lip. The flow within the volute pulses between these divided discharge ducts as each duct experiences the pressure pulsation imposed upon it by the approaching vane as defined by Kikuyaman et al (1987).

The unsteadiness within both the short and long diffusing volute passageways is significantly less than around the periphery of the impeller.
This is demonstrated by fig 4.6.5 –fig.4.6.11 which illustrates a pressure fluctuation of 10% within the short passage and 8% within the long passage.

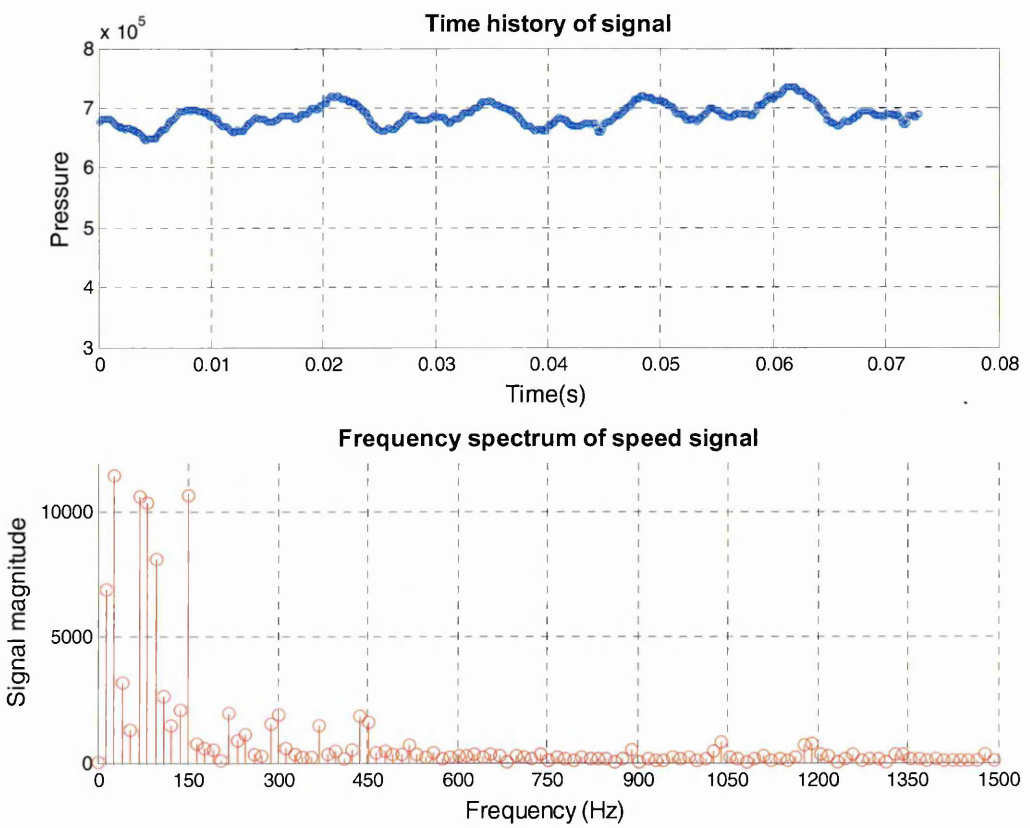

Fig 4.6.8 Spectra For Points Across Position B from Fig 4.1.3

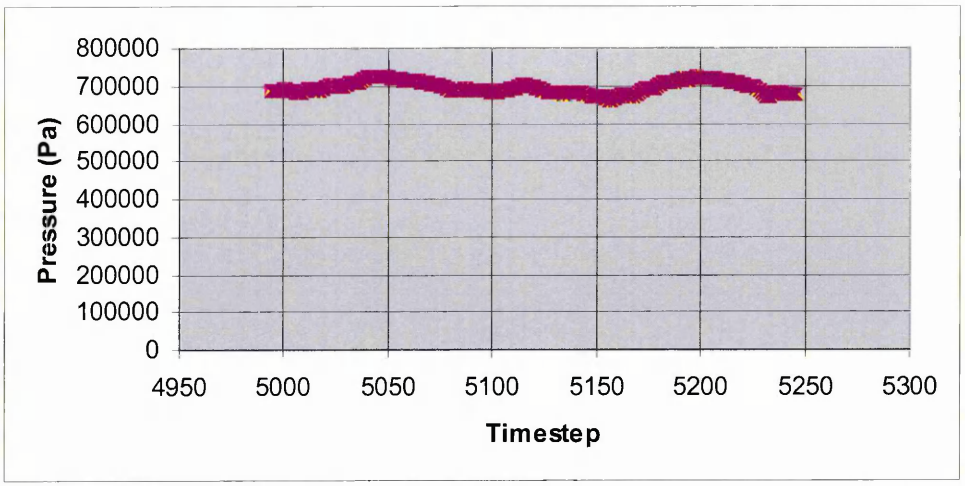

Fig 4.6.9 Pressure Map across Position C from Fig 4.1.3

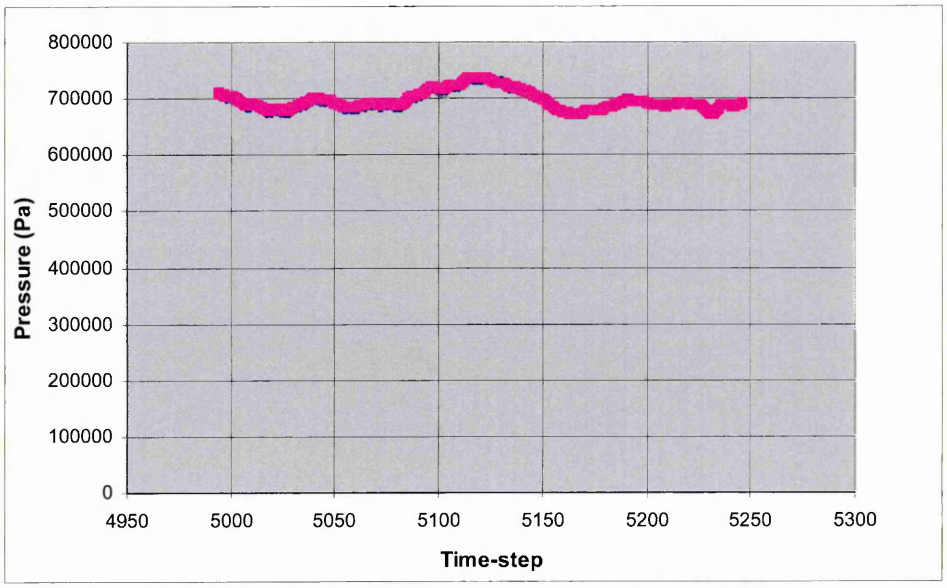

Fig 4.6.10 Pressure Map across Position B from Fig 4.1.3

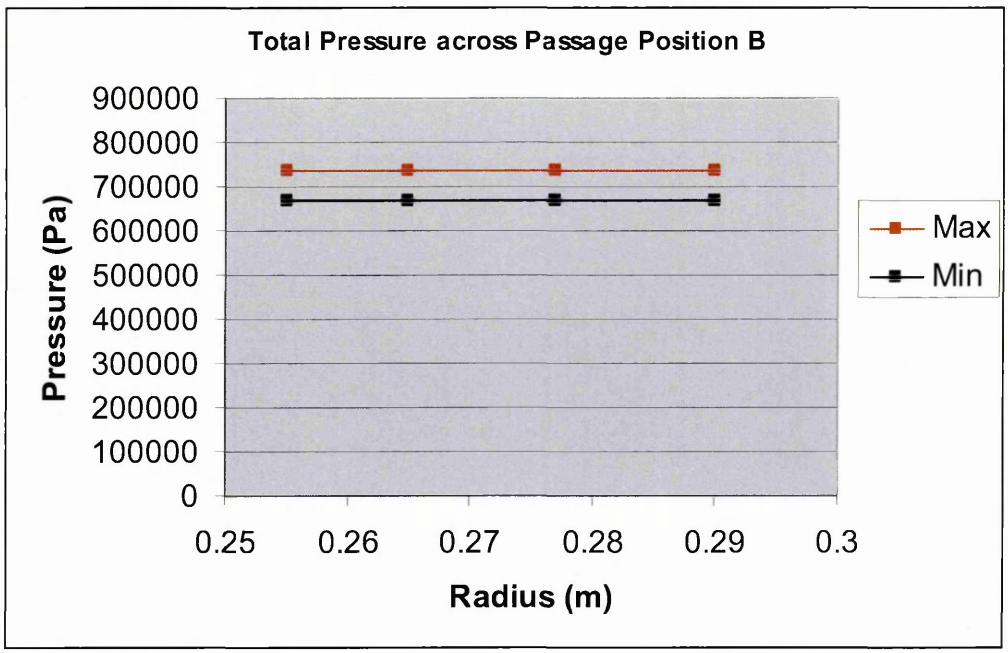

Fig 4.6.11 Pressure Map across Position B from Fig 4.1.3

This fluctuation is also represented within the discharge proportion of the volute casing when the two diffusing passages join together. The pressure fluctuation is 10 %. This is significant as the time averaged closed valve pressure is taken within this region for all centrifugal machine performance curves.

The dominance of the blade pass frequency allows us to conclude that the blade interaction frequency has an effect on the closed valve head of a machine. This agrees with the analysis of Peck (1950) who concluded that the impeller diffusion ratio w1/w2 (which is related by vane number) could be controlled to ensure pump stability. This theory is, though, based on empirical analysis of steady state data.

From these figures it can also be shown that the pressure profile within the volute are consistent across the passage. Unsteady pressure maps taken in the radial direction do not differ from each other. This is as observed Worster (1953).

Fig.4.6.12-fig 4.6.17 features the unsteady pressure fluctuations within the diffusing passageways and across the discharge as illustrated in Fig.4.1.3.

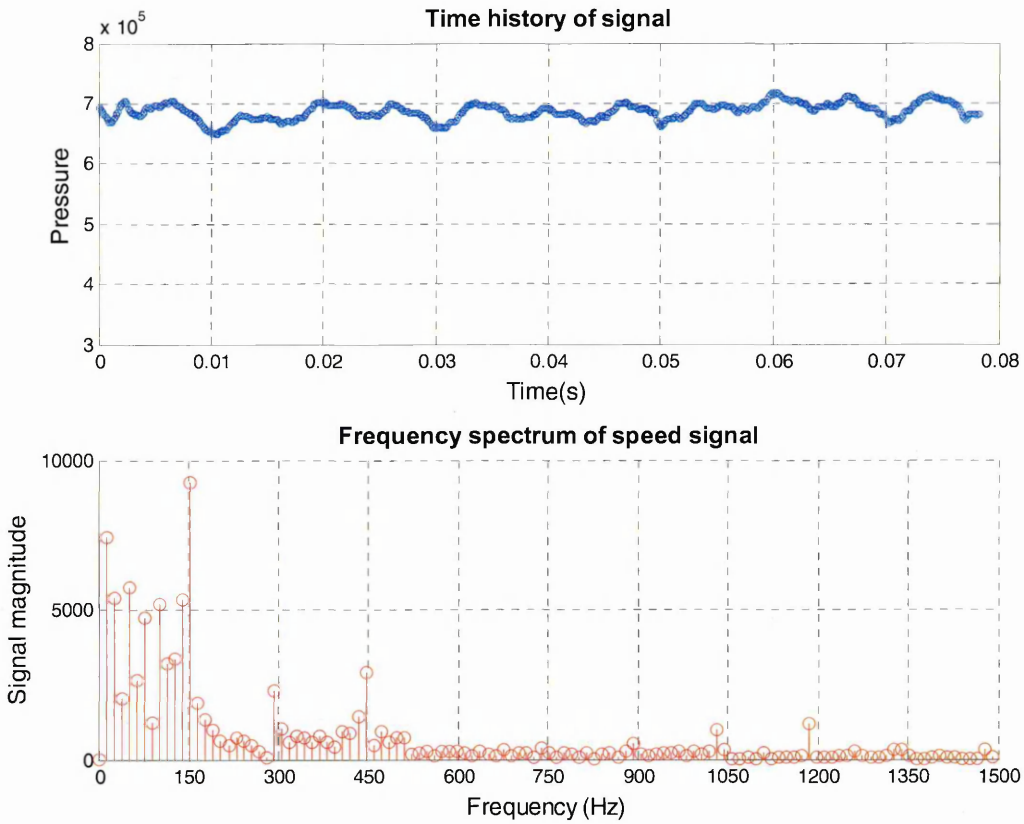

Fig 4.6.12 Pressure Map Position C Across All Points from Fig 4.1.3

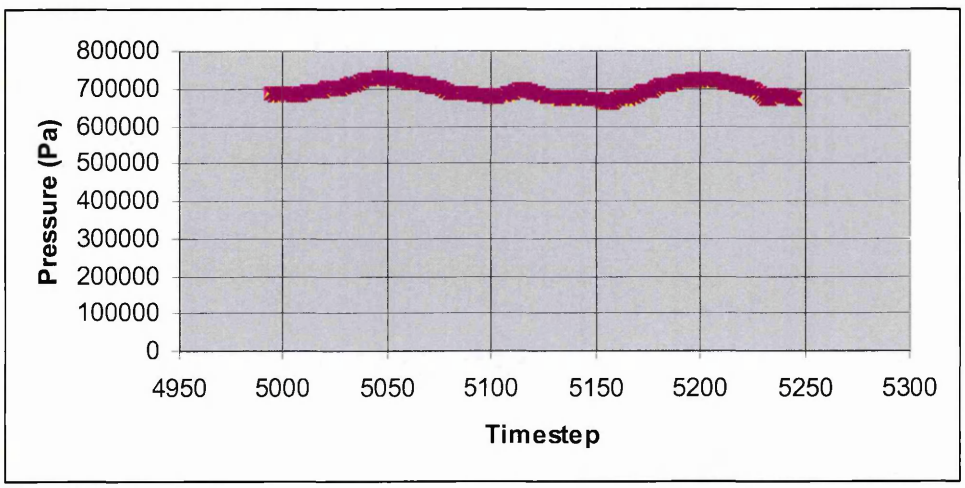

Fig 4.6.13 Pressure Map Across Position D from Fig 4.1.3

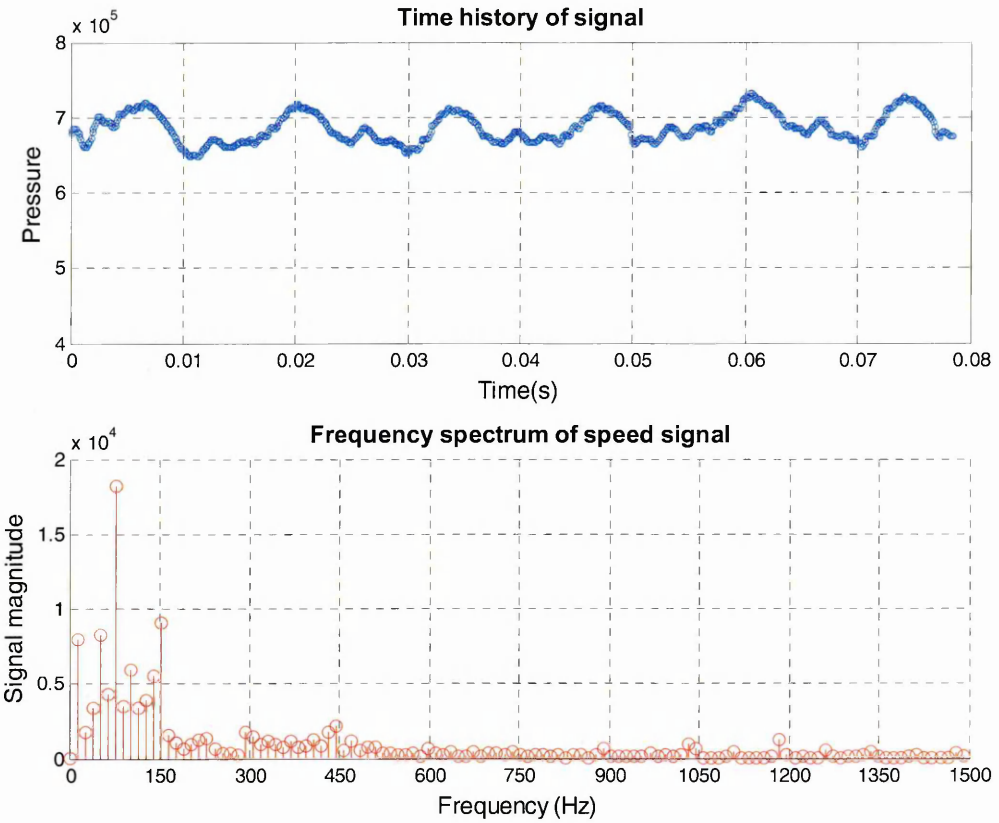

Fig 4.6.14 Position D Freq Spectrum from Fig 4.1.3

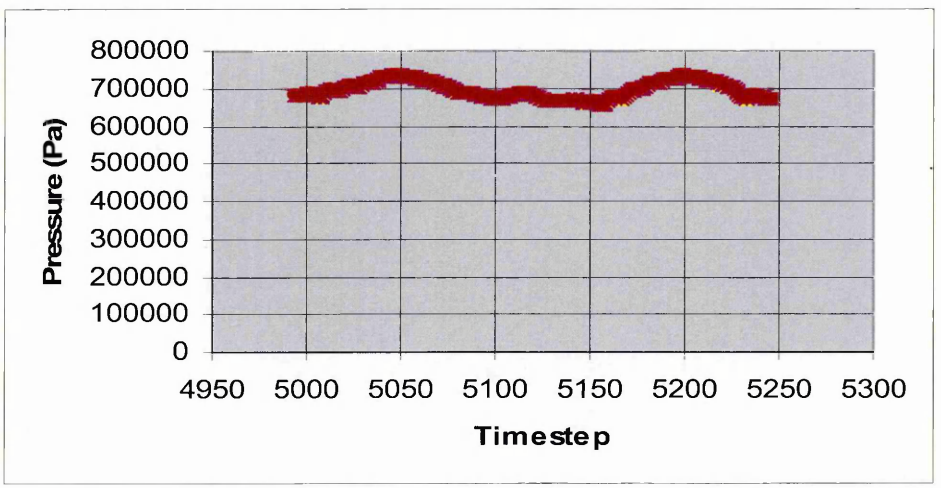

Fig 4.6.15 Pressure Map Across Position E from Fig 4.1.3

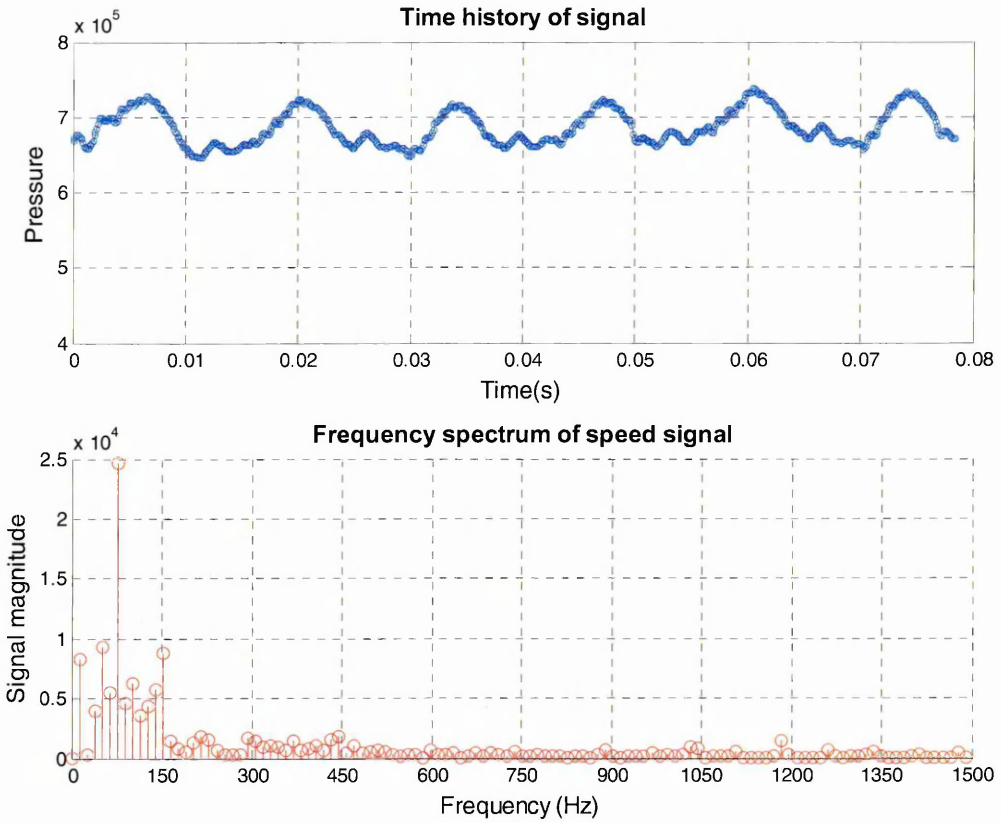

Fig 4.6.16 Spectrum For Position E from Fig 4.1.3

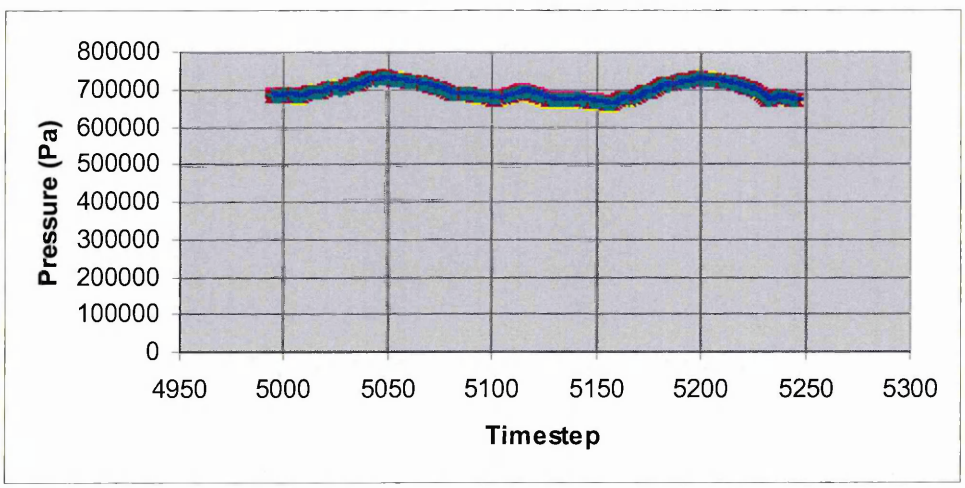

Fig 4.6.17 Pressure Map Position F from Fig 4.1.3

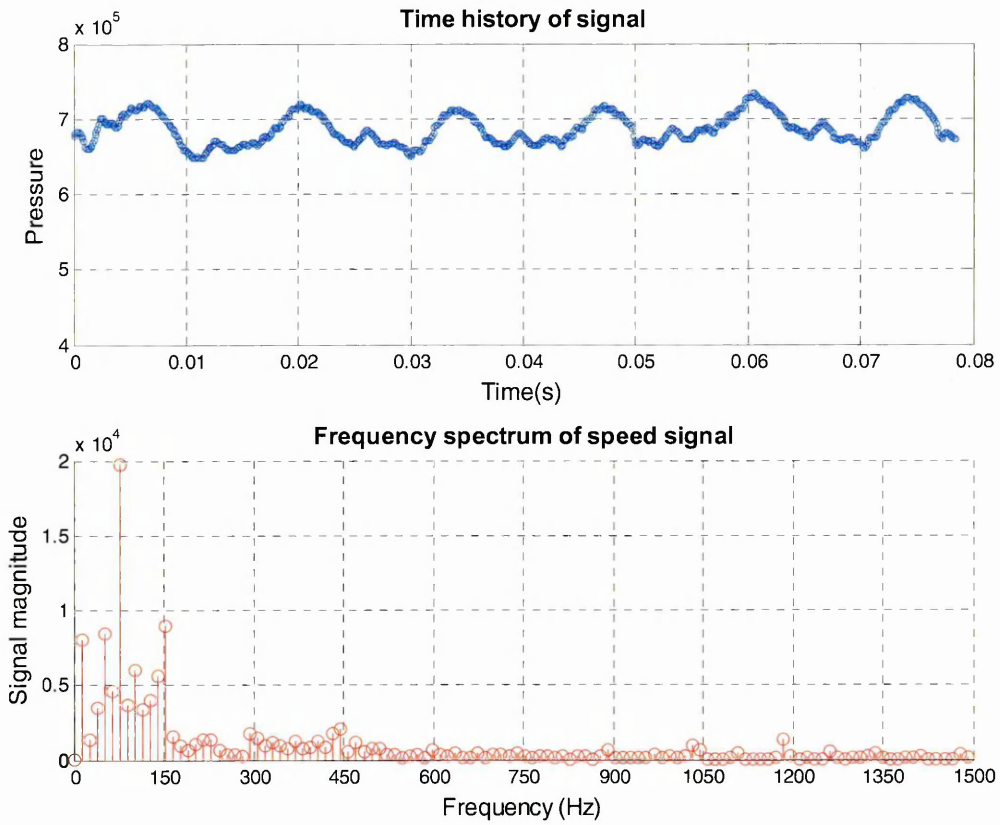

Fig 4.6.18 Spectrum across Discharge Position F from Fig 4.1.3

The two predominant frequencies of pulsation in these figures are rotational speed and vane passing.

At all positions the unsteadiness induced by the rotor stator interaction has diminished. All the time histories centre on the $7.0x10^5$Pa and there is no pressure recovery due to the passage shape or length.

The closed valve head of the machine is directly linked to the interaction effects between the impeller and casing volute lip. The average pressure is determined by the peristaltic action and pressure recovery of the impeller blades as the pass the volute lips. The casing diffusing passageways have a lesser effect on this and are filled with slow moving liquid trapped by the impeller outlet flux. This outlet flux migrates from the long diffusing passageway into the short diffusing passageway. For the purposes of the development of a design prediction methodology the passage flow regime could be considered steady.

It is significant to compare the flow direction within the volute long and short diffusing passageways with the flow direction given within the Newton research.

Fig 4.6.19 illustrates the flow around the splitter which divides these two passage ways

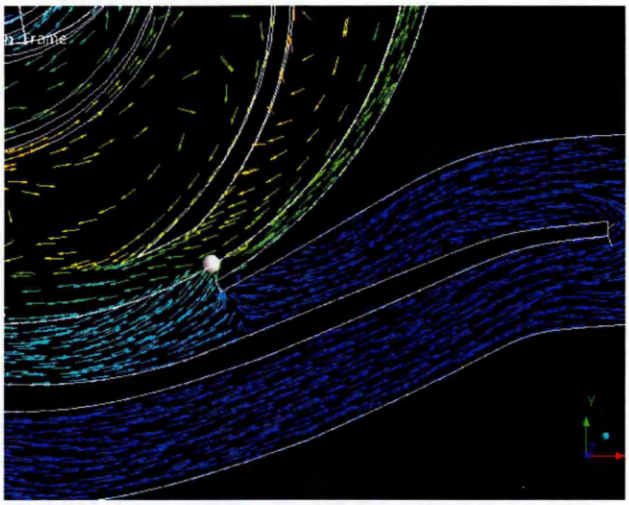

Fig 4.6.19 Long - Short Passage Flow

Research on single volute machines gives a different flow picture to the one encountered within a double volute pump.

Of particular interest within the double volute pump is the nature of cross passage slow moving liquid. Within the single volute this cross passage flow regime is allowed to form into a vortex within the discharge channel. This vortex pulses as the velocity streams from the impeller vanes interact with the slow moving liquid bound within the discharge passage. Viscous forces which alter with impeller phase position drive this bound vortex.

Within a double volute pump the driven vortex cannot form and a cross channel flow is setup as seen by Kikuyaman et al (1987). Liquid is driven from the long passage into the short passage.

4.7 Impeller Flow

The mental model proposed by Simpson and Cinnamond (1964) for flow within the impeller defines the inner proportion of the impeller as filled with a standing vortex of a common radius of ½ of the impeller diameter. The proportion of liquid trapped above it drives this vortex, forcing fluid to re-circulate through the impeller eye and into the suction duct. The flow phenomenon from the CFD analysis generally conforms to the observations, but superimposed on this steady state picture must be the unsteady effects.

The unsteady effects are evident when analysing a 3 vane impeller within a double volute casing. The impeller blade passages experience a different flow field with respect to their position relative to the volute cut-water.

Position A fig 4.7.1-fig.4.7.2– The upper proportion of the impeller passage, close to the discharge area of the impeller, is filled with a standing eddy. The viscous forces applied by the stalled collector passages drive this eddy as the fluid around the impeller periphery is squeezed between the volute lip and the approaching impeller blade. This further drives the intensity of the inlet vortex.

Position B fig 4.7.1-fig.4.7.2– This represents the interface between the discharge rotating eddy and the inlet backflow eddy. This suction eddy is characterised by a local separation from the pressure side of the blade, close to the hub. This local development is manifest as the volume flux is reduced, becoming more stable as the flux approaches zero. Unsteadiness of the flow develops coupled to transient operational loading. At closed valve this complex inlet discontinuity gives rise to a span wise flux from pressure to suction side. The flow re-circulation zone viewed from the relative frame is characterised by this standing eddy rotating counter to the machine rotation.

Position C fig 4.7.1-fig.4.7.2 – At this position the flux stream has passed from the hub across the passage span to the blade suction side in the meridional plane. The region is associated with strong secondary flow phenomenon and three-dimensionality, as the inlet eddy is driven out from the impeller and into the suction channel as described in section 4.8.

Position D fig 4.7.1-fig.4.7.2– The largest proportion of the streamline passage is characterised by strong flow re-circulation at mid position on the blade pressure side. The vortex, driven by the viscous interaction with the fluid trapped within the volute, experiences stochastic fluctuations that are characterised by the size of the discharge vortex with respect to the volute lip position. When a blade approaches the volute lip the relative volume flux is squeezed between the lip and the rotor-stator interface gap[1].

[1] ~This can be as small as 2% of the impeller maximum diameter. For centrifugal pumps reducing this gap has a beneficial effect. The wake shed by the upstream rotor is stretched out into the stator passage generating a smaller mixing loss than if the wake were completely mixed out before entering the volute.

This suppresses the vortex development by providing a firm viscous boundary. As the impeller blade moves past the volute lip the diffusive contribution of the volute decays the intensity of the trapped casing fluid, allowing the impeller discharge vortex to move forwards along the pressure side of the impeller blade. A snapshot of this phenomenon can be seen in fig.4.7.1 by comparison of the flow regime in individual impeller passages. The arrows in fig.4.7.1 represent the position of the volute lips.

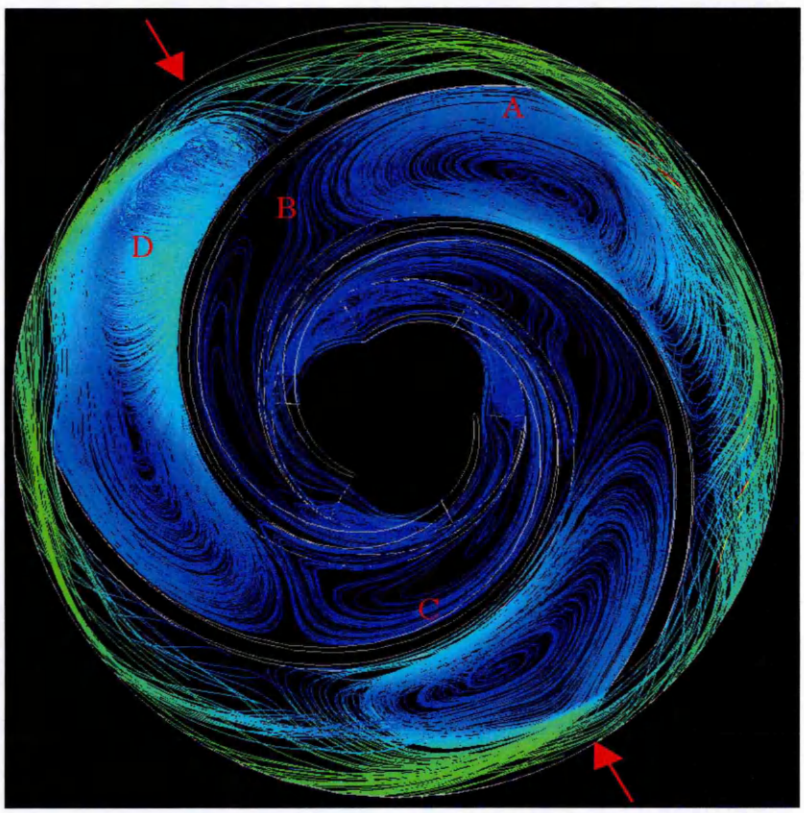

Fig 4.7.1 Impeller Streamlines at Closed Valve Low Solidity Impeller

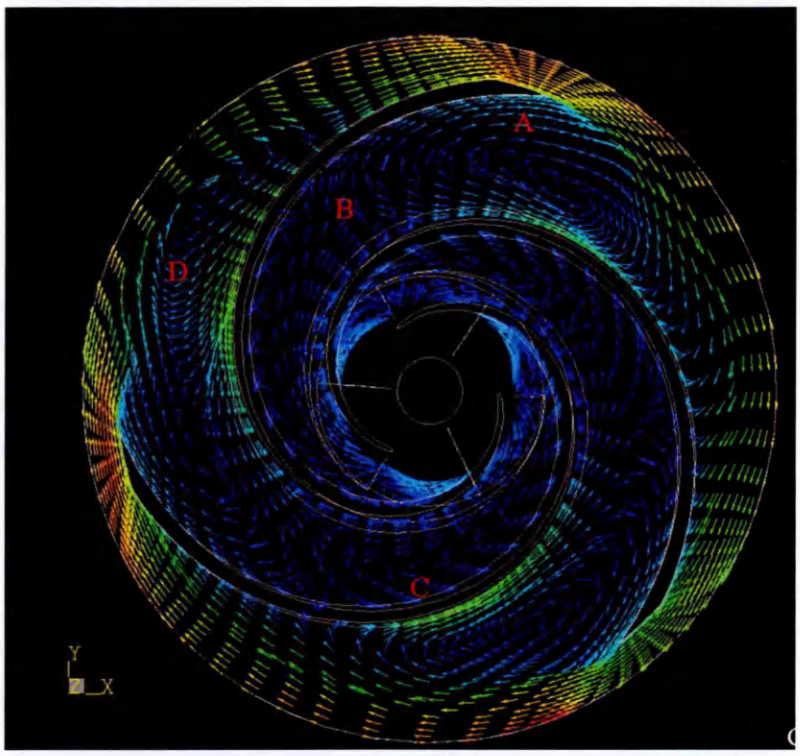

Fig 4.7.2 Velocity Vectors Within 3 Vane Pump Impeller at Closed Valve for a Low Solidity Impeller

The true nature of the unsteady pressure fluctuations can be defined by plotting the pressure fluctuations at varying impeller diameters. Within the impeller passage the unsteady pulsation is at a maximum close to the cutwater lip.

This demonstrates that as the impeller blade approaches the casing cut-water the velocity of the fluid, forced through this gap, increases. This suggests that the volute is completely stalled within the discharge proportion of the casing filled with dead liquid. Whilst directly within the throat the casing experiences a fluctuating pressure field, this is greatly reduced when compared to the unsteady pressure at the pump discharge flange.

4.7.1 Points on Horizontal Centre Line

5 points lie on the horizontal centre line of the impeller as illustrated in Fig4.7.1.1 These points are used to monitor the unsteady pressure readings.

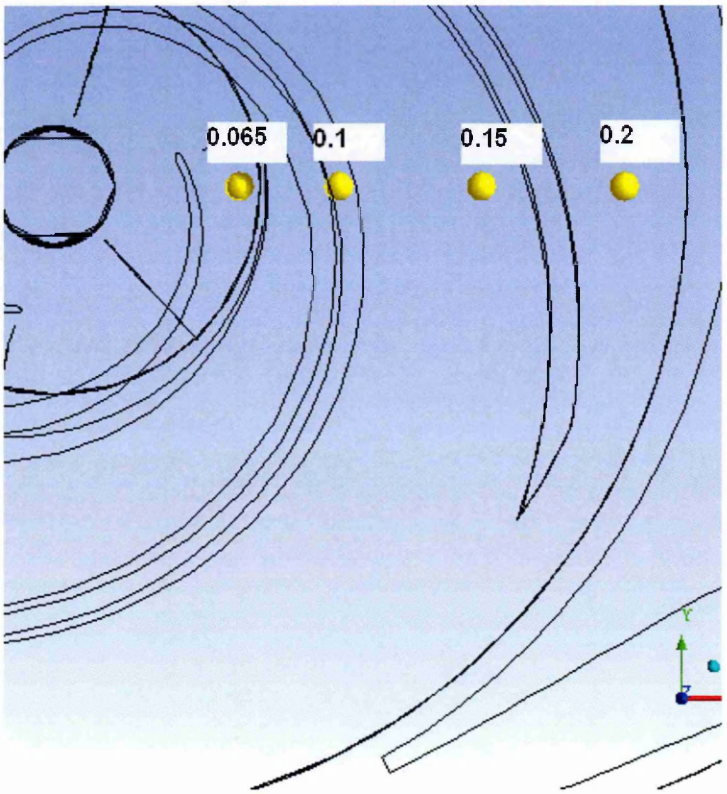

Fig 4.7.1.1 Position Of Impeller Points

Fig.4.7.1.2- fig.4.7.1.6 contain the unsteady pressure signal and the subsequent FFT analysis of that signal. Each of these signals is generated on the at the impeller blade centre. The monitor points chart the change of unsteady pressure and FFT signal from the outer rim of the impeller inwards.

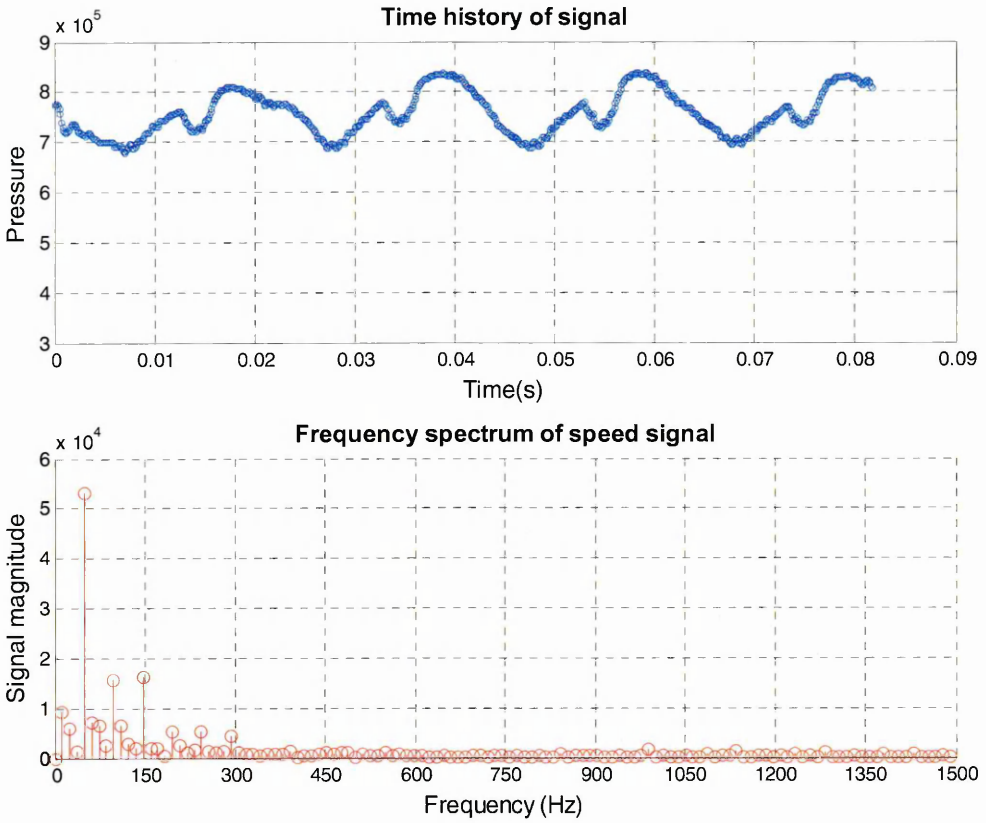

Fig 4.5.1.2 Pressure In Stationary Frame At 0.2m Radius

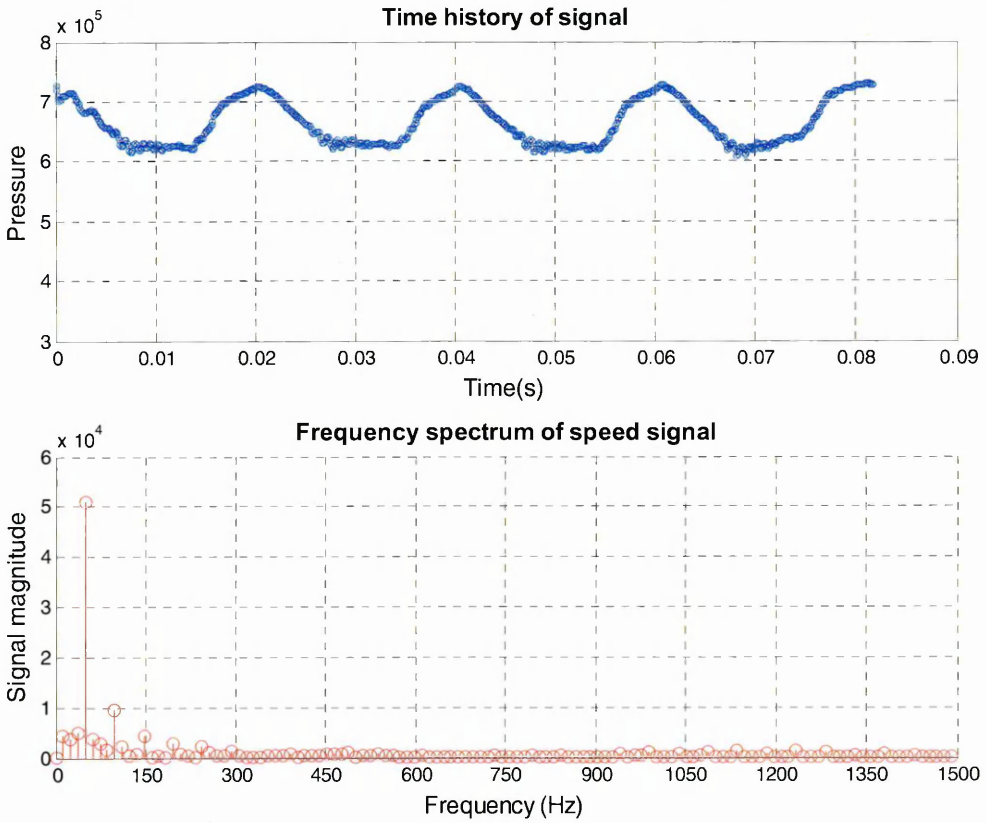

Fig 4.7.1.3 Pressure In Stationary Frame At 0.15m Radius

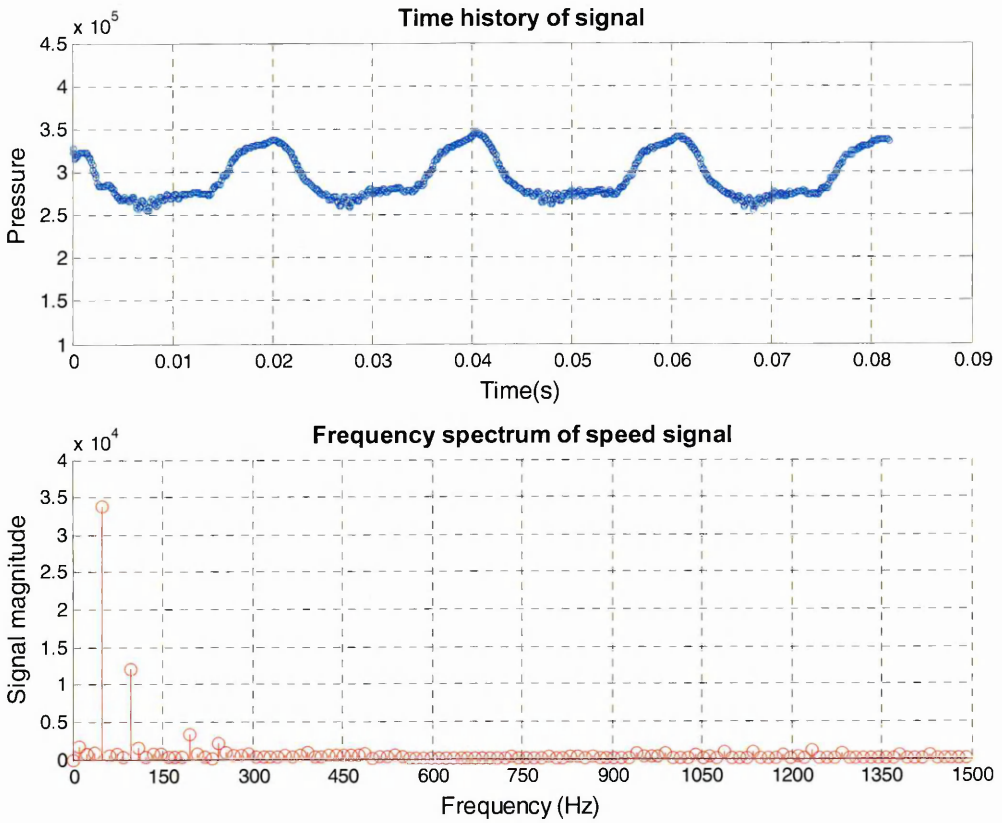

Fig 4.7.1.4 Pressure In Stationary Frame At 0.1m Radius

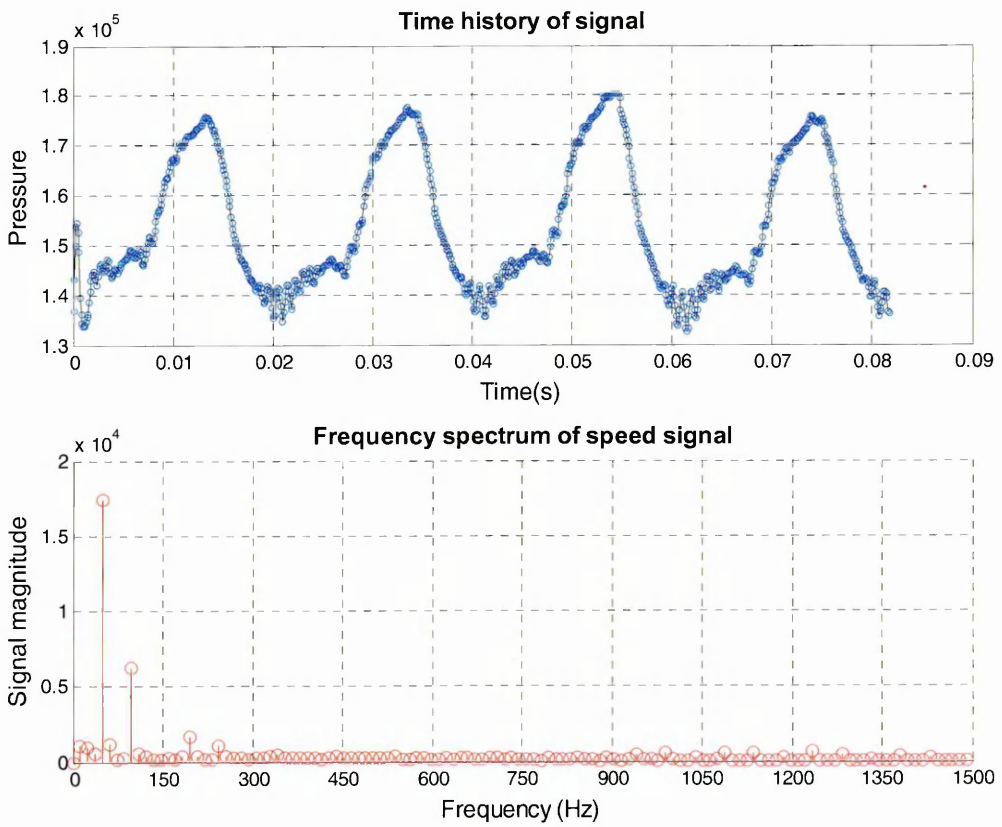

Fig 4.7.1.5 Pressure In Stationary Frame At 0.065m Radius

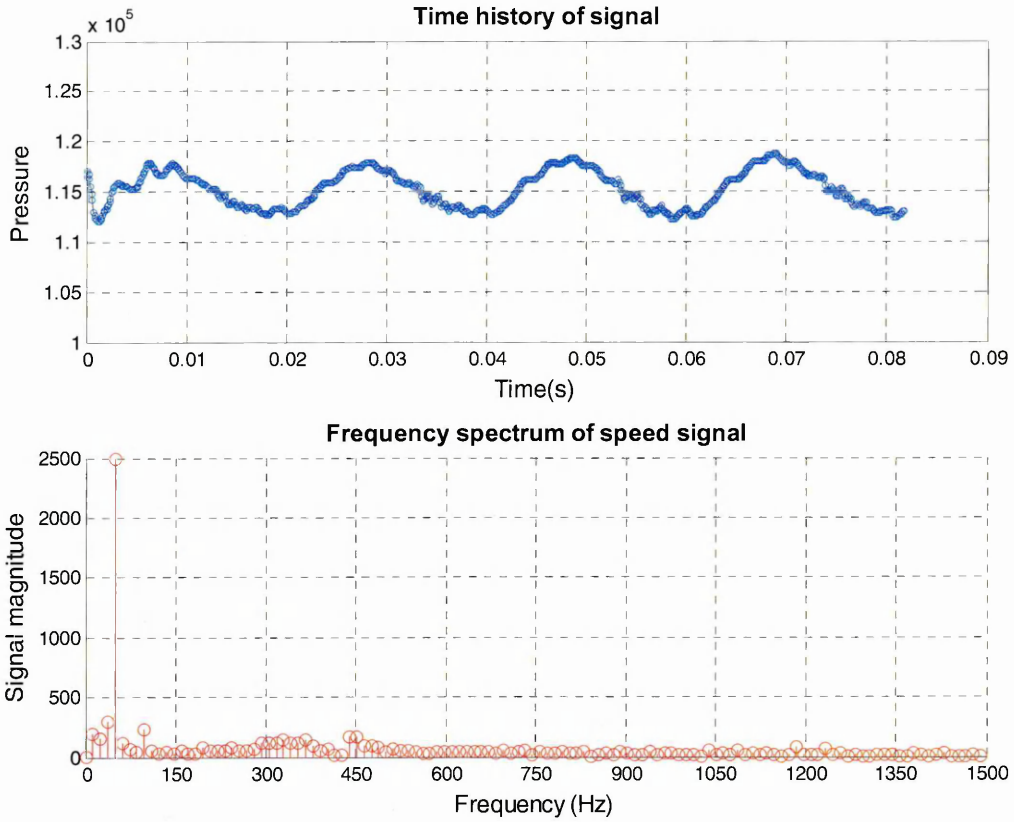

Fig 4.7.1.6 Pressure In Stationary Frame At 0.05m Radius

At 0.2m radius he spectrum is dominated by the rotational component of the frequency spectrum. From a practical standpoint, rotating machines always have some component of rotational speed within their frequency spectrums due to mechanical unbalance. These FFTs indicate that the impeller also contributes to the vibration level at running speed.

Vibration peaks also exist at the vane pass frequency which is attributable to the impeller casing interactions. This peak occurs at $1.75x10^4$ Pa.

The time signal indicates two peaks one attributable to the impeller vane and the other attributable to the wake. This appears at 2xvane pass frequency in the FFT spectrum.

At 0.15m radius the spectrum continues to be dominated by the rotational component of the frequency spectrum. The vibration peaks also exist at the vane pass frequency which is attributable to the impeller casing interactions. This peak occurs at $0.75x10^4$ Pa. The 2x vane pass frequency component has almost disappeared as the wake has little effect at this radius.

At 0.1m radius the spectrum is dominated by the rotational component of the frequency spectrum. The vibration peaks also exist at the vane pass frequency which is attributable to the impeller casing interactions. This peak occurs at $1.25 x10^4$ Pa.

The 2x vane pass frequency component is again low as the wake has little effect at this radius. The time signal indicates that the level of unsteadiness has reduced.

At 0.065m radius the spectrum is dominated by the rotational component of the frequency spectrum. No vibration peak exists at the vane pass frequency which suggests the influence of the volute does not extend into the inlet eddy. The 2x vane pass frequency component also does not appear. The time signal is dominated by the pulsations caused by the rotation speed but the unsteadiness is again reduced.

Fig.4.7.1.6 illustrates the diminished unsteadiness of the pressure pulsations that exist within the inlet eddy of the impeller. The frequency is again dominated by the rotational speed with no indication of the vane passing frequency and its multiples. This again supports the supposition that the casing and impeller vane interactions are not primarily responsible for this frequency. Away from the interface of the rotating and stationary components the frequency spectrum is likely to be dominated by the rotational speed.

4.7.2 Points on Vertical Centre Line

5 points lie on the vertical centre line of the impeller as illustrated in Fig 4.7.2.1 These points are used to monitor the unsteady pressure.

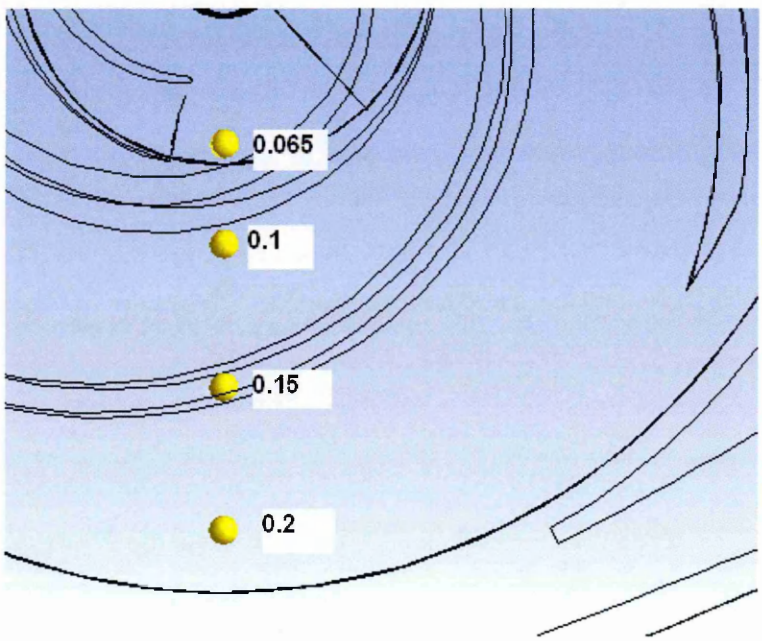

Fig 4.7.2.1 Position Of Impeller Points

Fig.4.7.2.2-fig.4.7.2.6 contain the unsteady pressure signal and the subsequent FFT analysis of that signal. Each of these signals is generated on the at the impeller blade centre. The monitor points chart the change of unsteady pressure and FFT signal from the outer rim of the impeller inwards.

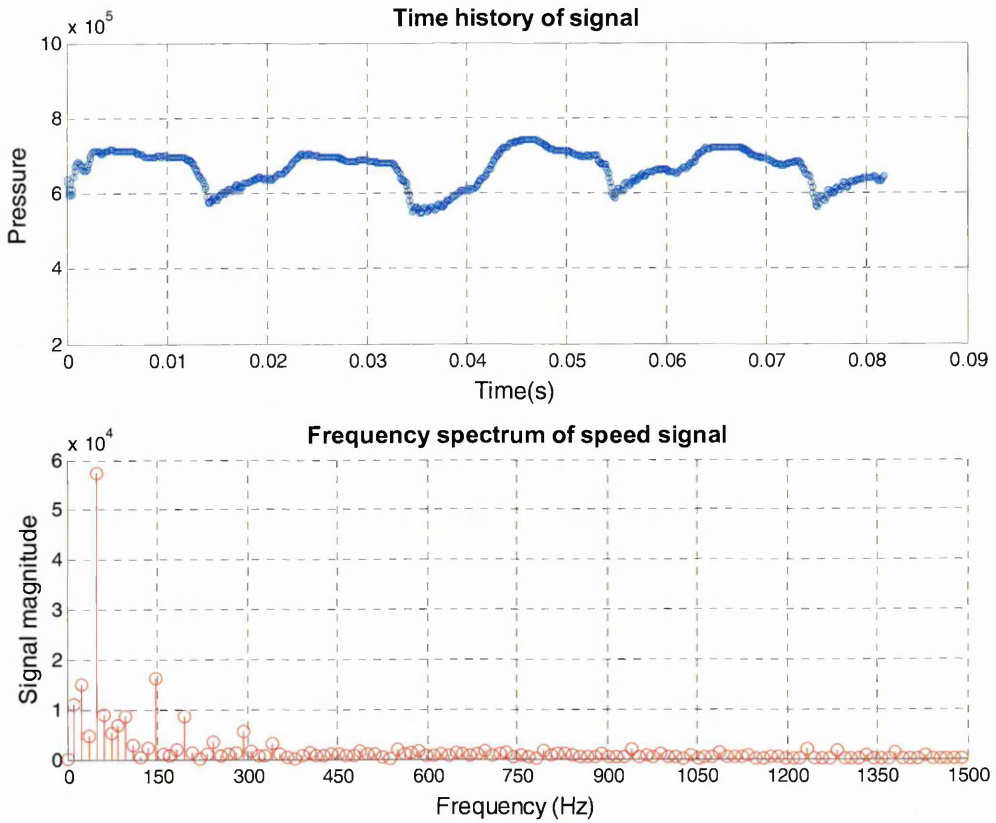

Fig 4.7.2.2 Pressure In Stationary Frame At 0.2m Radius

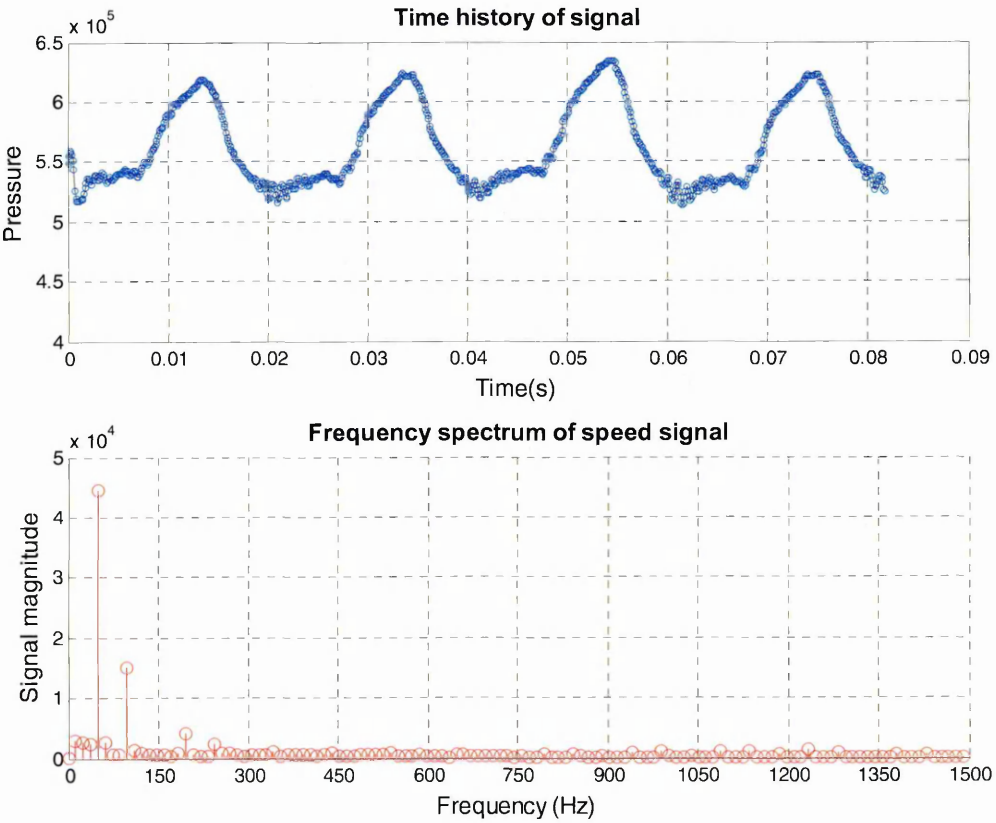

Fig 4.7.2.3 Pressure In Stationary Frame At 0.15m Radius

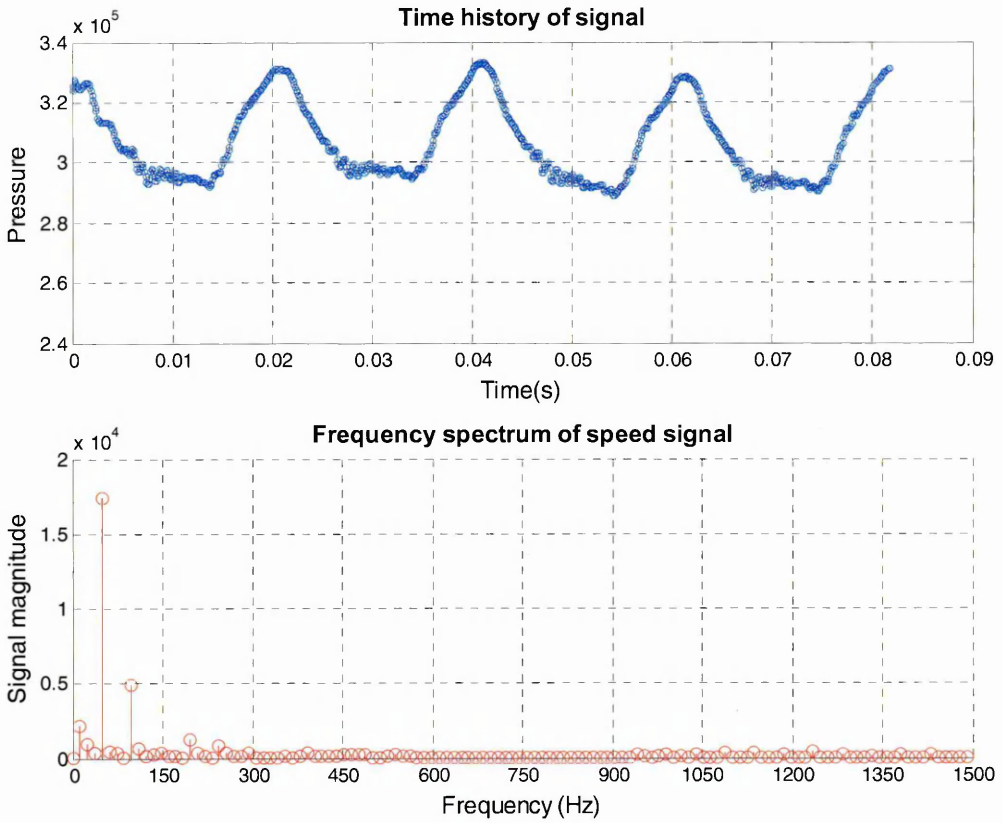

Fig 4.7.2.4 Pressure In Stationary Frame At 0.1m Radius

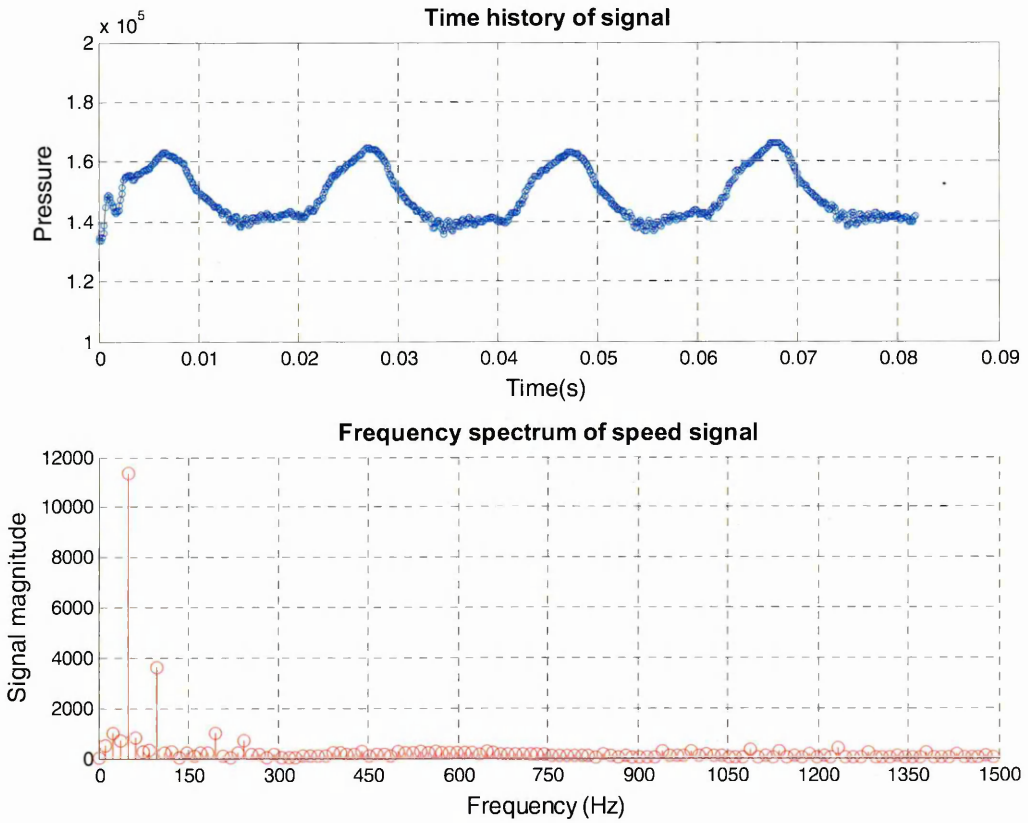

Fig 4.7.2.5 Pressure In Stationary Frame At 0.065m Radius

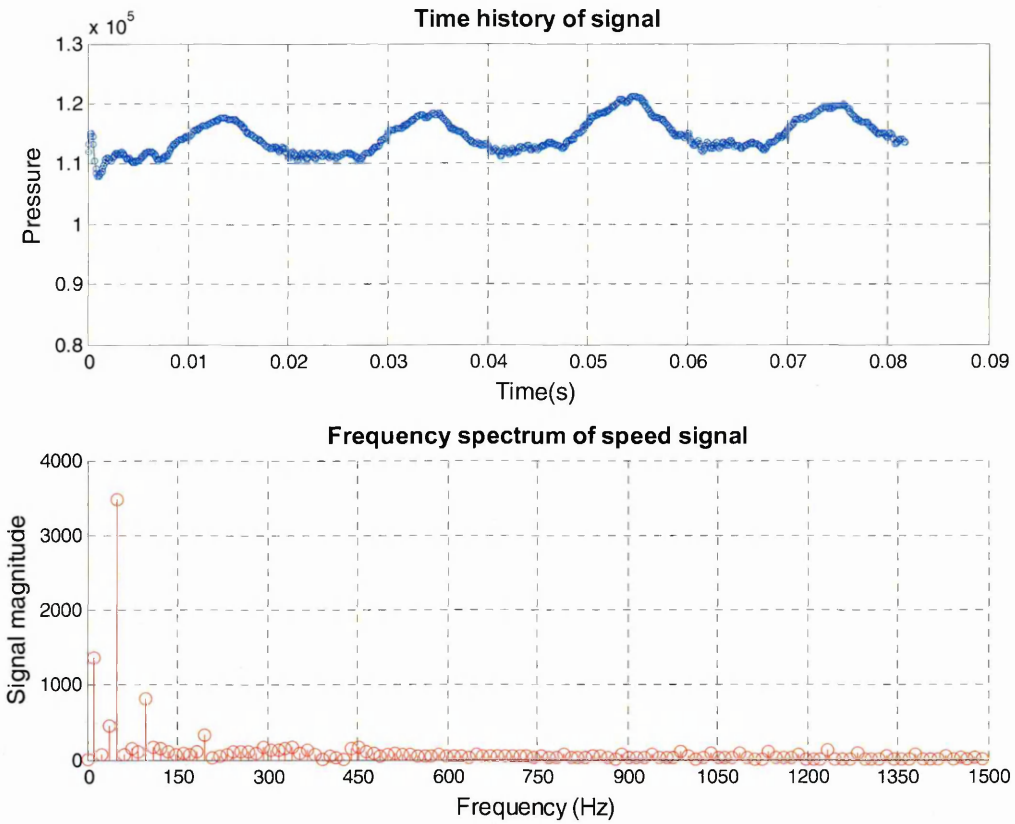

Fig 4.7.2.6 Pressure In Stationary Frame At 0.05m Radius

At 0.2m radius the spectrum is dominated by the rotational component of the frequency spectrum. From a practical standpoint, rotating machines always have some component of rotational speed within their frequency spectrums due to mechanical unbalance. These FFTs indicate that the impeller also contributes to the vibration level at running speed.

Vibration peaks also exist at the vane pass frequency which is attributable to the impeller casing interactions. This peak occurs at 1.75 $x10^4$ Pa as in the horizontal plane described in the previous section.

The time signal indicates two peaks, one attributable to the impeller vane and the other attributable to the wake. These are less defined in this plane due to the extra distance from the volute lip. This wake phenomenon appears at 2xvane pass frequency in the FFT spectrum.

At 0.15m radius the spectrum continues to be dominated by the rotational component of the frequency spectrum. No vibration peaks exist at the vane pass frequency attributable to the impeller casing interactions. The 2x vane pass frequency component has not reduced as the wake influence will be steady and less influenced by the volute lip position.

At 0.1m radius the spectrum is dominated by the rotational component of the frequency spectrum.

The 2x vane pass frequency component is again missing as the wake has little effect at this radius. The time signal indicates that the level of unsteadiness has reduced.

At 0.065m radius the spectrum is dominated by the rotational component of the frequency spectrum. No vibration peak exists at the vane pass frequency which suggests the influence of the volute does not extend into the inlet eddy. The 2x vane pass frequency component does not appear. The time signal is dominated by the pulsations at rotation speed but the unsteadiness is again reduced.

Fig.4.7.2.6 illustrates the diminished unsteadiness of the pressure pulsations that exist within the inlet eddy of the impeller. The frequency is again dominated by the rotational speed with no indication of the vane passing frequency and its multiples. This again supports the supposition that the casing and impeller vane interactions are not primarily responsible for this frequency. Away from the interface of the rotating and stationary components the frequency spectrum is likely to be dominated by the rotational speed.

4.7.3 Points at 45 Degrees

These 5 points lie on the 45 degrees from centre line of the impeller as illustrated in Fig 4.7.3.1. These points are used to monitor the unsteady pressure.

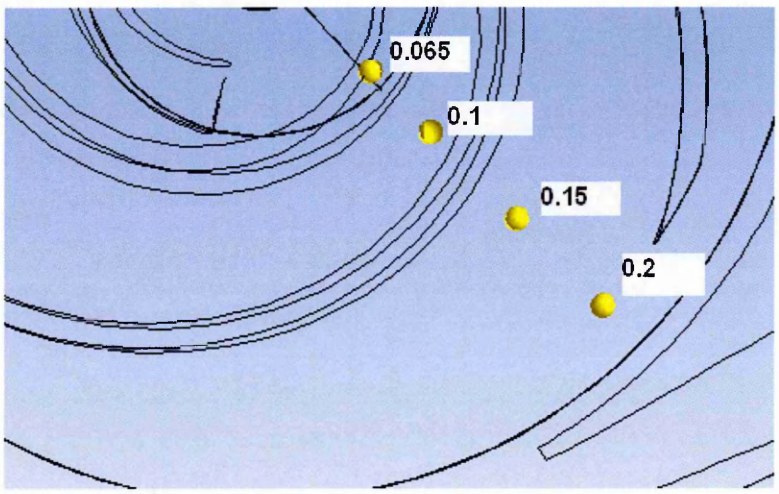

Fig 4.7.3.1 Position Of Impeller Points

Fig.4.7.3.2 - Fig.4.7.3.6 contain the unsteady pressure signal and the subsequent FFT analysis of that signal. Each of these signals is generated on the at the impeller blade centre. The monitor points chart the change of unsteady pressure and FFT signal from the outer rim of the impeller inwards.

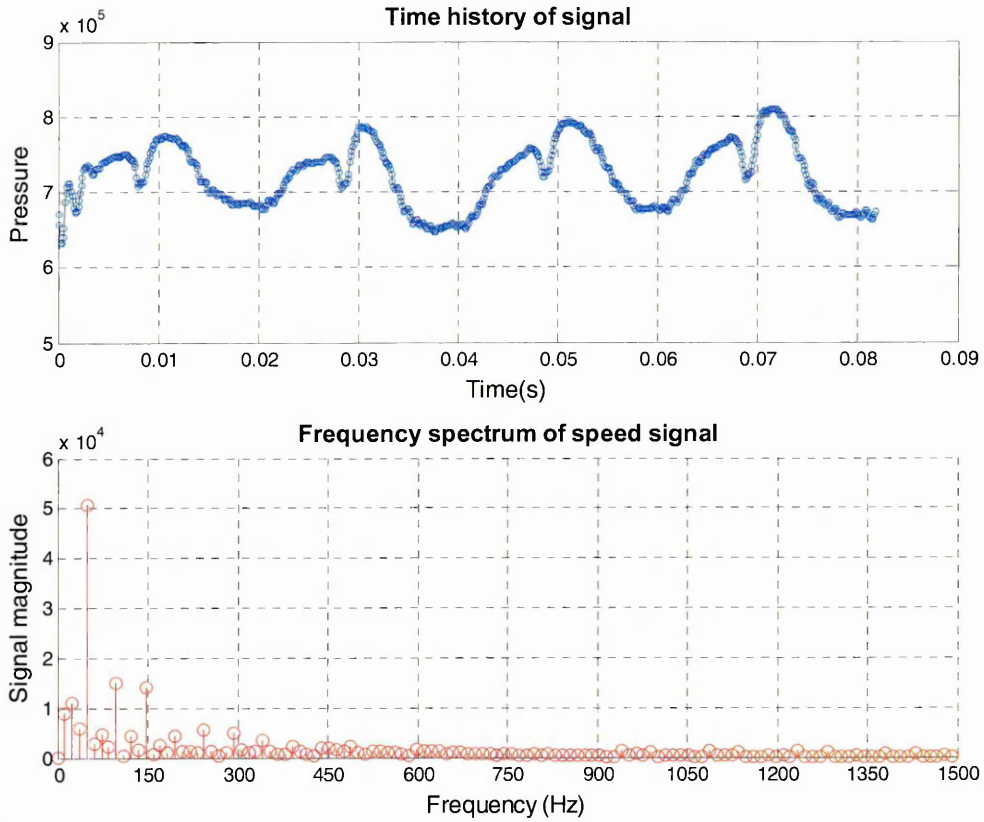

Fig 4.7.3.2 Pressure In Stationary Frame At 0.2m Radius

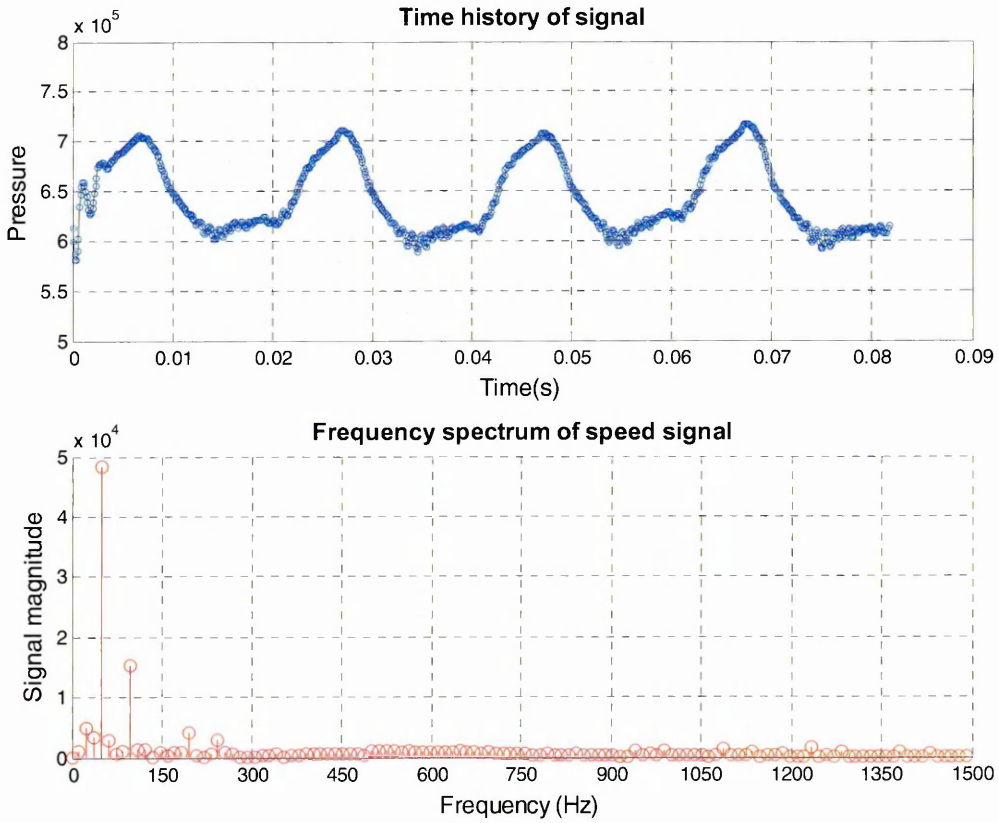

Fig 4.7.3.3 Pressure In Stationary Frame At 0.15m Radius

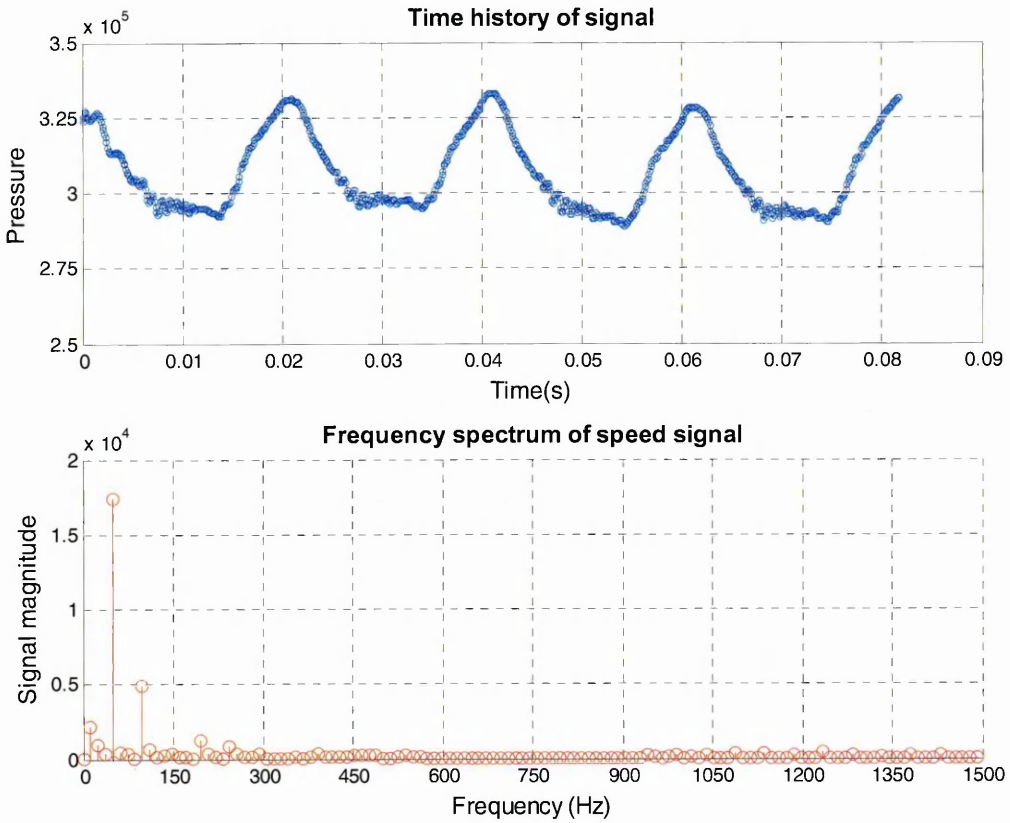

Fig 4.7.3.4 Pressure In Stationary Frame At 0.1m Radius

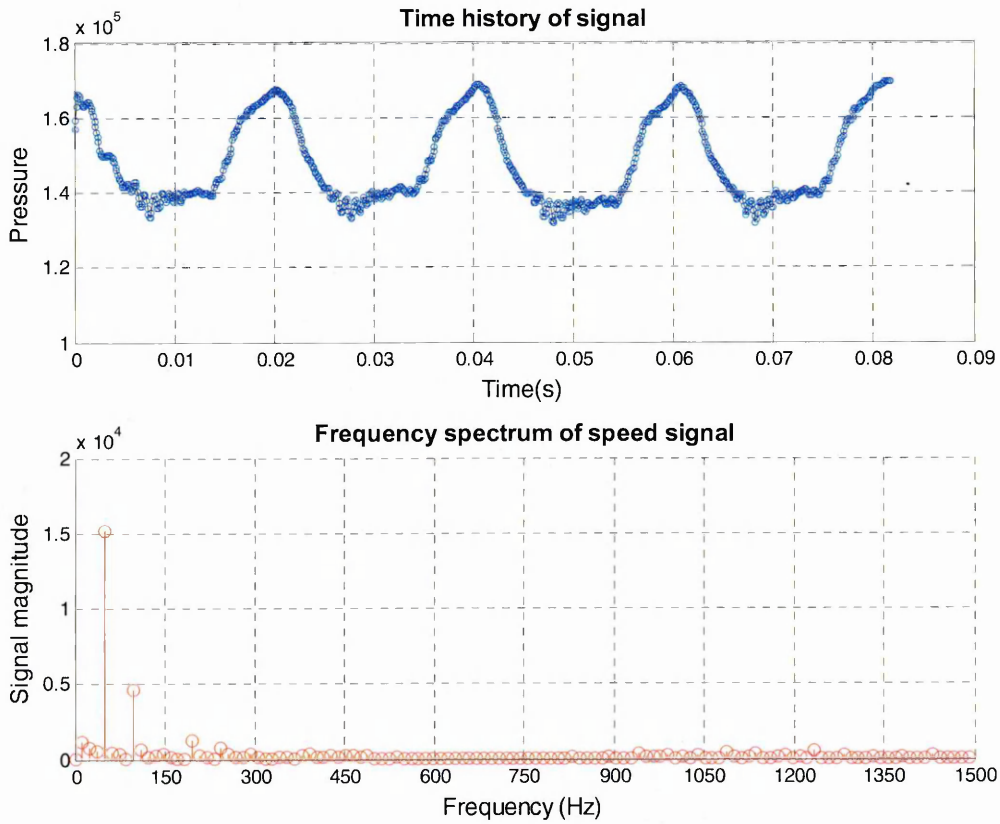

Fig 4.7.3.5 Pressure In Stationary Frame At 0.065m Radius

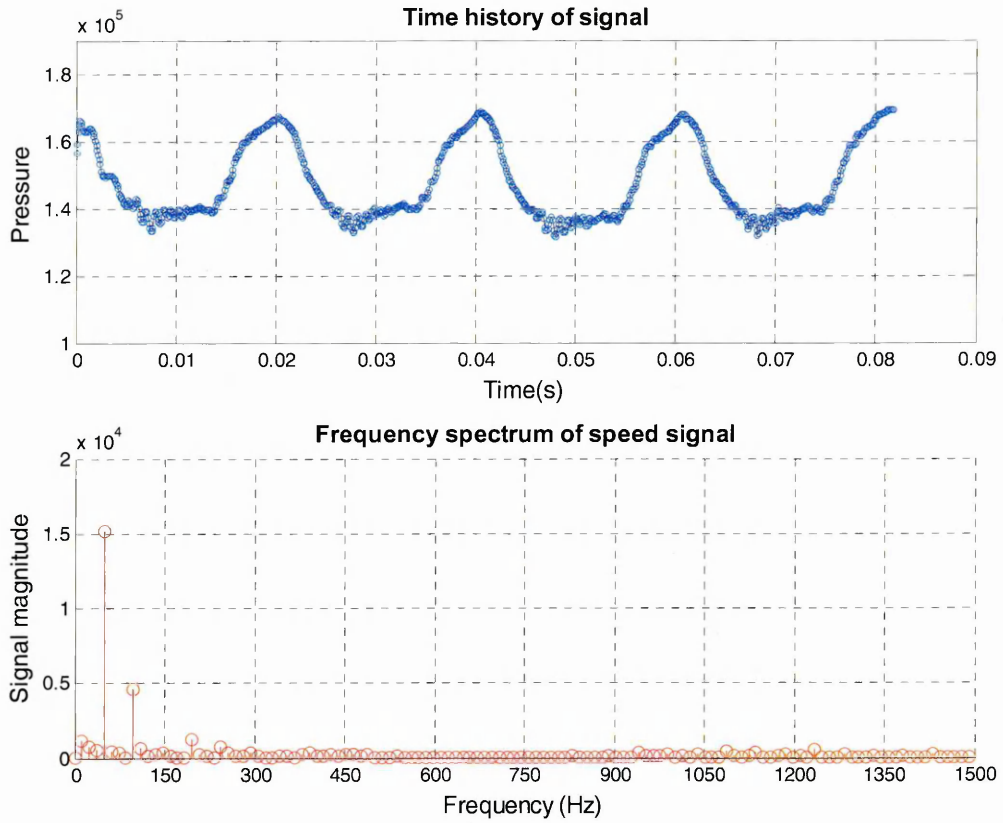

Fig 4.7.3.6 Pressure In Stationary Frame At 0.05m Radius

At 0.2m radius the spectrum is dominated by the rotational component of the frequency spectrum. From a practical standpoint, rotating machines always have some component of rotational speed within their frequency spectrums due to mechanical unbalance. These FFTs indicate that the impeller also contributes to the vibration level at running speed.

Vibration peaks also exist at the vane pass frequency which is attributable to the impeller casing interactions. This peak occurs at $1.5x10^4$ Pa.

The time signal indicates two peaks one attributable to the impeller vane and the other attributable to the wake. This appears at 2xvane pass frequency in the FFT spectrum. These are again pronounced as the point is closer to the volute lip.

At 0.15m radius the spectrum continues to be dominated by the rotational component of the frequency spectrum. No spectrum peaks exist at the vane pass frequency. The 2x vane pass frequency component in not present as the wake has little effect at this radius.

At 0.1m radius the spectrum is dominated by the rotational component of the frequency spectrum. The vibration peaks also exist at the 2xrotational speed. This peak occurs at $0.5x10^4$Pa.

The 2x vane pass frequency component is not present. The time signal indicates that the level of unsteadiness has reduced.

At 0.065m radius the spectrum is dominated by the rotational component of the frequency spectrum. No vibration peak exists at the vane pass frequency which suggests the influence of the volute does not extend into the inlet eddy. The 2x vane pass frequency component does not appear. The time signal is dominated by the pulsations caused by the rotation speed but the unsteadiness is again reduced.

Fig.4.7.3.6 illustrates the diminished unsteadiness of the pressure pulsations that exist within the inlet eddy of the impeller. The frequency is again dominated by the rotational speed with no indication of the vane passing frequency and its multiples. This again supports the supposition that the casing and impeller vane interactions are not primarily responsible for this frequency. Away from the interface of the rotating and stationary components the frequency spectrum is likely to be dominated by the rotational speed

4.8 Inlet Pipe flow

Levin and Poliokovsky (1965) carried out work to ascertain the suction re-circulation at shut-off conditions. Investigations took place on a radial un-shrouded machine. The investigation uncovered two distinct zones of fluid, which interact together within the suction channel. The mental model they proposed is somewhat simplified as it does not cover the three-dimensional interactions. Investigations using CFD yield the following observations for the two zones.

High-energy liquid is expelled from the impeller eye. This expelled liquid dominates the suction passage, occupying the 2/3 of the flow area from the pipe outer diameter downwards towards the channel centreline Fig.4.8.1.

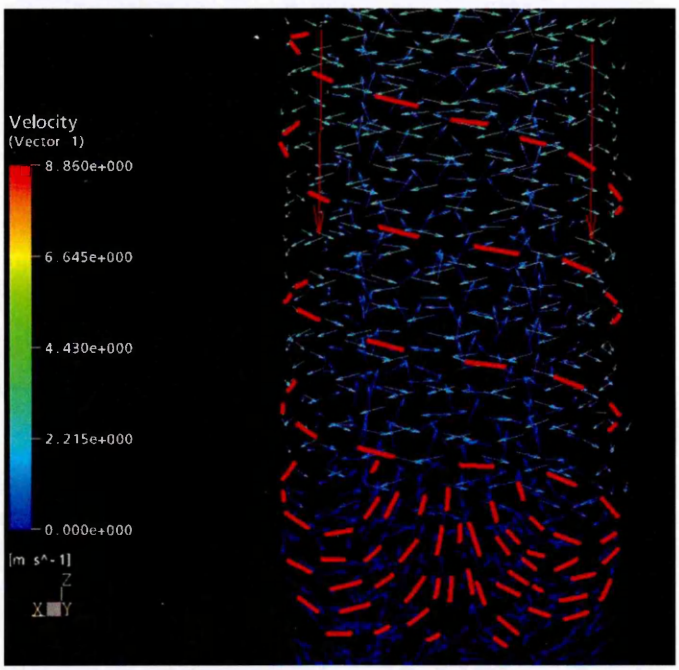

Fig 4.8.1 Helical Spiralling Inlet Backflow at Suction Duct Periphery

The extent that the expelled liquid fills the suction channel remains unchanged with distance from the impeller. This flow spirals helically down the periphery of the suction pipe in a direction counter to the impeller rotation at a constant helical angle.

Each impeller blade generates individual streams. The tangential velocity imposed on the regime by the impeller dominates the flow causing the helical spiral angle to be approximately equal to the blade inlet angle. This angle does not diminish with distance from the impeller implying that both the tangential and axial components of the velocity decay proportionally to maintain this angle. Independent streams can be viewed in Fig.4.8.2

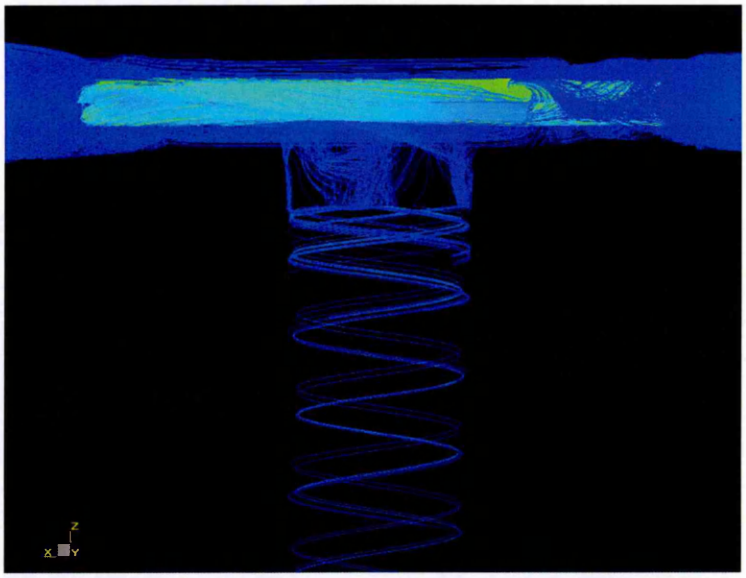

Fig 4.8.2 CFD Streamline of Backflow Discharge down the Suction Line

The inner 1/3 of the suction channel area contains a spiralling core of slower moving fluid. Viscous effects transmit tangential energy from the high-energy peripheral flow and drive this core in a helical spiral counter to the direction of pump rotation. Flow is dominated by the axial component of the velocity and tangential forces exerted by the peripheral flow cause the inner helical flow angle to be approximately double the outer angle. Again the helical spiral angle remains constant. Fig.4.8.3

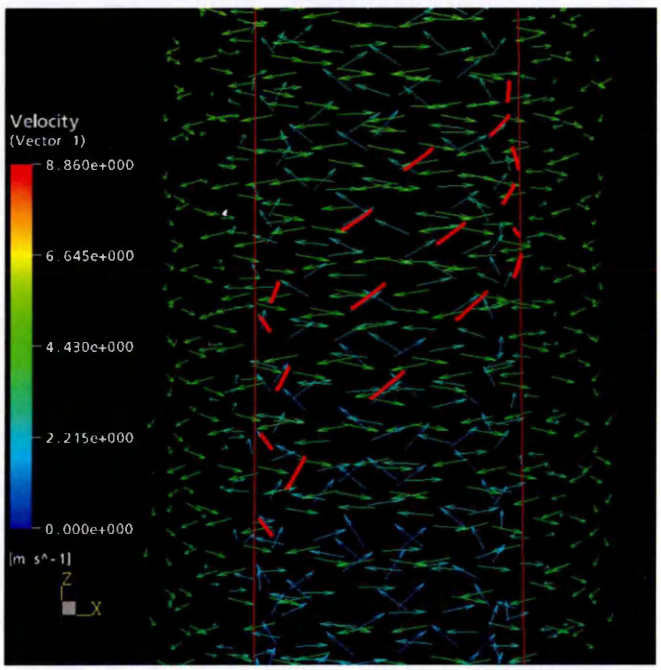

Fig 4.8.3 Internal Core of Spiraling Fluid in Suction Channel

Visual experimental data is available to support the CFD solution. Fig 4.8.4 contains photographs taken through a plexi-glass tube inserted at the suction of a centrifugal pump running at extreme low mass flux.

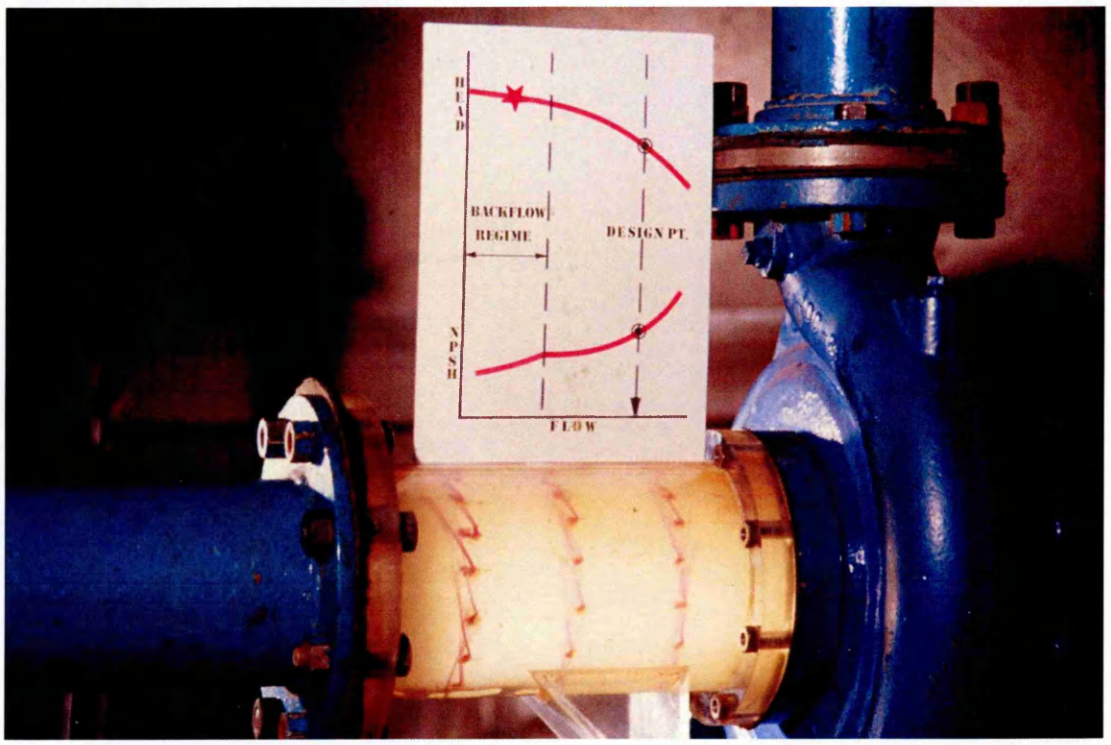

Fig 4.8.4 Pump Test To Qualitatively Illustrate The Suction Re-Circulation Effect At Extreme Part Load

Fibre tufts on the internal surface of the tube are used to illustrate the motion of the fluid as it exits the eye of the impeller and spirals down the suction pipe.

The interface between the re-circulating flow is predicted, by the CFD model, to be 14 multiples of the eye diameter. The position of this interface occurs when the viscous and friction effects have slowed the net velocity within the channel to zero. This "plugs" the suction pipe, encouraging the outer flow to reverse and form the inner core fig.4.8.1. The extent that the re-circulating flow pushes into the suction duct is linked to the suction peripheral speed of the impeller. Increasing rotational speed of the impeller or the eye diameter pushes the extent of the re-circulation further down the suction passage.

Of particular interest with this analysis is the experimental FFT data provided in fig 4.8.5. This data is dominated by the vane pass rate of the frequency spectrum. The CFD data, in contrast, predicts a steady flow regime unaffected by the vane rate.

There is a simple explanation for this apparent inconsistency. It is the standard practice for many pump designers to include within their machines a suction splitter in the suction annulus. This is used to eliminate suction pre-swirl into the impeller maximising the generated head at design flow.

The experimental FFT data was taken in such a machine. Although the regime may be steady when the outer spiralling core is unimpeded by the absence of a splitter, the opposite is true when a splitter is present. The spiralling fluid from each blade impacts on the splitter causing an unsteady interaction.

The CFD solutions attempted in this simulation were carried out without the presence of the splitter. This greatly simplifies the solution as only the unsteady interaction at the pump discharge is taken into consideration.

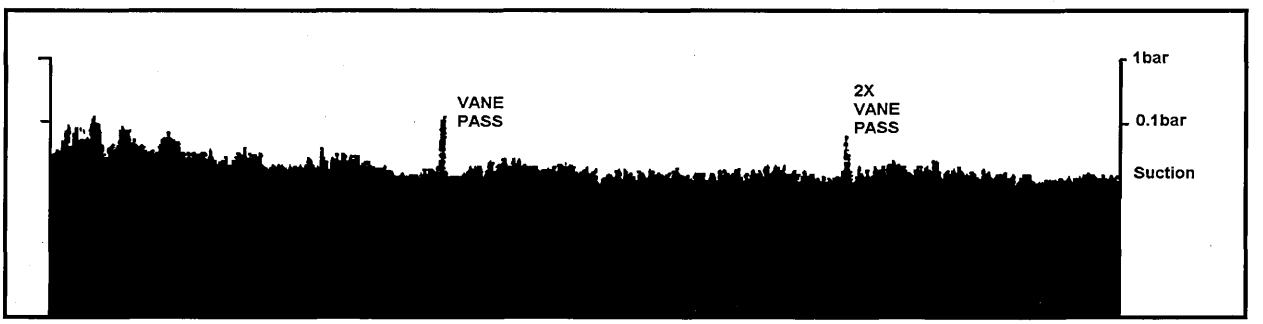

Fig 4.8.5 Experimental Pressure Spectrum Taken In Suction Channel

4.9 Conclusion and Summary

The nature of the flow fields when the volume flux of a centrifugal pump approaches zero is demonstrated by the analysis to be undoubtedly unsteady. The Volute is filled with a slow moving low energy liquid which experiences pressure pulsations dominated by the vane pass frequency. Double volute pumps have discharge ducts that experience these pulsations independently of each other as the vanes approach the volute lips.

The outer proportion of the impeller is filled with a discharge vortex imposed on the impeller by the stationary vanes. The numbers of vanes within the stator influences the development and direction of this discharge vortex. The first 1/3 of the impeller is filled with a vortex generated by the boundary layer breakdown along the pressure side of the impeller vane close to the hub.

Within the suction of the impeller the liquid passes span-wise across the meridional plane and is expelled from the impeller eye at a constant helical angle approximately equal to the impeller inlet tip angle. This spiralling liquid has an influence on the inner core of the suction flow causing a rotation in this core, which reduces the incidence to the hub side of the vane. These effects all work together. The exchanges in energy from suction to impeller and on to the volute all influence the closed valve head value. The success of the model in predicting the closed valve head lies with its ability to capture all these flow effects.

The analogy of solid body rotation when applied to the closed valve head situation whilst appearing statistically significant does not truly represent the sophisticated energy exchanges required to fully describe the nature of the flow field. All of the prediction methods available rely on some form of empirical and statistical analysis (Dyson 2002). Whilst these methods are of value the advances in computational modelling and processor speed will ultimately see them replaced by CFD analysis as a routine function of the design process.

The casing volute sections experience a non-linear pressure rise between the throats. This is attributable to the stalled nature of the long and short diffusing passages which join the casing throats to the discharge nozzle. The unsteadiness within these regions is 17% less than that experienced within the volute casing sections.

The long and short passages experience out-of-phase fluctuations driven by the casing and impeller interactions. The closed valve head of the machine is determined by the strength of these interactions and the pressure recovery which takes place due to the peristaltic from the impeller, driving the unsteadiness.

5.0 Description of Flow Features through a Diffuser Pump

Within the conventional design geometry of centrifugal pumps both the volute passage and the bladed diffuser are popular.
Bladed designs are used in multi-stage machines; they give the designer the ability to tailor the generated machine head by adding extra impeller and diffuser stages without major modifications to the manufacturing process.

There is little work available which adds to the understanding of the flow regime within a centrifugal diffuser pump.

This chapter contains an analysis of a diffuser pump. Although little published work is available on closed valve head diffuser pump simulations, anecdotally diffuser pumps exhibit higher closed valve head coefficients than volute machines.

This chapter will focus on a commercial machine where the generated closed valve head can be compared to time averaged test data. A number of similarities between the diffuser and volute pumps are apparent.

The geometry is similar to the volute geometry in the following ways:

- The pump suction enters the impeller along the rotating axis of the machine. This limits inlet pre-swirl. Although this is not typical of a conventional diffuser design, it is a simplification of the geometry. This simplification is required so that the backflow proportion of the flow expelled from the impeller inlets at closed valve can be accommodated. In this type of machine the inlet mass flux commonly enters the suction channel vertically and is turned and guided radially by a swept radius and an anti-swirl guide vane. The net result of this is a uniform, non-swirling flow into the first stage impeller
- The impeller discharges into an annular space subsequent to the diffusion. There are a number of geometric arrangements used to transport the diffused fluid energy into the subsequent impeller. All these schemes use vanes to guide the slow moving fluid into the next impeller stage. This is fundamentally an exercise in limiting the pre-swirl into subsequent impeller eye.

The pump contains the following features that are typical of modern pump design that were not included in the Newton (1998) research.

- The impeller inlet angles are arranged for zero incidence at design flow.
- The impeller meridional profile is curved to accept the inflow.
- The impeller blade width is not equal to the throat width, although for this analysis only mid-streamline effects are considered for comparison.

The machine has a specific speed of 1100 (US units). This would be considered a medium Specific speed machine.

5.1 Geometry

A diffuser pump differs from a volute pump in respect of the diffusion on the fluid expelled from the impeller. Rather than a two channel diffusion mechanism over a long distance as in the volute method, the flow is divided into many channels and diffused by a passage formed between adjacent blades.

This type of machine is popular when high heads are required. Diffuser pumps are used to provide a flexibility of head generation at a common flow. The configuration allows banks of impellers and diffusers to be arranged in series on a common shaft. The discharge from each impeller is handled by the diffuser and transported to the inlet eye of the subsequent impeller. Each pump stage generates the same amount of head. Fig 5.1.1 illustrates one common construction of a diffuser pump.

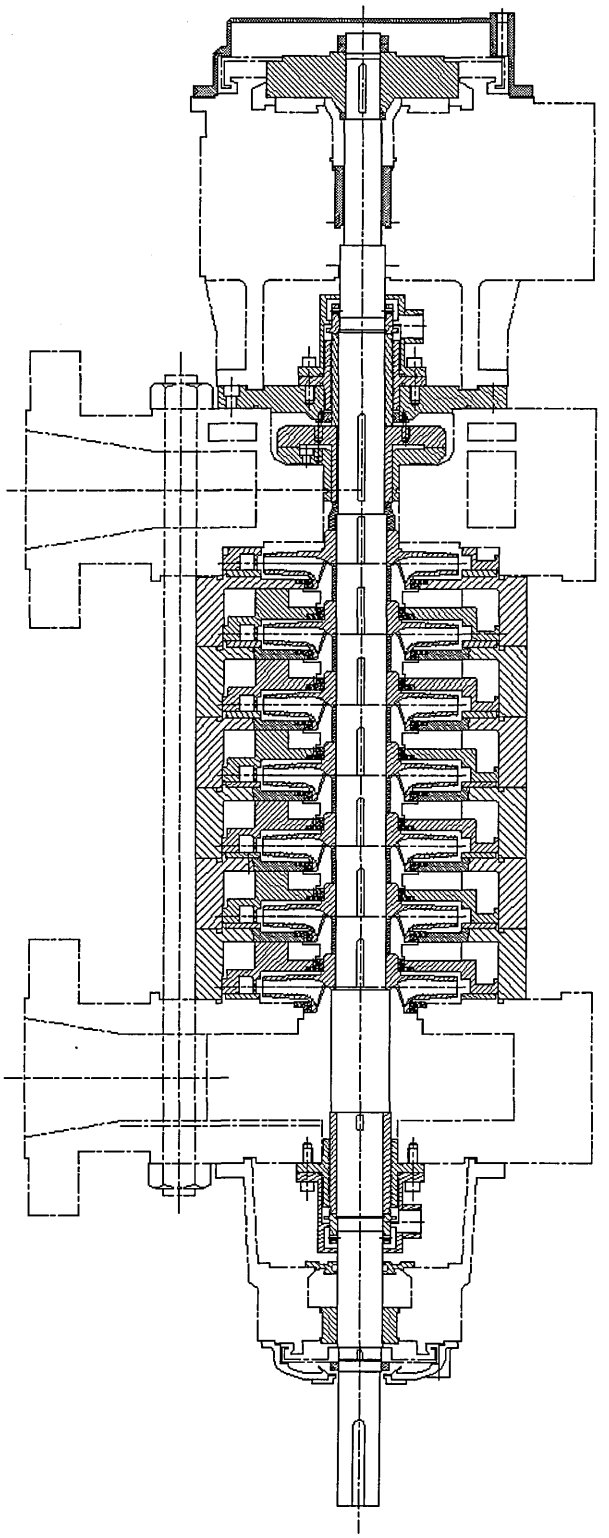

Fig 5.1.1 Section through a Diffuser Pump

For the case of computational simplicity the impeller and diffuser are considered for one stage only. The transportation geometry between stages is not considered in the computational analysis. This transport geometry is replaced by a blocked diffuser outlet which allows a mass flux less than the internal volumetric leakage to pass through the boundary.

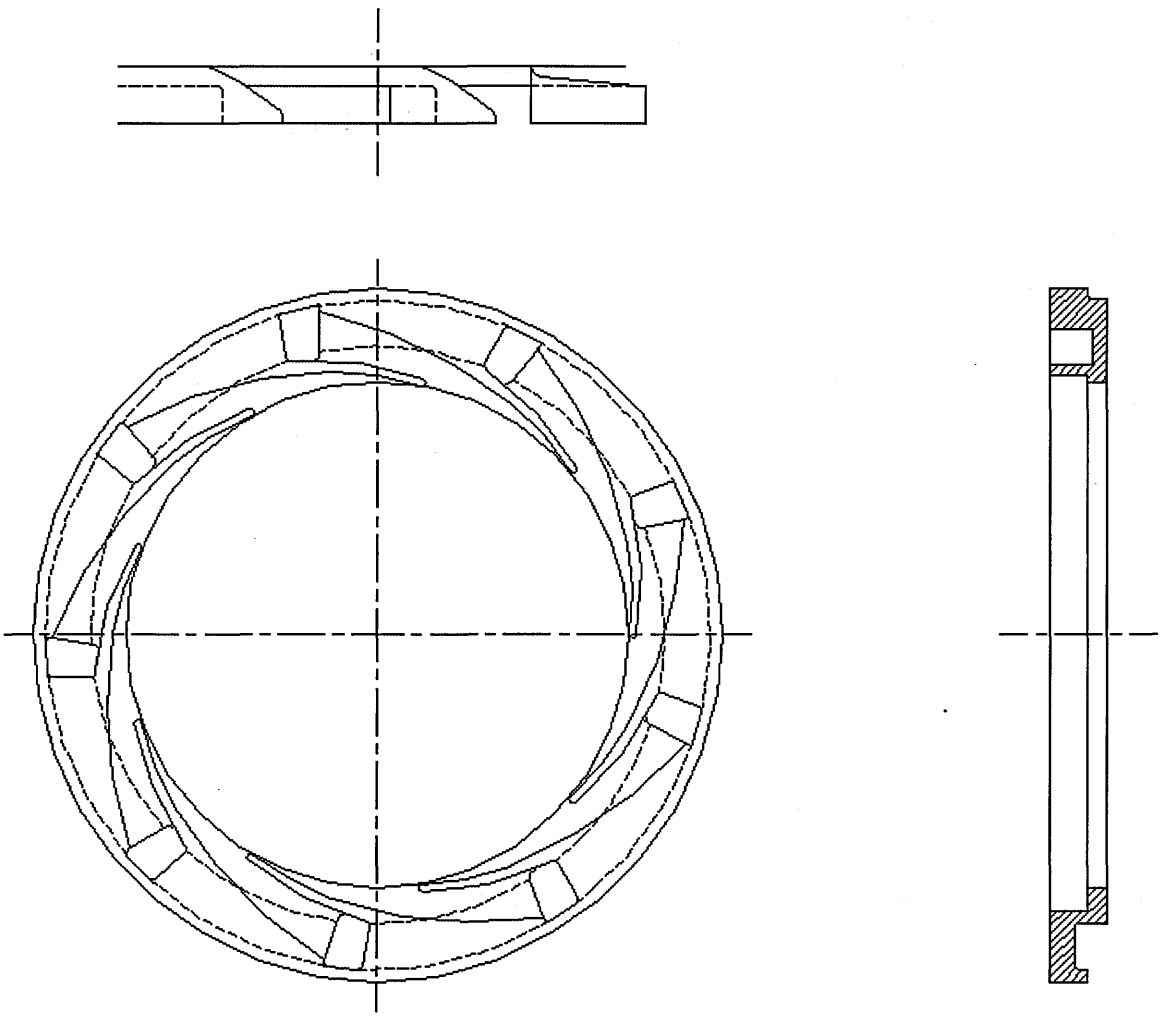

Fig 5.1.2 Diffuser Geometry

The diffuser design used in this analysis is shown in Fig 5.1.2.
The diffuser contains nine stationary vanes arranged with an appropriate inlet angle to accept the best efficiency incidence.

In this particular design the flow is also moved span-wise along the axis to facilitate the inter stage fluid transportation. Within the computational model this axial motion is not facilitated, but the diffusion ratio is maintained.

Within the computational model the liquid, post diffusion is expelled into a free annular space around the diffuser periphery. This geometry is more typical of older diffuser designs. The modern methodology employs a span-wise liquid channel which is commonly used to keep channel ring diameters smaller thus keeping the cost of manufacture lower. That being said, the computational design is still representative of contemporary pump design and the transportation mechanisms have, anecdotally, not affected the generated head of the machines. The important hydraulic features are the blade inlet angle, the diffuser throat area and the diffusion ratio. Fig 5.1.3 shows the diffuser blade model

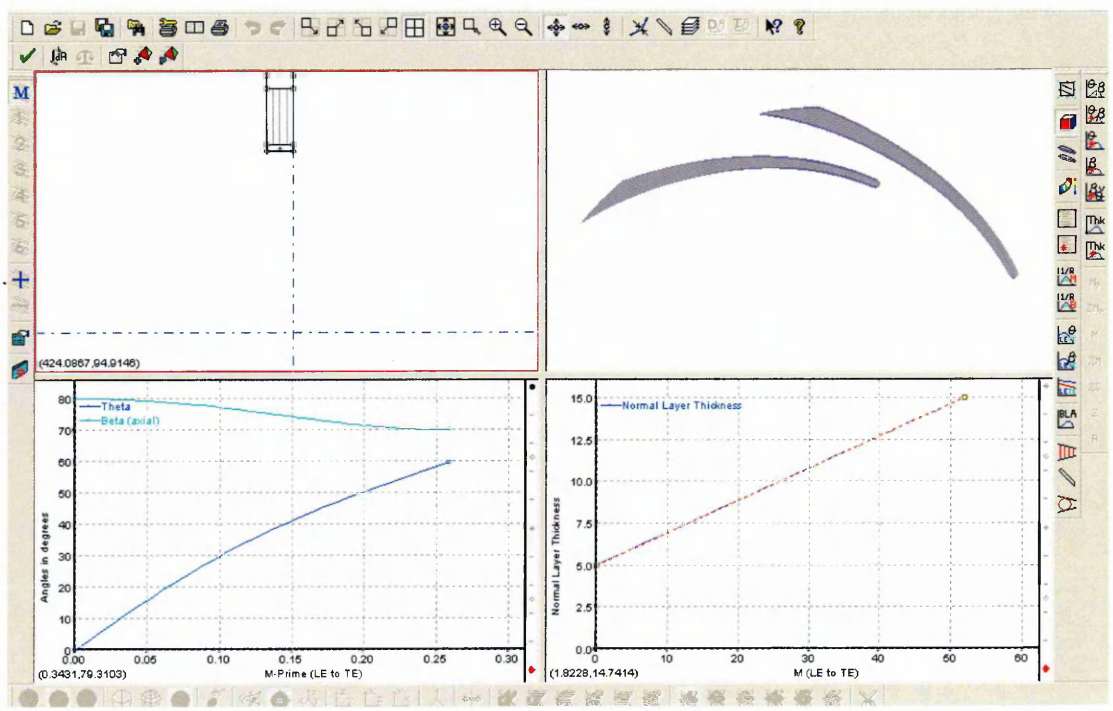

Figure 5.1.3 Diffuser Model

The impeller design is typical of a radial machine. Fluid enters the blade passageways through the impeller eye. The impeller inlet blade angles are arranged to accept zero incidence at the design condition.

The impeller contains 5 blades equally spaced in this shrouded design. The impeller outlet angle is set at 23 degrees for each blade.

The impeller contains two plane cylindrical landings which accommodate fine clearance rings. These annular rings are used to separate the impeller discharge pressure from the suction pressure. This is described in detail, for a single stage machine, in Chapter 1.

Fig 5.1.4 contains the impeller model and geometry.

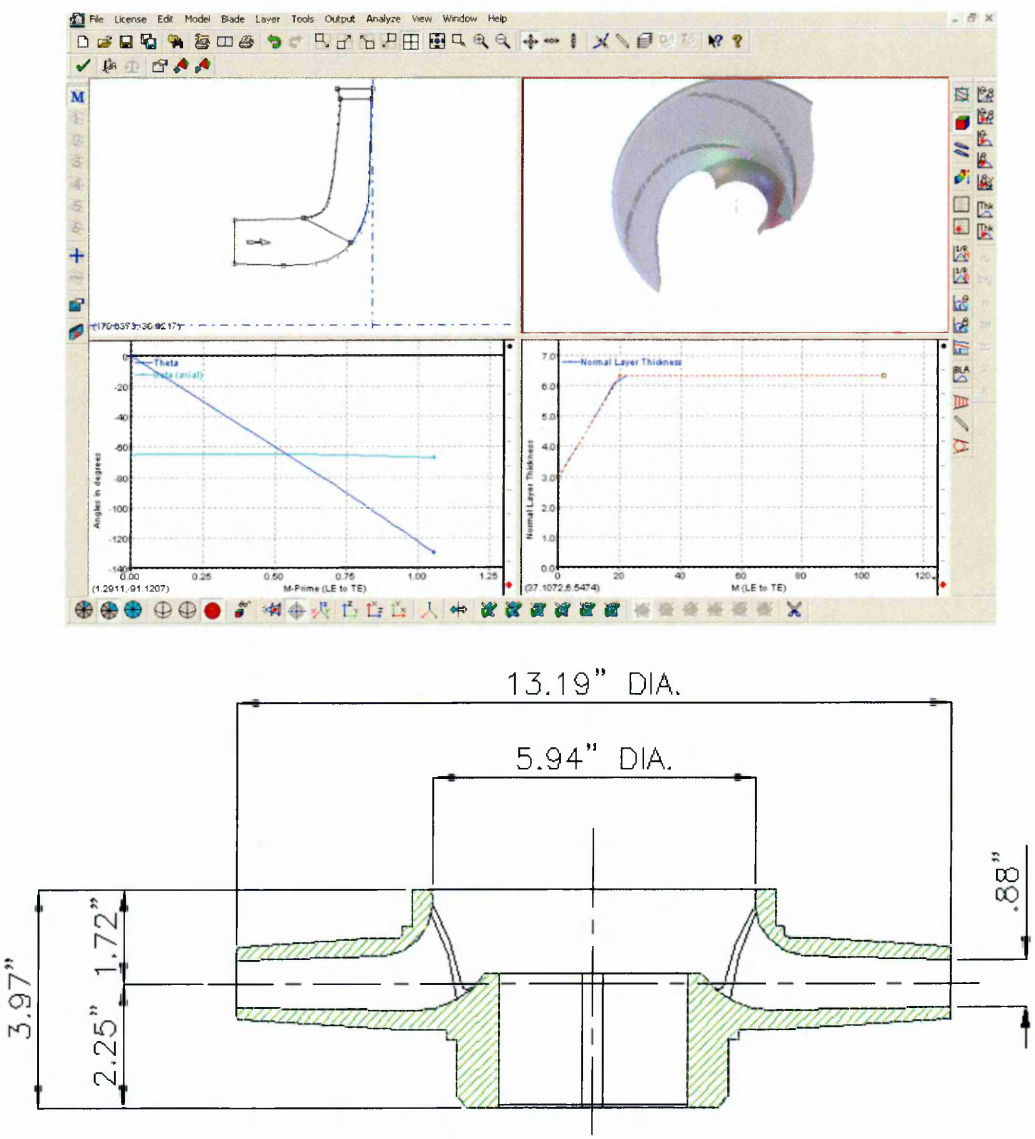

Fig 5.1.4 Impeller Model and Geometry

It can be seen from Fig 5.1.4 that the impeller width at outlet is not identical to the diffuser width. This situation always occurs within pump design.

Constructional considerations force designers to accommodate some axial flexibility in their machines to accommodate cumulative build tolerances.

This disconnect between the impeller and a diffuser width is handled axially by flaring the impeller width within the annular clearance between impeller and diffuser. This then conforms to a common width half way between the impeller blades and diffuser blades.

The grids for the impeller and diffuser are illustrated in Fig 5.1.5. Both these grids were constructed using CFX turbo grid. This tool allows the designer the ability to manipulate a structured mesh. Particular care is required controlling the mesh skew-ness within the annular space above the impeller blades and below the diffuser blades. The skew-ness values of 18 degrees were encountered as the high density mesh was constructed in a confined region between the impeller and diffuser.

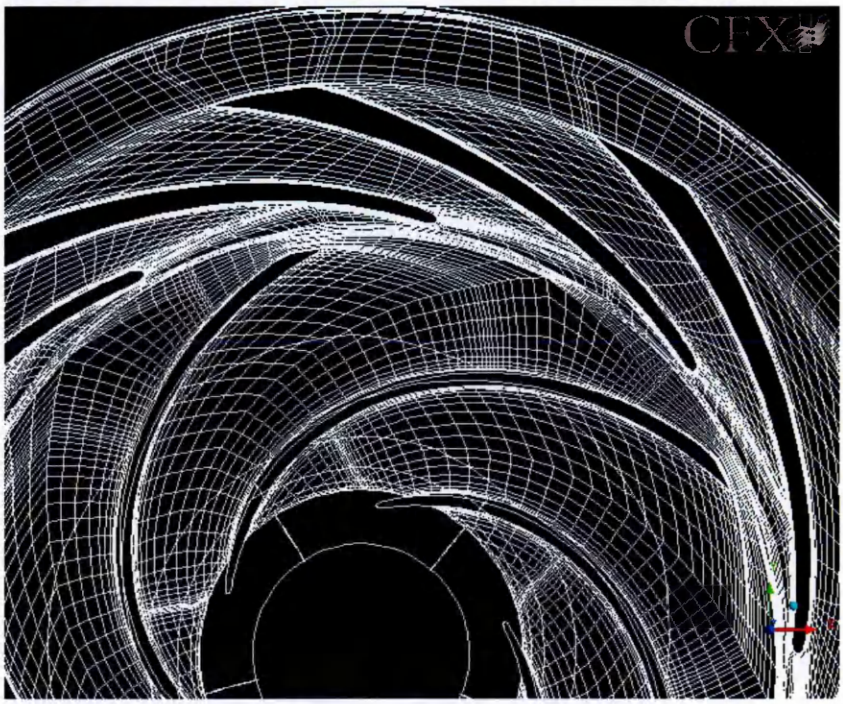

Fig 5.1.5 Impeller and Diffuser Mesh

5.2 Experimental Testing

The diffuser pump was subject to a performance test on the Union Pump Test stand and is pictured below in Fig 5.2.1.

Fig 5.2.1 Diffuser-Ring Section Pump pictured on Union Pump test stand

The Union Test stand provides facilities for the performance testing of centrifugal machines manufactured or repaired by Union Pumps.

The Union Pump test stand loop is illustrated in Fig 5.2.2.

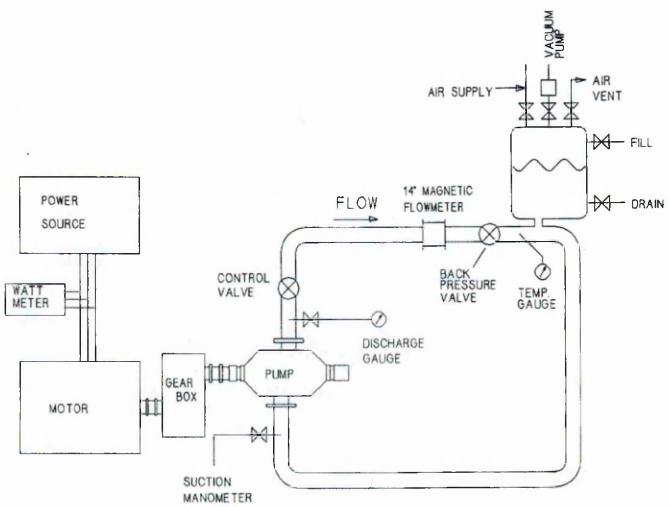

Fig 5.2.2 Union Pump Large Test Loop

The flow rate within the large loop is measured using Danfoss magnetic flow meters calibrated at a NAMAS accredited facility.

The flow loop consists of a 350mm diameter manifold that allows a range of flows between 5.3m3/hr-3464m3/hr to be accommodated.

Suction and discharge pressures are measured using Rosemount Pressure Transmitters type 3051C.

Water temperature is taken within the suppression tank by using RTD's installed in the tanks.

Pump speed is measured using a digital tachometer.

The pump is driven by a 687kW 1480rpm electric motor.

All performance tests are conducted and set up to comply with BS 5316: 1976: Part 1 Class 'C' Acceptance Tests for Centrifugal, Mixed Flow and Axial Flow Pumps.

Conversions are calculated for rated speed from actual test speed. Using the pump affinity laws, the following conversions apply:

Capacity Q_2	=	Q1 x (N2/N1)
Head H_2	=	H1 x $(N2/N1)^2$
Power P_2	=	P1 x $(N2/N1)^3$

Where:

Q_1	=	Capacity on test
Q_2	=	Capacity at rated speed
N_1	=	Speed on test
N_2	=	Rated speed
H_1	=	Head on test
H_2	=	Head at rated speed
P_1	=	Power on test
P_2	=	Power at rated speed

All readings are corrected to common units. Corrections are made for speed, and specific gravity due to test loop temperature.

The Performance data shown in Fig 5.2.1.1 has been generated using this multi stage machine has been subsequently modified to illustrate the performance of a single impeller and diffuser.

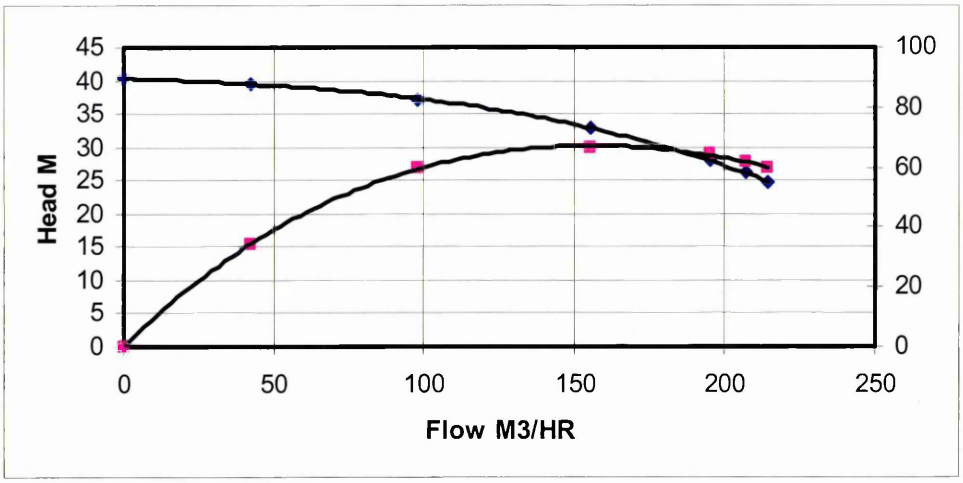

Fig5.2.3 Performance test curve

The single stage data corrected to a common speed of 1480 rpm and a common diameter of 12.83" as per the computational model gives a closed valve differential head measured at 40.3m. This figure is compared to the closed valve head predicted by the computational solution of 40.43m.

This closed valve head prediction is less than 0.3% deviation from the experimental figure. Whilst this level of accuracy is far better than any of the existing empirical prediction methodologies it must be viewed against the background of the difficulties that are encountered in taking the closed valve head reading.

5.3 Solution Parameters

The development of the computational procedure, based on the research incorporated in Chapter 3, uses the following parameters and boundary conditions.

As with the volute the pump requires a specific suction pressure, this suction pressure is used to suppress and cavitation within the pump inlet. Pump designers are familiar with this concept so a pressure boundary as a pump inlet boundary condition is a favourable choice. Unlike the volute pump, which by construction has an axial inlet condition, a diffuser pump conventionally has a radial suction flow which is then turned and guided axially into the impeller eye. Stationary vanes are used to ensure the axial approach of the liquid into the impeller eyes. The existence of a splitter system prior to the impeller would require treatment with a sliding mesh interface as the expelled liquid streams due to the inlet backflow would impact upon the stationary splitter causing a rotor stator interaction effect.

For computational simplicity of the inflow, the splitter row at the inlet is not considered. The impeller inflow for this problem is considered axial and the solution procedure used for the volute pump is adopted.

Inlet boundary – Pressure Boundary: - 100000 Pa

Inlet boundary conditions based on mass flow input were found to be produce walling of the inlet boundary by the solver. This was perceived to be caused by the solvers attempt to simulate the inlet backflow proportion of the flow where outflow may be apparent at the inflow boundary. Switching to a pressure boundary and moving the inflow further form the impeller prevented this walling. Further solution investigation based on subsequent flow reduction from b.e.p flow, outlined in the following section, provided a consistent successful approach.

The outlet boundary requires a finite outflow through the boundary to enable a converged solution. Since pump designers talk in terms of discharge flow, from a perception standpoint an outlet mass flow is desirable.

Final Outlet boundary – Mass flow outlet: - 0.001 kg/s

The outlet boundary for the diffuser pump is different than the volute pump. Rather than a fixed discharge pipe the diffuser pump diffuses the fluid through a diverging row of blades. These blades feed into a free annular space.
Above the discharge the free annular space is pinched to form a narrow outlet which extend around the diffuser periphery. This plane is assigned as the diffuser row outlet.

Other boundary conditions are as follows

Rotational Speed: - 1480rpm

This is a synchronous speed of a 50hz motor and would be recognisable to pump designers

Working Fluid:- Water

Although pumps are used for many liquids they are commonly tested by pump manufactures on water and then the results are adjusted for specific gravity and viscosity after the water test.

5.4 Solution Procedure

Using the above solution parameters we can apply the following solution procedure to the problem.

5.4.1 Initial Conditions

The initial conditions are established using the methodology available within the CFX code. These conditions require refinement by allowing the rotating impeller grid to rotate 1 complete revolution with a 5 degree time-step.
These rotations are carried out in the following manner:-

- B.e.p flow – 1 complete sweep
- 50% b.e.p flow 1 complete sweep
- 25% b.e.p flow 1 complete

At the 25% b.e.p. flow condition the inlet backflow proportion of the flow is fully established.

5.4.2 Solution Process Part 2

The final solution is evolved using the 25% b.e.p flow solution as the initial condition. The outlet boundary flow condition is modified to its final value. Through this stage a process of time step reduction is followed:-

- 1 sweep of the impeller at 1 degree time-step
- multiple sweeps of the impeller at 0.5 degree time-step until the periodic pulsations monitored within the solved are converged to with 3% of each other
- 1 final sweep of one blade pitch with outputs to individual results for every degree of time-step for final analysis.

It is important to implement the final output run to conserve disc capacity. The individual results files can contain 60Mb of data. Individual file outputs of this size per time-step quickly utilise disk space and solver failure occurs when no disc space remains.

The results from the final sweep are used for the following analysis.

5.5 Time Averaged Evaluation

It is interesting to evaluate the averaged unsteady data from the computational solution across one diffuser blade pitch to examine the non-linearity in pressure development.

Averaging the unsteady pressure signal from the CFD around the pump volute described in Section 4.4 demonstrated a non-linear pressure around the impeller periphery within the volute. This can be compared with the situation within the diffuser. This non-linear pressure rise is apparent within the annular space around the periphery of a diffuser pump.

This is illustrated in Fig 5.5.1

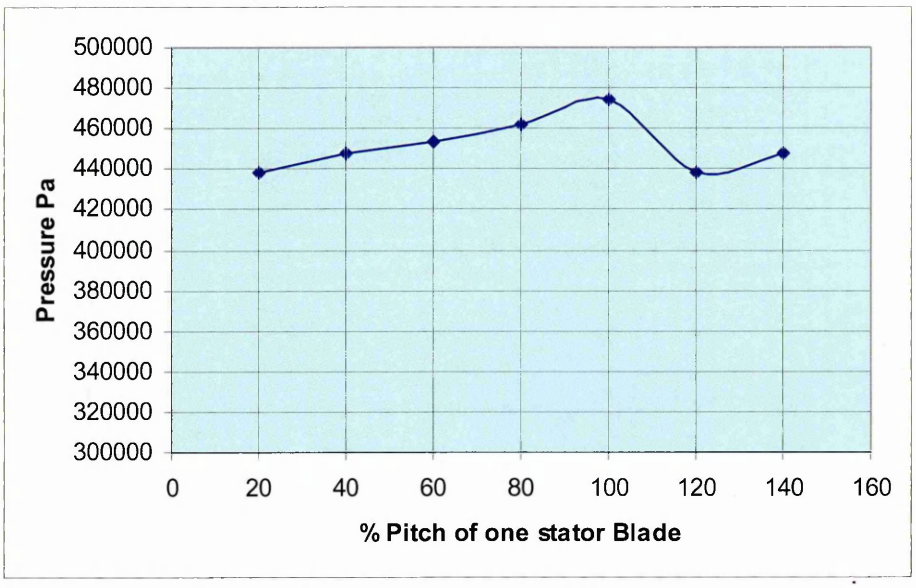

Fig 5.5.1. Averaged Pressure across One Pitch of the Diffuser Blade as It Experiences One Impeller Pitch Cycle

Within the volute pump the stalled nature of the long and short diffusing passageways inhibited the impeller out flow. Within the diffuser pump a similar situation occurs as the diffuser passageway is stalled preventing outflow to the diffuser. The liquid trapped between the upper proportion of the impeller and the diffuser is subject to velocity variations from the rotating impeller blades approaching the diffuser lip. When the vanes are congruent to the lip a finite volume of liquid is squeezed through the gap formed between rotor and stator vane thickness. This mass flow through a small volume increases the velocity and continuity consideration dictate the drop in pressure.

The volute pump experiences a greater pressure fluctuation. The pressure fluctuation is 20 % compared to 8% on the diffuser machine.

Examination of the difference in geometry between the two types of machine explains why this difference occurs.

Figure 5.5.2 illustrates the situation of the impeller vane with respect to the volute lip in its two extreme positions. The first image depicts a vane as it passes the volute lip. The second image depicts a vane row at mid pitch to the stator vane.

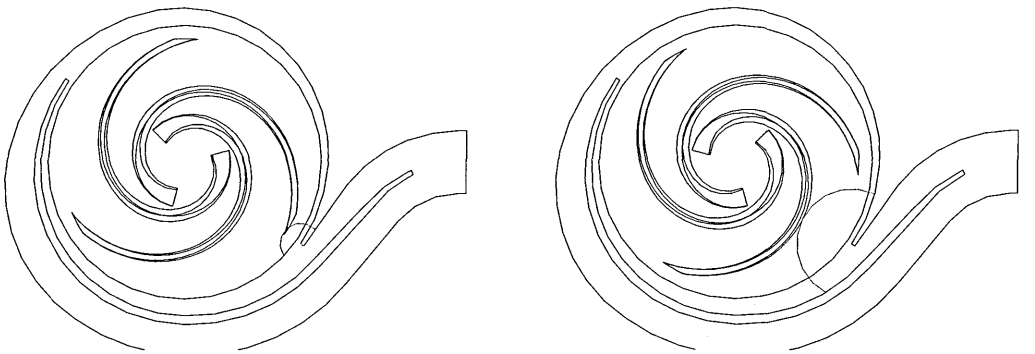

Fig 5.5.2 Illustration of Impeller Vane at Mid Pitch and Coincident To The Volute Lips

In contrast to this Figure 5.5.2 depicts impeller vane as per Figure 5.5.2 but this time with respect to a row of diffuser vanes.

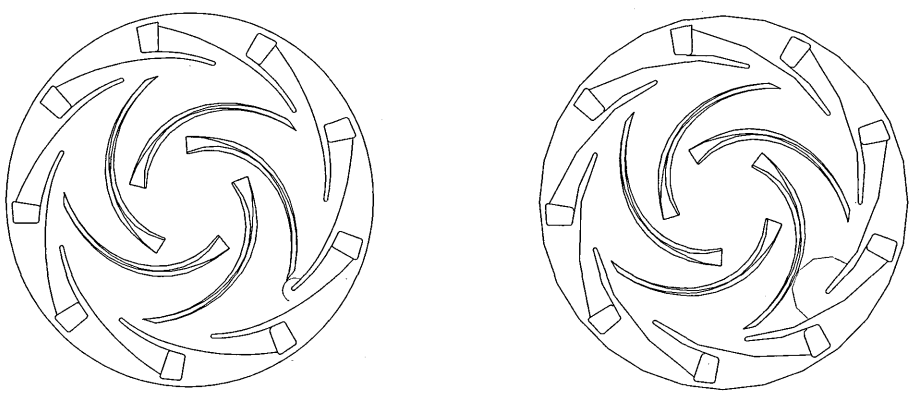

Fig 5.5.3 Illustration of Impeller Vane At Mid-Pitch And Coincident To The Diffuser Lips

The key difference is within the stator geometry. The volute pump has only two throat areas. To achieve the required throat area for the b.e.p the throat within a volute pump is taller. When the pumped product is expelled from the impeller, diffusion can take place around the impeller periphery along a path that extends to 50% of the impeller circumference and to a greater height.

In contrast the diffuser has 9 throat areas of a much lower height. The diffusion takes place along 11% of the impeller periphery.

The volute pump contains only 3 vanes. The distance from the volute lip to the mid pitch impeller blade is greater than that of the impeller in the diffuser pump, which has 5 blades.

The peristaltic effect that occurs as these impeller blades try to exchange fluid with the stalled stator passageways influences the unsteady pressure field within the impeller-stator annular gap and thus influences the pressure pulsation propagating through the stalled passageway.

This observation is an extension of the theory proposed by Frost and Nielsen (1988). In their paper the researchers suggested that the aspect ratio of the diffuser/volute throat had a distinct influence on the closed valve head of the machine.

Their research assumed that the velocity gradient over the diffuser throat could be integrated to provide a pressure contribution associated with the stator geometry. The impeller pressure was deemed to be analogous to a solid rotating disc as described previously in Chapter 2.

The Frost and Nielsen (1988) research neglected the rotor stator interaction effects. These contribute to the peristaltic pressure development between impeller and diffuser. Chapter 6 of this research evaluates the peristaltic contribution in greater detail and proposes an empirical formula for stability criteria based on changing rotor vane number and accounting for the increased pulsation frequency.

5.6. Unsteady Pressure Reading

Monitor points are arrange across as illustrated in fig 5.6.1 in the annular gap between the impeller and diffuser across the inlet to the diffuser. These points are used to assess the frequency and amplitude of the pressure within this annular gap

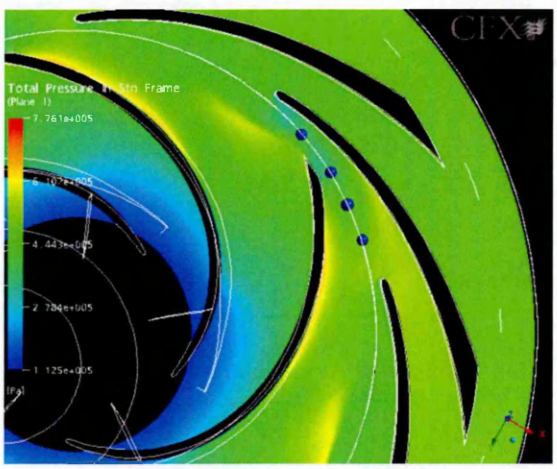

Fig 5.6.1 Monitor Point Position across the Diffuser Entrance.

5.6.1Unsteady Pressure Readings Taken at Point 1

Point 1 is positioned centrally between the impeller outside diameter and the diffuser lip diameter in the annular gap between rotor and stator. This is illustrated in figure 5.6.1.1

The figure 5.6.1.1 illustrates the temporal position at which the maximum pressure occurs. The maximum pressure precedes the blade as it approaches the monitor point.

Unsteady pressure readings generated by the computational solution are depicted in fig 5.6.1.2. The time signal history illustrates a repeating Pattern of pressure peaks.

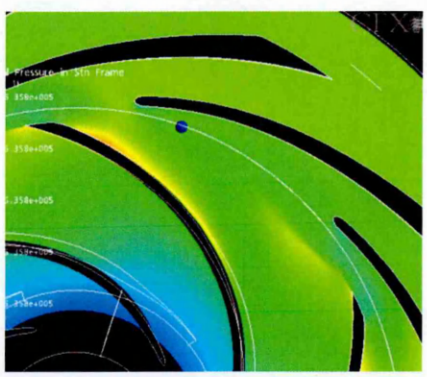

Fig 5.6.1.1 Monitor Point 1 Maximum Pressure

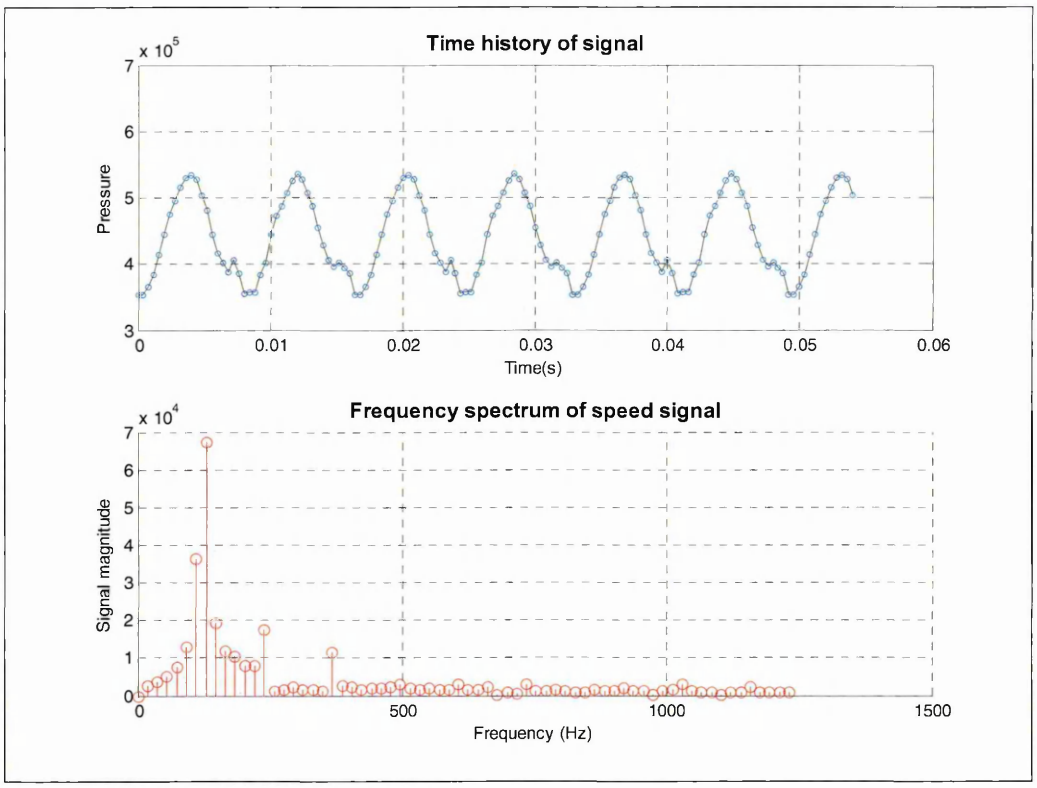

5.6.1.2 Pressure Pulsation at Monitor Point 1

The frequency spectrum is dominated by the vane frequency. This is a function of the number of vane passing the stationary lips. There is also a significant frequency at twice the vane passing frequency. This is generally attributed to the wake effect (Dyson and Palgrave 2000, Deans and Senoo 1953).

These dominant frequencies also exist within the volute design of machine. They are linked to the number of rotating impeller vanes. These frequencies are always apparent on any rotating impeller as the rotating vanes pass the stationary vanes. The industry measure the vibration signature generated by these pressure pulsations and uses its amplitude to draw conclusions about machine bearing and seal reliability

Figure 5.6.1.3 illustrates the position of the minimum pressure at point 1. This is close to the turbulent wake as it passes the monitor point. There is a pressure rise of 51% from the minimum. The maximum pressure at this monitor point is 553200Pa. The minimum pressure is 353000Pa. The average pressure from blade to blade is 438648Pa.

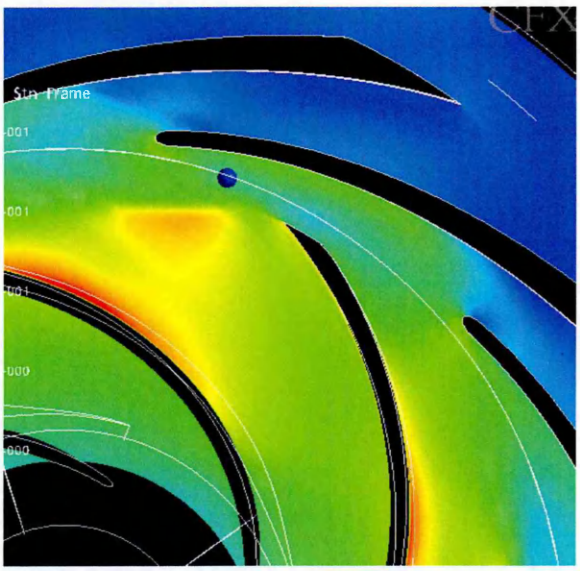

Fig 5.6.1.3 Monitor Point 1 Minimum Pressure

5.6.2 Unsteady Pressure Readings Taken at Monitor Point 2

Point 2 is positioned centrally between the impeller outside diameter and the diffuser lip diameter in the annular gap between rotor and stator. This is illustrated in Fig 5.6.2.1

The following Fig 5.6.2.1 illustrates the temporal position at which the maximum pressure occurs. The maximum pressure precedes the blade as it approaches the monitor point as observed for point 1.

Unsteady pressure readings generated by the computational solution are depicted in Fig 5.6.2.2. The time signal history illustrates a repeating pattern of pressure peaks.

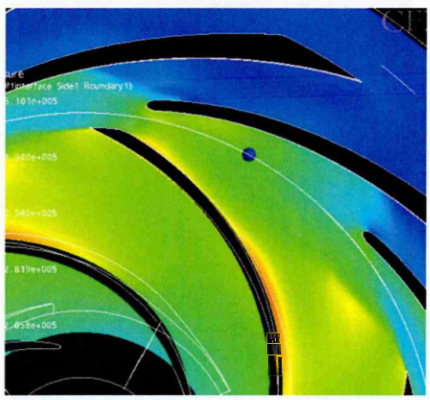

Fig 5.6.2.1 Monitor Point 2 Maximum Pressure

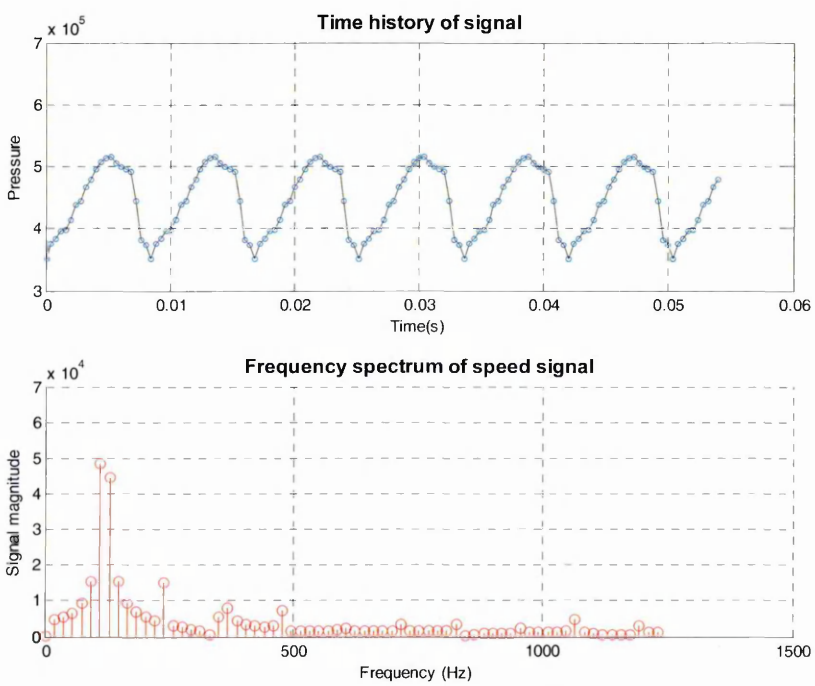

Fig 5.6.2.2 Pressure Pulsation at Monitor Point 2

Evaluation of the temporal pressure signal indicates that although the frequency of the pressure pulsation is unaltered the peak pressure is spread over a longer period. At point 1 the pressure peak was a defined peak. For Monitor point 2 the pressure decay in less immediate and the rate of pressure decay has diminished. The frequency spectrum is dominated by the vane frequency and twice vane frequency.

Fig 5.6.2.3 illustrates the position of the minimum pressure at point 2. This is close to the blade thickness as it passes the monitor point. There is a pressure rise of 47% from the minimum. The maximum pressure at this monitor point is 516900Pa. The minimum pressure is 351400Pa. The average pressure from blade to blade is 447306Pa.

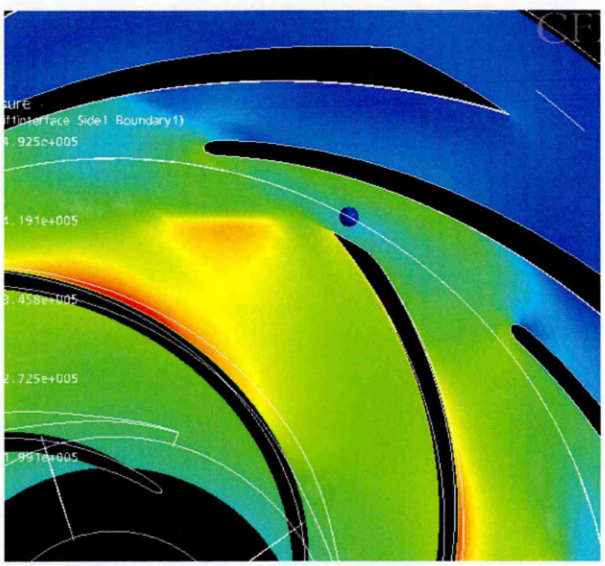

Fig 5.6.2.3 Monitor Point 2 Minimum Pressure

5.6.3 Unsteady Pressure Readings Taken at Monitor Point 3

Pont 3 is positioned centrally between the impeller outside diameter and the diffuser lip diameter in the annular gap between rotor and stator. This is illustrated in Fig 5.6.3.1

The Fig 5.6.3.1 illustrates the temporal position at which the maximum pressure occurs. The maximum pressure precedes the blade as it approaches the monitor point.

Unsteady pressure readings generated by the computational solution are depicted in Fig 5.6.3.2. The time signal history illustrates a repeating pattern of pressure peaks.

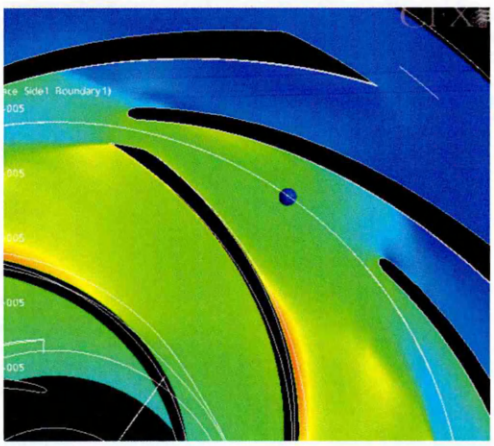

Fig 5.6.3.1 Monitor Point 3 Maximum Pressure

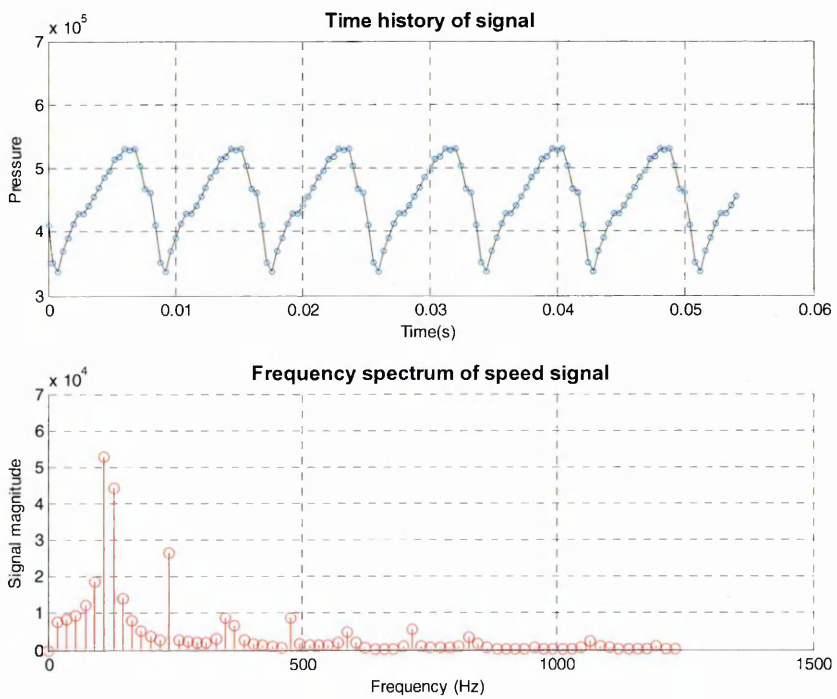

Fig 5.6.3.2 Pressure Pulsation at Monitor Point 3

Evaluation of the temporal pressure signal indicates that although the frequency of the pressure pulsation is unaltered the peak pressure spread is more defined as for monitor point 1. For monitor point 3 the pressure decay is rapid and almost immediate. The rate of pressure decay has increased. The frequency spectrum is dominated by the vane frequency and twice vane frequency.

Figure 5.6.3.3 illustrates the position of the minimum pressure at point 3. This is close to the blade thickness as it passes the monitor point. There is a pressure rise of 56% from the minimum. The maximum pressure at this monitor point is 530500Pa. The minimum pressure is 337400Pa. The average pressure from blade to blade is 453686Pa.

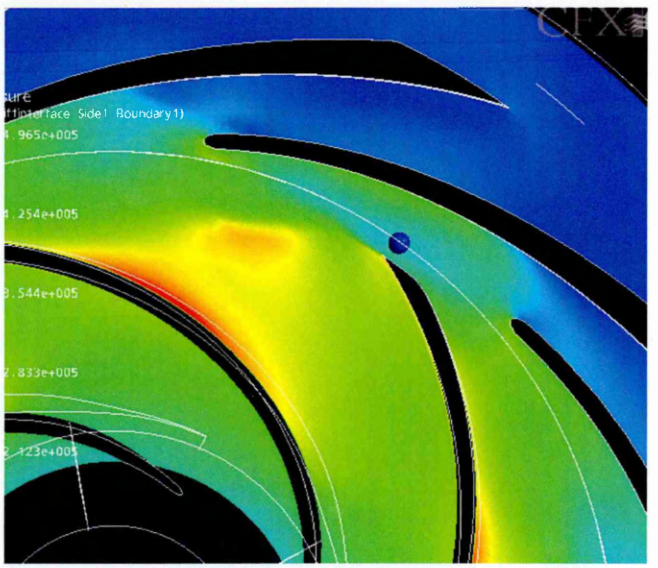

Fig 5.6.3.3 Monitor Point 3 Minimum Pressure

5.6.4 Unsteady Pressure Readings Taken at Monitor Point 4

Pont 4 is positioned centrally between the impeller outside diameter and the diffuser lip diameter in the annular gap between rotor and stator. This is illustrated in Fig 5.6.4.1

The Fig 5.6.4.1 illustrates the temporal position at which the maximum pressure occurs. The maximum pressure precedes the blade as it approaches the monitor point.

Unsteady pressure readings generated by the computational solution are depicted in Fig 5.6.4.2. The time signal history illustrates a repeating pattern of pressure peaks.

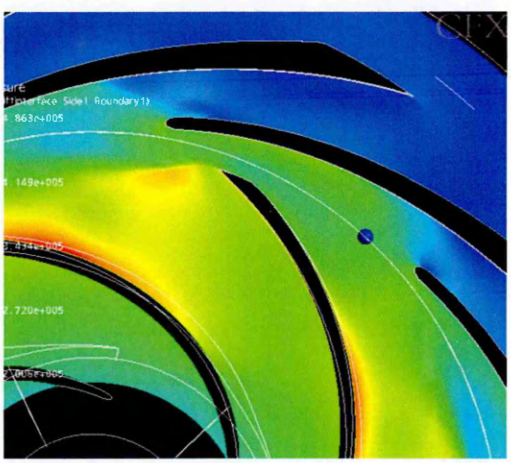

Fig 5.6.4.1 Monitor Point 4 Maximum Pressure

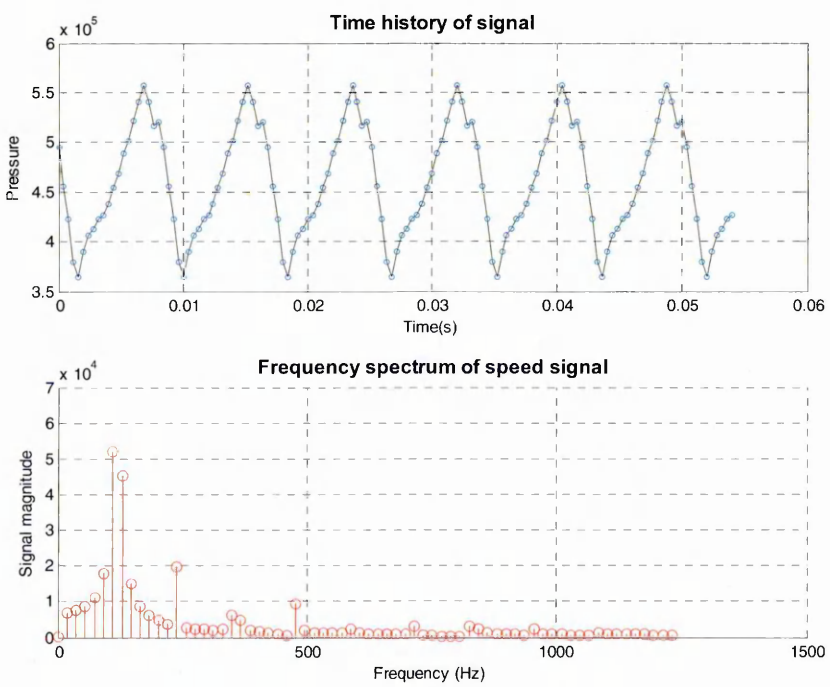

Fig 5.6.4.2 Pressure Pulsation at Monitor Point 4

Evaluation of the temporal pressure signal indicates that although the frequency of the pressure pulsation is unaltered the peak pressure is more defined as with monitor point 1 and 3. For Monitor point 4 the pressure decay is rapid and almost immediate. The rate of pressure decay has again increased. The frequency spectrum is dominated by the vane frequency and twice vane frequency.

Fig 5.6.4.3 illustrates the position of the minimum pressure at point 4. This is close to the blade thickness as it passes the monitor point. There is a pressure rise of 53% from the minimum. The maximum pressure at this monitor point is 557400Pa. The minimum pressure is 364400Pa. The average pressure from blade to blade is 463209Pa.

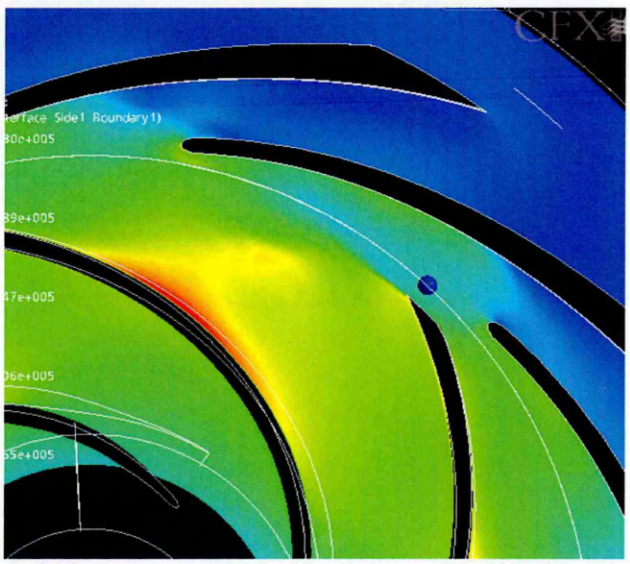

Fig 5.6.4.3 Monitor Point 4 Minimum Pressure

5.7 Overview of Diffuser and Impeller Flow Regime Interface

Fig 5.7.1 illustrates the velocity vectors between the rotating impeller and the stationary diffuser blades. These images are particularly relevant as they illustrate the flow condition as the impeller blade is close to the diffuser blade. The condition where the blade is one diffuser vane pitch away from the following blade is also captured. This is achieved as the blade numbers between the stationary and rotating components are different allowing multi frame capture in one image.

The flow regime presented is taken on a plane which cuts through the centre of the impeller and diffuser. Secondary flows are not investigated within this research.

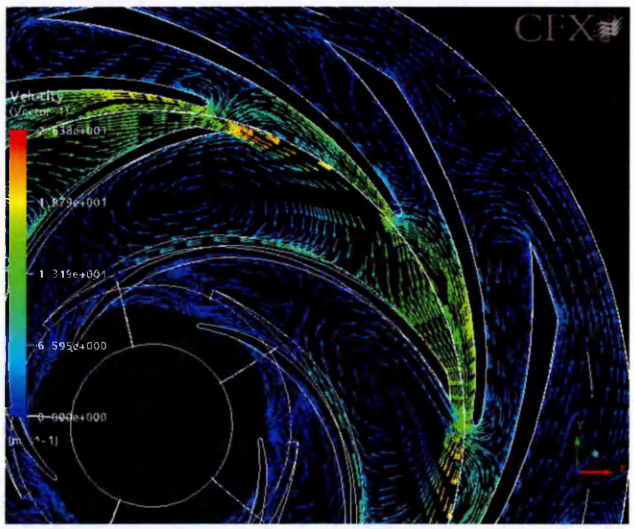

Fig 5.7.1 Velocity Vectors through the Impeller and Diffuser

Although further refinement of the vector picture is instructive, this image demonstrates that a distinct difference occurs between the mid-pitch and congruent temporal positions of the impeller blades.

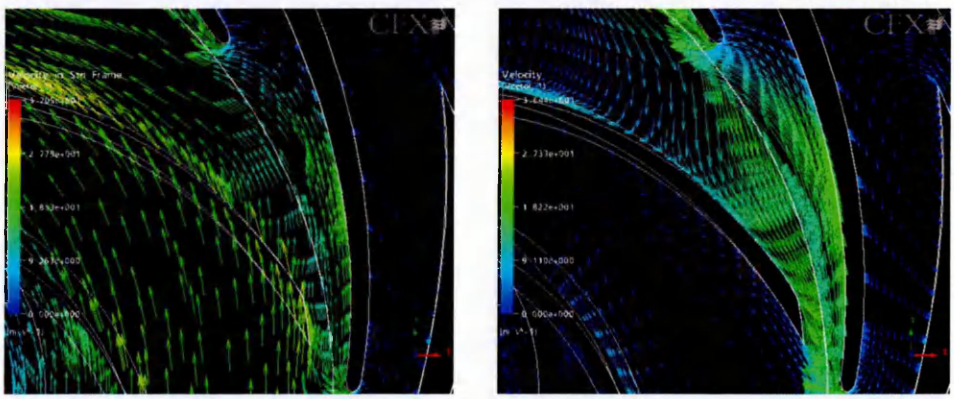

Fig 5.7.2 Velocity Vectors At Diffuser Tip

Fig 5.7.2 further refines the images to present absolute and velocity vectors of the impeller blade as it passes the diffuser tip.

Where the impeller blade is congruent with the diffuser blade, in both the relative and absolute images, the flow through the small annular gap, formed by the impeller blade thickness passing the diffuser tip, is ordered to meet the stream line formed by the geometry. This area experiences the highest velocity as the liquid is driven into the small clearance gap.

The velocity stream is attached to the diffuser blade suction face.

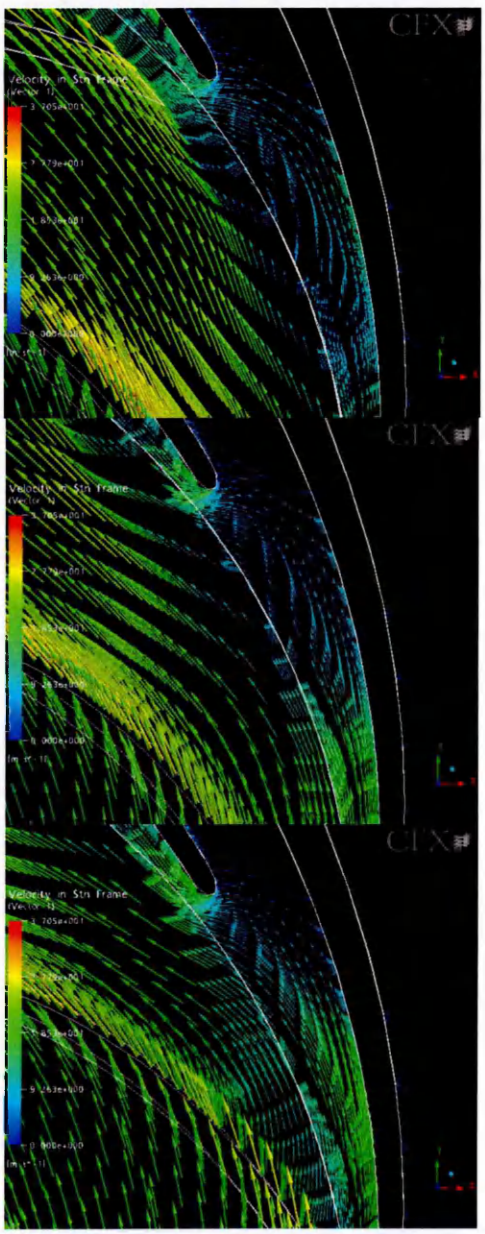

Fig 5.7.3. Diffuser Incidence Illustration

For rotor stator interaction it has previously been observed in the study by Cattanei et al (1998) that a fluctuating positive and negative diffuser incidence occurs as a consequence of the alternating passage of blade wakes and free-

stream flow. Fig 5.7.3 illustrates that this fluctuation of diffuser incidence does not occur at such an extreme low flow condition. The incidence to the diffuser blade remains negative. Only the proportion of negative incidence changes as the impeller blade influence acts upon it.

At the closed valve condition i.e. Q= 0 the diffusers are filled with stationary fluid preventing ingress of the impeller flow into the stationary passageways. This situation forces the expelled impeller flow to follow the suction side of the diffuser blade until it approaches the stalled diffuser throat.

At the diffuser throat the flow that has exited the impeller vanes is forced to re-enter the annular clearance that occurs as a consequence of the running the rotating impeller within the stationary diffuser.

Whilst the incidence close to the blade is consistently negative, the liquid progress back into the impeller/diffuser annular clearance is strongly influenced by the passing of the impeller blade.

At mid pitch of the impeller, the impeller blade to blade area is the greatest. This allows the negative incidence from the diffuser blade to progress at a negative angle back into the impeller blade to blade passageway.

The situation when the impeller blade is approaching and coincident with the diffuser blade is very different. The high pressure region close to the impeller tip on the discharge side of the vane, and subsequently the impeller vane thickness, force the flow rejected by the stalled throat to progress circumferentially.

These rotor-stator interaction effects set up a continual energy exchange based on continuity considerations. A pulsating flow is observed at each diffuser vane location as the annular flow fluctuates between the circumferential and the ingress back into the impeller vane channel.

This complex flow interaction has not previously been reported within the literature. This points, again, towards the difficulties encountered by researches investigating the closed valve head phenomenon. The computational interface between the impeller and diffuser must accept both inlet and outlet flow. Previous studies have found this boundary condition assignation difficult to accommodate so as not to influence the solution validity.

The annular space between the impeller and diffuser is subject to a fluctuating pressure field that affects the closed valve head of the machine.

The Fig 5.7.4 demonstrates the change in velocity along line ‘a-a’.

The outlet proportion of the impeller can be divided into two distinct regions. These are denoted in Fig 5.7.4 as ‘A’ and ‘B’.

These two region regions have a distinct influence on the flow regime within the impeller diffuser clearance.

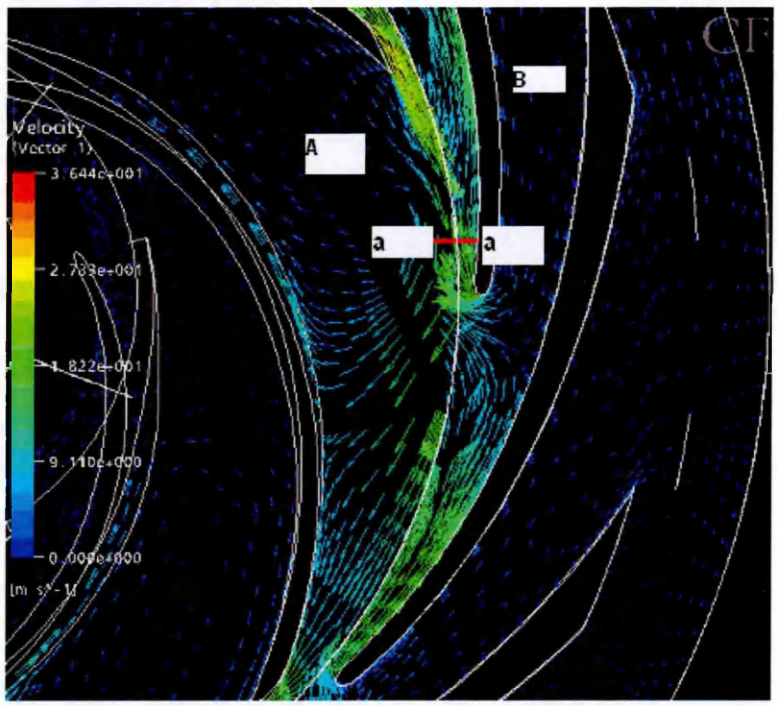

Fig 5.7.4. Division of Flow Areas

At portion A the impeller is filled with a standing vortex as observed within the volute pump. This vortex pulsates with the influence of the rotor stator interaction. This portion is filled with a proportion of trapped fluid bound by the liquid held within the annular gap between impeller and diffuser.

Point B is also full of dead liquid and prevents outlet mass flux. The pressure pulsations passed from the rotor stator action define the level of closed valve head of the machine within this region.

Monitoring of the unsteady velocity variation along line 'a-a' acknowledges the influence of the bound liquid within this clearance at the blade interactions occur.

The velocity variations along the illustrated line fall into two distinct regions.
The first region occurs from the approach of the impeller blade to the commencement of the discharge vortex diminishment.
The liquid is bound within the small gap by first the blade thickness and subsequently by the vortex.

Close to the impeller outside diameter there is little difference between stationary frame velocity readings over the vane thickness and the discharge vortex. As readings are taken at greater radii a negative velocity gradient becomes apparent. This gradient increases to a maximum as the impeller vortex is driven inwards into the rotating vane channel.

Fig 5.7.5 demonstrates the changing nature of the velocity gradient with respect to distance and phase angle. From this chart it can be seen that the gradient increases as the impeller blade moves away from the tip and the vortex influence becomes dominant. One third of the annular passage between the impeller and diffuser blades is filled with the negative velocity gradient.

As the influence of the pressure profile caused by the impeller vane passing reduces the viscous effects allow time/distance to mix out some of the velocity forces impinging on the passage velocity and the gradient becomes positive closer to the diffuser blades.

Of interest is the changing nature of the unsteadiness as the blade progresses along its pitch. At the interface, where the discharge vortex turns inwards into the impeller channel the nature of the velocity reaches an unsteady peak. This aligns to the largest negative velocity gradient coupled to a subsequent velocity recovery to a positive gradient.

This unsteady interaction is demonstrated in Fig 5.7.6 which illustrates the changes in velocity from the averaged streamline velocity, taken in the radial direction.

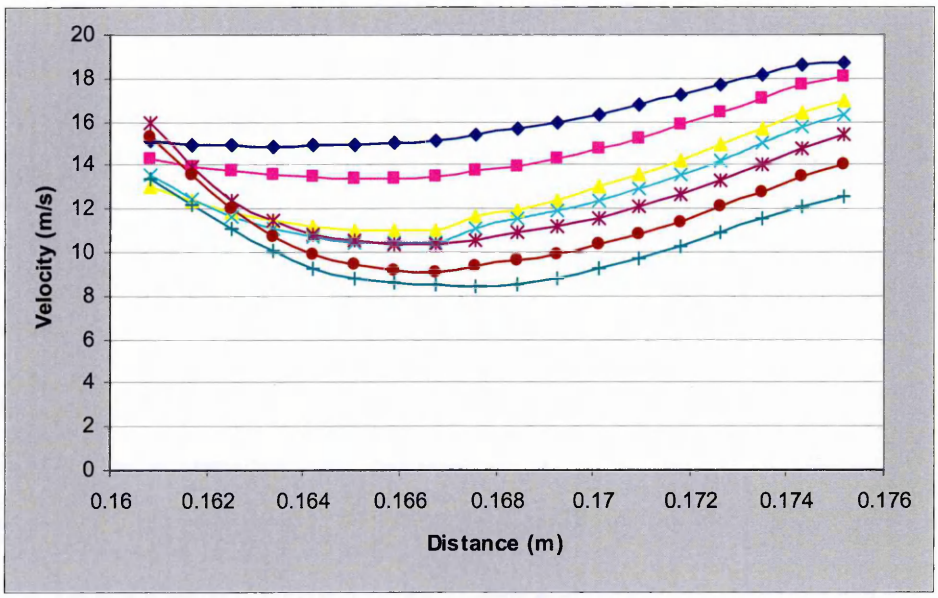

Fig 5.7.5 Radial Differences in Velocity Based On Phase Position Along Line 'A-A'

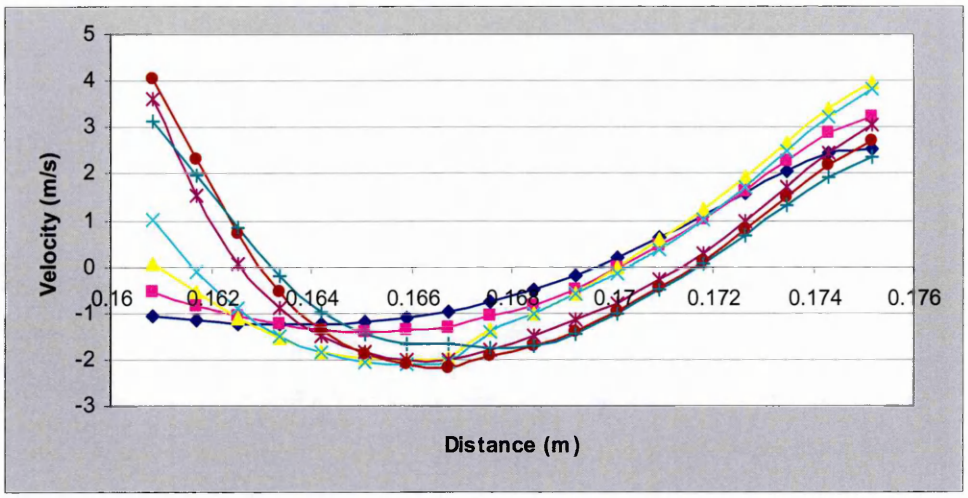

Fig 5.7.6 Unsteady Velocity Difference From Average Streamline Velocity

When the influence of the vane and discharge vortex has passed the unsteadiness is reduced. The velocity differences from the mean velocity range from -2m/s to +2m/s as opposed to -2m/s +4m/s.

Although the velocity changes with phase position its unsteadiness is greatly reduced compared to the analysis of a volute machine. This is attributable to the higher frequency but lower amplitude pulsation system set up by the blade row configuration.

Using this observation we can conclude that increasing the vane number with the rotating impeller provides smaller amplitude pulsations but at a higher frequency. This supports the work by Peck (1950) who observed that higher vane numbers contributed to a higher closed valve head coefficients.

5.8 Diffuser Passage Flow Regime

The nature of the flow within the diffuser channels is presented in this section. Research by Newton (1998) suggested that the volute pressure rise prediction within the CFD code was responsible for the inaccurate prediction of closed valve head.

In the previous chapter the volute pressure rise was correctly predicted. The closed valve head predicted by the CFD code was in line with experimental measurements taken on similar machines.

Within a diffuser pump the situation is similar to the volute pump except that the volute pressure rise is replaced by the pressure rise around the 9 diffuser blades.

Whereas the pressure rise around the volute consisted of only two channels the diffuser situation is much more complex, forcing the code to evaluate pressure rises at multiple points as the pitch differences between impeller and diffuser influences the timings of the pressure development.

The diffuser throat is an interesting area to begin an investigation into the diffuser flow regime. The aspect height of the diffuser channel was cited by Frost and Neilsen(1988) as a contributor to the closed valve head value.

An unsteady pressure map is instructive in illustrating the unsteady nature of the pressure development across the diffuser throat.

Figure 5.8.1. Illustrates the throat of the diffuser and the line across which the pressure development is measured.

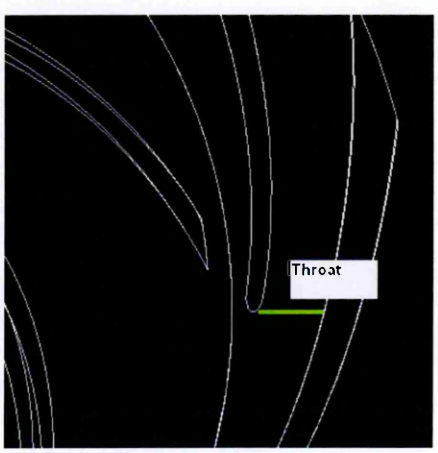

Fig 5.8.1 Diffuser Throat Location 'A'

Figure 5.8.2 illustrates the evolving pressure with time across this diffuser throat line. As the impeller vanes approach the diffuser vanes.

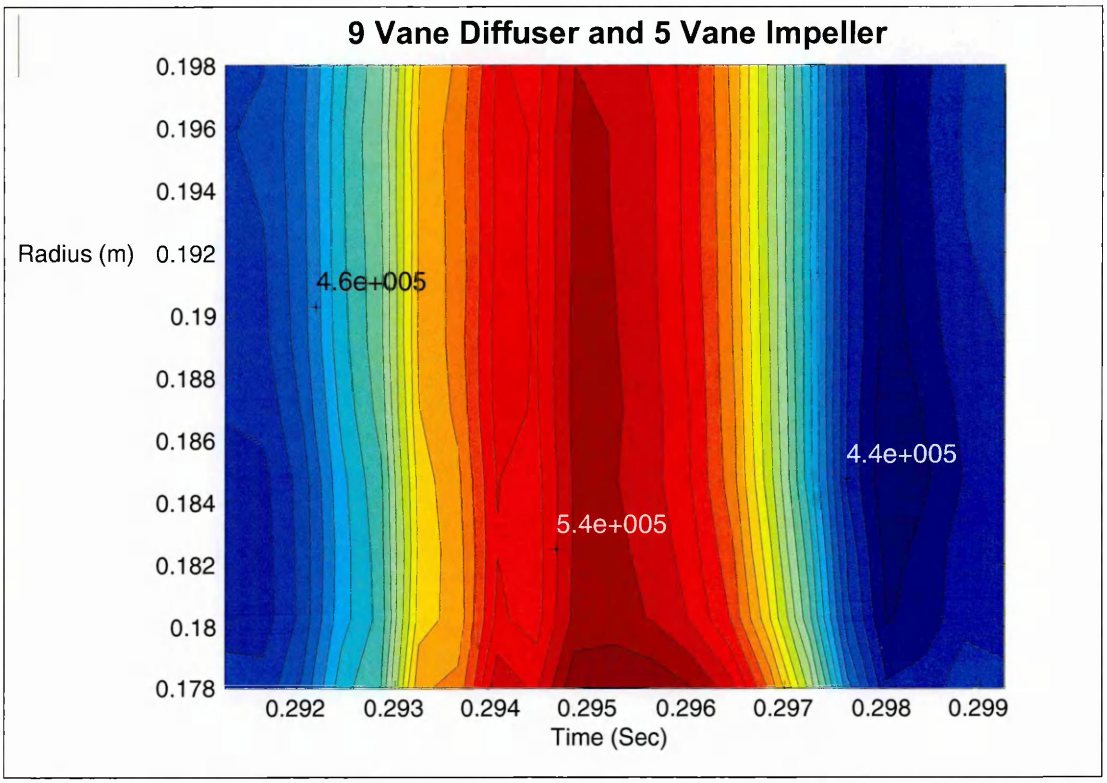

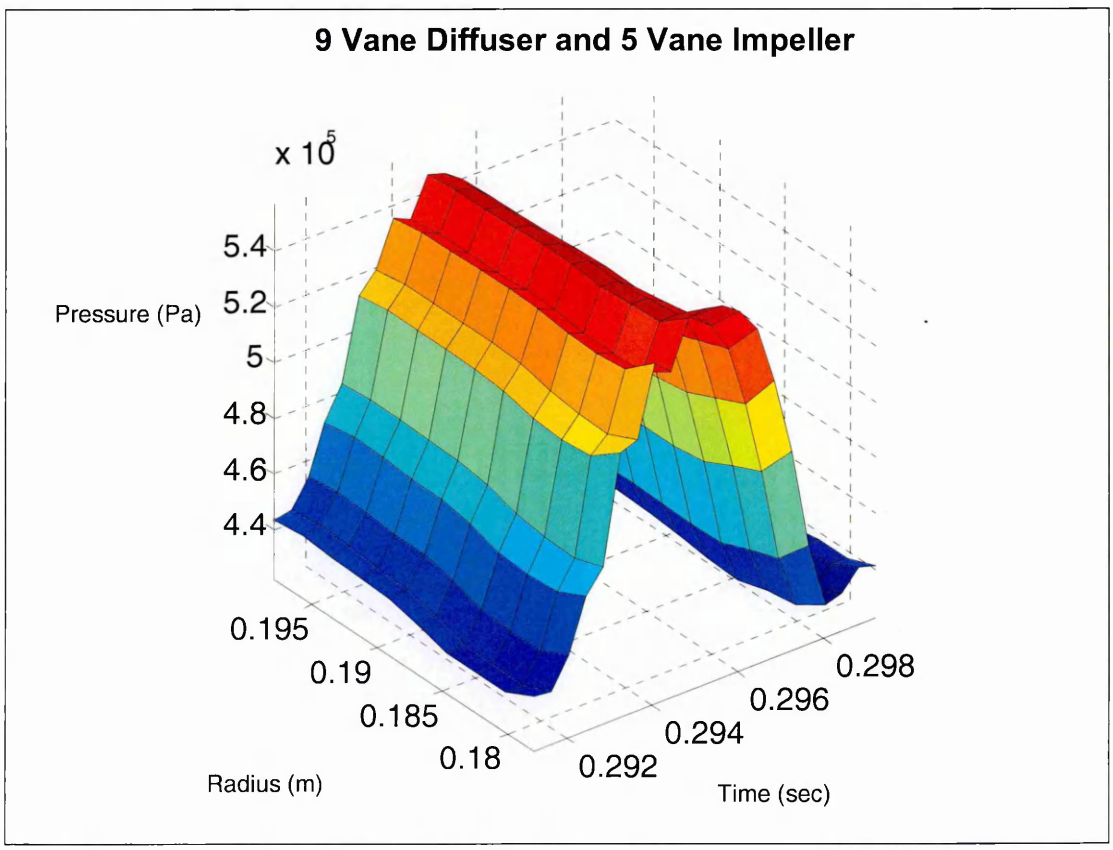

Fig 5.8.2 Pressure Map across the Diffuser Throat 'A'

The pressure map illustrated in Fig 5.8.2 encompasses the pressure development across a time period equal to the passage of one impeller blade pitch.

Figures 5.8.3 contains a map of all the diffuser blade passages. This is used to aid the description of the flow field. Figures 5.8.4-5.8.10 contains the throat pressure information for each of theses blade passages.

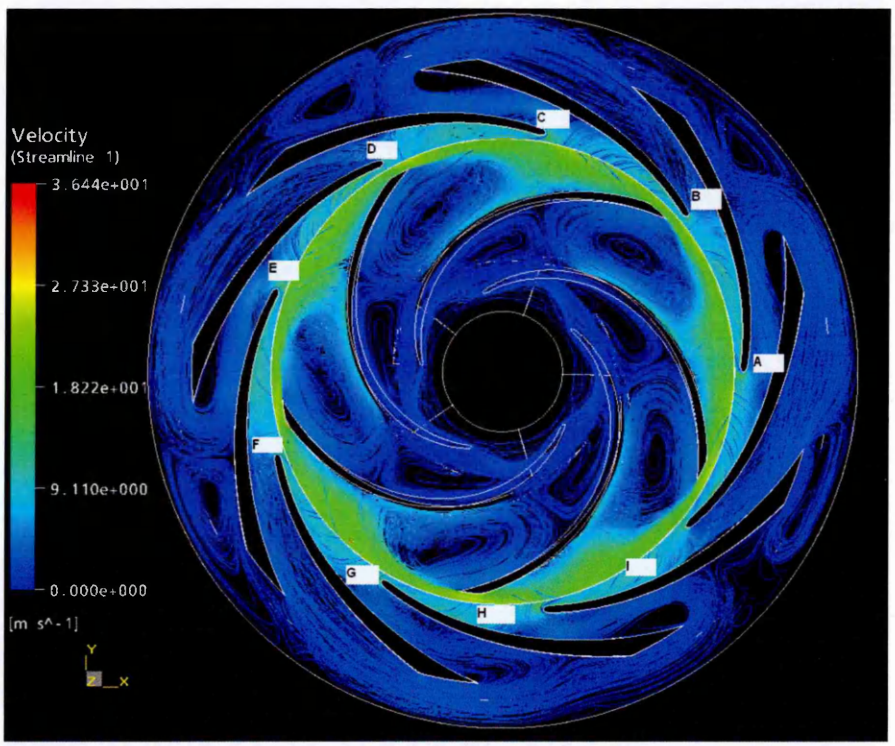

5.8.3 Diffuser Passage Location Map

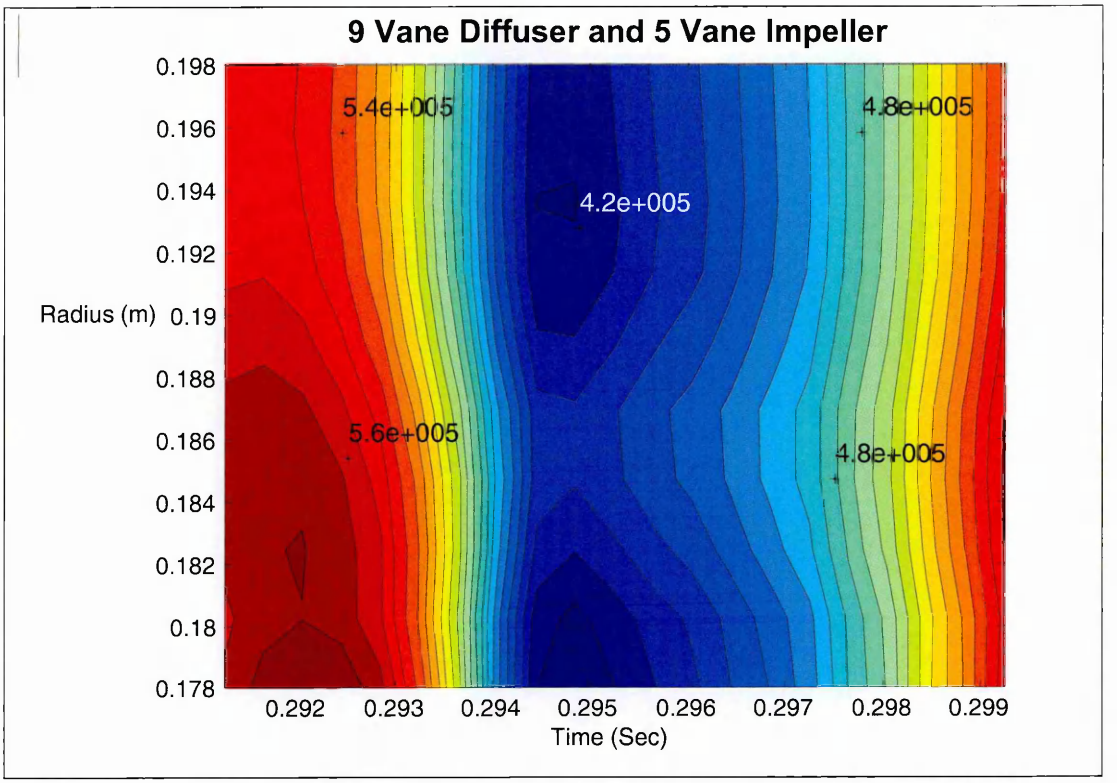

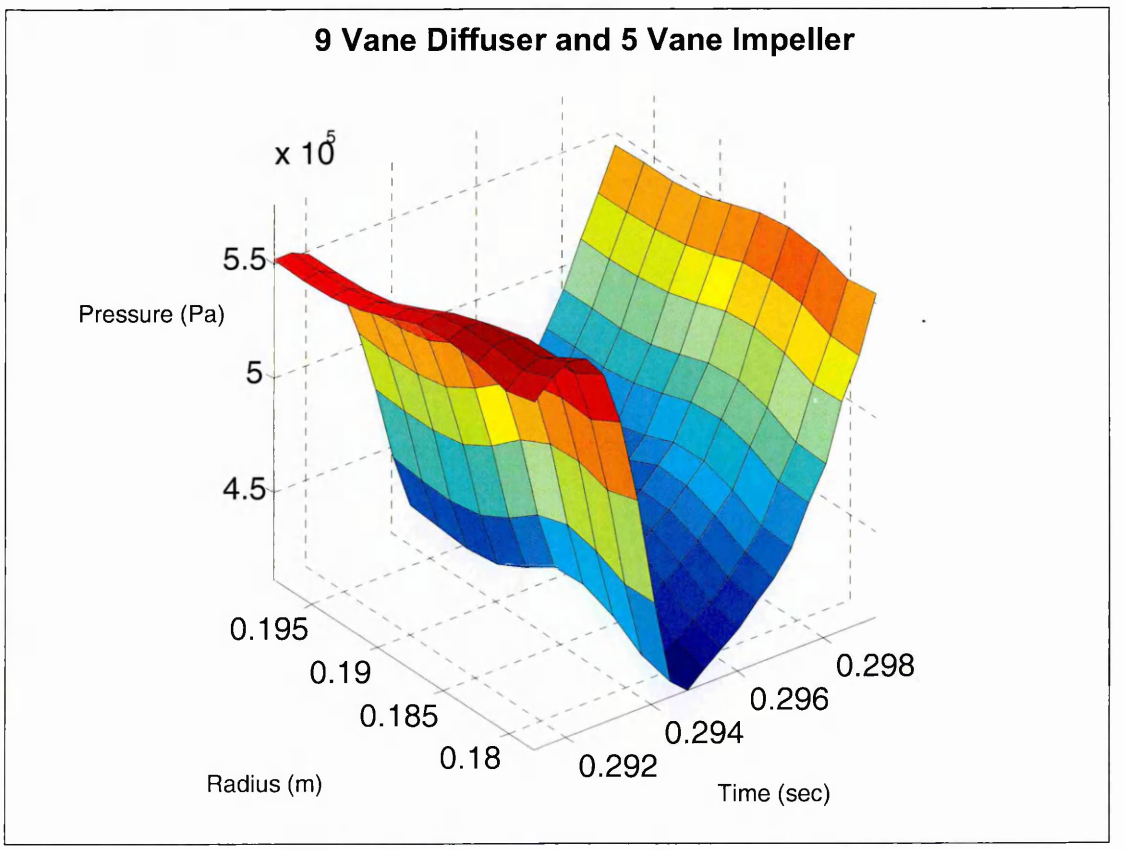

Fig 5.8.4 Pressure Map across the Diffuser Throat 'B'

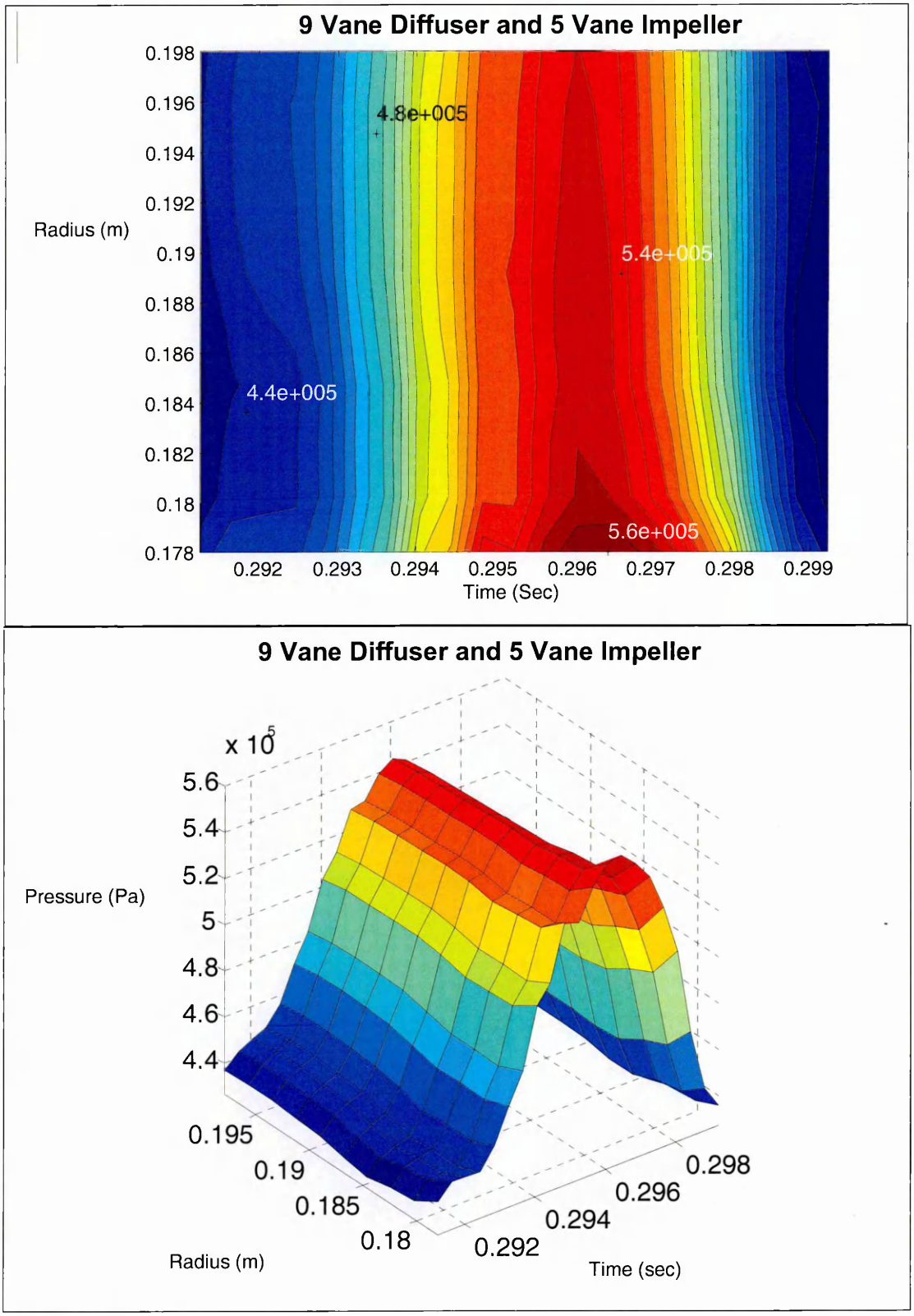

Fig 5.8.5 Pressure Map across the Diffuser Throat 'C'

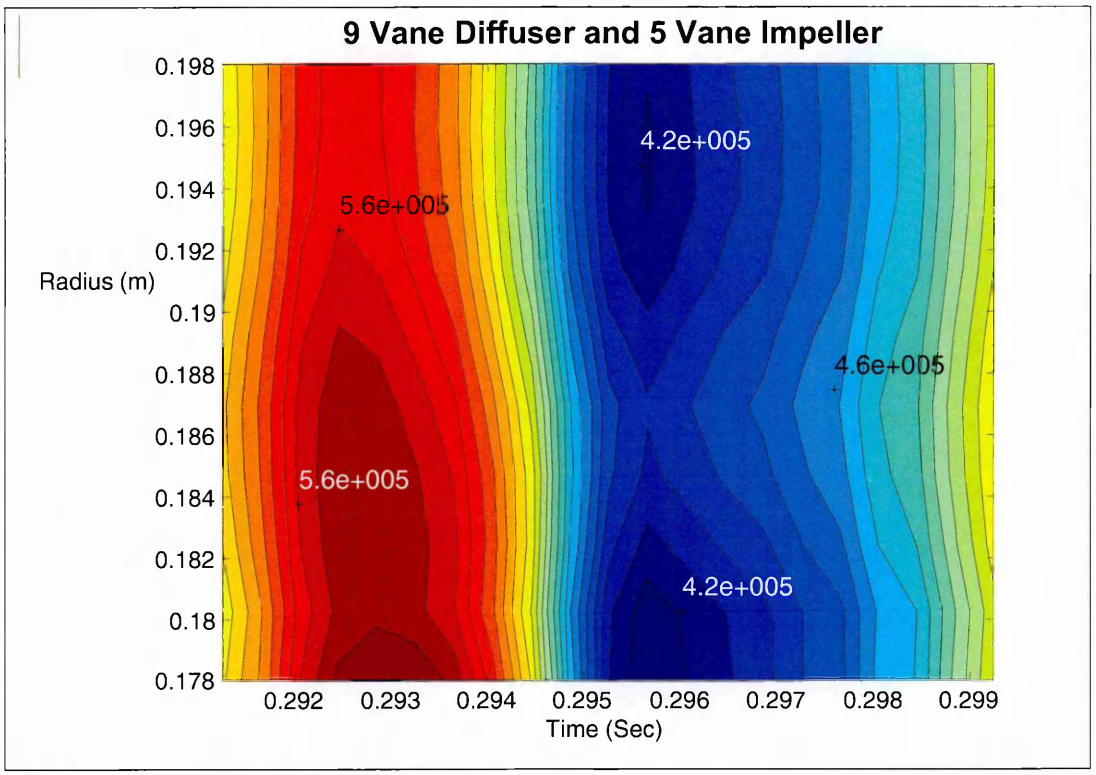

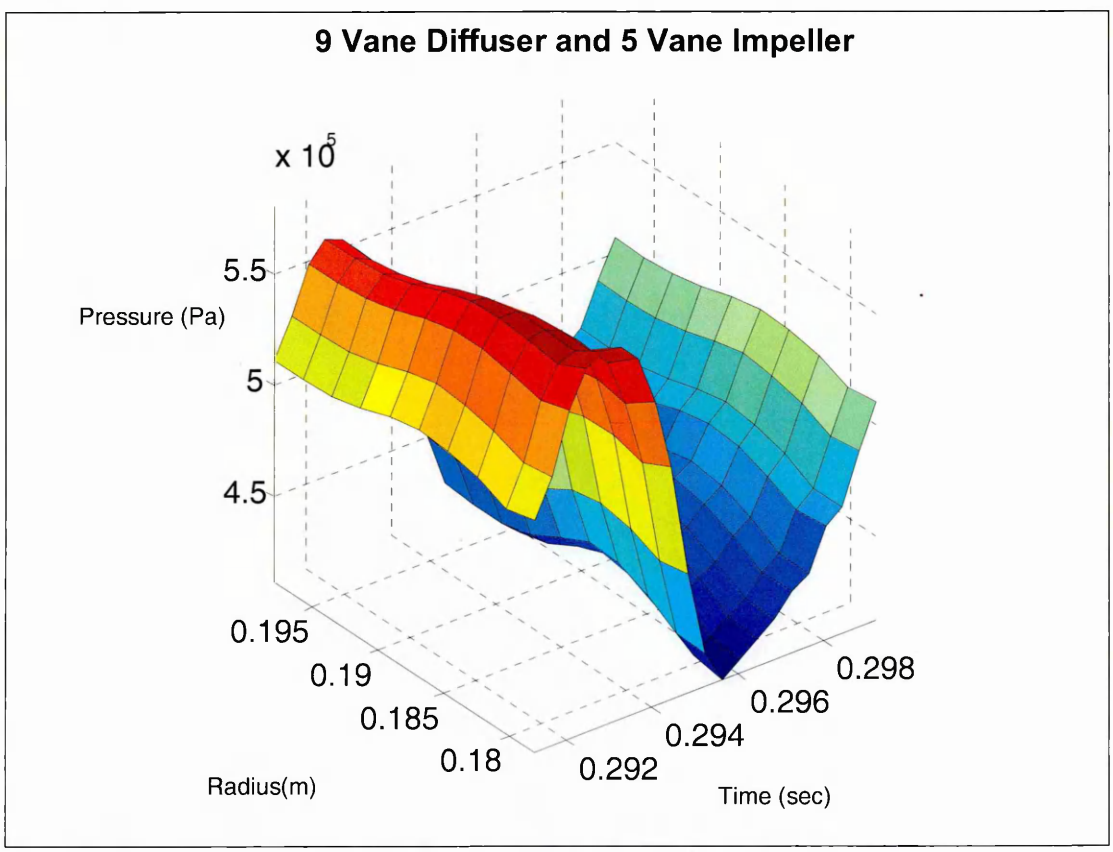

Fig 5.8.6 Pressure Map across the Diffuser Throat 'D'

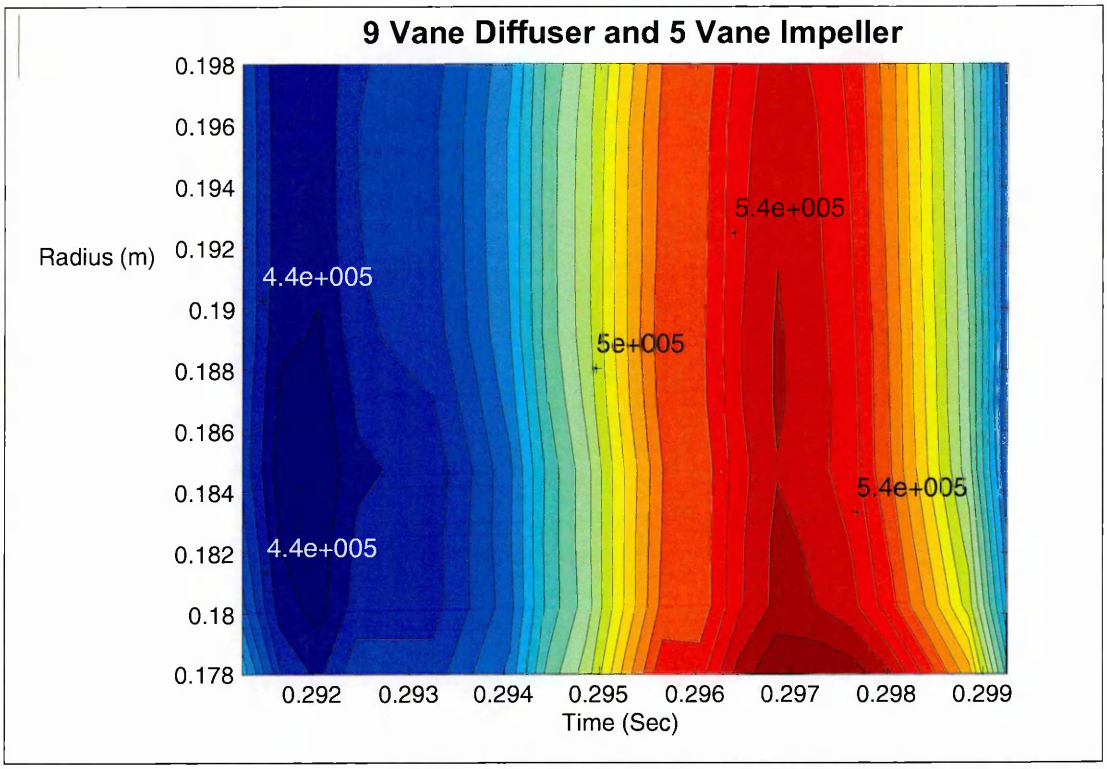

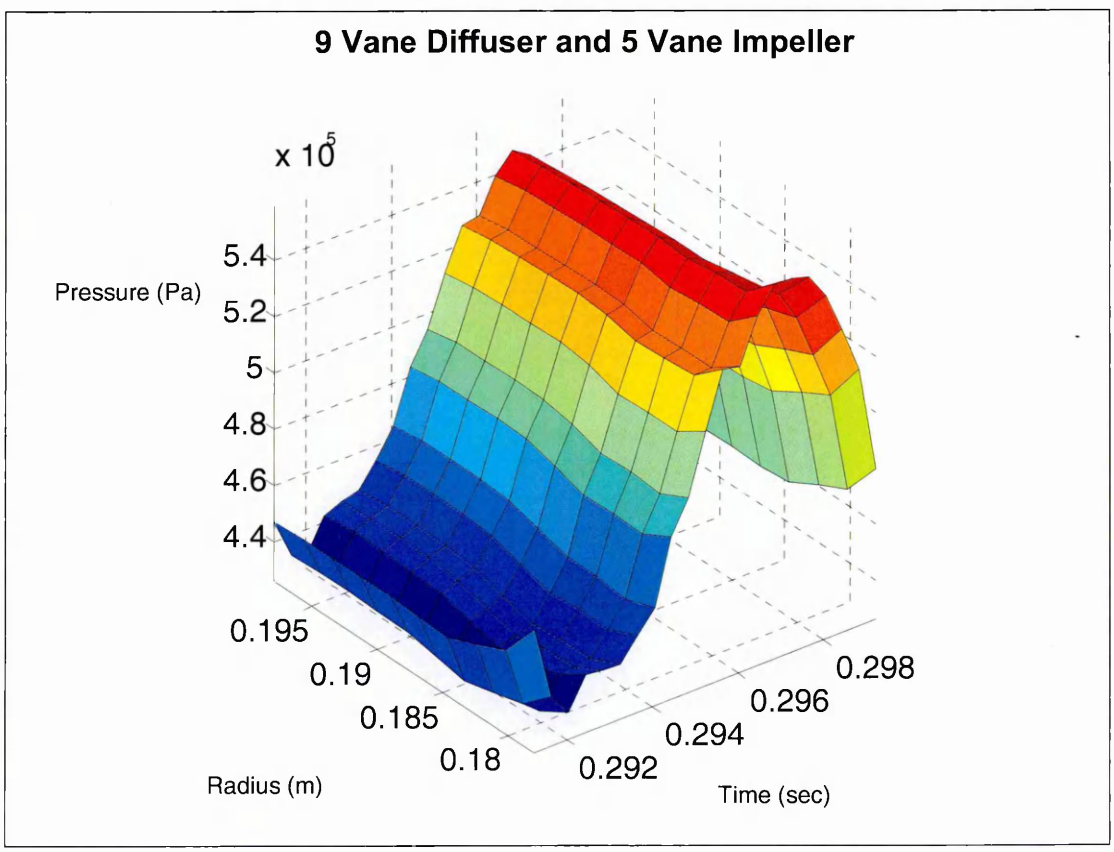

Fig 5.8.7 Pressure Map across the Diffuser Throat 'E'

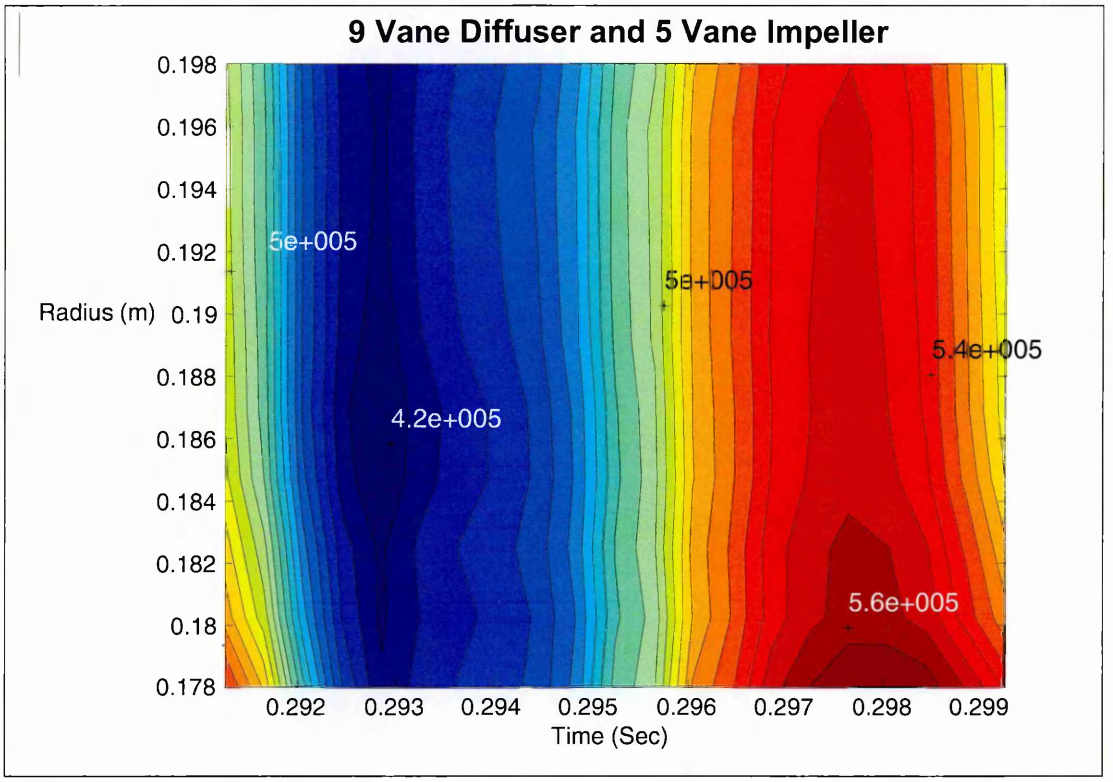

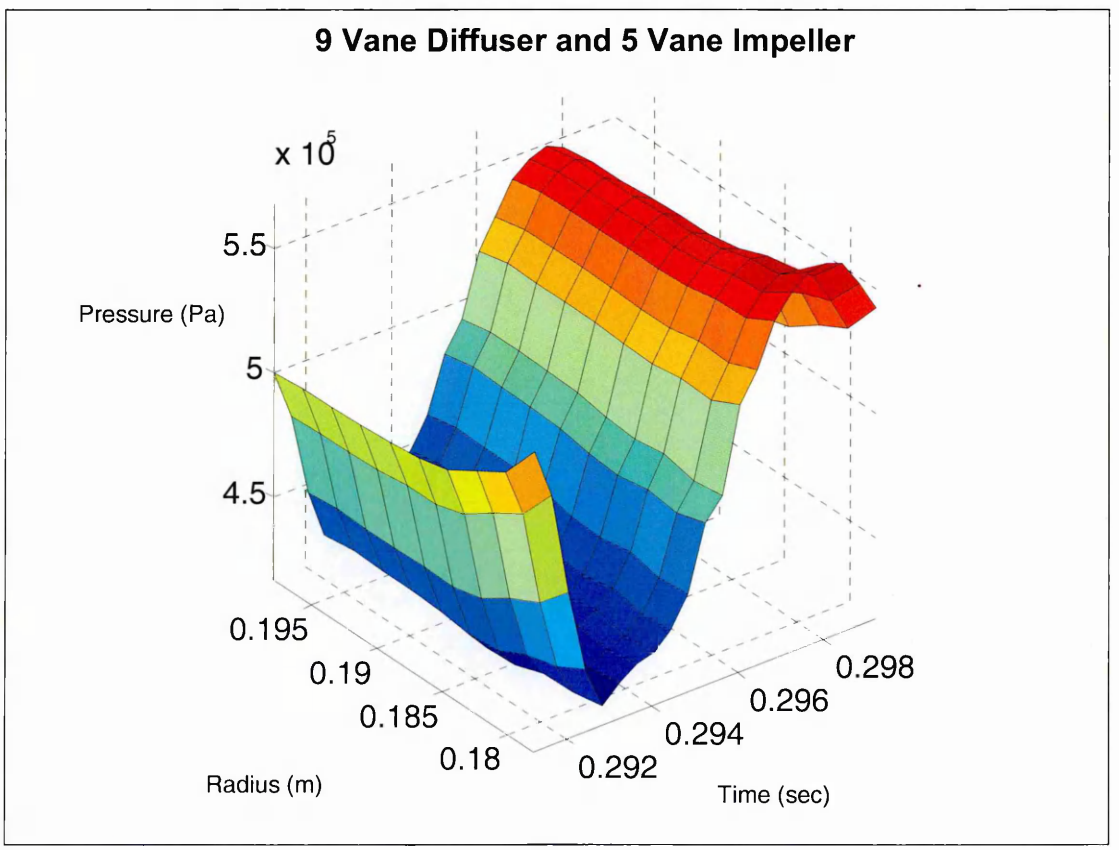

Fig 5.8.8 Pressure Map across the Diffuser Throat 'F'

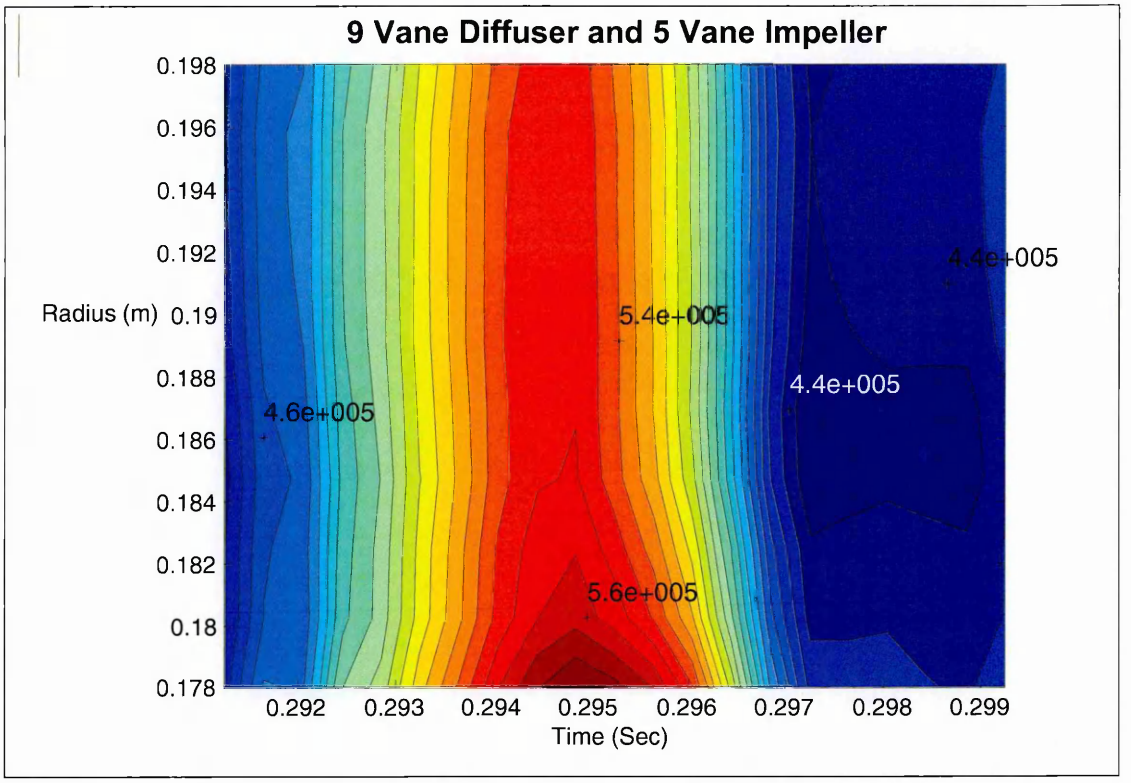

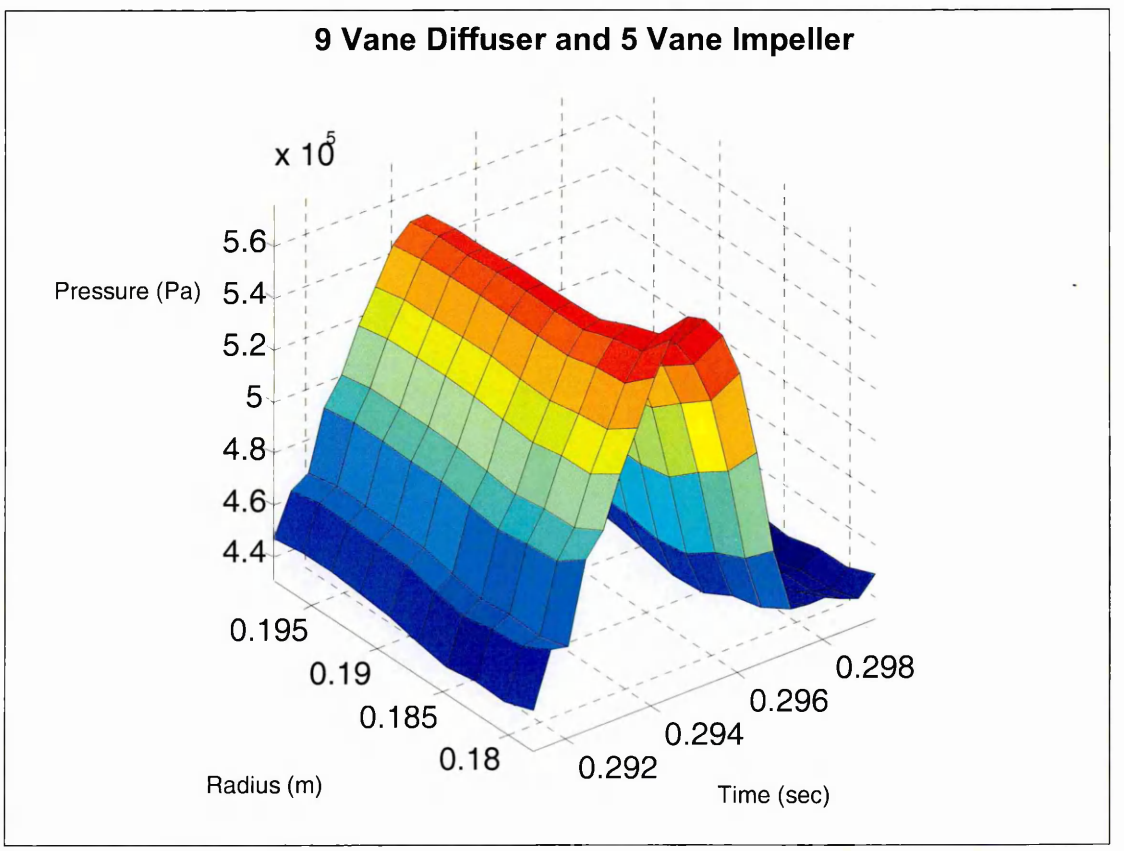

Fig 5.8.9 Pressure Map across the Diffuser Throat 'G'

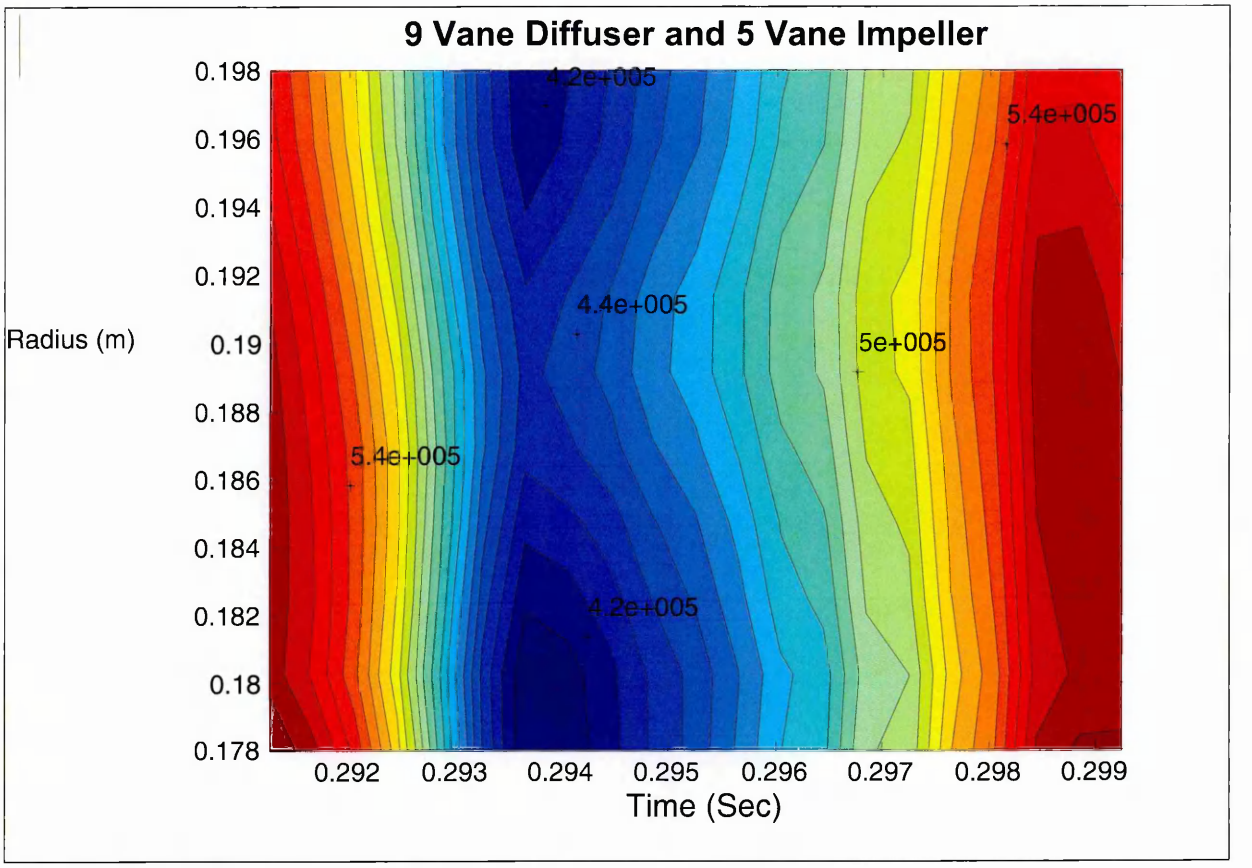

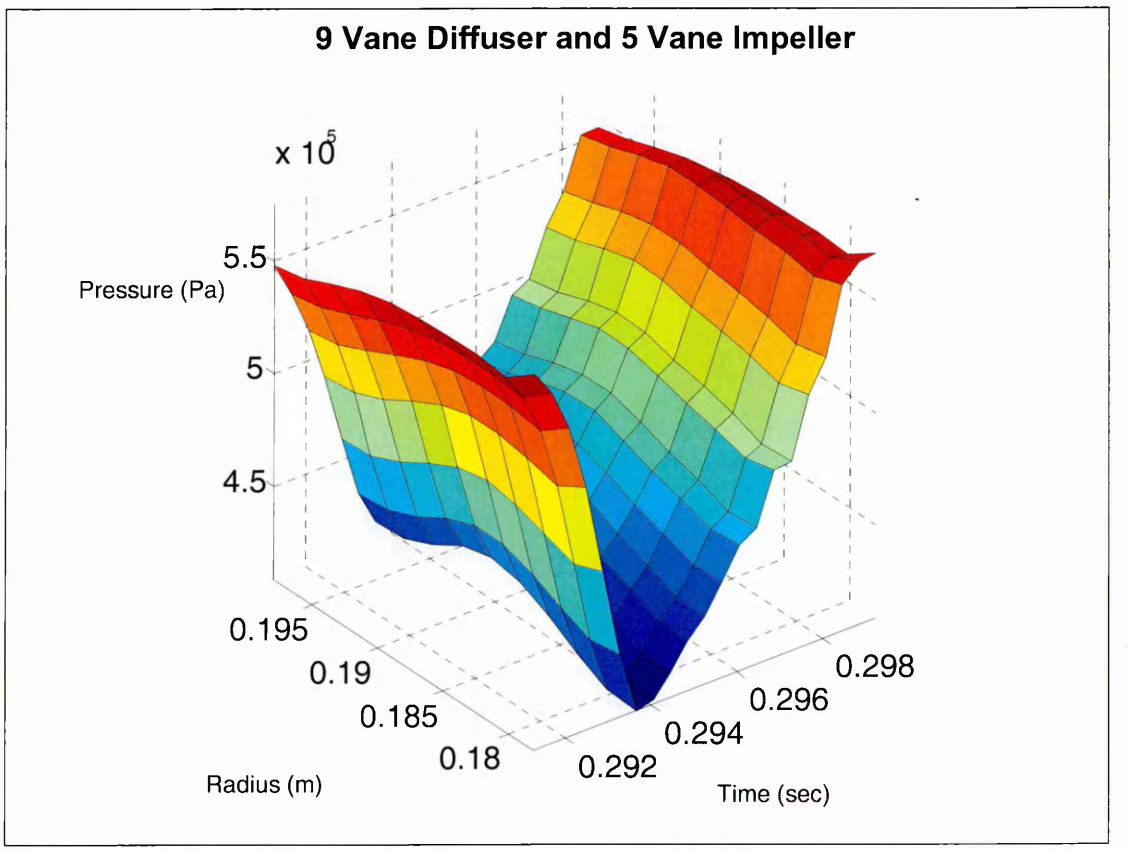

Fig 5.8.10 Pressure Map across the Diffuser Throat 'H'

The pressure fluctuation is strongly related to the position of the impeller blade as it approaches the diffuser passageway. This results in a rotating pressure field around the diffuser which propagates at a speed related to the number of vanes within the Impeller and Diffuser.

The Table below illustrates the maximum and minimum pressure values within each passageway for one pitch rotation.

Diffuser Passage	Max (Pa)	Min (Pa)
A	557152	436773
B	576640	412538
C	557152	438204
D	580714	412387
E	557152	422635
F	580132	414232
G	553209	417292
H	557152	422635
I	580132	414232

Fig 5.8.11 Comparison of Maximum and Minimum Pressure values

5.9 Pressure Evolution along the Diffuser Passage

The unsteady pressure within the machine experiences its maximum level as the impeller blade approaches the passage.

Figure 5.9.1 illustrates the 5 positions within the diffuser passage which are used to measure the pressure with respect to time. These positions are marked A-E. Figures 5.9.2 illustrates the evolution of the pressure pulsation at stages along the passage length.

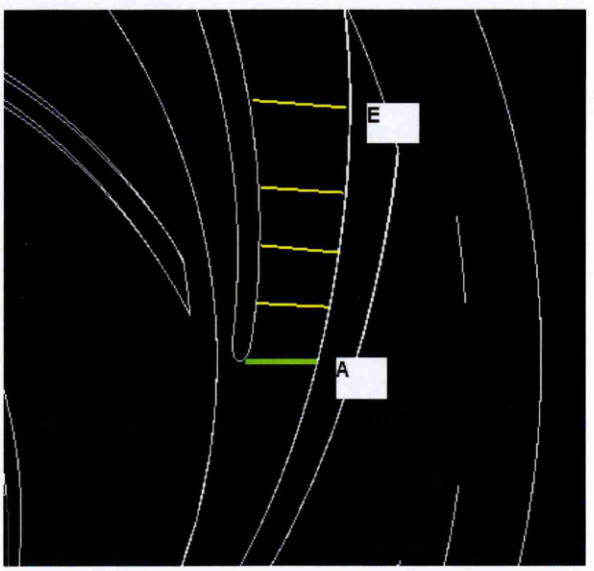

Fig 5.9.1 Location of Diffuser Passage Monitor Lines

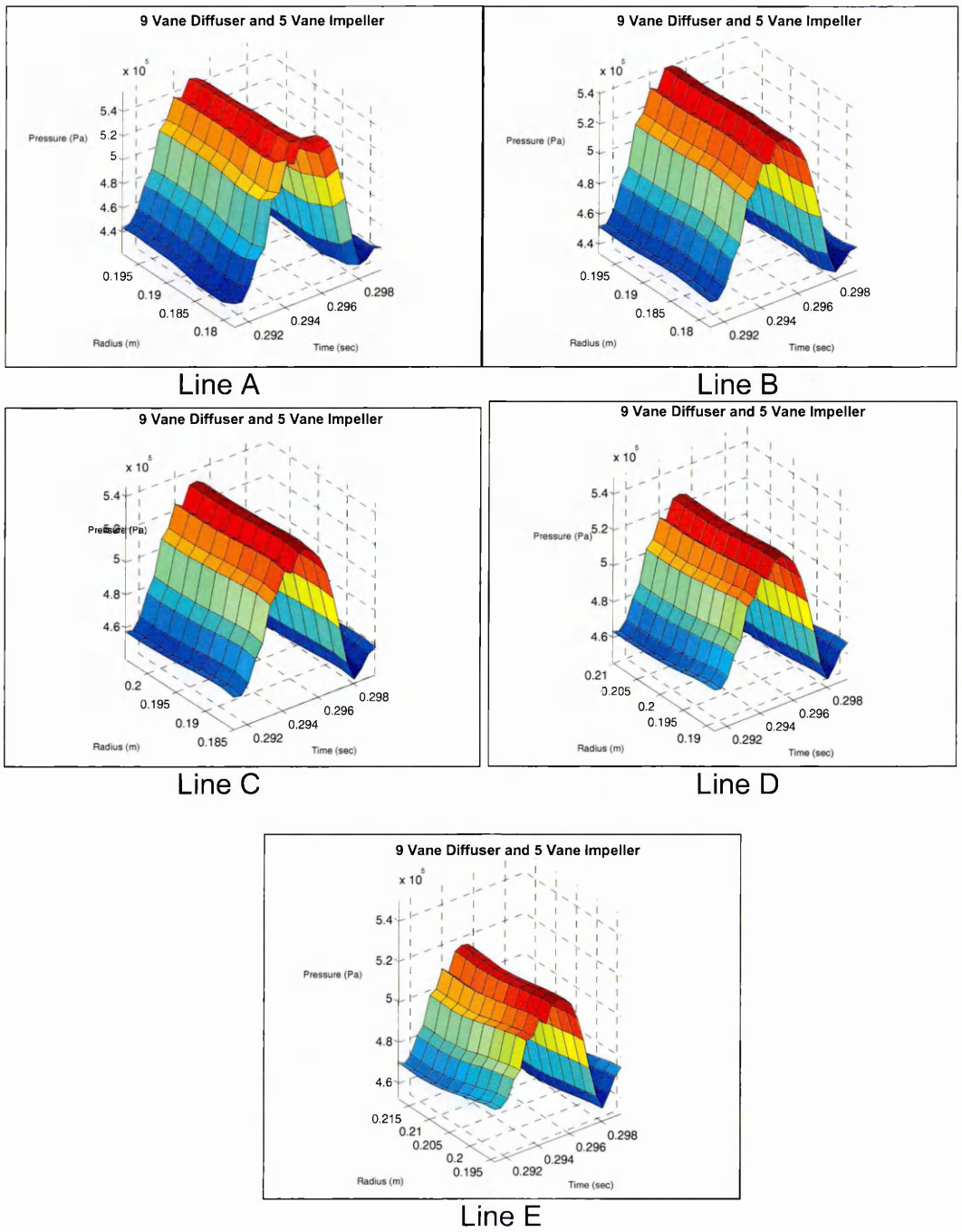

Fig 5.9.2 Pressure Deterioration along Diffuser Passage

Line	Max (Pa)	% change from A	Min (Pa)	% change from A
A	557152	-	436773	-
B	541922	97.266	450299	103.097
C	535765	96.161	456971	104.624
D	529222	94.987	462214	105.825
E	520229	93.373	468658	107.300

Fig 5.9.3 Pressure along Passage

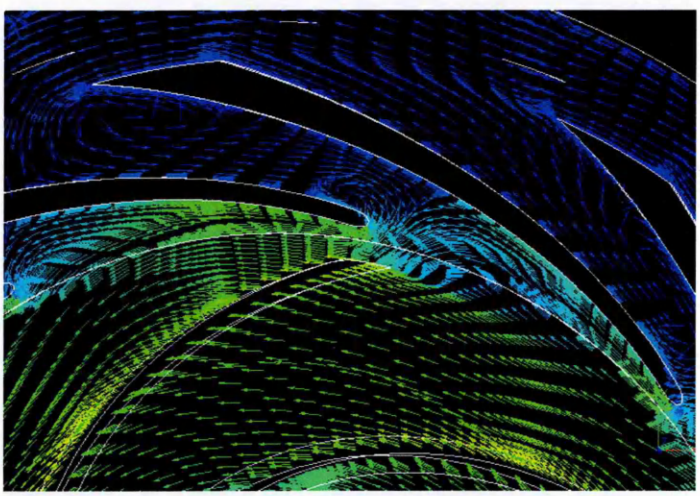

Fig 5.9.4 Flow Field in Adjacent Passageways

The mean flow direction does not change with the phase position of the impeller blade with respect to the diffuser blade Fig 5.9.4. The two adjacent diffuser channels experience a consistent mean flow direction but the intensity of the unsteadiness and the temporal pressure level fluctuates with the impeller blade position.

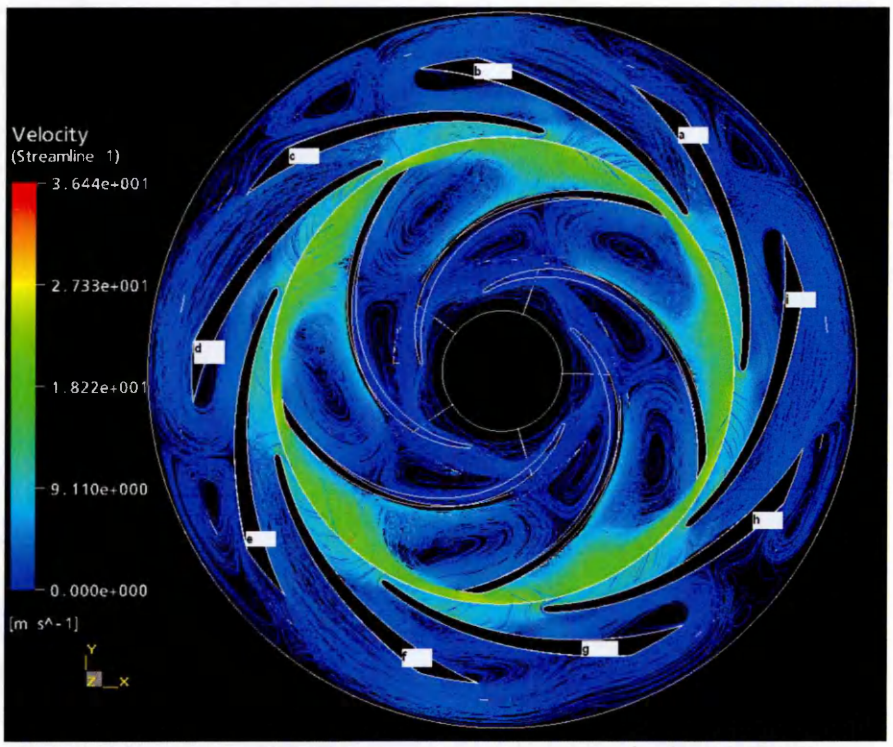

Fig 5.9.5 Diffuser Vane Location Map

Of interest is the non-uniform flow development around the diffuser periphery. Fig 5.9.5 contains a map of the diffuser blade positions to aid in the description of the diffuser flow regime. The blades are marked a-e.
Around the diffuser blade 'b' the flow analysis and temporal pressure experienced by the passages is as described above. The mass flux moves between the diffuser blade 'b' and 'a' before returning down the channel between blades 'b' and 'c'.

This situation is replicated around the periphery of the diffuser. At blades 'b','d','f' and 'i' the blade is bound on its top surface by the diffuser outflow and on its lower surface by a subsequent inflow.

The mean flow follows the passage contours. The impeller-diffuser blade pitch difference shows in this image that the mean flow is not strongly influenced by the position of the impeller blade.

All the impeller and diffuser passageways are shown in Fig 5.9.5 allowing the effect of the differing impeller pitch positions to be evaluated for each flow channel.

The impeller and diffuser blade number ratios are responsible for a non-uniform flow feature on blade 'g'. The impeller contains 5 blades and the diffuser contains 9 blades. Non divisible blade numbers cannot allow the

altering inflow-outflow regime to prevail over the complete periphery of the diffuser.

The diffuser blades expel their mass flow into a free annular space around the periphery. This annular space is commonly used to transport b.e.p. flow from one stage to the next without impacting on the machine efficiency.

Within the computational solution the free annular space is blocked around the outside edge preventing the outlet mass flux. Within a conventional pump design this can be considered analogous to having stalled inlet guide vanes.

The channels formed between blades 'f-g' and 'g-h' experience a mass inflow. Channel 'f-g' follows the flow situation described above but channel 'g-h' experiences an inflow from the free annular space that passes around the diffuser periphery.

This varying pitch wise pressure distribution accounts for differences in the predicted closed valve head level. The time averaged closed valve head consists of the sum of all the pressure pulsations at each location around the diffuser periphery.

Figure 5.9.6 illustrates this feature. The pressure level around the diffuser periphery varies directly in relation to flow feature demonstrated in figure 5.9.5.

Four passageways are filled with higher pressure outflow whist the 5 remaining passageways, which experience in-flow, are shown to be at al lower level of pressure.

For a prediction methodology we must consider that each passageway experiences a different level of pressure generation dependent on the blade number ratio between rotor and stator and the ratio of channel experiencing outflow or inflow.

The diffuser pump is ideally positioned to explore this differing peripheral pressure development as the diffuser geometry for each blade is identical. Variations of the impeller blade number should lead to differing diffuser flow regimes.

Consideration of the table in Figure 5.9.3 illustrates the different pressure regimes dependent on their flow direction within the diffuser passageways. Previous research has not highlighted the presence of a non linear pressure distribution within the diffuser passageways.

Diffuser passages a,c,e,h, all contain inflow towards the impeller. Diffuser passages b,d,f,i contain out flow away from the impeller. The flow direction is represented as a differing passage to passage pressure distribution.

An anomaly to this situation is Diffuser Passage 'g'. The rotor stator blade ratio is not an integer so a uniform inflow outflow pattern around the diffuser

blade cannot exist. Within the simulation Diffuser passage 'g' contains both inflow flow the proceeding diffuser passage and outflow from the impeller passage.

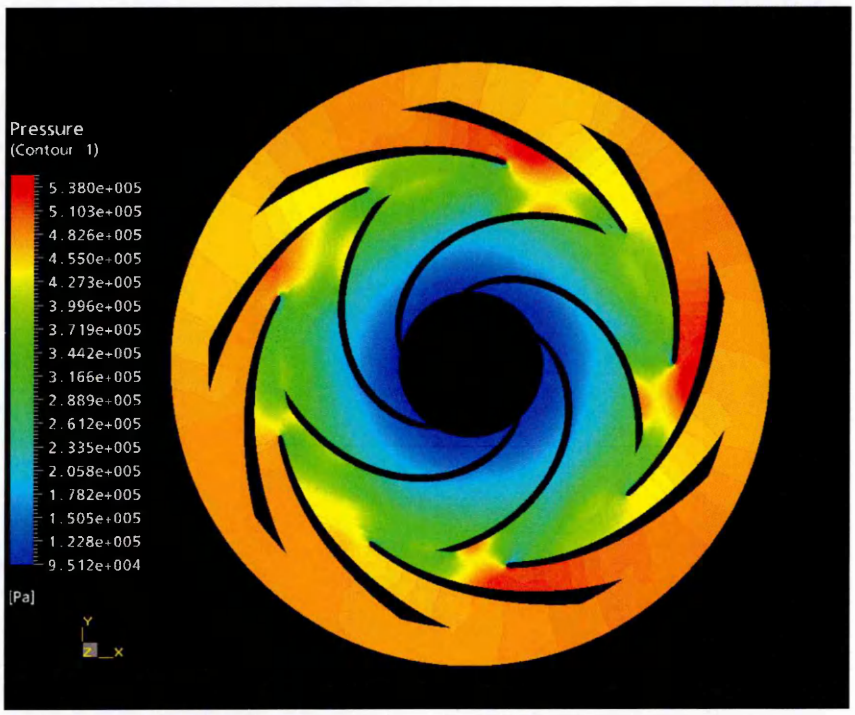

Fig 5.9.6 Pressure in Adjacent Passageways

Comparing the Pressure Map across the Diffuser Throat and relating this to the pressure fluctuation which are attributable to the vane passing frequency pressure evaluated at points along the mean stream line of the diffuser passage centre line. These points are indicated in figure 5.9.7 below.

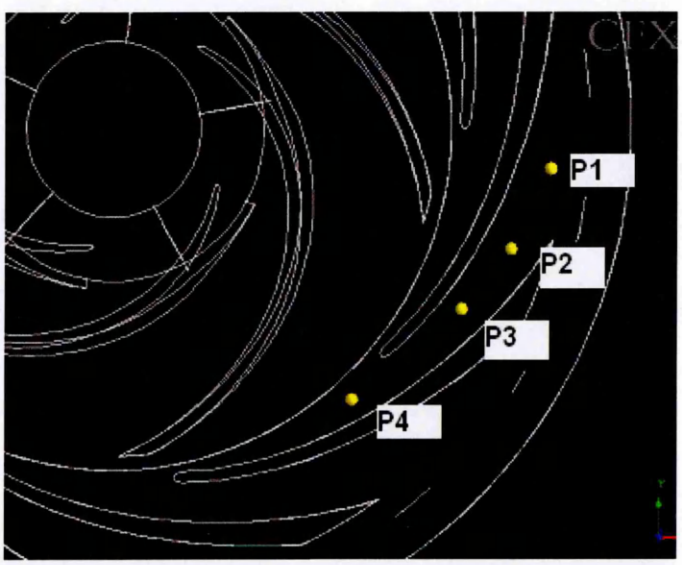

Figure 5.9.7 Point Positions in Diffuser Passage

These points are used to measure the unsteady nature of the pressure filed as the impeller rotates within the diffuser.

The pressure profile with respect to phase position is illustrated in the following figure 5.9.8. This figure represents the fluctuations about the mean pressure and can be considered a measure of the unsteady behaviour within the diffuser passageway.

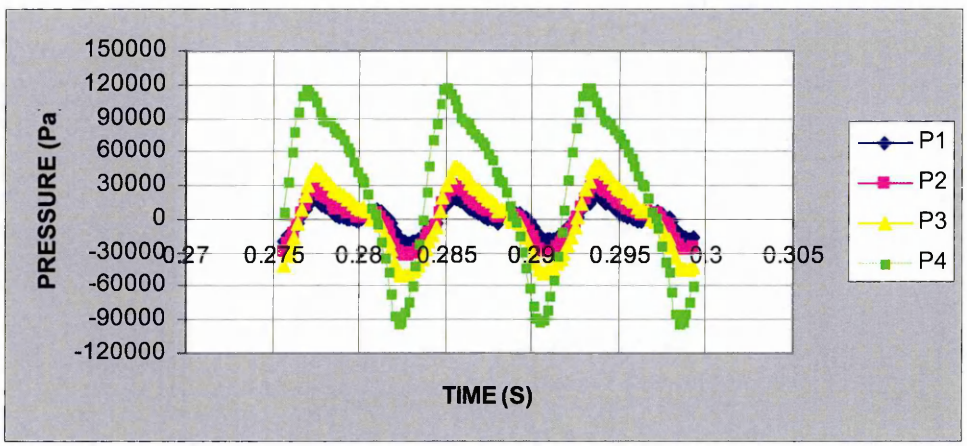

Fig 5.9.8 Difference from Mean Pressure

5.9.1 Unsteady Pressure Point 4

The pressure close to the diffuser inlet at position 4 has greatest unsteady component.

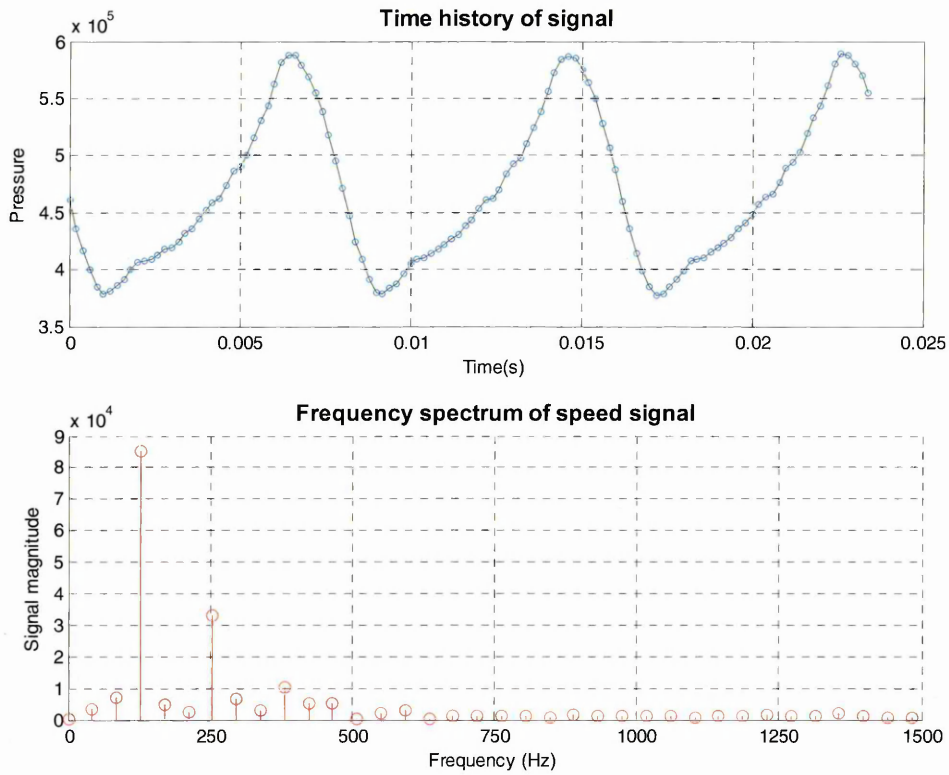

Fig 5.9.1.1 Pressure Pulsation at Monitor Point 4

Evaluation of the temporal pressure signal indicates that the frequency spectrum is dominated by the vane frequency and twice vane frequency as illustrated in Figure 5.9.1.1.
This point is closest to the impeller periphery and experiences the largest unsteady fluctuations.

Analysis of the temporal pressure wave shows a distinct pressure peak that is responsible for the dominant vane passing frequency.

Figure 5.9.1.2 illustrates the position of the minimum pressure at point 4. This is close to the blade thickness as it passes the monitor point. Figure 5.9.1.3 illustrates the impeller blade position that generates the maximum pressure. There is a pressure rise of 55% from the minimum. The maximum pressure at this monitor point is 588670Pa. The minimum pressure is 377610Pa.

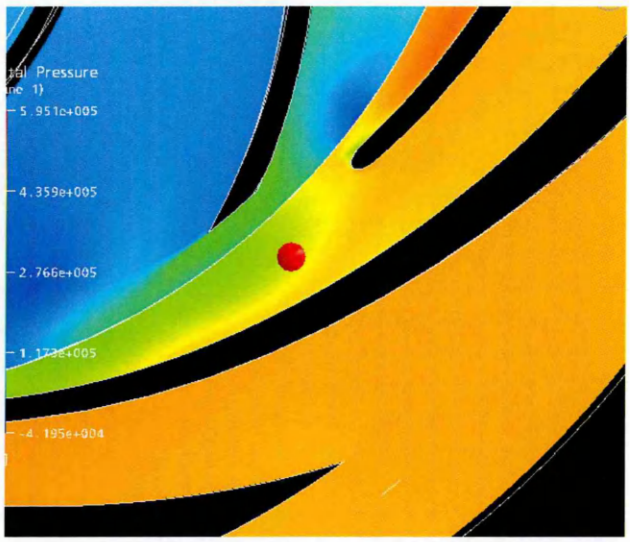

Fig 5.9.1.2 Monitor Point 4 Minimum Pressure

Fig 5.9.1.3 Monitor Point 4 Maximum Pressure

5.9.2 Unsteady Pressure Point 3

Evaluation of the temporal pressure signal at point 3 indicates that the frequency spectrum is dominated by the vane frequency and twice vane frequency as illustrated in Figure 5.9.2.1.

Figure 5.9.2.2 illustrates the position of the minimum pressure at point 3. This occurs as the impeller has passed the centre point of the diffuser passageway and its influence has diminished. Figure 5.9.2.3 illustrates the impeller blade position that generates the maximum pressure. As the impeller approaches the centre of the passage the influence of the impeller outflow is the greatest.

There is a pressure rise of 20% from the minimum. The maximum pressure at this monitor point is 543540Pa. The minimum pressure is 453190Pa. The peak pressure has diminished and is less defined

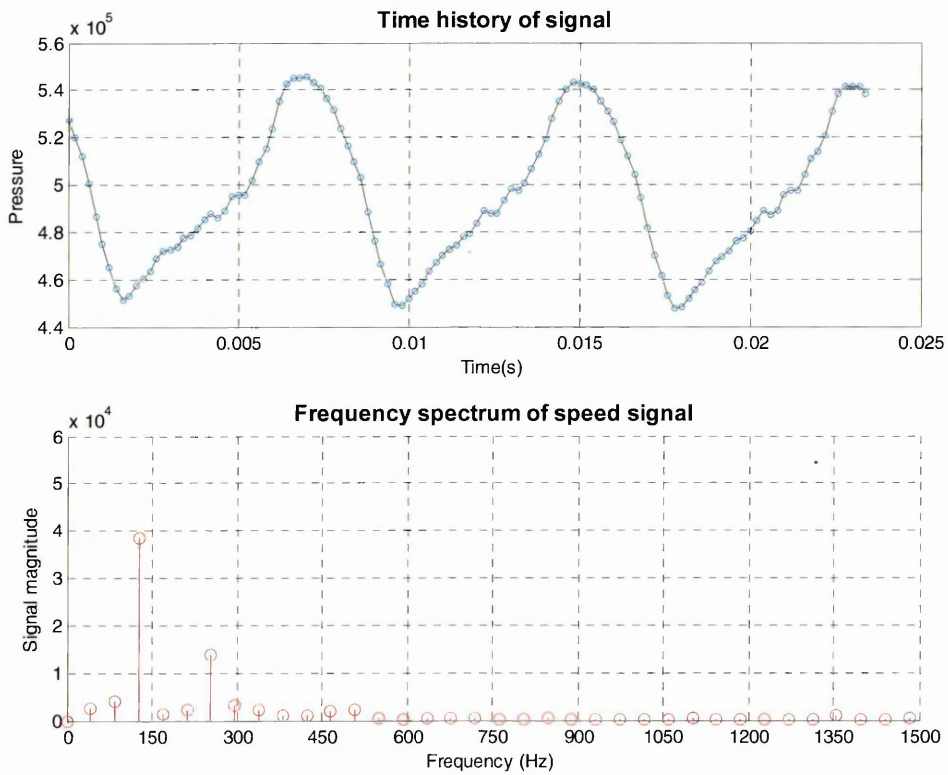

Fig 5.9.2.1 Pressure Pulsation at Monitor Point 3

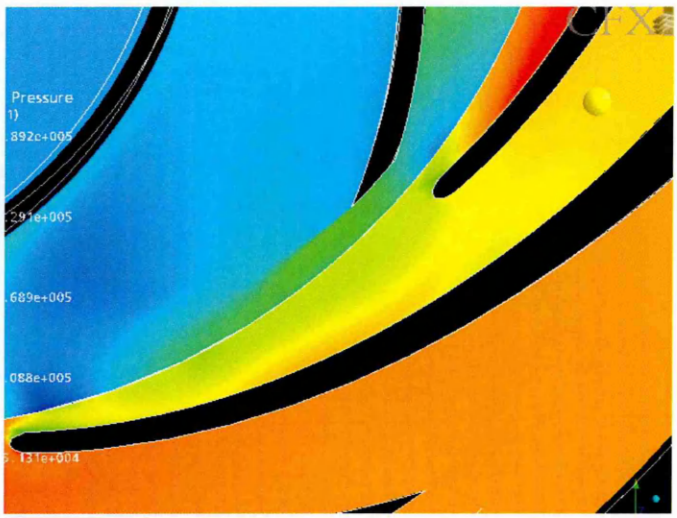

Fig 5.9.2.2 Monitor Point 3 Minimum Pressure

Fig 5.9.2.3 Monitor Point 3 Maximum Pressure

5.9.3 Unsteady Pressure Point 2

Evaluation of the temporal pressure signal at point 2 indicates that the frequency spectrum is dominated by the vane frequency and twice vane frequency. Figure 5.9.3.1 Illustrates that the vane passing frequency has diminished but the 2x vane pass has remained strong.

Figure 5.9.3.2 illustrates the position of the minimum pressure at point 2. This is close to the blade thickness as it passes the monitor point. Figure 5.9.3.3 illustrates the impeller blade position that generates the maximum pressure.

There is a pressure rise of 11% from the minimum. The maximum pressure at this monitor point is 522290Pa. The minimum pressure is 460790Pa.

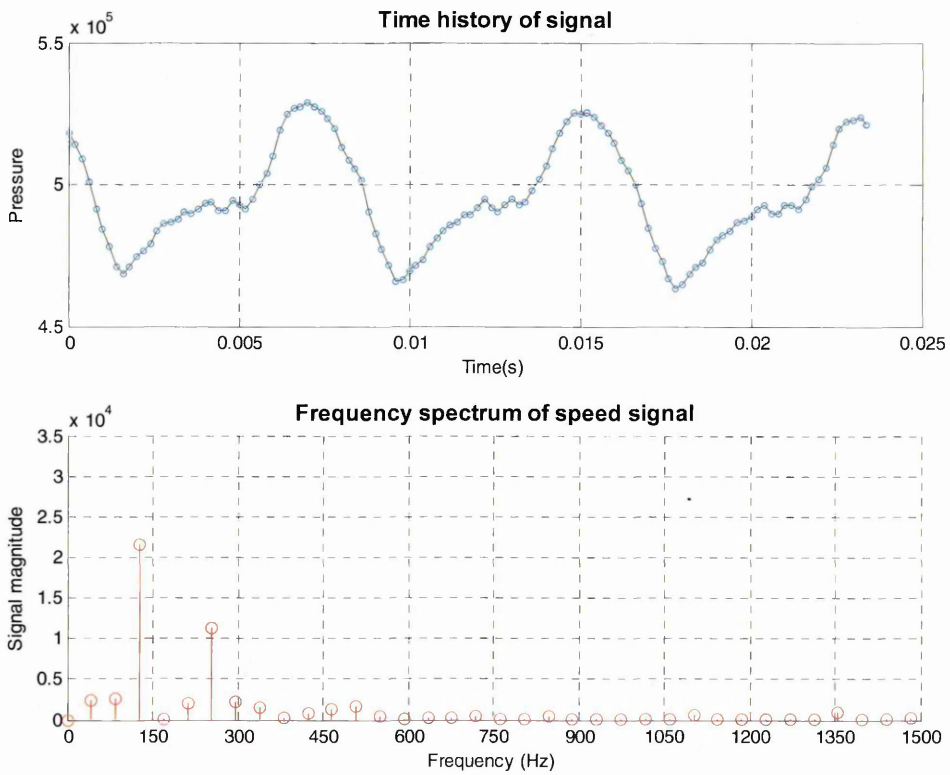

Fig 5.9.3.1 Pressure Pulsation at Monitor Point 2

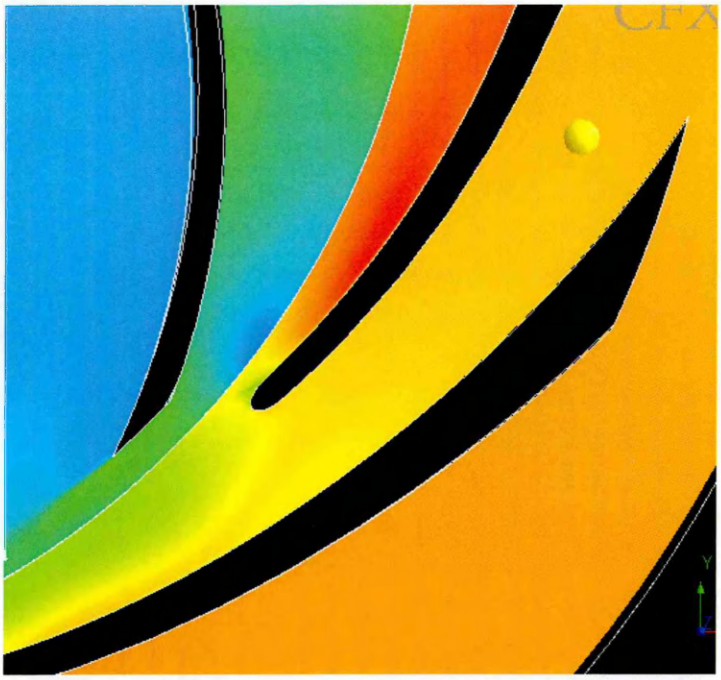

Fig 5.9.3.2 Monitor Point 2 Minimum Pressure

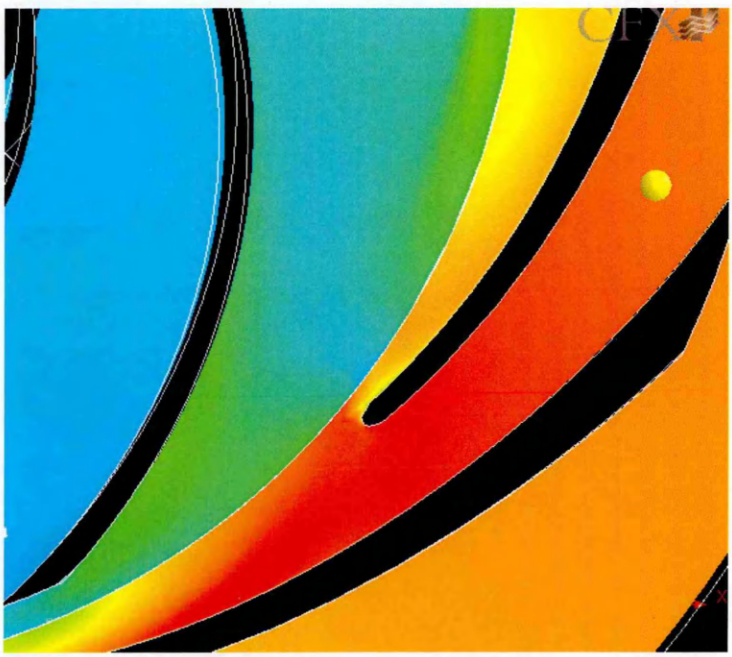

Fig 5.9.3.3 Monitor Point 2 Maximum Pressure

5.9.4 Unsteady Pressure Point 1

Evaluation of the temporal pressure signal at point 1 indicates that the frequency spectrum is dominated by the vane frequency and twice vane frequency. Fig 5.9.4.1 illustrates the unsteady pressure frequencies present. The domination of the vane pass frequency has diminished but the 2x vane pass frequency remains strong.

Figure 5.9.4.2 illustrates the position of the minimum pressure at point 1. This is close to the blade thickness as it passes the monitor point. Figure 5.9.4.3 illustrates the impeller blade position that generates the maximum pressure.

There is a pressure rise of 7.6% from the minimum. The maximum pressure at this monitor point is 513510Pa. The minimum pressure is 477140Pa.

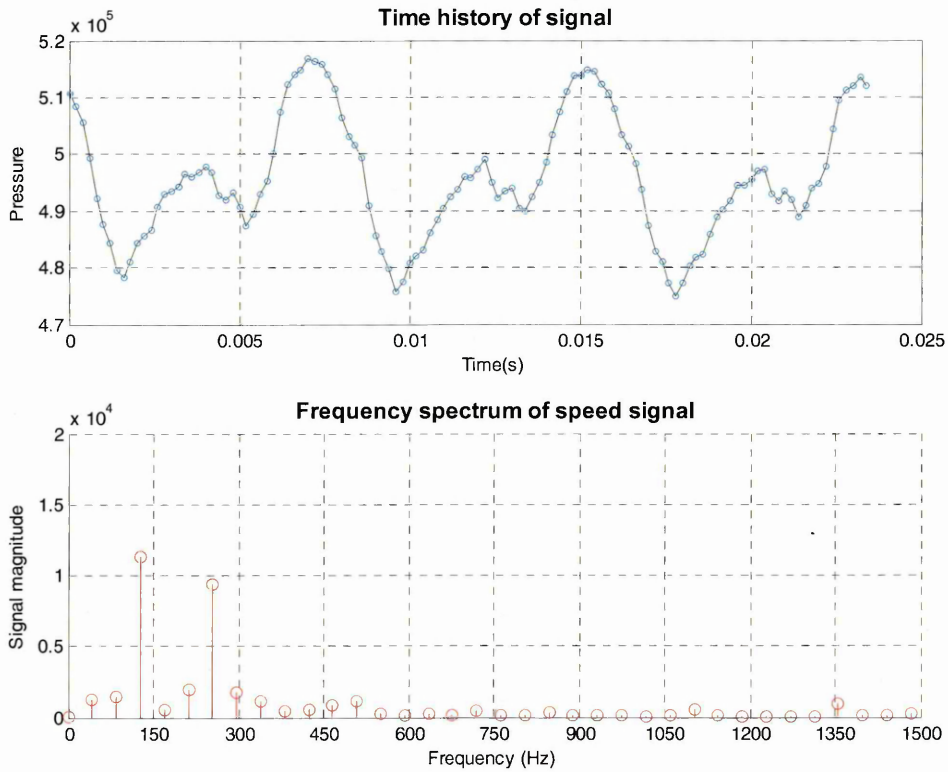

Fig 5.9.4.1 Pressure Pulsation at Monitor Point 1

Fig 5.9.4.2 Monitor Point 1 Minimum Pressure

Fig 5.9.4.3 Monitor Point 1 Maximum Pressure

5.10 Summary

A diffuser pump with 9 diffuser blades and 5 impeller blades was tested on the Union Pumps test stand. The closed valve head was calculated and these calculations were compared with those generated by a computational solution.
When comparing the time averaged closed valve head reading with computational result the measured value was within 0.3% of the computed value. This is more accurate than any of the existing empirical methodologies but it is just one instance of CFD correctly predicting closed valve head.

From the computational solution the time averaged pressure across one diffuser blade pitch was analysed. A non-linear pressure rise was noted over one blade pitch of the diffuser. This situation is in agreement with the situation experienced within the volute pump.

Within the volute pump the non linear pressure distribution occurred at two instances around the volute. This nonlinearity was driven by the rotor-stator interactions which occur at the two volute lips. Within the diffuser pump, with 9 blades, this time averaged non-linearity linked to the vane numbers within the stator also occurred.

One significant difference between the geometries was the throat height. The volute pump, with a taller throat height allowed for a greater amplitude of pressure evolution. The research by Frost and Neilsen(1988), which had previously been considered state of the art by the pump industry, was evaluated against the background of unsteady rotor-stator interactions which take place and their proposition that the steady state pressure resulting from the bound vortex that occurs within the throat was challenged.

The stator passages are influenced by the pressure pulsations generated by the interactions of the blades. Analysis of the temporal pressure within the annular gar between the impeller and diffuser blade presented a picture of fluctuation at vane passing frequency and the second multiple of this frequency.

An overview of the pressures with the diffuser flow channels demonstrated that there is an unsteady pressure component passed into the diffuser channel. Although viscous effects decay this pressure fluctuation with time/distance the unsteady pressure is still apparent at the outlet of the diffuser blade. The 2x vane pass frequency grows in dominance along the passage length.

The diffuser contribution to the closed valve pressure is not uniform despite uniform geometry. The stalled nature of the diffuser encourages an alternating picture of inflow and outflow across the diffuser channels. This differing flow picture contributes to a differing unsteady pressure level between the impeller and diffuser.

6.0 Diffuser Pump Discussion - Introduction

The flow features observed and outlined in Chapter 5 lead to an understanding of the nature of the regime when a pump operates at closed valve. Of particular significance is the rotor-stator interaction pulsations generated by the impeller vane as they pass the diffuser vanes.

The flow within the annular gap between the impeller and diffuser is shown, undoubtedly, to be unsteady. This flow is dominated by the multiples of the vane passing frequency, in particular the 1x vane pass.

This chapter contains discussion on the flow regime within the impeller and diffuser, against the background of the existing prediction methodology, solid body rotation. Flow features observed within the CFD and the literature review are analysed in terms of the rotor – stator influence and its effects on the flow features.

The chapter finishes with an analysis of the pressure pulsations within the annular gap of a diffuser pump and the effect the change in impeller vane number has on the pulsation amplitude and frequency.

6.1 Impeller Regime - Theory of Solid Body Rotation

The closed valve head of a centrifugal pump has been split, in the literature by both Frost and Stirling into impeller and volute components. For a complete analysis of the closed valve problem it is necessary to consider the contribution made for each main constructional component. These can be split into the impeller and diffuser contributions. This has proved impossible in experimental situations but is straightforward from the computational standpoint

The impeller contribution has been previously proposed by both Frost and Neilsen (1988) and Stirling (1982) to be that of the head generated by a solid spinning disc. Newton (1998) in his investigative thesis carried out experimental investigation on a centrifugal fan by closing off the discharge proportion of his research impeller and measuring the closed valve head. Whilst detailed measurements are not given within the work, Newton (1998) disagreed with the theory of solid body rotation. Despite this, the theory of solid body rotation is still recognised within the pump industry as the "state of the art".

This theory of solid body rotation does not describe the unsteady pressure generated by the impeller, whilst empirically approaching the head generation of the limited number of machines that were studied; it does not take into consideration the unsteady interaction effects that are inevitable within the small annular gap between impeller and diffuser. Anecdotally designers know that increasing vane numbers can have a distinct effect on the closed valve head of a machine. Newton's (1998) work on a 4 bladed impeller is based on limited data regarding this vane change effect.

Empirical analysis has been unable to assign, accurately the contribution split between the major components of the machine. This has lead to varying opinions regarding the geometry appropriate for the solid body calculation. Propositions exist from Stirling (1982) and Frost (1988) that the inner proportion of the solid spinning disc can be the impeller eye, the impeller hub, or even the RMS diameter of the two. The proposition of solid body rotation has grown, within the pump community, to become the mental model pump designers use when they analyse closed valve head generation.

Fig 6.1.1 illustrate the fluctuating nature of the area averaged closed valve head. This fluctuating nature is attributed to the pitch change between impeller and diffuser.

Fig 6.1.2 illustrates the unsteady proportions of the closed valve differential pressures.

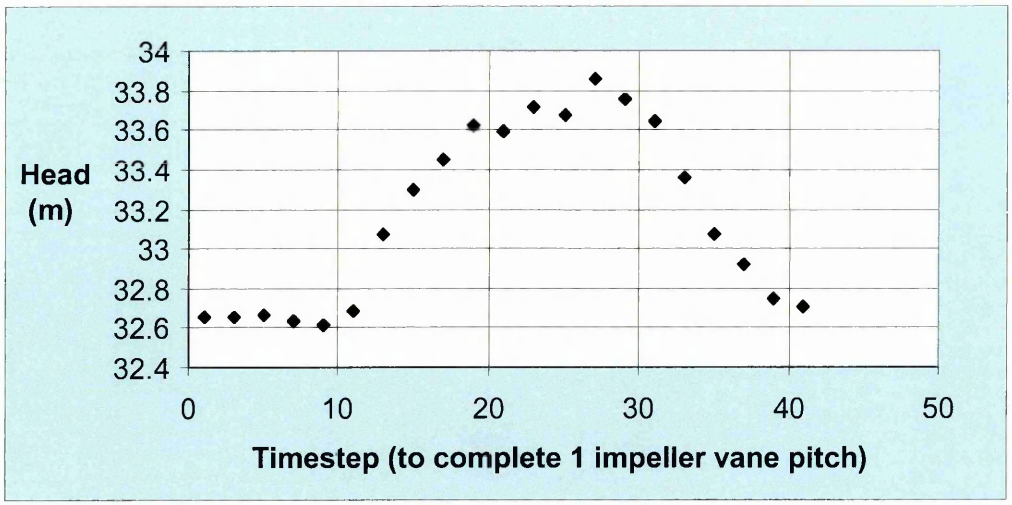

Fig 6.1.1 Average Closed Valve Head vs. Time Step at Impeller Periphery

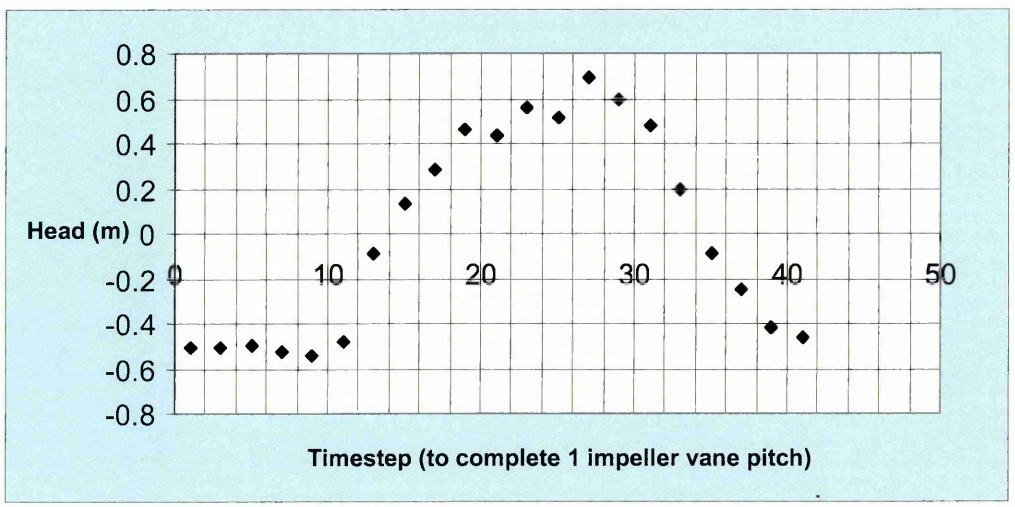

Fig 6.1.2 Difference from the Average Differential Head

Analysis of the fluctuations in the periodic unsteady pressure supports the proposition that the vane interactions are responsible for the fluctuations in the area averaged pressure.

Figure 6.1.3 demonstrates the unsteady pressure fluctuations that occur at a fixed point at the periphery of the impeller. The spectrum is dominated by the vane passing frequency.

Significant from this figure are the two pressure pulsation amplitudes of each passage. This indicates that each impeller vane does contribute identical proportions of pressure to the closed valve head generated but the extent of the instantaneous pressure generated is influenced by the blade position with respect to the monitor point. These two pressure peaks occur in distinctly different areas of the rotation cycle but are both closely associated with the wake.

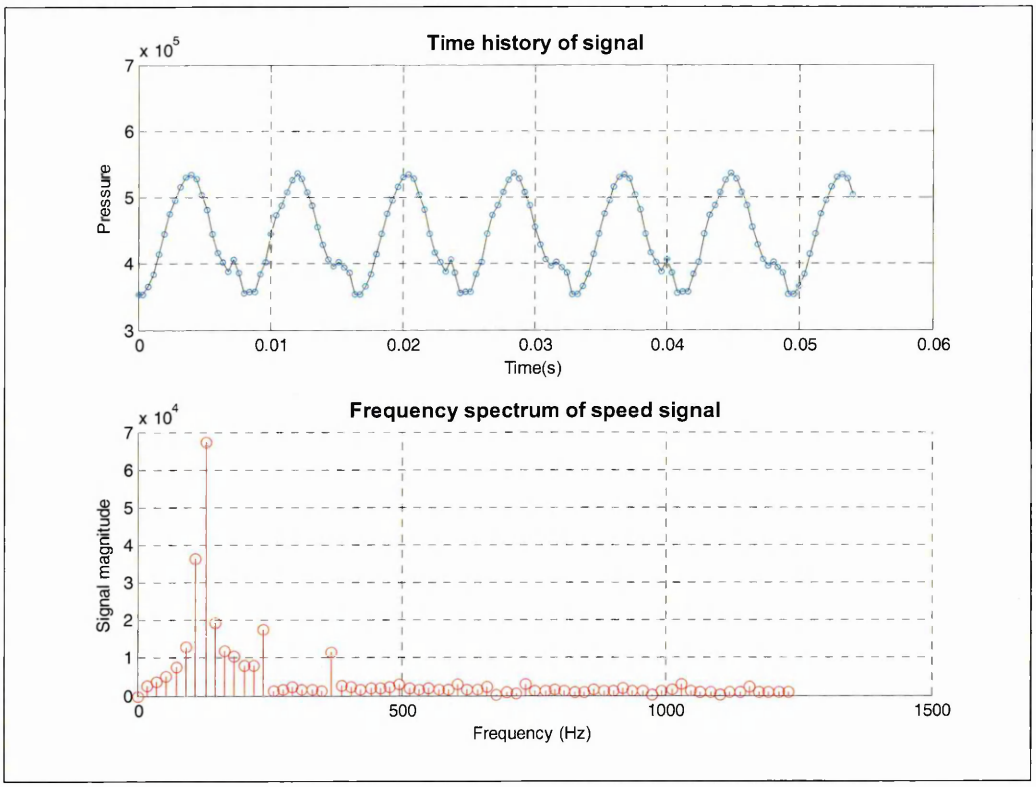

Fig 6.1.3 Unsteady Pressure Map and Frequency Spectrum

6.1.1 Annular Channel between Impeller and Diffuser

The state of the art prediction methodologies for the closed valve head of centrifugal pumps rely on the theory of solid body rotation to predict the head generated by the impeller. This theory is previously outlined in Chapter 2. Methods by Stirling (1982), Frost and Neilsen(1988) all use the sold body theory.

This theory suggests that at closed valve the impeller outflow is steady. Analysis of the pressure within the annular space which divides the impeller and diffuser indicates that there is a strong pressure pulsation related to the impeller vane position in relation to the diffuser vane.

Fig 6.1.1.1 illustrates these pressure fluctuations and indicates that the phenomenon of solid body rotation is actually an unsteady pressure fluctuation driven by the rotor stator interaction.

For Solid body rotation to actually exist the pressure within the annular clearance between the impeller and diffuser vane rows would need to be steady.

Newton (1988) in his experimental work using a centrifugal fan blocked the fan outlet with a plane strip of material to simulate solid body rotation. Despite his findings, that solid body rotation did not exist, the pump industry has been slow to adopt this proposition. The nature of the fan design and the use of air as the working fluid have all added to the doubt about Newton's (1998) work. The computational solutions within this work agree with Newton. The phenomenon of solid body rotation does not exist.

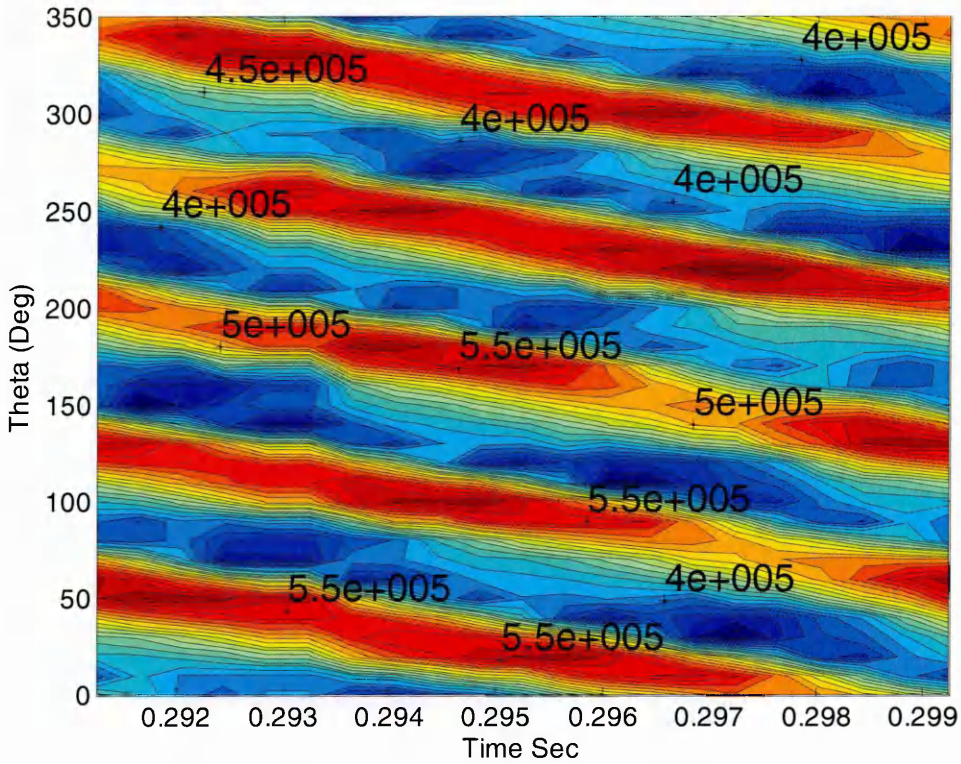

9 Vane Diffuser and 5 Vane Impeller

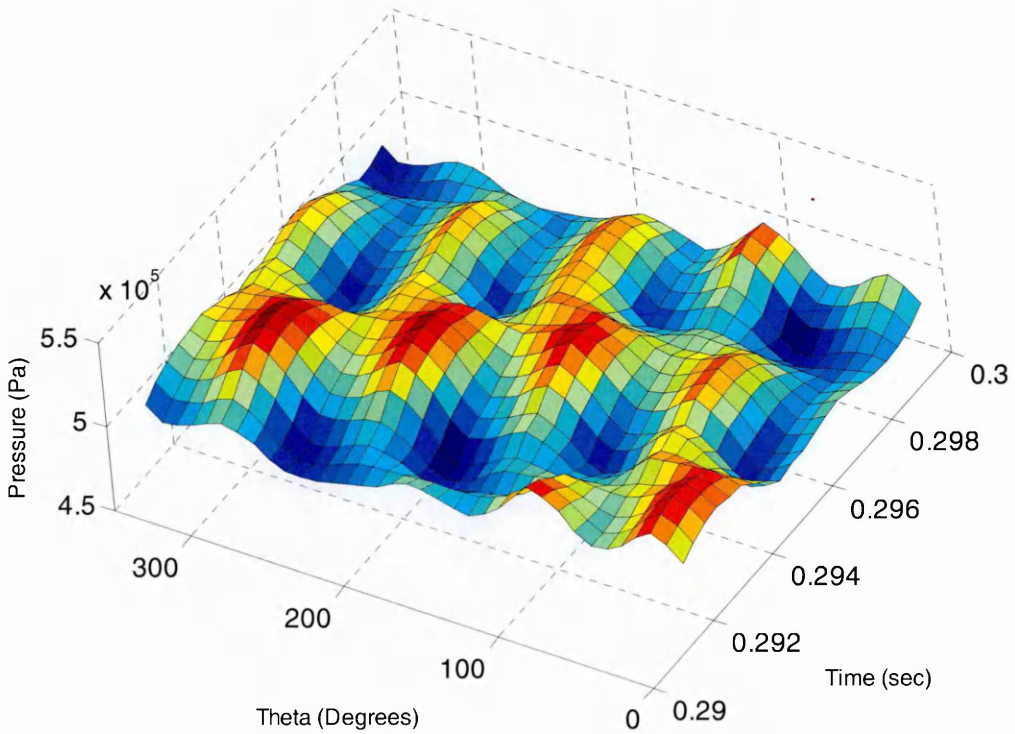

Fig 6.1.1.1 Illustration of Evolving Pressure in Annular Gap between Impeller and Diffuser

6.2 Blade Geometry Effects on Discharge Eddy Development

The region at the impeller exit, driven by the interaction with the stalled volute flow, is a phenomenon which is not consistently accounted for in the literature. It has been previously suggested by Newton (1998) that it is difficult to see within a volute pump and may have been missed by some researchers. Many CFD studies indicate its presence.

The vortex is linked to the position and number of blades in both the rotor and stator. The physical size and its development within the impeller passage is controlled by the number of impeller vanes. Its rotational direction and speed is firmly linked to the impeller & diffuser vane ratio. This may account for the difficulty when using visual observation techniques to view this feature.

When we compare the geometry of a volute to the geometry of a diffuser the obvious difference is the number of stator passage to accept the impeller fluid. That also means the interaction effects are multiplied i.e. one interaction event occurs as an impeller blade passes each diffuser stator vane.

For a low solidity impeller design with a low blade number, the vortex develops in the radial direction down into the impeller passage until it fills 50% of the channel (Fig.6.2.1) The intensity of this vortex increases as the impeller blade approaches the casing cut water as the driving viscous force of the liquid trapped between the lip and tip becomes dominant.

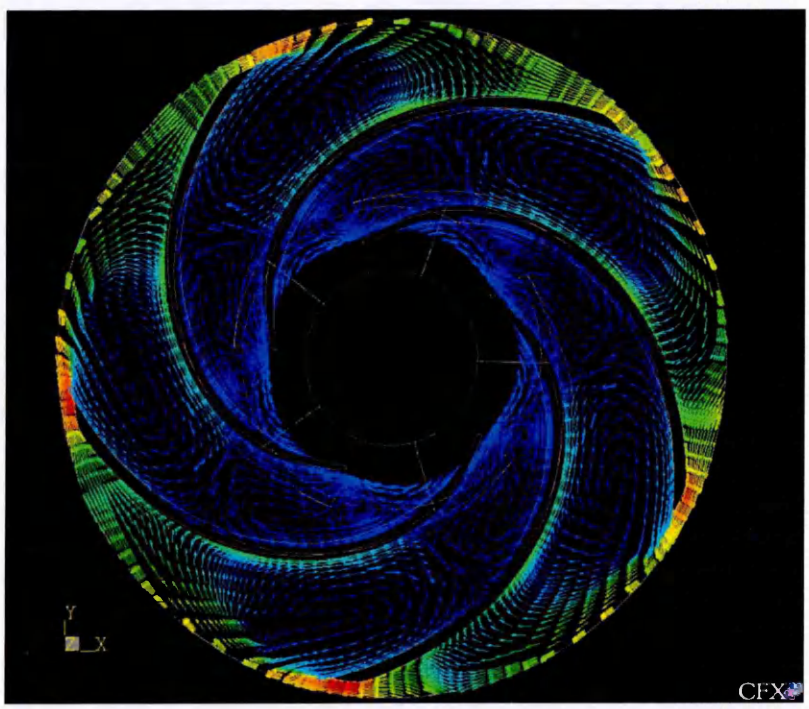

Fig 6.2.1 Velocity Vectors within 5 Vane Pump Impeller at Closed Valve

The converse is true when the impeller blade solidity is increased. The vortex at impeller exit extends in the radial direction only 20% into the impeller passage (Fig 6.2.2).

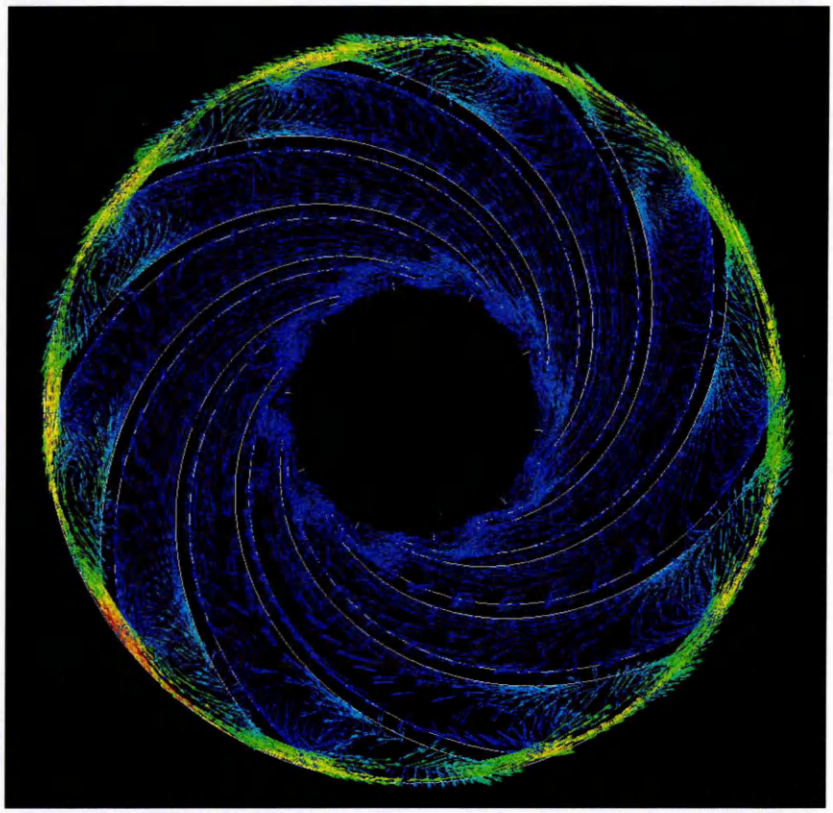

Fig 6.2.2 Velocity Vectors Within 10 Vane Pump Impeller at Closed Valve

Comparisons of Fig 6.2.1-6.2.2 indicate the extent of the vortex development within the passage with respect to increasing solidity. Experimental observations, which refer to this vortex, such as Acosta and Bowerman (1957) define its motion as counter to the machine motion i.e. it rotates at a sub-synchronous speed counter to the pump rotation.

Whilst in the limited experimental studies available, this observation is true, it neglects the importance of the rotor-stator interaction between the varying rotor and stator blade systems which have a direct influence on the direction of vortex motion.

6.2.1 Impeller Blade Number Less Than Stator Blades

Considering a case where the impeller blade number is less than the number of stator blades the vortex will appear to move counter to the machine rotation.

Fig 6.2.1.1 represents a machine with a 5-vane impeller and a 10-vane diffuser. Passages 2,4,6,8 and 10 are congruent with impeller blades a-e. The

standing vortex within the impeller exit, influenced by the stator vanes, will be identical within each of these impeller passages

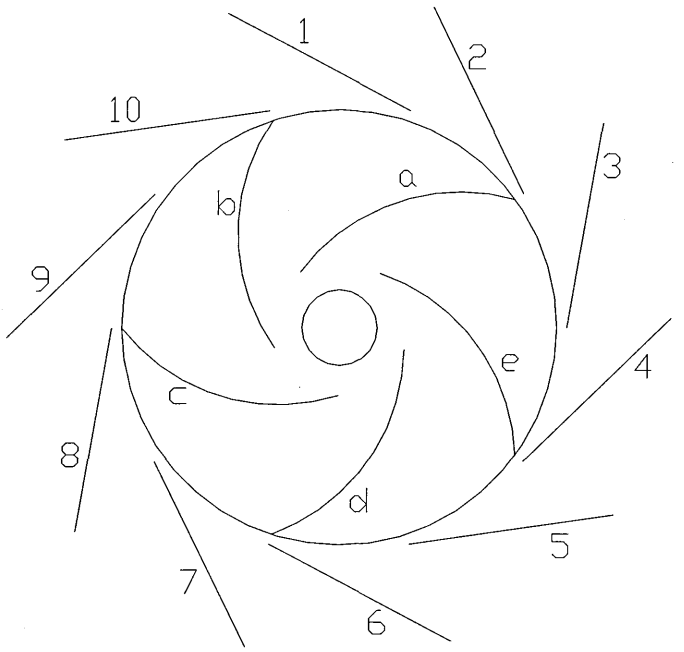

Fig 6.2.1.1 Representations of Impeller and Diffuser Vanes

When the impeller has rotated 0.5 of the impeller blade peripheral pitch, this situation will be repeated as stator blades 3,5,7,9 and 1 become congruent with the impeller blades. In this manner the stalled vortex at impeller exit appears to rotate backwards, counter to the machine rotation. This vortex will rotate at 50% of the synchronous speed.

This key observation is not apparent in the present literature. The researchers who have observed this vortex have only noted its motion. They have not attempted to link this motion to the interaction effects.

The overall impression when the blade rows are viewed in entirety is one of 5 identical flow regimes occurring simultaneously. As the impeller rotates the subsequent blade encounters the identical influence of a subsequent stator blade after 0.5 impeller pitch rotations. This identical flow regime experienced after this 0.5 pitch rotation gives the impression that the vortex has passed counter to machine rotation at twice the synchronous speed when viewed from the relative frame.

If the impeller blade number and the stator blade number[1] are equal the vortex will appear not to move, as the pitch change influence of the stator is equal to the rotor effect at any instance. Each impeller passage experiences identical influence from the stator at the same instance so the standing vortex will pulse due to the interaction effects.

[1] Pump Designers try to avoid this situation to limit the vibration potential of the machine

Extending this logic further, when the impeller vane number is greater than the stator number the vortex will appear to move in the same direction as the machine rotation.

To put this into the context of a simple single volute pump, as analysed by Newton, the influence of the stator would occur once per blade pitch and no stator influence is passed onto subsequent vanes. It is understandable why some researchers did not register the phenomenon of the counter-rotating eddy, as it is entirely dependent upon the influence of the rotor and stator vanes.

6.3 Linking the Unsteady Pressure to Impeller Vane Number

To aid designers of pump equipment in predicating the closed valve head of a new machine the link between geometry and pressure is important. Conventionally pump designers do not begin with a completely new design. The new designs are grounded in reality by using the laws of similarity to scale existing machines. These laws of similarity are outlined by Stepanoff (1957) are outlined in Chapter 1.

One area where designers introduce unpredictability into the similarity laws is by changing the impeller vane number. Vane number changes can occur for a number of different reasons i.e. NPSHR, Vibration potential or efficiency consideration. With this change the prediction methodology for head changes at best efficiency point is well proven. The prediction of changes at closed valve is far from predictable and is based on empirical constants. No study exist which quantifies for designers the changes in pressure generation that occur when the impeller vane number is increased.

Yeddidah (1993) suggests that the mechanism for an unstable head curve is linked to the energy exchange close to the lip but neither the volute nor diffuser CFD studies suggest that this mechanism does not readily exist. The strong influence of the rotor vane thickness at it passes the volute lip forces the flow to follow the volute lines. It is more likely that the rotor-stator influence in terms of amplitude and frequency dominates the pressure development.

To investigate the changes within the annular gap between the impeller and diffuser with respect to changing vane number further simulations were carries out with rotor blade numbers 6,7,9,10.

These simulations are identical to that which is documented in Chapter 5. The boundary conditions and diffuser grid remained the same. The impeller blade design remained unaltered apart from the vane number increase.

6.3.1. Solution Procedure

The following procedure and parameters were used to solve for the different vane numbers.

- The impeller blade number was increased. No other changes were made to the impeller geometry. The inlet and outlet blade angle remained the same, as did the blade length.
- The impeller mesh size was reduced to 20000 nodes. Although this is below the threshold recommended in Chapter 3 the increased total grid size required for the solution of the 9 and 10 vane impellers was beyond the computational capacity available
- The diffuser grid remained unaltered from the solution outline in chapter5.

- The boundary conditions remained unaltered from the solution outlined in chapter5.
- The solution form the 5 vane model outlined in chapter 5 was used as the initial conditions for the subsequent models.

Pressure was monitored by points within the annular gar between the impeller and the diffuser. These points are used to evaluate the consequences of the impeller vane number increase.

6.3.2Development of the Stability Criteria - Background

It has been demonstrated by the experimental and computational research on centrifugal pumps that the blade number has an effect on the closed valve head of the machine.

Anecdotally, as we increase the number of blades within the impeller we expect a change in the closed valve head coefficient. Designer's of centrifugal pumps use increasing blade numbers to push up the duty head of the machine flattening the performance curve. This is desirable as greater pressure per impeller diameter reduces the cost of the machine. To refine the design an empirical ratio proposed by Peck (1950) is used to judge the effect of raising the blade number.

Peck's (1950) stability prediction evaluation method used the ration w1/w2 to evaluate if the pump would be stable. This does not take into account the rotor-stator interactions. Peck's (1950) evaluation is based on diffusion criteria within the impeller. Using the analysis, an impeller would be considered unstable if the relative diffusion from inlet to outlet was greater than unity.

Impellers with a large diffusion over a short distance experience a boundary layer breakdown on the pressure side of the impeller blade, this phenomenon can be present even at best efficiency flow. Whilst diffusion within the impeller passageways may contribute to the early inception of the discharge standing eddy as the mass flux is already separated into two varying velocity streams, it is not the greatest contributor to the closed valve head coefficient.

At some point in the design process increasing the impeller vane number and/or outlet angle combination induces a closed valve head coefficient which begins to fall. This may not be the limit of stability as this should be referenced to the b.e.p. head level but it is an indicator to the commencement of closed valve head degradation.

As the vane number and/or outlet angle increases the b.e.p head of the machine increases. If the rise in b.e.p. head is greater than the change in closed valve head coefficient then the HRTSO will reduce. Continuing to reduce the HRTSO will lead to an unstable machine.

A further consideration, based on the Euler equation and the Busemann(1928) slip factor described in Chapter 1, is the effect of discharge blocking. As the number of vanes increase the blocking effect of the vane thickness through increasing vane number reduces the outlet area of the machine to such an extent that the HRTSO increases.

Designers of the high speed geared machines use this technique to keep their pumps stable. These machines use high vane number and run at high speed, maximising the head per diameter. To use such technique on a conventional centrifugal machine is impractical due to the high efficiency penalties involved.

These practical anecdotal situations outline the key considerations for any unifying theory of closed valve head prediction.

Any theory for stability analysis must satisfy the following practical conditions:-

1. The closed valve head analysis must take into account the changes in closed valve head for a fixed impeller tip velocity. Changes to speed and diameter can be accounted for by the Euler equations. The criteria must take into account the differentials experienced due to vane interaction effects.
2. The closed valve head coefficient must change as the vane number increases
3. When a specific geometric condition is satisfied the impeller closed valve head condition should then begin to fall.
4. Further increase in the vane number should provide an increase in head coefficient as the blocking effect of the machine comes into effect

Applying some simplifications to the observed flow fields within diffuser pumps we can develop criteria for the prediction of unstable curve on-set using the following assumptions.

- The diffuser blade design and number remains constant
- The inlet tip speed is unchanged
- The closed valve head is linked to the amplitude and frequency of the pressure pulsations generated by the rotor stator interaction events and passed upstream through the diffusers.
- The diffuser has a common additive effect on the closed valve head irrespective of vane number
- The inlet tip speed and incidence contributions are considered constant

Using these criteria we can define closed valve head changes purely with respect to impeller vane number changes.

6.3.3 Pressure Fluctuations with Vane Number

If we consider the pressure wave form generated by the CFD solutions in chapters 4 and 5 it is evident that the pulsations within the diffuser system are directly linked to the number of vanes within the impeller.

The pressure pulsations generated by the impeller and the propagation of these pulsations are predominantly responsible for the closed valve head of the machine. Chapters 4 and 5 have outlined these pulsations within a volute and diffuser machine. Taking the diffuser and impeller design configuration from Chapter 5 we can analyse the effect on the pressure pulsations for increasing vane number.

From the simulation outlined in Chapter 6.3 we can evaluate the change in frequency and amplitude of the pressure development within the annular space between impeller and diffuser.

Figure 6.3.3.1-6.3.3.5 illustrates the differing levels of pressure development for impeller vane numbers 6,7,9,10. The only change to the impeller design was blade number. No other geometric modifications were made to the impeller blades. Hence the solidity of the impeller was increased.

Figure 6.3.3.5. The pulsation for the 6 vane impeller shows a strong component of 2x blade frequency. This frequency diminishes as the vane number increase to such an extent that the 10 vane impeller exhibits little 2x blade frequency pulsation.

The influence of the vane effect is increased in frequency and the wake effects are subdued by the high solidity of the impeller vanes.

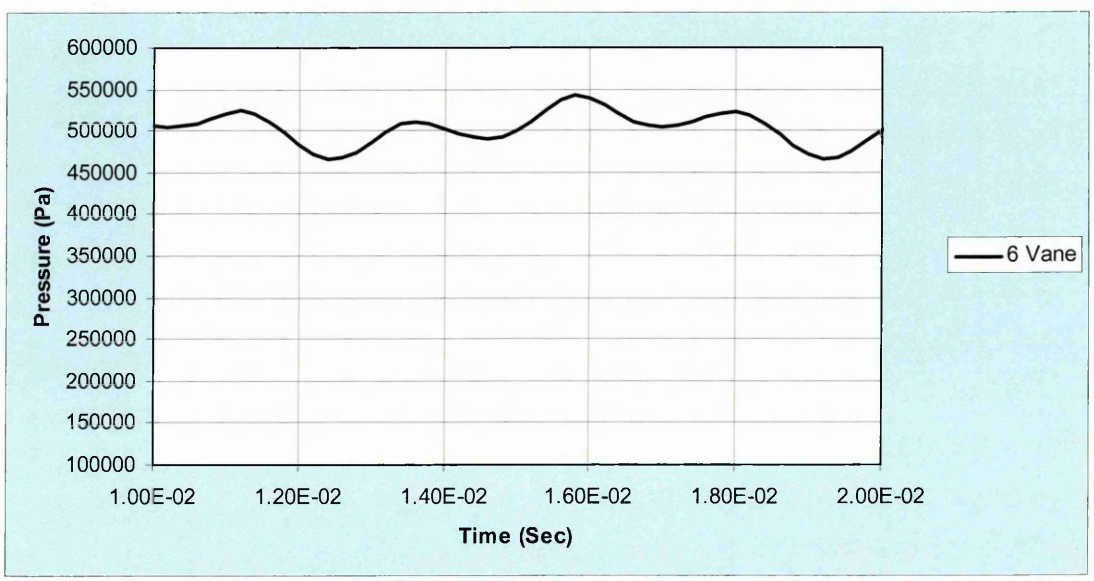

Fig 6.3.3.1 Pressure Pulsations 6 vane impeller

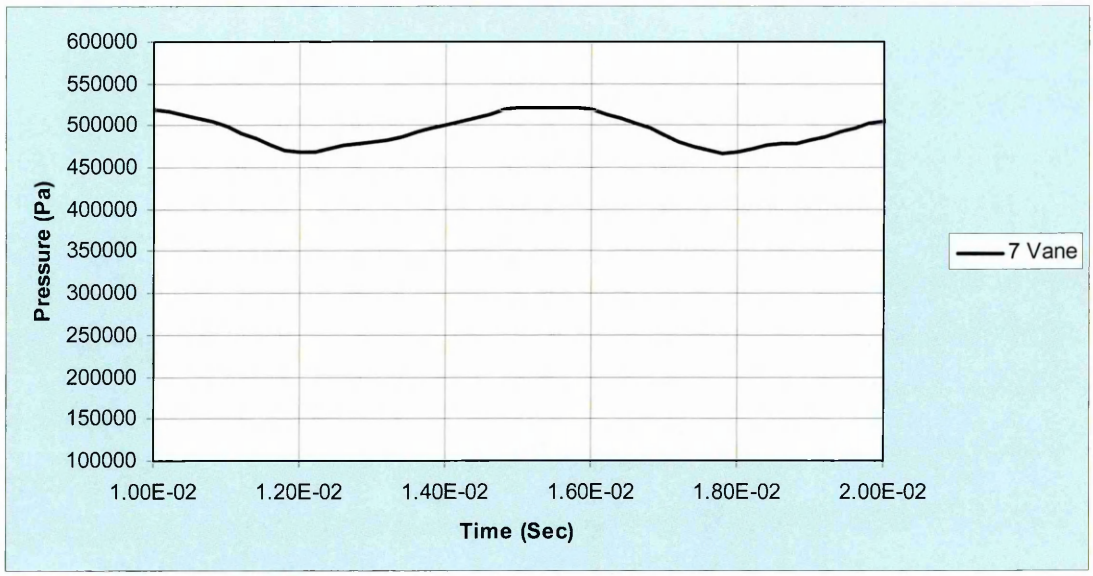

Fig 6.3.3.2 Pressure Pulsations 7 vane impeller

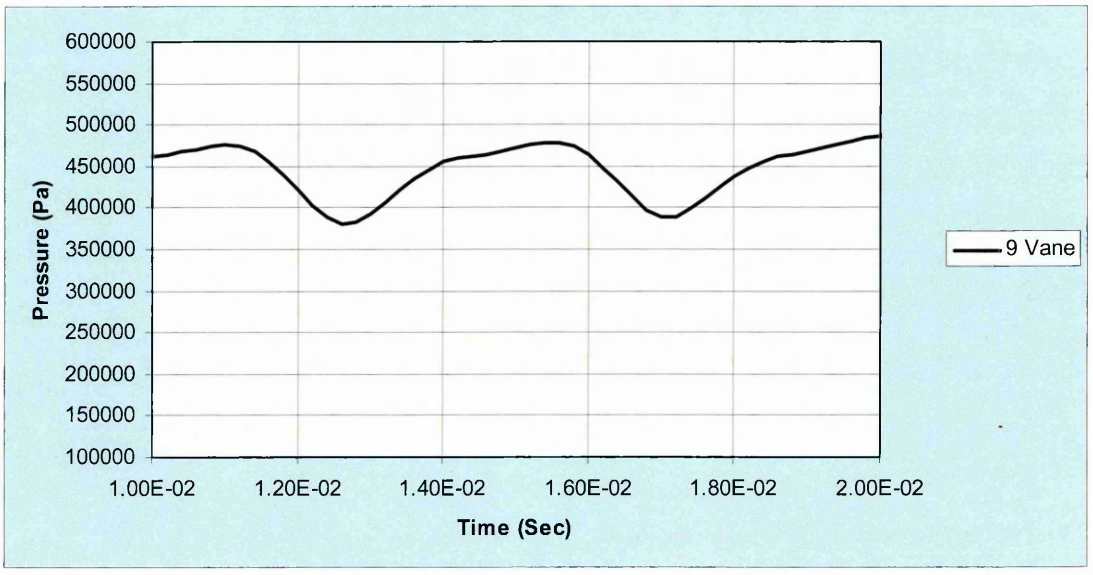

Fig 6.3.3.3 Pressure Pulsations 9 Vane impeller

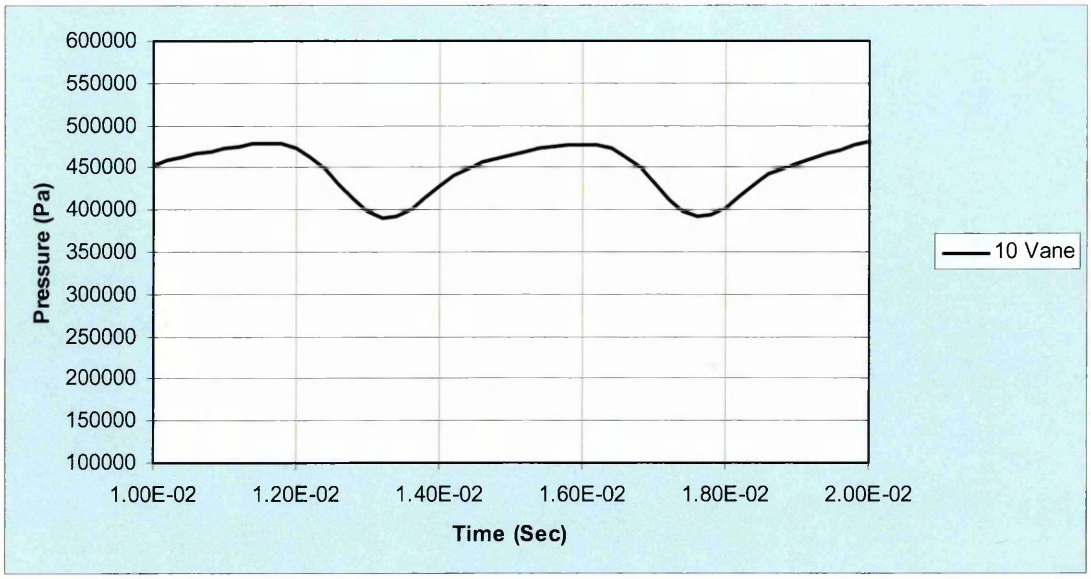

Fig 6.3.3.4 Pressure Pulsations 10 Vane Impeller

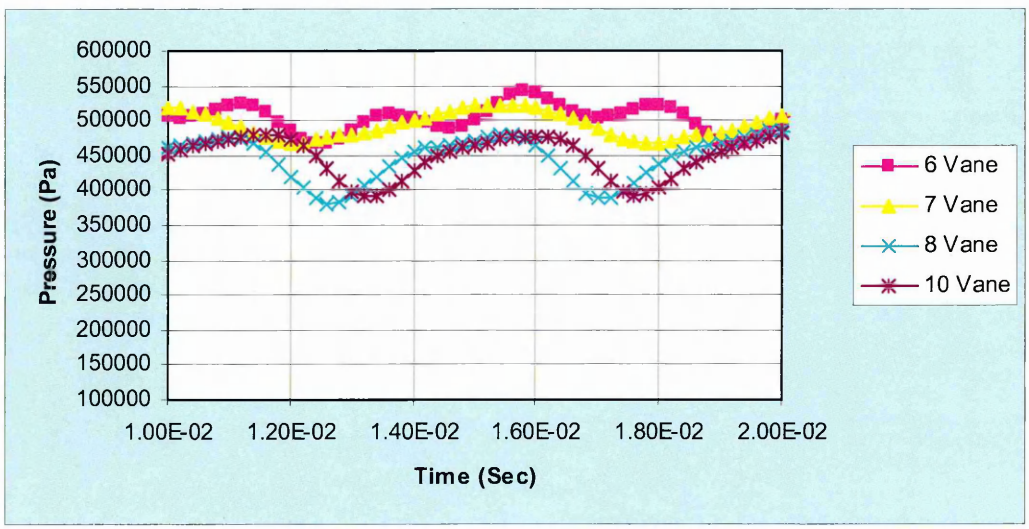

Fig 6.3.3.5 Pressure Pulsations all Impellers

6.3.4 Analysis of Pressure - Maximum and Minimum Levels

Consideration of the pressure change due to the increase in impeller vane number provides an insight into way the impeller diffuser system reacts to vane modifications.

The frequency of the maximum pressure level influences the closed valve head pressure and this frequency is directly linked to the impeller vane number. The table in Figure 6.3.4.1 illustrates the maximum pressure levels within the annular space between diffuser and impeller for different vane numbers.

Impeller Vane Number	Pressure Pa
4	561240
6	542080
7	521950
8	508924
9	490210
10	485200

Fig 6.3.4.1 Table of Maximum Pressures

A plot of these maximum vane numbers indicates a near linear decay in the maximum pressure level as illustrated in Figure 6.3.4.2

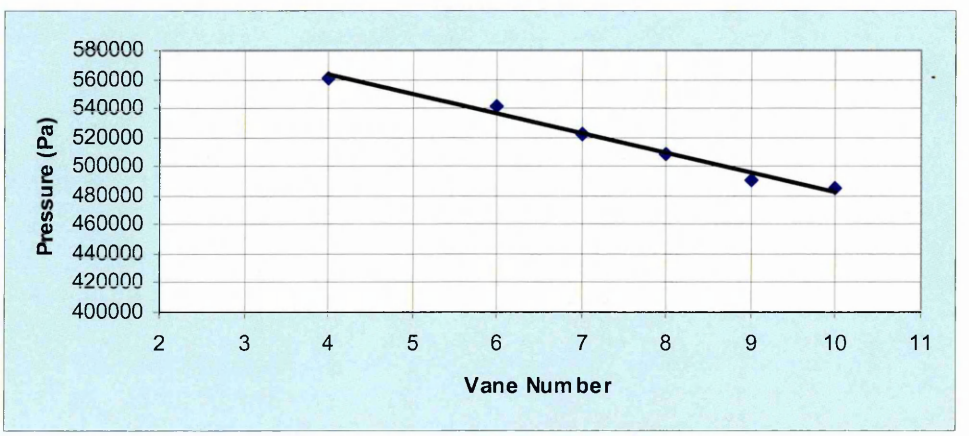

Fig 6.3.4.2 Plot of Maximum Pressures

Although these pressures are decreasing with vane number the contribution to the closed valve head is also linked to the frequency of the pulsations encountered within the annular space. This frequency is increasing. Taking this into consideration by multiplying the maximum pressures by their frequency change we get the following plot Fig 6.3.4.3.

This situation would partially satisfy the condition 2 laid down in Chapter 6.3.2.

Using the same methodology for the minimum pressure levels we can develop the Table featured in Fig 6.3.4.4. This illustrates the minimum pressure levels.

Impeller Vane Number	Pressure Pa
4	471600
6	466080
7	466100
8	457181
8	379670
10	386360

Fig 6.3.4.3 Table of Minimum Pressures

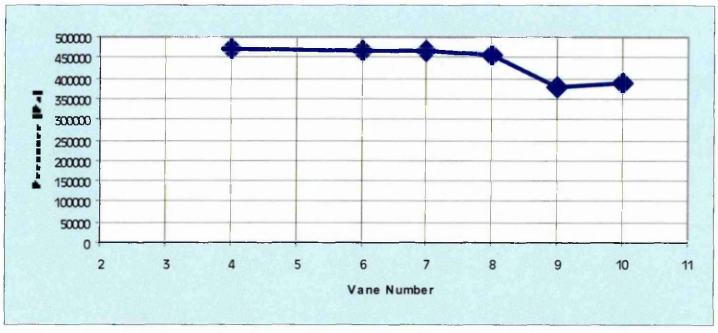

Fig 6.3.4.4 Plot of Minimum Pressures

Analysis of Fig 6.3.4.4 presents the situation where the minimum pressure is practically constant until we increase the vane number to 9. As this integer of vane number is reached there is a rapid pressure drop. In this condition the impeller vane number is equal to the diffuser vane number. This would satisfy condition 3 outlined is section 6.3.2. At this particular condition a loss of closed valve head would be experienced. This would be classed as the unstable condition.

As with the analysis of the maximum pressure peaks the minimum pressure levels should also be considered in terms of the increased frequency.

6.3.5 Pressure Maximum and Minimum Levels – The Link to Geometry

From analysis and comparison of the flow regime, if we assume the stator passageways contain steady pressure based on the level of unsteadiness passed through to the stator passages by the unsteady rotating vane system, and the rotating impeller blades contain unsteady pressure, then only the unsteady pressure generated by the blades and their interaction with the stator can influence the value of the closed valve head coefficient.

For impellers of identical blade designs we can also assume that changes in the pressure level of the bound volume within the stator passages are determined solely by the change of rotor blade number.

Inspection of the flow regime within the gap between impeller and diffuser shows a pulsating flow dependent on rotor blade position. This results in a peristaltic action of velocity-pressure exchange. The liquid in the upper proportion of the impeller blade channel is trapped between the stalled stator passages which exhibits steady pressure and the inlet backflow eddy which exhibits steady pressure.

From the description in the previous section it can be demonstrated that the extent of the bound outlet eddy and its protrusion into the impeller channel is linked to the area between the vanes. An impeller with a high vane number, but low A2bb, contains a small outlet eddy. Figure 6.3.5.1 illustrates the A2bb dimension for a pump impeller. The converse is true for an impeller with a low vane number.

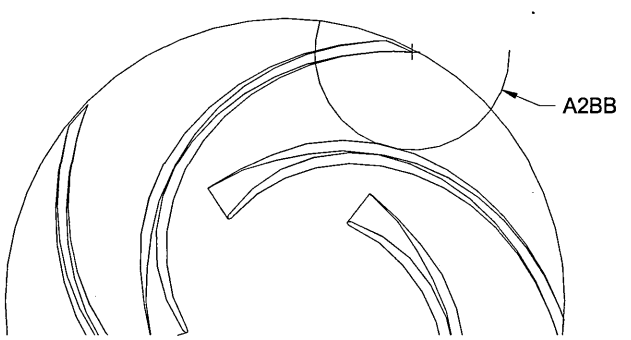

Fig6.3.5.1 Illustration of A2bb

If we consider the passage of one blade and its pressure recovery, we observe that a pressure velocity exchange occurs within the annulus around the impeller.
When the impeller blade is close to the diffuser blade the volume of liquid trapped between the stalled stator and the inlet eddy is forced between the annular gaps.

As the impeller blade moves away from the diffuser lip, the large area between the impeller vanes facilitates the velocity exchange, giving the pressure pulsation. From this analysis the closed valve head of the machine is determined by the extent of the pressure recovery between one impeller blade pitch and the number of times that pressure recovery takes place.

Taking these two situations into account we can propose that the pressure recovery is determined by the A2bb distance, Figure 6.3.5.1, and the frequency of the pulsation per revolution. To link the geometry to the analysis of maximum and minimum pressure pulsation we need to establish a geometric condition within the impeller that simulates the shape of either the minimum or maximum pulsation change with respect to the vane number.

Figure 6.3.5.2 contains an illustration of the maximum pressure level multiplied by the number of pressure events in one rotation. This relationship is linear. This figure is used to represent not just the change in pulsation level but also the frequency of pressure event experienced by one stator blade.

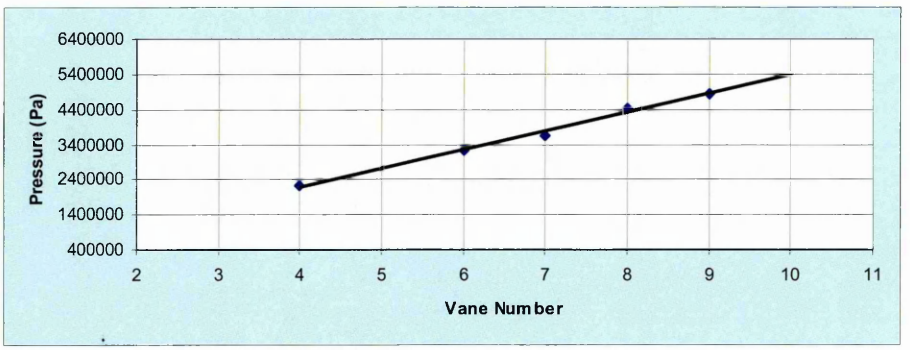

Fig 6.3.5.2 Frequency x Maximum Pressure vs. Vane Number

Figure 6.3.5.3 extends this frequency event through to also consider the effect on minimum pressure levels.

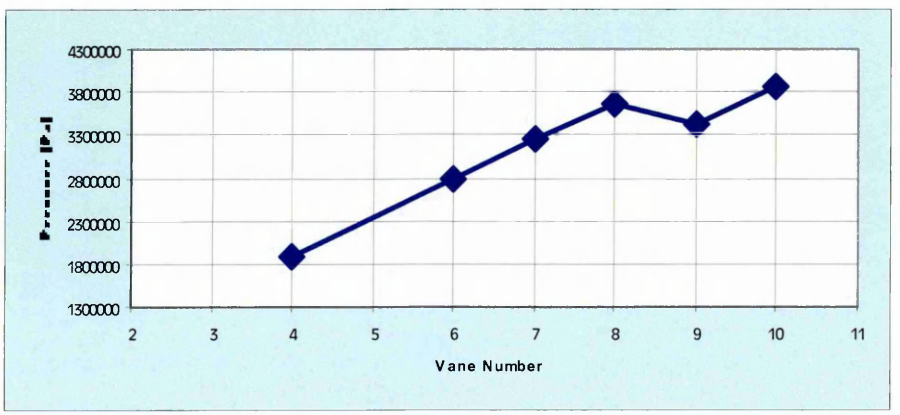

Fig 6.3.5.3 Frequency x Minimum Pressure vs. Vane Number

These two figures capture the nature of both the pressure pulsation amplitude and frequency events experienced by an individual stator blade. From this

situation we need to determine how these two propositions link to the geometric changes attributable to changes in the A2bb dimension within the impeller.

The table in Figure 6.3.5.4 contains the A2bb dimensions for the subject impeller.

Vane No Z	A2bb
4	69.565
5	59.035
6	50.574
7	44.715
8	40.585
9	35.115
10	31.835

Fig 6.3.5.4 A2bb Variation with Vane Number

Normalising this data so we have use the 4 vane impeller as the benchmark for the analysis we get the table in figure 6.3.5.5

Vane No Z	A2bb
4	1
5	0.8486308
6	0.7270035
7	0.6427801
8	0.5834112
9	0.5047797
10	0.4686983

Fig 6.3.5.5 A2bb Normalisation to 4 Vanes

Applying the pressure event frequency to this table by multiplying by the number of pulsation event per revolution (i.e. number of vanes) we get the graph represented in Fig 6.3.5.6.

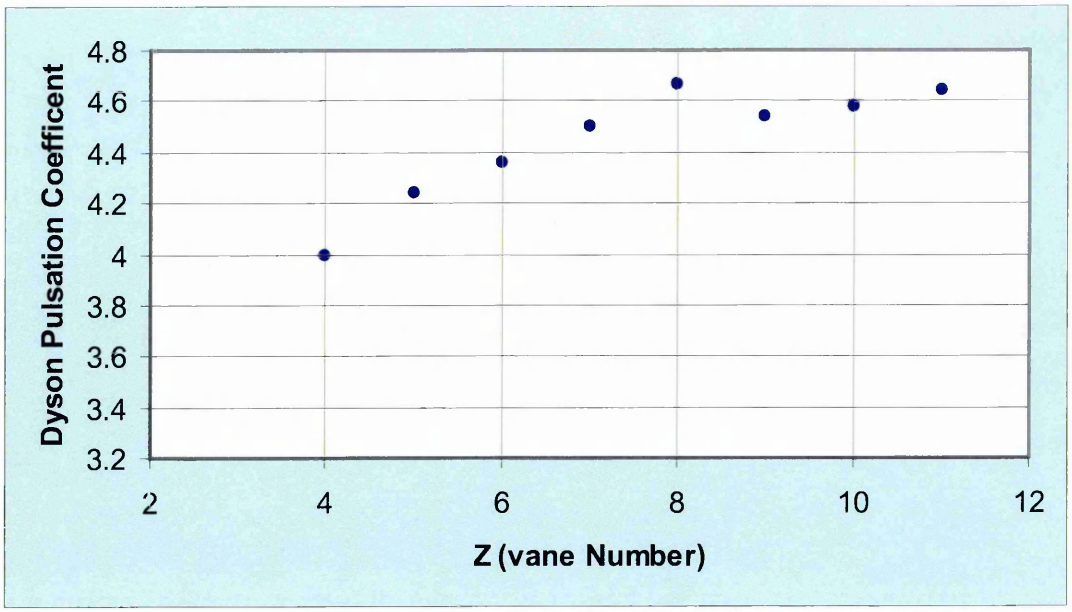

Fig 6.3.5.6 Pulsation Coefficient

Comparing this to the Figure 6.3.5.7 below, we can see similarities attributable to the minimum pressure levels.

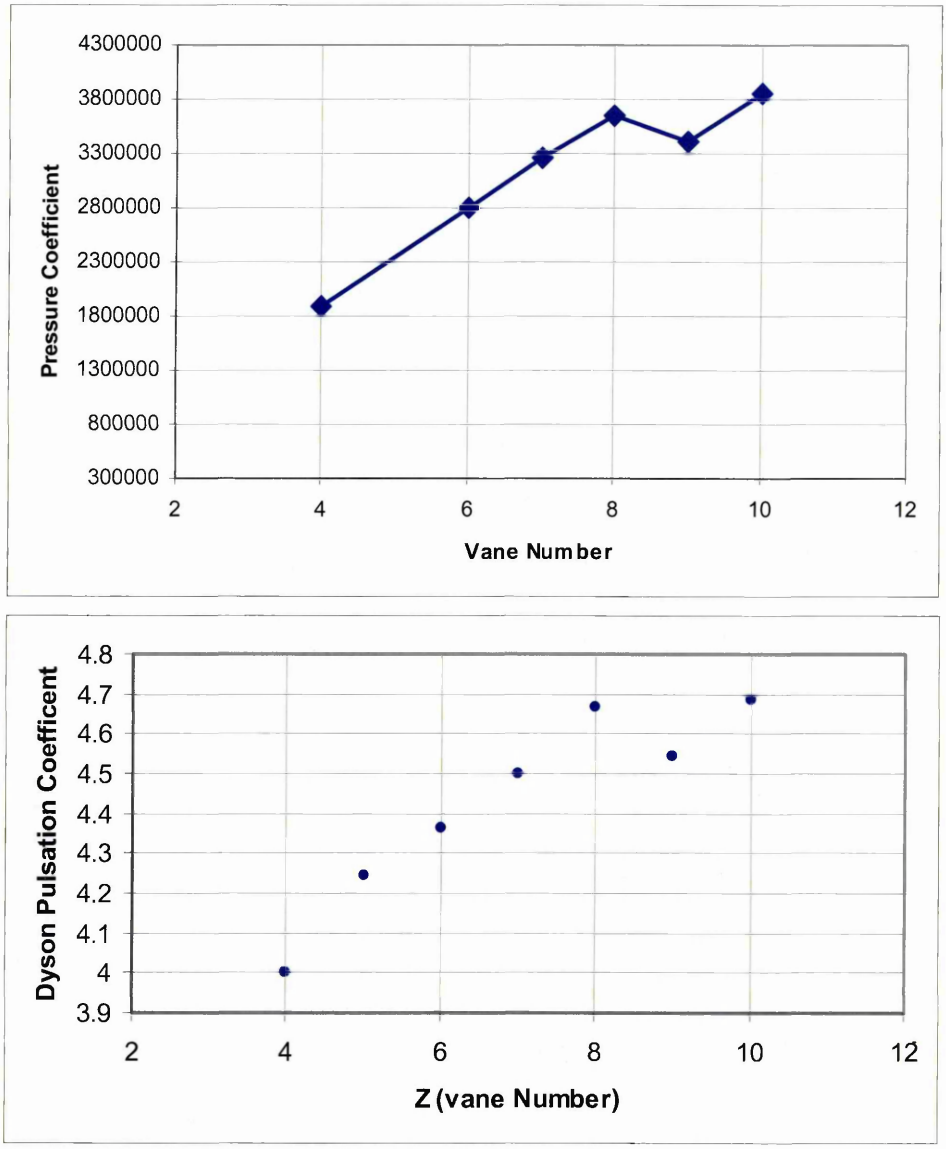

Fig 6.3.5.7. Comparison between Curves

From this comparison conditions 3 and 4, outlined in Section 6.3.2, are satisfied and the minimum pressure level change can be linked to the impeller A2bb geometric change causing a change in the peristaltic pressure effect as the impeller vane passes the diffuser vane.

The A2bb dimension and its effect on closed valve head provides a closer analogy to the actual flow situation, and how it changes with time, than the theory of solid body rotation. The A2bb not only links to the vane number but also the vane angle. Increasing the impeller outlet angle also has a subsequent effect on the A2bb dimension and the ultimately an effect on closed valve head.

Using the mental picture of a the energy interchange that occurs as the liquid is squeezed between the approaching stator and rotor blade, then relieved as

the A2bb dimension grows as the blade rotates, represents the flow field and is consistent with the regime demonstrated in previous chapters for both diffuser and volute pumps.

Although CFD has been demonstrated as a successful tool for accurately predicting the closed valve head of centrifugal pumps, the process is time consuming and computationally expensive. Building on the flow regimes identified by the CFD we can present designers with links to geometry and better refine their mental models. We have given pump designers a tool to rank the consequences of design changes with respect to changes in the flow regime and also to assess the consequences for the time averaged closed valve head value.

6.4 Summary

This chapter takes the flow features identified within the CFD simulations and uses those simulations to assess and identify the nature of the flow regimes and how these are linked and influenced by the geometry.

The theory of solid body rotation is investigated and this theory is proposed within the chapter to be only an analogy. Solid body rotation does not present the pump designer with a believable mental model from which he can propose new design theories linking geometry and flow regimes. The existence of pressure pulsation is demonstrated for impeller vane integers 6-10.

Within the outlet of the impeller the movement and extent of the discharge vane eddy is demonstrated to be linked to the ratio of impeller and diffuser vane numbers. If the impeller vanes are less than the stator vanes, which is common, the vortex will rotate counter to the machine rotation. If the converse is true and the impeller vanes are increased to be more then the stator vanes the vortex will move with the machine rotation. Equal numbers of vanes will present a standing vortex which pulses due to the influence of the rotor-stator interaction effects.

The chapter also proposes the link between the peristaltic actions of the impeller vane passing the diffuser vanes and considers the effect of changes in closed valve head as the frequency of this peristaltic phenomenon increases. By increasing the number of blades within the impeller and considering this effect on the amplitude and frequency of pressure pulsation we can propose that there is a linear relationship between pressure maximum amplitude and vane number. As the impeller vane number increases the pressure amplitude falls.

The same cannot be predicted for the minimum pressure level. The minimum level is predicted, by the computational solutions, to remain constant then fall dramatically before recovering. This is in line with the anecdotal behaviour of pumps which have their vane numbers increased and experience unstable characteristics at closed valve.

This change in minimum pressure development can be linked through an analysis of the A2bb geometry, as the A2bb measurement falls at the same vane integer as the minimum pressure level. Analysis of the change in A2bb is proposed as a method of predicting the fall in closed valve head as a pump becomes unstable.

Overall this chapter gives designers of centrifugal pumps a mental model based on vane interactions rather than solid body rotation theory. This mental model better represents the flow features that are defined through the previous chapters. The link to the A2bb geometry gives the designer a tool to rank the consequences of vane increase with respect to closed valve head and stability. Although this link is still an analogy it is firmly linked to the rotor stator interaction events, something that solid body rotation cannot claim.

7.0 Conclusions

Performance prediction of centrifugal pumps based on empirical analysis has hampered the development of new machines. Producing a new configuration of machine has traditionally required experimental knowledge of similar machines, extensive testing and refinement before a final design is acceptable. Given the relative low capital cost of centrifugal pumps, compared to other turbo-machinery, pump manufacturers do not invest heavily in development.

The scope of this project has three objectives. The first, to assess the current state of the art of closed valve head prediction for centrifugal pumps.

The second, to develop a methodology to use a commercial CFD code to predict the closed valve head of a centrifugal pump and assess its success based on the experimental background available from the literature.

The third objective is to set out the flow features predicted by the CFD code for a volute machine and a diffuser machine. These flow features are viewed against the background of the available experimental data to resolve some of the misunderstandings that are held within the pump industry as "state of the art".

7.1Conclusions of the Computation

The CFD simulation of a pump running at closed valve is possible using a commercial CFD code using a single processor machine. The following conclusions can be drawn from the techniques used to complete the simulation:

Grid sensitivity is an issue and the impeller blade passage requires more than 50000 nodes to capture the rotor-stator interaction effects. That being said, less refined grids are still qualitatively instructive. This research was carried out on a single processor machine. Grid sizes increased to approach the computational capacity.

Further grid refinement within the diffuser passage way, where the interaction effects are weakest, would be prudent. The Newton (1988) research suffered from difficulties predicting the pressure rises around the volute where the interaction effects are weakest. With the rapid growth of computational capacity the issue of grid size should not remain a barrier.

The standard k-epsilon turbulence model has little impact on the solution. The selection and evaluation of turbulence models was difficult. The influence of turbulence models was assessed, in this research, using an impeller, without collector, operating at design point. The analysis would be more appropriate if carried out at an off-design condition using an impeller and collector combination. Experimental validations for the turbulence models in similar off-design situations are not available.

It is important to include the rotor/stator interaction effects in any off-design solution where unsteady interactions are expected. Flow features are passed across the rotating and stationary domains. Averaging planes do not capture this transition of flow features and cannot be used

Time-step independence is important and steps greater than one degree introduced errors into the prediction of pressure pulsation amplitude. The time step independence study indicated that step sizes of 0.5 degree were appropriate.

The outlet domain of the volute was allowed to expel a flow less than the volumetric internal flow of the machine. In this way the boundary condition assignation was simplified. In an actual closed valve situation the impeller flow is equal to the volumetric flow whereas the flow expelled from the outlet of the volute is zero. This simplification when, viewed in terms of the experimental data available, is appropriate as the overall flow value is small compared to the on-design flow.

A more complete solution could be proposed which includes the volumetric flow through the wear ring annulus and the pumping effect of the impeller shrouds. Incorporating these two features greatly complicates the geometry and the associated grid but would better represent the actual closed valve situation.

The simulation of closed valve cannot be attempted without reference to the system in which the pump sits. There is a need to model elements of the piping at the suction, to accept the inlet backflow phenomenon, and the discharge, to simulate a closed control valve, to aid the solution validity. The phenomenon of inlet backflow should be accommodated by extending impeller inlet domain axially so the inlet boundary is remote from any unsteady affects. The entire inflow boundary can then be assigned as a one direction flow plane.

The simulation of the diffuser pump was greatly simplified. The approach to the impeller was considered to be axial which is not representative of a typical diffuser pump. Conventional designs incorporate suction bay geometry which accepts the pump radial inflow before using splitters to change the flow direction from radial to axial. This type of geometry at closed valve would have an unsteady impact on the fluid streams rejected from the impeller as the inlet backflow proportion of the flow regime develops. This would complicate the solution as an averaging interface may not be appropriate.

Despite the compromises forced upon the solution by the limited computational resources the simulation technique does not over-predict the volute pressure rise in the same manner as the Newton (1988) research. Using commercially available software the computational technique gives time averaged closed valve predictions that are within pump performance test measurement tolerances. This is a commercially valuable contribution which enables pump manufacturers to confidently design machines with closed valves characteristics that are both predictable and stable. The consequences of the actual machine geometry are considered, eliminating the need for design coefficients.

7.2 Volute Pump Insight

Using CFD the flow field through a double volute centrifugal pump, which was representative of conventional pump design, was investigated. Fig 7.2.1 presents an overall instance of the predicted flow regime.

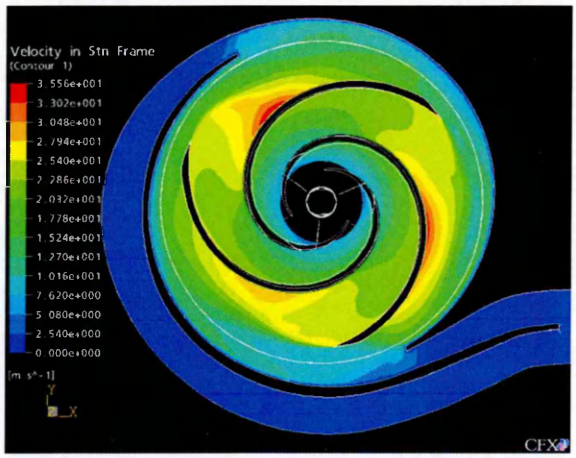

Fig 7.2.1 Overall Picture of Volute Pump Flow Regime

The nature of the flow fields when the volume flux of the pump approaches zero is shown to be unsteady. The volute passages are filled with a slow moving, low energy liquid, which experiences pressure pulsations dominated by the vane pass frequency Fig 7.2.2.

Double volute pumps have discharge ducts that experience these pulsations independently of each other as the vanes approach the volute lips. These independent pulsations combine at the pump discharge. The amplitude and the frequency of the pulsations passed through the volute passageways are strongly influenced by the impeller blade geometry.

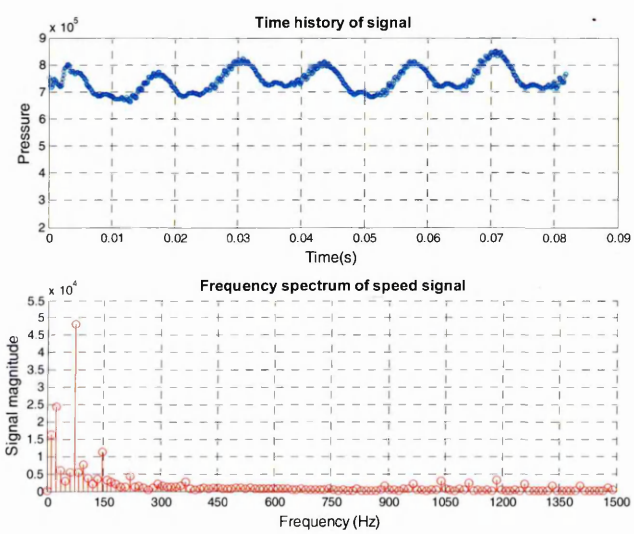

Fig 7.2.2 Frequency Spectrum of Pressure Pulsations Close To the Volute Lip

The volute sections around the periphery of the impeller experience a non-linear pressure rise between the throats. This is attributable to the stalled

nature of the long and short diffusing passages which join the casing throats to the discharge nozzle. The impeller blade motion causes an energy exchange as the bound liquid in the annular gap between the impeller and volute is influenced by the peristaltic motion as the impeller blade coincides and then moves away from the volute lip.

The long and short passages experience out of phase fluctuations driven by these casing and impeller interactions. The impeller blade number accounts for the phases shift. There is a cross passage flow from the long to the short diffusing passageway as illustrated in Fig 7.2.3. The closed valve head of the machine is influenced by the strength of the rotor stator interactions and the pressure recovery which takes place due to the peristaltic action from the impeller blades, driving the unsteadiness.

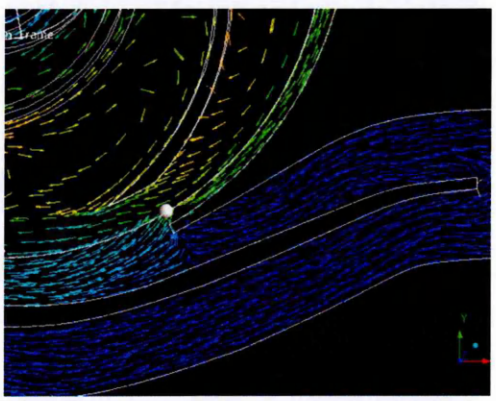

Fig 7.2.3 Long - Short Passage Flow

Within the impeller blade passage the outer proportion is filled with a discharge vortex, imposed on the impeller by the stalled stationary passageways and vanes as illustrated in Fig 7.2.4. The number of vanes within the stator influences the development and direction of this discharge vortex.

The proposition that the impeller behaves as would a solid rotating disc (solid body rotation) when applied to the closed valve head situation, whilst appearing statistically significant, does not truly represent the sophisticated energy exchanges required to fully describe the nature of the flow field. As a mental model for designers this analogy is flawed.

All of the prediction methods available rely on some form of empirical and statistical analysis, the more sophisticated methods using sold body rotation to account for the impeller contribution to closed valve head. The proposition of solid body rotation is not representative of the actual flow regime.

The gap between the impeller and casing is dominated by pressure pulsations caused by the impeller-casing interaction. These pulsations, at vane passing frequency, are generated as the impeller blade approaches the casing lip and propagate through the volute at acoustic velocity.

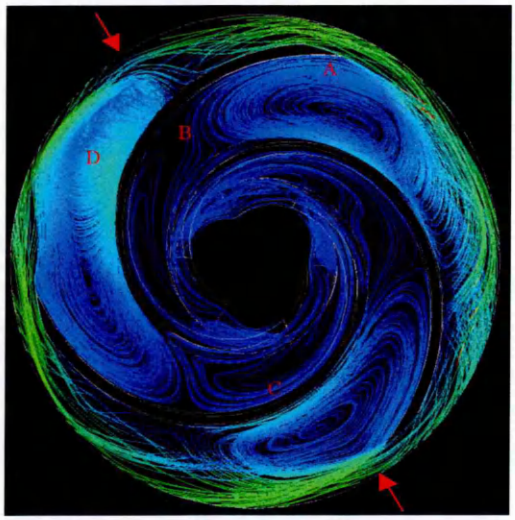

Fig 7.2.4 Impeller Streamlines at Closed Valve Low

Within the impeller inlet the first 1/3 of the impeller is filled with a vortex generated by the boundary layer breakdown along the pressure side of the impeller vane close to the hub.

The liquid passes span-wise across the meridional plane and is expelled from the impeller eye at a constant helical angle approximately equal to the impeller inlet tip angle as shown in Fig 7.2.5. This spiralling liquid has an influence on the inner core of the suction flow causing a rotation in this core, which reduces the incidence to the hub side of the vane. These effects all work together. The exchanges in energy from suction to impeller and on to the volute all influence the closed valve head value. The success of the model in predicting the closed valve head lies with its ability to capture all these flow effects.

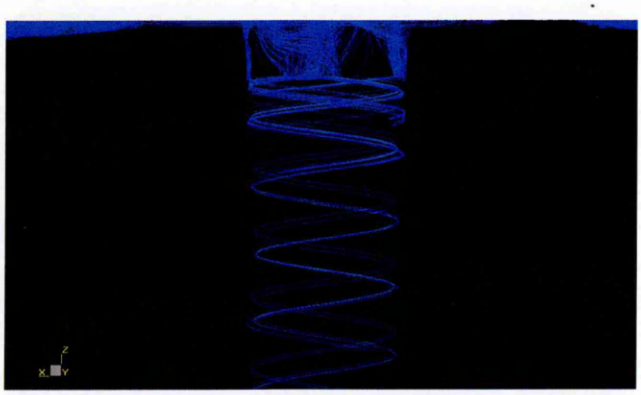

Fig 7.2.5 CFD Streamline of Backflow Discharge down the Suction Line

The strong flow features present in the CFD code agree with the body of experimental investigation within the literature.

7.3 Diffuser Pump Insight

From the computational solution of a bladed diffuser pump the time averaged pressure across one diffuser blade pitch was analysed. A non-linear pressure rise was noted over one blade pitch of the diffuser. This situation is in agreement with the situation experienced within the volute pump.

Within the volute pump the non linear pressure distribution occurred at two instances around the volute. Within the diffuser pump, with 9 blades, this time nonlinearity occurred across each diffuser blade pitch.

The stator passages are influenced by the pressure pulsations generated by the interactions of the blades. Analysis of the temporal pressure within the annular gap between the impeller and diffuser blade presented a picture of fluctuation at vane passing frequency and the second multiple of this frequency as illustrated in Fig 7.3.1.

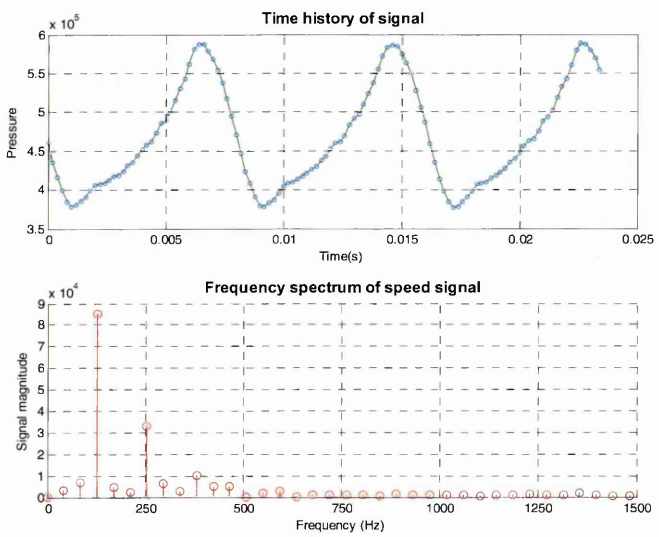

Fig 7.3.1 Pressure Pulsation within Annular Gap

An overview of the pressures within the diffuser flow channels demonstrates that there is an unsteady pressure component passed into the diffuser channel. Although viscous effects and diffusion decay this pressure fluctuation with time/distance the unsteady pressure is still apparent at the outlet of the diffuser blade (Fig 7.3.2).

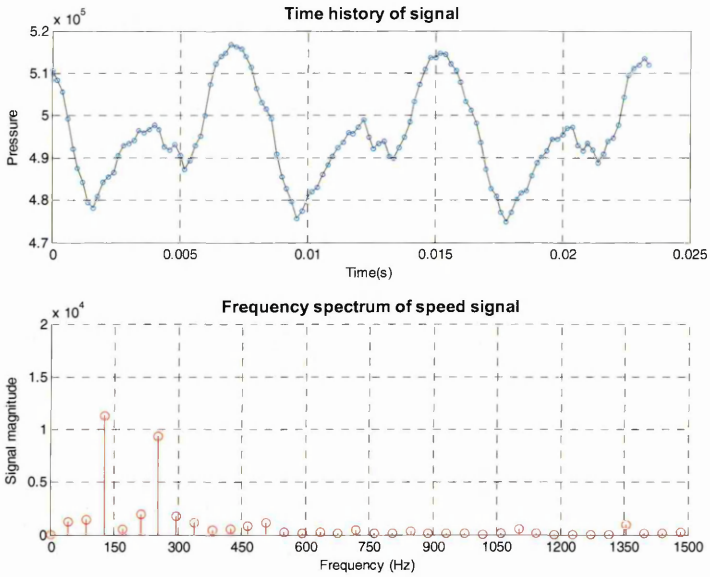

Fig 7.3.2 Pressure Pulsation at Diffuser Exit

The diffuser contribution to the closed valve pressure is not uniform despite uniform geometry. The stalled nature of the diffuser encourages an alternating picture of inflow and outflow across the diffuser channels. This differing flow picture contributes to a differing unsteady pressure level between the impeller and diffuser (Fig 7.3.3).

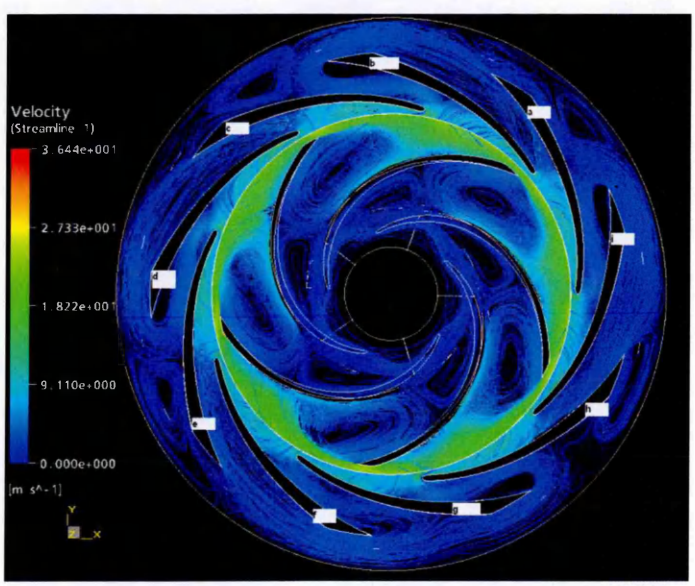

Fig 7.3.3 Diffuser Flow Regime Overview

7.4 Blade Geometry Effects on Discharge Eddy Development

The low pressure region at the impeller exit, driven by the interaction with the stalled volute flow, is a phenomenon which is not consistently accounted for in the literature.

The vortex is linked to the position and number of blades in both the rotor and stator. The physical size and its development within the impeller passage is controlled by the number of impeller vanes. Its rotational direction and speed is linked to the impeller & diffuser vane ratio.

For a low solidity impeller design with a low blade number, the vortex develops in the radial direction down into the impeller passage until it fills 50% of the channel (Fig.7.4.1) The intensity of this vortex increases as the impeller blade approaches the casing cut water as the driving viscous force of the liquid trapped between the lip and tip becomes dominant.

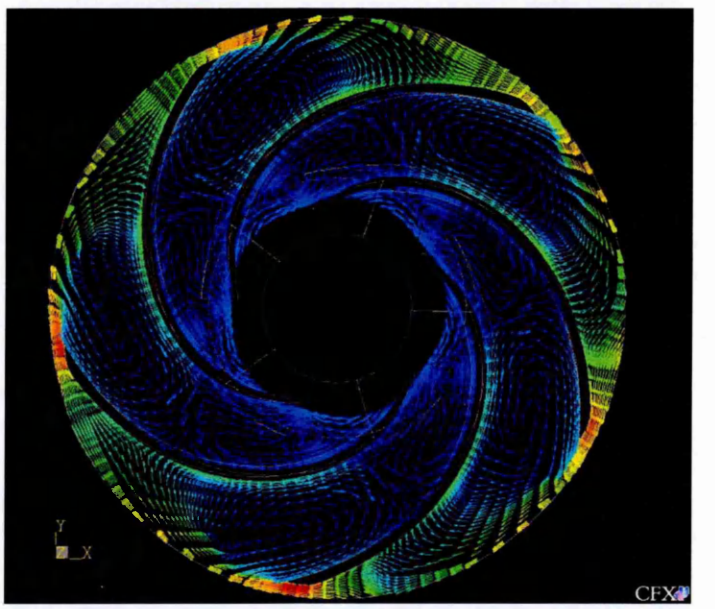

Fig 7.4.1 Velocity Vectors within a 5 Vane Impeller at Closed Valve

The converse is true when the impeller blade solidity is increased. The vortex at impeller exit extends in the radial direction only 20% into the impeller passage (Fig 7.4.2).

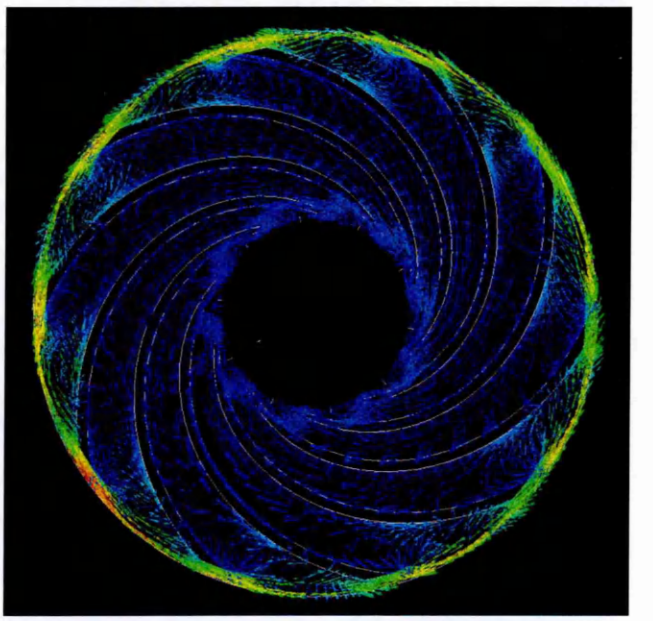

Fig 7.4.2 Velocity Vectors Within a 10 Vane Impeller at Closed Valve

Comparisons of Fig 7.4.1-7.4.2 indicate the extent of vortex development within the passage with respect to increasing solidity. Experimental observations, which refer to this vortex define its motion as sub-synchronous and counter to the pump rotation. This observation neglects the importance of the rotor-stator interaction on the direction this vortex motion.

For a case where the impeller blade number is less than the number of stator blades the vortex will appear to move counter to the machine rotation.

If the impeller blade number and the stator blade number are equal[1] the vortex will appear not to move, as the pitch change influence of the stator is equal to the rotor effect at any instance. Each impeller passage experiences identical influence from the stator at the same instance.

When the impeller vane number is greater than the stator number the vortex will appear to move in the same direction as the machine rotation.

The amplitude and frequency of the pressure within the annular gap between the impeller and diffuser is also influenced by the number of impeller vanes. This is attributable to the peristaltic action that occurs as the impeller vane passes across the stator vane. This A2BB dimension can be linked to this peristaltic pressure development Fig 7.4.3.

[1] Pump Designers try to avoid this situation to limit the vibration potential of the machine

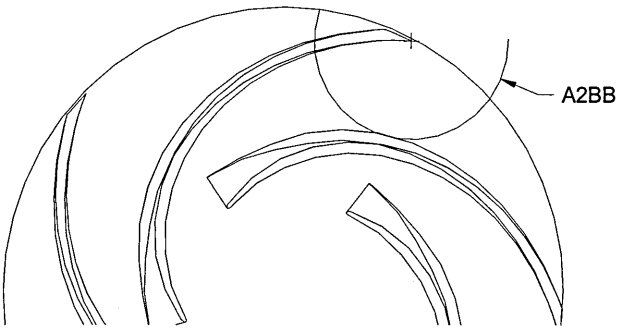

Fig 7.4.3 Illustration of the A2BB Dimension

The A2BB dimension is presented as a major influence on the development of the closed valve pressure. Increasing the vane number decreases the A2BB dimension. The consequence of this reduction in A2BB is a reduction in the peristaltic pressure development and subsequently a change in the closed valve pressure.

7.5 Final Conclusions

The accuracy of the closed valve prediction using CFD is better than the empirical corrections available. This is despite the compromises made within the simulations to limit the size of the computational domains. This is commercially valuable, allowing pump manufacturers to extend their product offerings beyond their current pump configurations.

CFD gives a valuable insight into the nature of the flow mechanisms. The available prediction methodologies, Frost and Nielsen (1991) notwithstanding, have no link to the flow physics.

The following Insights were gained from the study:

- The flow within the impeller at closed valve is not solid body rotation as proposed by Stirling (1982) and Frost and Nielsen (1991). The nature of the flow between the impeller and stator is unsteady. Rotor stator interactions cause pressure pulsations at vane pass frequency. These pulsations propagate at acoustic velocity, diffusing within the stator passageways.

- The flow pattern around both the volute and diffuser blade is different from that proposed by Newton (1998) and Frost (1991). The central splitter of the double volute pump divides the passageways into two stalled regions which experience pressure pulsations at vane pass frequency. There is a cross channel flow around the central splitter from the long to the short diffusing passageway. The diffuser blade row experiences a similar cross channel flow and pressure pulsation propagation at blade pass frequency

- The impeller geometry which affects the A2BB dimension, particularly the vane integer, has an affect on the impeller flow regime. The peristaltic action setup by the interchange of A2BB and blade thickness directly influences the closed valve pressure.

This research has contributed to the understanding of closed valve head by proposing a mental model based on rotor stator interactions rather than steady state solid body rotation.

Commercially a valid prediction methodology is valuable. Using computational simulation techniques to replace empirical coefficients and experimental analysis shortens the design cycle and increases the capability of manufacturers to design machines outside their traditional product configurations.

7.6 Further Work

This section considers potential further work which would improve the understanding and prediction of closed valve head.

- This research uses a combination of experimental data available from the literature and test data available from production machines to build a validating case for the accuracy of the computational simulation. Whilst these point towards the validity of the solution they do not capture the true nature of the flow regime in the subject machine. A comparative study on a commercial machine would be a more appropriate validation method.

- The influence and appropriateness of turbulence models is an area of research that is not well defined. This research used a steady analysis of a single impeller channel as validation for using the k-epsilon turbulence model. The influence of turbulence models at off design performance is an area where there is little research or guidance within the literature.

- The simulation neglected a number of features which may have an influence on the closed valve head. These are:
    - The flow through the wear ring annulus back to the suction channel
    - The radial nature of the approach to the impeller within a conventional diffuser pump.
    - The influence of the inlet guide vanes prior to the diffuser vanes
    - The pumping action of the impeller shrouds

  Investigation of the influence of these features is a realistic aim as a further step towards full machine modelling. As computational power increases the listed features can be added to the simulation technique.

- When a machine operates at severe partial capacity it experiences inlet backflow recirculation. This recirculation is also linked to cavitation surge damage within the impeller. Current CFD methodologies cannot predict the inter-relationship between inlet backflow recirculation and cavitation surge. It is unclear both experimentally and computationally if cavitation influences the closed valve head pressure. Further investigation in this area would be appropriate.

- By building on the prediction methodology developed within this work it is possible to investigate the consequences for closed valve head of different geometry changes. The literature points towards the impeller inlet geometry as a contributor to the closed valve head. Investigations into the effect on closed valve head of eye size, blade angle and inlet area could provide further insight into the constituents of closed valve head.

The ultimate goal of the solution methodologies should be to provide a platform to assess and rank the consequences of changing geometry. This is done with a view to developing a new prediction methodology for closed valve head. A new methodology should assess common geometric changes without the need for reference back to CFD. This would have dramatic consequences for the design cycle time for a new development.

References

Abramian M. and Howard J.H.G(1998) "Experimental investigation of the steady and unsteady relative flow in a model centrifugal impeller passage" ASME Journal of Turbomachinery. Vol116 pp269-279.

Acosta A J and Bowerman RD(1957)."An experimental study of centrifugal pump impellers"
Transactions of ASME pp1821-1839

Acosta A J (1954). "An experimental and theoretical investigation of two-dimensional centrifugal pump impellers" Transactions of ASME Pp749-763

Alder D. and Levy Y (1979). "A laser Doppler investigation of the flow inside a backswept, closed, centrifugal impeller" Imeche Journal Mechanical Engineering Science Vol 21 No1 Pp1-6.

API610 Standard 10th Edition (2004), Centrifugal Pumps for Petroleum, Petrochemical and Natural Gas Industries

Barrand J P, Caignaert G Canavelis R and Guiton P(1984). "Experimental determination of the reverse flow onset in a centrifugal impeller" Proceedings of the 1st International Pump Symposium Pp63-71. Cited in Newton T M (1988). Rotor –Stator interaction in radial flow pumps and fans at shut-off conditions. Pdh Thesis. Newcastle University.

Binder R.C. and Knapp R.T. (1958)."Experimental determinations of the flow characteristics in the volutes of centrifugal pumps." Trans ASME Paper No. HYD-58-4. Cited in Newton T M (1988). Rotor –Stator interaction in radial flow pumps and fans at shut-off conditions. Pdh Thesis. Newcastle University.

Brownell R.B., Flack R.D. and Kosrezewsky G.J. (1985). "Flow visualisation in the tongue region of a centrifugal pump." The Journal of Thermal Engineering Vol. 4, No. pp 35-45. Cited in Newton T M (1988). "Rotor –Stator interaction in radial flow pumps and fans at shut-off conditions". Pdh Thesis. Newcastle University.

Busemann A (1928), Das Forderverhaltniss radialer Kreiselpumpen mit logerithmischspiraligen Schaufeln, Zeitschrift fur Angewandte Mathematik und Mechanik, Vol.8 October pp372-384 as cited in Tuzon J (2000) Centrifugal Pump Design.

Caignaert G. and Morel P. (1995). "Mean pressure measurements within a centrifugal pump impeller at partial flow rates." Conf. Proceedings Turbomachinery: Fluid Dynamic and Thermodynamic Aspects: 1st European Conf. Vol. 2 Experimental fluid dynamics. Cited in Newton T M (1988). "Rotor –

Stator interaction in radial flow pumps and fans at shut-off conditions". Pdh Thesis. Newcastle University.

Chen and Liaw (1997) "The Flowfield calculation of a centrifugal pump with volute". Proceedings of the International Gas turbine and Aerospace Congress and Exhibition. 97-GT-49.Pp1-10

Cooper P. and Graf E. (1994) "Computational Fluid Dynamical analysis of complex internal flows in centrifugal pumps". Proceedings of the eleventh annual international pump users symposium. Pp83-94

Dong R., Chu S. and Katz J.(1992b). "Quantitative visualisation of the flow within the volute of a centrifugal pump. Part B: results and analysis." Vol. 114, No. 3 pp 396-403

Dong R., Chu S. and Katz J. (1992a) "Quantitative visualisation of the flow within the volute of a centrifugal pump. Part A: technique." ASME Journal of Fluids Engineering Vol. 114, No. 3 pp 390-395. Cited in Newton T M (1988). "Rotor – Stator interaction in radial flow pumps and fans at shut-off conditions". Pdh Thesis. Newcastle University

Dyson G.(1999)" CFD as a Design Tool" ImechE conference, Up and Coming in Engineers Fluid Machinery

Dyson G (2005) Impeller Re-Rate to Reduce Hydraulically Generated Vibration. Proceedings of the International Pump Symposium, Houston

Ficher K. and Thoma D.(1932) "Investigation of the Flow in A Centrifugal Pump" Presented at the meeting of ASME June27 1932

Fraser WH (1991) Recirculation in Centrifugal Pumps. World Pumps 1982 vol188 p.227-235

Frost T.H. and Nilsen E.(1991) "Shut-off head of centrifugal pumps and fans." Proc. Instn. Mech. Engrs. Vol 205 pp 217-223

Gostelow J.P. (1977) "A new approach to the experimental study of Turbomachinery flow phenomena." ASME Journal of Engineering for Power, January pp 97-105

Goulas A. and Truscott G. (1988) "The flow at the tip of an impeller at off-design conditions."C336/88 Proc. IMechE Conf. "Part-Load Pumping operation, control and behaviour."

Graf E. (1993) "Analysis of centrifugal impeller BEP and recirculation flows; comparison of Quasi-3D and Navier-Stokes solutions." ASME FED – Vol 154 Pumping Machinery

Grotjans H and Menter FR. (1998) Wall functions for general application CFD codes. In K. D. Papailiou et al., editor, ECCOMAS 98 Proceedings of the Fourth European Computational Fluid Dynamics Conference, pages 1112-1117. John Wiley & Sons, 1998. as cited in CFX Tascflow Theory Documentation.

Hamill I.S., Hope C.B., Ng R. (1995) "Pump-related applications of CFDS-FLOW3D" 14th BPMA Technical Conference, Using Pumps Better pp 653-667

Hereau F., Kermarec J., Stoffel B. and Weiss K. (1993) "Study of internal recirculation in centrifugal impellers." ASME FED-Vol. 154 Pumping Machinery pp 151-157

Iversen H.W., Rolling R.E. and Carlson J.J. (1960) "Volute pressure distribution, radial force on the impeller, and volute mixing losses of a radial flow centrifugal pump."ASME Journal of Engineering for Power pp 136-144

Kaupert K.A and Staubli T (2001) The unsteady pressure field in a high specific speed centrifugal pump impeller- Pt11: transient hysterisis in the characteristic. Journal of Fluids Engineering Vol 121 p627-632

Kaupert and Thomas (1999) "The Unsteady Pressure Field in a High Specific Speed Centrifugal Pump Impeller Part1 – Influence of the Volute". Journal of Fluids Engineering. Vol 121 pp621-626

Kikuyama K., Minemura K., Hasegawa Y., Asakura E. and Murakami M. (1987) "Unsteady pressure distributions on the impeller blades of a centrifugal pump-impeller operating off-design."
ASME Gas Turbine Conf. And Exhibition Paper No. 87-GT-144.

Kovats A.(1979) "Effect of Non-Rotating Passages on Centrifugal Pumps and Subsonic Compressors" Flow in Primary Non-Rotating Passages in Turbomachines Presented at Winter Annual Meeting of ASME, December 2-7 1979

Kumar T.C.M and Rao Y.V.N (1977) "Quasi 2D Analysis of A Flow Through a Centrifugal Pump Impeller". Joint Applied Mechanics. Fluid Engineering and BioEngineering Conference. June 15-17 1977. ASME.

B.E. Launder and D.B. Spalding (1974). The numerical computation of turbulent flows. *Comp. Methods Appl. Mech. Eng.*, 3:269-289.

Lennemann E. and Howard J.H.G (1970) "Unsteady Flow Phenomena in Rotating Centrifugal Impeller Passages". Journal of Fluid Engineering for Power. ASME Series A Vol 92 No1 pp65-72

Levin A.A. and Poliokovsky (1965) "To calculate the pressure characteristic of centrifugal pumps and fans at zero discharge." Isvestya AN SSSR Energetika 1, Transport 2 pp 129-133. Cited in Newton T M (1988). "Rotor –Stator interaction in radial flow pumps and fans at shut-off conditions". Pdh Thesis. Newcastle University.

McDonald G.B, Lennemann E. and Howard J.H.G (1971) "Measured and Predicted Flow Near the Exit of a Radial Flow Impeller". ASME Paper 71-GT-15 pp1-6

Miner S.M., Beaudoin R.J. and Flack R.D (1989). "Laser velocimeter measurements in a centrifugal pump." ASME Journal of Turbomachinery Vol. 111 pp 205-212

*Miner S.M., Flack R.D. and Allaire P.E.(*1992). "Two-dimensional flow analysis of a laboratory centrifugal pump." ASME Journal of Turbomachinery Vol. 114 pp 333-339

Miner S.M. (1988) "Potential flow analysis of a centrifugal pump: Comparison of finite element calculation and laser velocimeter measurement." PhD Thesis, University of Virginia, USA.

Newton T M (1988). "Rotor –Stator interaction in radial flow pumps and fans at shut-off conditions". Pdh Thesis. Newcastle University.

Palgrave. R(1985) –"Operating centrifugal pumps at partial capacity", 9th BPMA Technical Conference, Paper 6, Warwick University, Coventry (April 1985)

Palgrave & Dyson (2000) "Assessing a Pump's Vibration Potential From CFD Analysis". Centrifugal Pumps-The State of Art and New opportunities. ImechE

Patel D.P., Srivastava R.K. and Shah C.S. (1981)."Performance prediction in complete range of centrifugal pumps."Seventeenth Technical Conference British Pump Manufacturers' Association

Peck J.F.(1950) "Investigations Concerning Flow Conditions in a Centrifugal Pump and the Effect of Blade Loading on Head Slip". Proceedings of the ImechE Vol162 p409

Peck, J.F. (1968) "Design of centrifugal pumps with computer aid." Proc. Instn. Mech. Engrs. Vol. 183, Part 1, pp 321-352

Patel D.P., Srivastava R.K. and Shah C.S. (1981)."Performance prediction in complete range of centrifugal pumps."Seventeenth Technical Conference British Pump Manufacturers' Association

Roco M.C., Hamelin P., Cader T. and Davidson G (1990) "Animation of LDV measurements in a centrifugal pump." Fluid Machinery Forum 1990, Vol. 96. Cited in Newton T M (1988). "Rotor –Stator interaction in radial flow pumps and fans at shut-off conditions". Pdh Thesis. Newcastle University.

Rose M.G. (1987). "Flow in the impeller of a centrifugal water pump with three-dimensional blading."
C274/87 Proc. IMechE Conf.

Simpson H.C. and Cinnamond (1964) "Studies of flow through centrifugal pump impellers." IMechE Proc. 1963-64 Vol. 178, Pt. 3 1(ii) Paper 8

Simpson and Cinnamond 1964 Studies of flow through centrifugal impellers ImechE Proc 1963-64 Vol178 Pt3.1 (ii) Paper 8

Stepanoff A.J. (1957) "Centrifugal and axial flow pumps." John Wiley, New York Chapman and Hall, London

Stirling T.E. (1982) "Analysis of the design of two pumps using NEL methods." C183/82 Proc. ImechE Conf. "Centrifugal Pumps-Hydraulic Design."

Stoffel B. and Weiss K. (1994) "Experimental investigation on part load flow phenomena in centrifugal pumps."World Pumps, October Elsevier Science Ltd No. 337pp 46-50

Throne E.W. (1988) "Head and power at closed valve." C331/88, Proc. IMechE Conf. Part-Load Pumping operation, control and behaviour.

Tourret J., Badie-Cassagnet G., Foucault J.P. and Kermarec J.
(1985) "Experimental studies of the noise emission and noise generation from a centrifugal pump." Presented at the ASME Winter Annual Meeting, Miami Beach, Florida November 17-21 Paper No. 85-WA/FE-8. Cited in Newton T M (1988). "Rotor –Stator interaction in radial flow pumps and fans at shut-off conditions". Pdh Thesis. Newcastle University.

Tourlidakis A, Elder R.L. and Tan S.C. (1995)
"Applying computational fluid dynamics to real fluid machinery and pump flow problems."
14th BPMA Conference, Using Pumps Better, April 25-27 pp 623-651

J.Sun and H. Tsukoamoto (2001) Off -design performance prediction for diffuser pumps. Proceedings of the Institute of Mechanical Engineers Vol 215 Part A pp 191-201

Versteeg HK and Malalasekera W (1995) An introduction to computational fluid dynamics : the finite volume method. Longman Scientific and Technical

Wiesner F.J. (1967) "A review of slip factors for centrifugal impellers." Journal Engineering Power Vol. 89(4) pp 558-572

Worster R.C.(1963) "The Flow in Volutes and its Effect on Centrifugal Pump Performance". Proc. ImechE Vol177 (31)pp843-865

Yausa and Hinita(1979)." Fluctuating Flow behind an Impeller of a Centrifugal Pump". JSME Vol22 No.174 Paper 174-7 Cited in Newton T M (1988). "Rotor – Stator interaction in radial flow pumps and fans at shut-off conditions". Pdh Thesis. Newcastle University

Yates M.K., Rhodes I.N. and Elder R.L. (1995) "The application of computational fluid dynamics (CFD) to centrifugal fuel pumps – A user's perspective." 14th BPMA Technical Conference, Using Pumps Better pp 669-687.

Yeddiah S. (1985) "Certain unexplained phenomena, observed in centrifugal pumps part A and B." Joint ASME/ASCE Applied Mechanics & Fluids Engineering and Bioengineering Conference Paper No. 85-FE-3

Young G.A.J (1956) "Flow in the Rotating Passages of A Centrifugal Pump Impeller". British Hydromechanics Research Association paper SP530

Yedidiah (1993). "The drooping curve of a centrifugal pump." Proc. ROCON 93 Rotating Machinery Conf. And Exposition, Nov. 12-13 New England, USA